Identifying Shared Pathways Across Multiple Muscle Groups of the Human Upper Limb

Thomas Christopher Richards

Submitted in accordance with the requirements for the degree of
Doctor of Philosophy

The University of Leeds
School of Biomedical Sciences

September 2018

The candidate confirms that the work submitted is his/her own and that appropriate credit has been given where reference has been made to the work of others.

Acknowledgements

I would like to acknowledge my parents, Dave and Tina for the unwavering support and encouragement they have shown me throughout my time studying, to thank them, and for them to know that they are appreciated.

Samit – I thank you for all the faith, time and patience you have invested in me over many years, and for the intellectual challenges that you continually pose.

Amey Desai I would like to acknowledge for his efforts helping with the initial scripting and mathematical aspects of Chapter 3, for the friendship we have cultivated during his visits to Leeds, and for the rare qualities of being a completely genuine and unique character.

Kevin Power, thank you for providing the dataset used in Chapter 3, and for hosting me in St Johns whilst I collected the data for Chapter 5.

Thank you to Tom Pearson at CED for the many hours of his own time that I know he put in order to help me with scripting for the ‘coher and phase’ script which was applied in Chapter 4.

I would also like to acknowledge Ioannis Delis for allowing me to use his script for the cluster analysis which was applied in Chapter 4.

To all my friends, thank you for the joy in the good times and the support in the less good times over the course of my PhD.

Last but not least, thank you to the Motor Control (Out of Control) Group at the University of Leeds, particularly Piyanee, Mungo, and Rich. Lovely bunch of coconuts.

Abstract

Experimental limitations in humans mean that neurophysiological recordings must usually be limited to non-invasive, indirect measures. Consequently, we often overlook pathways in areas such as the spinal cord and brainstem in favour of pathways which are more accessible for stimulation and recording, such as cortical areas and the corticospinal tract. However, we currently lack the tools to effectively examine these systems. This may explain the large variability between the predicted and observed recovery which is common in clinical populations such as those affected by stroke. Whilst this significantly hampers clinical assessment, it has also led to large gaps in our understanding of shared pathways between shoulder and upper limb muscles, which is important information since the shoulder supports the weight of the arm. Applying algorithms for muscle synergy analysis to muscle activation patterns gives us interesting mechanistic insight. In clinical scenarios, it has also been used to show aberrant muscle activation patterns which are thought to relate to dysfunction in specific pathways. However muscle synergy studies do not reveal the neural drive to the muscles. This thesis addresses these problems by applying novel analytical approaches to non-invasive electromyographic (EMG) recordings of behavioural tasks and by using stimulation techniques to activate specific pathways. To accomplish this, it was necessary to generate new analytical systems which would enable us to be able to extract the relevant information.

Synaptic input to motoneurones can be identified non-invasively by performing frequency coherence analysis on EMG signals. Coherent frequencies between 6-60 Hz are often assumed to reflect efferent activity of

direct projections from the motor cortex to the spinal motoneurones. By applying a high resolution time-frequency analysis of evoked responses, we were able to show for the first time that EMG activity in the 15-60 Hz range is present at latencies which match those expected for the corticospinal pathway. We were also able to show the contribution of subcortical pathways, likely reticular, in the 35-100 Hz range, and spinal pathways in the 60-100 Hz range. This could be applied as a useful clinical metric for assessing remaining functional pathways following injury. We then assessed intermuscular coherence within these frequency bands across muscles of the upper limb to classify muscles into modules based on specific pathways. Using this technique, we provide a catalogue of muscle pairs sharing common drive across joints of the upper limb, and show how muscle interactions shift depending on task and limb position. We also propose a novel behavioural task for use in the clinic which we can use to identify key muscle interactions which are indicative of a functional descending drive. Finally, we demonstrate the involvement of high and low threshold peripheral pathways in a dynamic and static task of the upper limb.

List of Abbreviations

AD – Anterior deltoid

BB – Biceps brachii

CD – Contralateral middle deltoid

C-L – Contralateral

CMC – Corticomuscular Coherence

CMEP – Cervico-medullary Evoked Potential

CNS – Central Nervous System

CPG – Central Pattern Generator

CST – Corticospinal Tract

EEG – Electroencephalography

EMG – Electromyography

ER – Extensor carpi radialis

FDB – Flexor digiti minimi brevis

FFT – Fast Fourier Transform

FR – Flexor carpi radialis

GABA – Gamma aminobutyric acid

IMC – Inter-muscular Coherence

IS – Infraspinatus

LD – Latissimus dorsi

LT – Lateral triceps brachii

M1 – M1 Area of the Motor Cortex

MD – Middle deltoid

MEG – Magnetoencephalography

MEP – Motor-Evoked Potential

Mmax – Maximum amplitude of the compound muscle action potential

MT – Medial triceps brachii

MUAP – Motor Unit Action Potential

MVC – Maximum Voluntary Contraction

MVE – Maximum Voluntary Effort

NMF – Non-Negative Matrix Factorisation

PAD – Peripheral Afferent Depolarisation

PD – Posterior deltoid

PM – Pectoralis major

RMS – Root Mean Square

RST – Reticulospinal Tract

SA – Serratus anterior

sEMG – Surface Electromyography

TM – Teres major

TMES – Trans-mastoid Electrical Stimulation

TMS – Transcranial Magnetic Stimulation

UT – Upper trapezius

WSST – Wavelet Synchro-Squeezed Transform

TABLE OF CONTENTS

Acknowledgements ..... **ii**

Abstract ..... **iii**

List of Abbreviations ..... **v**

List of Figures ..... **xii**

Chapter 1: General Introduction **1**

1.1 Rationale 1

1.2 Clinical justification 1

1.3 Theoretical models of motor systems 2

1.3.1 Redundancy in motor control 2

1.3.2 The muscle synergy hypothesis 3

1.4 Physiological and anatomical structure of motor systems 3

1.4.1 The motor unit 3

1.4.2 Muscle interactions 4

1.4.3 Adaptation of muscle function to task-specific requirements 4

1.4.4 Organisation of descending pathways 5

1.4.5 Expression of the flexion synergy post-stroke 5

1.4.6 Reflex organisation 6

1.4.7 Muscle and joint interactions at the shoulder 9

1.5 Application of Digital signal processing to motor control 10

1.5.1 Frequency coherence studies 10

1.5.2 The beta band in corticomuscular coherence 10

1.5.3 Gamma band activity 11

1.6 Aims 11

1. Define frequency bands in the EMG which correlate with activation of descending and spinal pathways. 11

2. Establish pathway-specific shared neural drive between muscle pairs based on frequency bands outlined in aim 1. 12

3. Determine the regulation of muscle activity by peripheral pathways during static and dynamic tasks 12

Chapter 2: General Methods **13**

2.1 Ethical Approval 13

2.2 Introduction 13

2.2.1 Isometric tasks such as MVCs and MVEs 14

2.2.2 Using repetitive tasks to invoke CPG activity 14
2.2.3 Time and Frequency Domain analysis 14
2.2.4 Rectification and power in high frequency bands 15
2.2.5 Muscle synergies and Intermuscular coherence 16
2.3 Amplitude Matching, Evoked Responses and Time-Frequency Analysis during Arm Cycling and Tonic Contractions 16
2.3.1 Frequency Analysis of TMS/TMES Response Reveals Task-Dependent Shift in Central Drive to Biceps Brachii 16
2.3.2 Regulation of Group I and II Reflexes from Human Forearm and Hand to Upper Limb Muscles during Arm Cycling and Tonic Contractions..... 24
2.4 Using Intermuscular Coherence to Identify Common Input to Muscles Activated During Shoulder Abduction and Adduction.... 26
Chapter 3: Frequency analysis of TMS/TMES response reveals task-dependent shift in central drive to Biceps Brachii..... 40
3.1 Abstract 40
3.2 Introduction 41
3.2.1 The clinical and research needs for a means to identify neural drive in humans 41
3.2.2 Caveats and limitations of existing methods..... 42
3.2.3 Wavelet Synchro-Squeezed Transform (WSST) as a high resolution time-frequency analysis to identify transient of physiological events 44
3.2.4 Corticospinal Excitability of the Biceps Brachii is higher during Arm Cycling than an Intensity-Matched Tonic Contraction (Forman 2014) 45
3.2.5 Experimental rationale..... 47
3.3 Hypothesis 48
3.4 Methods 48
3.5 Results 49
3.5.1 Time to peak Measurements..... 49
3.5.2 Time-Frequency Analysis 49
3.5.3 Wavelet Coherence Analysis..... 54
3.6 Discussion..... 58
3.6.1 Time to peak..... 59
3.6.2 Frequency domain..... 60
3.6.3 Wavelet Transform and Wavelet Coherence taken together..... 63

3.6.4 Comparison of our results to those within the literature 64
3.6.5 High Resolution Benefits of Application of WSST to EMG data 66
3.6.6 High frequency components of EMG should be studied more closely 67
3.6.7 Clinical Applications 68
3.6.8 Considerations 68

Chapter 4: Using Intermuscular Coherence to Identify Common Input to Muscles Activated During Shoulder Abduction and Adduction 70

4.1 Abstract 70
4.2 Introduction 71
4.2.1 Pathways for Control of the Upper Limb 71
4.2.2 Muscle Synergy Analysis and Clinical Applications 72
4.2.3 Intermuscular Coherence Analysis 73
4.2.4 Maximum Voluntary Contractions (MVCs) are unreliable as a Normalisation Factor and for Corticospinal Assessment 73
4.2.5 Maximum Voluntary Effort (MVE) Task for Identifying Muscle Pairs activated by Common Descending Pathways 75
4.2.6 Outcome Measures 76
4.3 Methods 76
4.4 Results 77
4.4.1 Amplitude analysis 77
4.4.2 Power spectrum 77
4.4.3 Cross correlations and coherence 77
4.4.4 Muscle interactions - Postural Differences 85
4.4.5 Muscle interactions - Task Differences 104
4.4.6 Cluster Analysis 125
4.5 Discussion 127
4.5.1 Cluster Analysis 128
4.5.2 Cross-joint Interactions 129
4.5.3 Involvement of Peripheral Pathways in Defining Muscle Interactions 133
4.5.4 Coherence between Agonist and Antagonists at the Shoulder 135
4.5.5 Maximum Voluntary Effort Task to Differentiate Peripheral and Descending Interactions 137

4.5.6 Inter-subject Variability as a Useful Clinical Tool 141
4.5.7 Experimental Limitations 143
4.5.8 Conclusions 144

Chapter 5: Regulation of Group I and II reflexes from the forearm and hand to the human upper limb during arm cycling and tonic contractions 146

5.1 Abstract 146
5.2 Introduction 147
5.3 Methods 148
5.4 Results 148
5.4.1 Responses between different behavioural tasks 148
5.4.2 Responses at different stimulation intensities 150
5.5 Discussion 152

Chapter 6: General Discussion 154

6.1 Summary of Findings 154
6.2 Discussion of Key Results 155
6.2.1 Contribution of Different Pathways to Specific Frequency Bands 155
6.2.2 High Resolution Wavelet Transform Reveals Frequency Content of Evoked Potentials at Physiologically Relevant Latencies 156
6.2.3 Intermuscular Coherence Reveals Neural Muscle Synergies and Task-Dependent Shift in Neural Drive 156
6.2.4 MVE Task as a Means to Reveal Muscle Pairs Receiving Shared Descending Drive 157
6.2.5 Inter-Subject Variability 157
6.3 Transferability of Methods to other Contexts 158
6.3.1 Custom-Written System for Time-Frequency Analysis of Evoked Potentials 158
6.3.2 Custom-Written System for Onset/Offset, Amplitude, Power, Coherence, Phase, and Cross-Correlation Analysis 158
6.4 A Catalogue of Common Synaptic Inputs to Motoneurones across the Human Upper Limb 159
6.5 Clinical significance 160
6.5.1 Assessment of Descending Pathways by Time-Frequency Analysis of Evoked Responses 160
6.5.2 Arm Cycling as an Activity Based Therapy 160

6.5.3 Intermuscular Coherence to Improve Clinical Diagnostics 160
6.6 Future directions 161
6.6.1 Incorporation of Clinical Data 161
6.6.2 Moving forward with the study of High frequency components of EMG 161
6.6.3 Investigating Differences in Proximal and Distal Innervation in Relation to Coherence 163
6.7 Concluding Remarks 163
References 165
Appendix 180
Appendix 1. Scripts associated with Chapter 3 180
Appendix 2. Scripts associated with Chapter 4 183

List of Figures

Figure 1. A general summary of reflex pathways in the spinal cord. 8

Figure 2.1. Data collection from Forman et al. (2014). 18

Figure 2.2. Screenshot of Spike 2 display during identification of events in evoked potentials. 20

Figure 2.3. EMG data, Wavelet Synchro-squeezed Transform and examples of filtering process..... 22

Figure 2.4. The Biodex System 3 Dynamometer..... 28

Figure 2.5. Screenshots showing Spike 2 user interface during demarcation of burst onsets and offsets. 31

Figure 2.6. Example of the confidence intervals used for analysis. 35

Figure 2.7. Number of clusters plotted against residual error. 38

Figure 3.1. Data collection and findings from Forman et al. (2014). 46

Figure 3.2. Task-dependent change in corticospinal drive to arm muscles..... 51

Figure 3.3. Raw EMG, and corresponding WSST and wavelet coherence Spectrograms for biceps and triceps brachii during the cycling and tonic tasks. 52

Figure 3.4. Power spectral density measured from WSST at the time of response to Erb's point stimulation 53

Figure 3.5. Power spectral density measured from WSST results..... 56

Figure 3.6. Biceps-triceps coherence measured from wavelet coherence. 57

Figure 4.1. Raw EMG for ABD, ADD and MVE task recorded at 30° from a representative subject. 78

Figure 4.2. Raw EMG for ABD, ADD and MVE task recorded at 75° from a representative subject. 79

Figure 4.3. Raw EMG for ABD, ADD and MVE task recorded at 120° from a representative subject. 80

Figure 4.4. Group mean of mean RMS amplitude from EMG recorded during ABD, ADD and MVE tasks. 81

Figure 4.5. Group mean of mean normalised power spectrum for ABD ADD and MVE tasks. 82

Figure 4.6. Cross-correlations from ABD, ADD and MVE tasks for a representative subject. 83

Figure 4.7. Coherence spectra from ABD, ADD and MVE tasks for a representative subject. 84

Figure 4.8. Matrices of coherence between muscle pairs during ABD task, compared across angles. 87

Figure 4.9. Matrices of cross-correlations between muscle pairs during ABD task, compared across angles. 89

Figure 4.10. Matrices of coherence between muscle pairs during ADD task, compared across angles. 94

Figure 4.11. Matrices of cross-correlations between muscle pairs during ADD task, compared across angles. 96

Figure 4.12. Matrices of coherence between muscle pairs during MVE task, compared across angles. 100

Figure 4.13. Matrices of cross-correlations between muscle pairs during MVE task, compared across angles. 102

Figure 4.14. Matrices of coherence between muscle pairs at 30°, compared across tasks. 106

Figure 4.15. Matrices of cross-correlations between muscle pairs at 30°, compared across tasks. 108

Figure 4.16. Matrices of coherence between muscle pairs at 75°, compared across tasks. 113

Figure 4.17. Matrices of cross-correlations between muscle pairs at 75°, compared across tasks. 115

Figure 4.18. Matrices of coherence between muscle pairs at 120°, compared across tasks. 120

Figure 4.19. Matrices of cross-correlations between muscle pairs at 120°, compared across tasks. 122

Figure 4.20. Results of cluster analysis. 127

Figure 4.21. Differences in proximal and distal innervation from corticospinal and reticulospinal pathway. 131

Figure 4.22. Task-dependent involvement of descending pathways. 133

Figure 4.23. Possible effect of presynaptic inhibition on muscle interactions. 136

Figure 4.24. Effect of afferent drive on muscle interactions 138

Figure 4.25. Utility of MVE task to identify descending modules. 140

Figure 4.26. Variability across the sample. 142

Figure 5.1. Example of group I and group II responses. 149

Figure 5.2. Representative traces from one subject. 150

Figure 5.3. Summary table of evoked responses. 151

Figure 6. Proposed diagnostic App for use in the clinic. 162

Appendix figure 1. Flowchart detailing the parallel processing sequence used for wavelet analysis. 182

Chapter 1: General Introduction

1.1 Rationale

The muscle synergy theory states that muscles facilitating common movements are combined into modules in order to reduce dimensionality during movement (Bernshteĭn, 1967). Muscle synergy studies classify muscles into functional groups but currently do not account for the neural pathways forming these groups (Tresch et al., 2006; Torres-Oviedo, 2007; d'Avella et al., 2008). The assumption is often that muscle selection occurs in the brain (Drew et al., 2008; Overduin et al., 2015) though reflex pathways and spinal pathways also interact with descending signals to affect muscle activity (Sinkjaer et al., 2000; Guzmán-López et al., 2015). Descriptions of reflex pathways affecting proximal muscles at the human shoulder (which is important for reaching) are incomplete (Pierrot-Deseilligny and Burke, 2012). Taken into a task specific context, this would explain the contribution of reflexes to recruiting muscles into synergies. In humans, analysis in the frequency domain can be applied to observe common synaptic inputs to spinal motoneurones (Farmer et al., 1993; Conway et al., 1995; Castronovo et al., 2015). We can use EMG-EMG frequency coherence analysis to study spinal and reflex pathways in humans by assessing task-dependence and spatial patterns of common input to muscles. The first step is to clarify which pathways contribute to which frequency bands in EMG signals. With this information, we can then assess intermuscular coherence between muscle pairs, and provide a catalogue of shared pathways between muscles based on coherent frequencies. This catalogue can then be used as a clinical reference to improve patient stratification.

1.2 Clinical justification

The shoulder must bear the weight of the arm, making it key to everyday movements. The requirement of this joint to be highly mobile means that most

shoulder muscles serve several roles. These factors mean that loss of shoulder control, post-stroke for example, have implications for quality of life (Carod-Artal and Egido, 2009). Currently, predictors of recovery following stroke are inconsistent (Prabhakaran et al., 2007) and clinical assessments give subjective qualitative measurements which cannot fully describe the state of the motor systems (Bohannon and Smith, 1987; Gladstone et al., 2014). Whilst activity-based therapies such as constraint-induced movement therapy show promise in clinical trials for stroke therapy (Wolf et al., 2006), the pathways responsible for facilitating therapeutic benefits are unknown. To be able to assess these pathways would mean a clear picture of lost and remaining pathways which could be used as a prognosis from which to plan rehabilitation. An objective, synergy-based assessment of muscle drive would allow us to improve predictions of recovery and detail plasticity during recovery. It would also improve personalised neurorehabilitation regimens and reveal targets for activity based therapy.

1.3 Theoretical models of motor systems

1.3.1 Redundancy in motor control

During any movement, there is a high number of potential muscle and joint interactions presenting many degrees of freedom. This means an infinite number of motor strategies can be implemented to achieve the same motor outcome. In the field of motor control, this problem is known as redundancy. There are several theories as to how the central nervous system (CNS) deals with this problem. Two predominant theories, which are not mutually exclusive, are the muscle synergy hypothesis, and the optimal control hypothesis (Hirashima and Oya, 2016). The optimal control hypothesis states that sensory feedback is used to inform command impulses which deliver optimal performance for a specific motor parameter, such as power or accuracy (Scott, 2004). The muscle synergy hypothesis, proposed by Bernshteĭn (Bernshteĭn, 1967) states that motor systems are organised into hierarchical control structures.

1.3.2 The muscle synergy hypothesis

In Bernshteĭn's terms, the neural machinery at the highest levels of the model would be the motor cortex and cognitive centres in the brain, and the lowest level would be spinal motor pools controlling individual muscles. In this model, individual muscles would be grouped together into vectors which are controlled as a unit in order to reduce dimensionality during movements. Many mathematical algorithms are available which attempt to extract muscle synergies from activation patterns during behaviour, the most commonly applied being non-negative matrix factorisation (NMF) (Lee and Seung, 2001; Tresch et al., 2006). However, proof of the muscle synergy theory must come from the neural pathways involved in recruiting muscle synergies, which currently are not known. The predominant theory is that the motor cortex that selects spinal muscle synergies; indeed there is evidence that cortical stimulation activates muscle synergies similar to those observed behaviourally in primates (Overduin et al., 2012). The Bizzi group have explored the theory that populations of neurones form primitives in the spinal cord which are contacted by the motor cortex and are combined to produce movement (Tresch et al., 1999; Tresch et al., 2002; Bizzi et al., 2008). Much of these data are from the bullfrog. Using this model, they have described how depriving the spinal cord of peripheral sensory input does not appear to affect muscle synergies during motor behaviour (Cheung et al., 2005). These studies regularly utilise NMF to identify the muscle synergies. NMF can classify muscle synergies based on an output measure, such as amplitude of muscle activity. However, due to pre-processing steps applied before analysis, this does not directly reveal the neural substrates involved in synergy formation.

1.4 Physiological and anatomical structure of motor systems

1.4.1 The motor unit

The musculoskeletal system consists of the muscles, tendons and fascia's which act as the mechanical actuators for movement, which without neural control, would be useless. Muscles are innervated by spinal (or lower)

motoneurones which are located in the ventral horn of the spinal cord. One motoneurone contacts several muscle fibres. Motor unit types can vary greatly depending on the specialization of the muscle, both in number and in morphology of the muscle fibres (Burke, 1981). This combination of a motoneurone and its respective muscle fibres is known as the motor unit.

1.4.2 Muscle interactions

Two muscles which provide an opposite effect to one another - such as the biceps and triceps brachii in the upper limb - are referred to as an antagonist pair. Muscles and muscle groups are commonly characterised by the action they have in the context of a particular joint. Muscles acting on the wrist and elbow joints are primarily flexors, extensors, pronators or supinators. Muscles acting on the shoulder joint can be flexors and extensors, abductors and adductors, and rotators. Two muscles which serve to facilitate the same action on a limb – such as biceps brachii and brachialis – are referred to as agonists. Agonist interactions can be homonymous or heteronymous – homonymous if the effector muscle provides sensory input to itself, and heteronymous if the effector muscle is a different muscle. Muscles which are co-activated during a task are referred to as synergists. Whilst synergistic muscles are active at the same time, they do not necessarily serve the same action, or act at the same joint.

1.4.3 Adaptation of muscle function to task-specific requirements

Few muscles exhibit true antagonistic interactions since this requires them to act either side of a hinge joint with one degree of freedom. This means that relationships between muscles are not always held constant and can often be affected by factors such as rotation of the joint or position of the limb (Eccles et al., 1957; Buchanan and Almdale, 1986; Knikou et al., 2002). Classification of muscles based on their developmental compartments and anatomical function is useful, but can fall short when muscles display more diverse functionality. Whether or not a muscle is recruited into a task depends on the excitability of the spinal motoneurone. The spinal motoneurone receives many neuronal inputs from a wide range of sources from cortical, subcortical, spinal, and peripheral origin.

1.4.4 Organisation of descending pathways

Synaptic inputs from the brain are critical for voluntary control of muscles. Much of our knowledge of these pathways comes from tract tracing studies in primates. Hans Kuypers used silver-impregnated anterograde fibre degeneration techniques to compare descending pathways across species (Kuypers, 1981). Cortical motoneurones (upper motoneurones) descend through the corticospinal tract, which originates in the primary motor cortex. Around 90% of corticospinal projections make direct synaptic contact with contralateral spinal motoneurones. This is considered the most important descending input for fine motor control. Kuypers noted that in species with high capacity for dexterous hand control, there was a high density of corticospinal collaterals which projected to the more lateral motor pools in the ventral horn, which contain motoneurones innervating distal muscles. In contrast, reticulospinal (corticobulbar) projections were higher in density to more medial motor pools controlling proximal muscles. More recently it has become apparent that reticulospinal pathways may have more influence on control of distal limbs than previously thought, and synapse directly with motoneurones of hand muscles (Baker, 2011). This may have implications for recovery following stroke, though we do not currently have a reliable way to assess whether reticulospinal inputs remain intact.

1.4.5 Expression of the flexion synergy post-stroke

Destruction of a specific pathway can have a characteristic effect on muscle activation patterns. For example, post-stroke, a particular muscle synergy known as the flexion synergy occurs, whereby shoulder adductor and internal rotator, and elbow and wrist flexor activity is pathologically coupled (Twitchell, 1951). This results in reduced reaching distance when the shoulder abductors are weight-loaded (Sukal et al., 2007). One reason for expression of this synergy is believed to be due to an increased reliance on reticulospinal pathways (Dewald et al., 1995) over the corticospinal pathway which is more active in a non-pathological state (Lemon, 2008). Another theory in the generation of the flexion synergy involves a spinal mechanism. The reticulospinal pathway appears to supress the activity of flexor reflex

interneurones (Engberg et al., 1968). Following a cortical stroke, release of cortical excitation of the reticulospinal pathway would increase the excitability of these flexor reflex interneurones through disinhibition, causing them to have a continuous facilitatory effect on the flexor motor pool.

1.4.6 Reflex organisation

1.4.6.1 *Reflex definition*

A reflex is an involuntary motor response to a sensory stimulus. The nomenclature of different reflexes is based on anatomical differences in fibres in major nerves of the hind limb of the cat which are involved in evoking the response (Lloyd, 1943). They are grouped I-IV depending on diameter, with the largest in group I and the smallest in group IV. Larger diameters and higher degrees of myelination result in faster conduction velocity. Group I and II are both exclusively muscle afferents while group III and IV can be either muscle or cutaneous fibres, including afferents from both nociceptors and mechanoreceptors. This classification has been revisited to account for data relating to the human (Macefield et al., 1989). Group I fibres are the most prevalent and most widely studied.

1.4.6.2 *Group I reflex pathways*

Group I afferents are large diameter, fast conducting, low threshold fibres which include the subtypes Ia and Ib.

1.4.6.3 Group Ia reflex pathways

Ia afferents transmit sensory information from muscle spindle organs of intrafusal fibres and provide information about velocity of muscle stretch in relation to force. Group Ia fibres make monosynaptic connections with motoneurones which are excitatory and produce the myotatic reflex (or stretch reflex) in both homonymous and heteronymous muscles. Density of monosynaptic projections are usually, but not always (Clough et al., 1968), greater to homonymous motoneurones, producing a larger response (Mendell and Henneman, 1970). Classically, it was thought that most heteronymous monosynaptic projections supply synergistic muscles at the same joint (Eccles

et al., 1957). However, many muscles have monosynaptic projections spanning to muscles of other joints, and others do not innervate muscles of the same joint (Rothwell, 1987). Ia fibres also give rise to antagonistic responses through inhibitory interneurones, which reduce the activity of antagonistic motoneurones (Hultborn et al., 1971; Iles, 1986). This action is known as reciprocal inhibition. A visual summary of pathways which exist between a pair of antagonistic motoneurones can be found in ***figure 1*****.**

1.4.6.4 Group Ib reflex pathways

Ib afferent fibres transmit sensory information from Golgi tendon organs (GTO) and provide information about load or tension. Homonymous projections from group Ib fibres inhibit firing of motoneurones to the effector muscle via inhibitory interneurones in a process known as autogenic inhibition. Ib fibres also give rise to reciprocal excitation in the autogenic reflex by exciting antagonistic muscles (***figure 1***).

1.4.6.5 *Group II, III, and IV pathways*

Owing to the difficulty of studying these pathways in humans, they are not well defined. However, in cats, group II pathways and interneurones have been identified and associated pathways defined (Wada and Shikaki, 1999; Jankowska et al., 2002). Like Ia afferents, group II afferents transmit sensory information from intrafusal muscle fibres. Unlike group Ia afferents, group II afferents continuously transmit information about overall muscle length (Darby and Frysztak, 2013). Group III fibres are thinly myelinated and include cutaneous and muscle afferents. Group II and III pathways are all polysynaptic, and are referred to as flexor reflex afferents as when stimulated they both produce the flexor reflex and crossed extensor response (***figure 1***). Group IV afferents are unmyelinated and include, muscle, nociceptive and cutaneous afferents. Group III and IV afferents are involved in the nociceptive withdrawal response, and the pressor reflex, which provides an autonomic reflex response to contraction of skeletal muscle.

1.4.6.6 *Recurrent inhibition*

Recurrent inhibition is provided by Renshaw cells, a population of inhibitory interneurones which receive inputs from many sources (***figure 1***). Renshaw cells provide autologous inhibition of the same motoneurone from which it

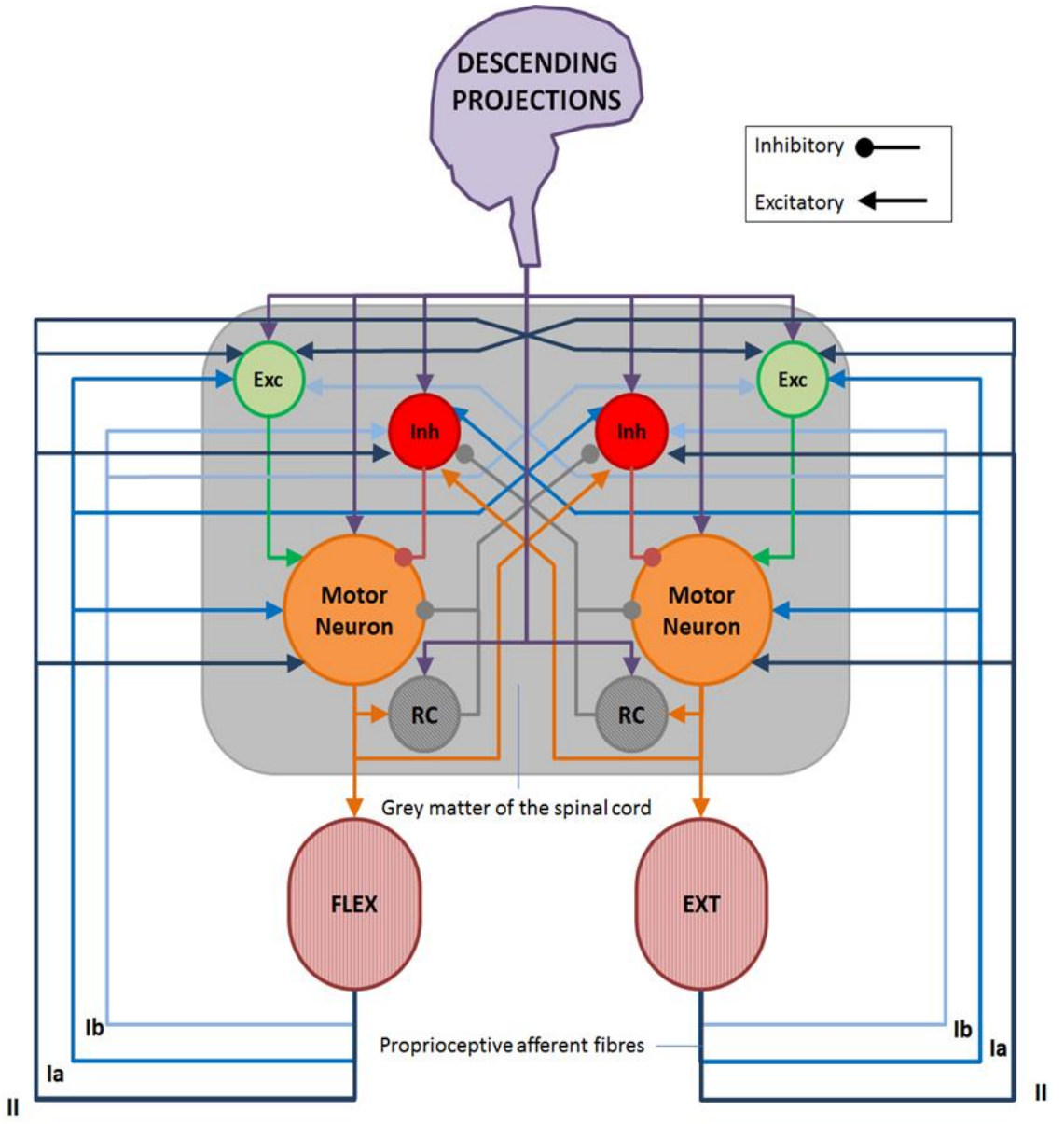

Figure 1. A general summary of reflex pathways in the spinal cord. Figure shows a simplification of pathways described in both humans and animals between motor pools innervating a pair of antagonistic muscles. Exc = excitatory interneurone, Inh = inhibitory interneurone, RC = Renshaw cells, Flex = flexor muscle, Ext = extensor muscle, Descending projections = general, but largely representative of corticospinal tract projections. Apart from Renshaw cells, distinctions are not made between different interneurone populations but are simply categorised as either excitatory or inhibitory. This means that this diagram cannot be considered to accurately describe factors such as spatial summation and convergence. Data from (Baldissera et al., 1981; Pierrot-Deseilligny and Burke, 2012).

receives axon collaterals, as well as homonymous motoneurones located in close proximity. In humans, recurrent inhibition is widespread in the lower limb, but more restricted in the upper limb (Katz and Pierrot-Deseilligny, 1999). Renshaw cells provide a negative feedback loop for which there are many functional theories, including: providing a cessation of motoneurone firing post activity in order to minimise muscular damage by tetanus, regulation of motoneurone gain, or providing more dynamic changes in motoneurone firing.

1.4.7 Muscle and joint interactions at the shoulder

Roh et al. (Roh et al., 2013) used NMF to identify synergies of shoulder and elbow muscles activated during shoulder abduction/extension tasks, (biceps brachii, anterior deltoid, middle deltoid, and pectoralis major) and adduction/flexion tasks (brachioradialis, medial triceps brachii, lateral triceps brachii, middle and posterior deltoid). However, the interactions between muscles and joints were not examined. This is important since any force exerted on a distal joint (wrist, elbow) affects activity of muscles which stabilise more proximal joints (shoulder) (Rothwell, 1987). Sensory information between distal and proximal joints must be coordinated to successfully achieve stability. In the baboon, interactions between muscles at different joints have been observed through Ia pathways in the upper limb (Hongo et al., 1984). Only recently have studies begun to cover interactions of muscles acting at different joints in man (Miller and Dewald, 2012). Reciprocal inhibition at the human wrist is mediated predominantly by Ib inputs though it is not known if these inputs extend to the shoulder (Wargon et al., 2006). Monosynaptic Ia and recurrent pathways have been studied in the upper limb in man but are also incomplete at the shoulder (Pierrot-Deseilligny and Burke, 2012). Better clarification of muscle interactions and the corresponding pathways would improve our understanding of the influence of peripheral afferents and spinal circuits on formation of muscle synergies. If different neural pathways can be correlated with specific frequency bands in muscle activity, we can use intermuscular frequency coherence analysis for this goal.

1.5 Application of Digital signal processing to motor control

1.5.1 Frequency coherence studies

Frequency coherence has been studied between signals recorded between a pair of muscles (intra- and intermuscular) (Farmer et al., 1993), and between a muscle and the cortex (corticomuscular) (Conway et al., 1995). Invasive studies using needle electrodes can be used to determine common drive to individual motor units (Farina et al., 2013), or surface EMGs (sEMG) can be used to view common drive to whole muscles (Chang et al., 2012). Whilst firing rates of motor units are usually within the range of 6 to 35 Hz, during strong contractions, firing rates can be seen to increase to around 50 Hz (Mima and Hallett, 1999). Coherence is most commonly discussed in the context of three distinct frequency windows or bands; alpha, α (8-12 Hz), beta, β (15-35 Hz), and gamma, γ (35-80 Hz), with the view that 15-30 Hz band is of cortical origin (Conway et al., 1995).

1.5.2 The beta band in corticomuscular coherence

Early coherence studies showed that motor units in hand muscles showed coherence in the 1-12 Hz and 16-32 Hz range during voluntary isometric contractions (Farmer et al., 1993). As the 16-32 Hz coherence remained in patients with peripheral neurological lesions, this was hypothesized to originate from the motor cortex. In agreement with this, oscillations in the primary motor cortex at 20-30 Hz have been observed in primates (Murthy and Fetz, 1996). Since then, many studies utilizing a precision grip task (ramp and hold) whilst recording from hand muscles have reported corticomuscular coherence using EEG/MEG-EMG (EEG - electroencephalography, MEG - magnetoencephalography) (Halliday et al., 1998; Kilner et al., 2000). Coherence around 20 Hz is seen to decrease after administration of a $GABA_A$ antagonist, suggesting that oscillations in the motor cortex are reliant on intracortical GABAergic circuits (Baker and Baker, 2003). The existence of corticomuscular coherence between 15-30 Hz is task dependent; it is absent during dynamic movement but is strongest during tonic contraction (Kilner et al., 2003; Mehrkanoon et al., 2014). Within the 15-30 Hz band there is also a reported ascending component (Witham et al., 2011). A recent study utilising

a dynamic motor task showed that whilst coherence in the beta and gamma bands may be due to cortex-lead events, sensorimotor components may also contribute to coherence in the alpha band (Mehrkanoon et al., 2014).

1.5.3 Gamma band activity

The gamma band describes activity in the range of 30-80 Hz. EMG power shifts to around 40 Hz during strong contractions. This was first described by Hans Piper in 1907 and is hence sometimes referred to as the Piper Rhythm. Corticomuscular coherence studies propose that this is also an oscillatory phenomenon driven by the contralateral cortex, and has been seen in submaximal as well as maximal contractions (Brown et al., 1998).

1.6 Aims

The primary objective of this work was to develop tools and data which allow non-invasive ways to measure activity in inaccessible but important pathways, such as those in the spinal cord and brainstem. These were then applied to create a catalogue of shared inputs to muscle pairs at the shoulder and across the upper limb. From this, we identified key muscle interactions which could be used in the clinic to study specific pathways. Another purpose for generating these data was to bring knowledge of pathways acting at the human upper limb closer to our knowledge of animals such as the cat, rat and monkey. To achieve these objectives, we took the following course of action.

1. **Define frequency bands in the EMG which correlate with activation of descending and spinal pathways.**

The first objective was to probe the source of muscular activity at frequencies between 5-65 Hz. This was achieved by observing responses to stimulation of the motor cortex (using transcranial magnetic stimulation) and the pyramidal tract (using trans-mastoid electrical stimulation) delivered during specific tasks. A time-frequency analysis was applied to the response to reveal differences in cortical, and subcortical stimulation.

2. **Establish pathway-specific shared neural drive between muscle pairs based on frequency bands outlined in aim 1.**

Using the frequencies identified in aim 1, we applied intermuscular coherence between muscle pairs across the upper limb to identify muscles which share common input from specific pathways.

3. **Determine the regulation of muscle activity by peripheral pathways during static and dynamic tasks**

By assessing how responses to peripheral nerve stimulation differs between static and dynamic tasks, we determined the involvement of peripheral drive in different task scenarios. This will allow us to assess whether peripheral drive contributes to different frequency bands in the EMG.

These data will give us a neurophysiological basis for muscle synergies in healthy adult humans. Following these studies, these techniques should be applied to patient populations to confirm findings with participants with known deficiencies. These data could be applied to a clinical situation in which a frequency analysis is used for diagnostic examination of specific pathways.

Chapter 2: General Methods

2.1 Ethical Approval

Experiments were performed under approval granted by the local ethical committee (University of Leeds BIOSCI 15-029).

2.2 Introduction

For the most complete understanding of motor control, we must take into account neurophysiological, biomechanical and behavioural context with combinations of the appropriate analytical techniques. In a clinical scenario, due to limitations on time and budget, we are often limited as to the complexity of assessments. Electromyography (EMG) is a simple non-invasive technique which we can apply clinically. It gives an indirect measure of the activity of the motoneurone pool innervating a muscle by recording the electrical activity of a muscle from the skin surface as a waveform. Evoked responses using magnetic or electrical stimulation can be recorded in order to extrapolate what is happening in the central nervous system (CNS) to produce an output. However, it is not always possible to stimulate neural pathways or populations in humans invasively, and responses to non-invasive stimulation represent an artificial function of the nervous system which may not accurately represent how pathways interact naturally. Ideally, we would be able to obtain pathway-specific data relating to neural feed to motoneurones without mechanical or electrical perturbation during natural behaviour. Whilst this may never be completely possible, we can further understanding of what pathways are active and how they can be measured by combining task context and stimulation with different analytical methods. Limits in our understanding and caveats in current methodology need to be addressed to approach this end goal. In this section I will outline these problems and explain our approach to overcoming these.

2.2.1 Isometric tasks such as MVCs and MVEs

Maximum Voluntary Contractions (MVCs) are recorded as the highest output an individual can achieve for a given muscle. The lack of standardisation of joint angles in the literature, too few MVCs being recorded for the participant to achieve 100% MVC, not recording from surrounding muscles, and trial to trial variability are all factors which detract from the value of taking MVCs. When the purpose of MVCs is to identify neural drive to muscles, this is problematic since all of these conditions are affected by or omit important aspects of neurophysiological drive. We approach these problems with shoulder MVC tasks recorded at different shoulder angles whilst recording from multiple muscles of the upper limb. We also use a novel Maximum Voluntary Effort task whereby subjects attempt to contract the muscle of interest without applying a force against a resistance as they do with MVCs.

2.2.2 Using repetitive tasks to invoke CPG activity

Isometric contractions are predominantly of a cortical origin (Sergio et al., 2005). However, networks of neurones in the spinal cord known as central pattern generators (CPGs) are capable of generating and sustaining repetitive movements in invertebrates and mammals (Grillner, 1981). CPG circuits also appear to function in the human upper limb during an arm cycling task (Zehr et al., 2004). We can compare how evoked responses differ between a cycling task and an isometric task to assess whether the prior activation of these circuits affects the response.

2.2.3 Time and Frequency Domain analysis

EMG waveforms can be subjected to time domain and frequency domain analysis, which show different aspects of the data. The time-domain shows changes in magnitude of a measured quantity with respect to time (e.g. signal amplitude). Frequency-domain analysis represents periodic or repetitive phenomena in the signal. Frequency domain analysis has been used to reveal common neural input to muscle pairs by measuring intermuscular coherence. This has promising clinical applications. A window based approach such as FFT or the Hilbert transform is useful for scenarios where the frequency

distribution within a signal is expected to be constant over time. This approach is useful for identifying coherence in key frequencies during sustained tasks where large windows of data can be selected. In case of transient changes in frequency distribution, window based approaches lack time resolution. To resolve transient events in the frequency domain, a better alternative is the wavelet transform, which operates with mathematical functions called ‘wavelets’ (Neto et al., 2010).

2.2.4 Rectification and power in high frequency bands

CMC and IMC studies show coherence in three bands: alpha (α) at 8-12 Hz, beta (β) at 15-35 Hz, and gamma (γ) at 35-100 Hz. Elements outside of the alpha, beta, and gamma bands are rarely discussed though the power spectrum of unrectified EMG often reaches 150-200 Hz or higher. Frequencies above 100 Hz are rarely studied, except for as a measure of fatigue by observing median frequency (Kattla and Lowery, 2010). It is commonly assumed that high frequencies in the EMG result from noise and synaptic events not responsible for motor unit (MU) coupling (De Luca and Erim, 1994). Another reason high frequencies are not studied is that before frequency coherence is performed, data are almost always rectified. This process shifts power from higher frequencies to lower frequencies thus improving coherence and definition in low frequencies considered to be of interest (Boonstra and Breakspear, 2012). The practice of rectification before coherence analysis is currently the subject of some debate. Since the skull naturally acts as a low-pass filter (Srinivasan et al., 1996), this is probably an appropriate step to improve detection of corticomuscular coherence. However, since high frequencies can still be detected in EMG recordings, applying rectification, which artificially suppresses high frequencies, may be inappropriate in this context. Rectification also has a non-linear effect on power spectrum, and whereas coherence analysis is a linear process (McClelland et al., 2012b). The intensity of the muscle contraction is also a factor to consider when deciding whether or not to apply rectification. Some groups argue that rectification improves coherence at lower levels of contraction (Ward et al., 2013), whilst during high intensity contractions it may have subtractive effects on coherence due to amplitude cancellation (Farina

et al., 2013). Since the tasks in the current study involved mainly mid-range or high intensity muscle contractions, data was analysed unrectified.

2.2.5 Muscle synergies and Intermuscular coherence

Muscle synergy analysis can give information about spatial, temporal, or spatio-temporal patterns of muscle activity (Cheung et al., 2012; Roh et al., 2013; Hilt et al., 2018), and has promising clinical applications (Cheung et al., 2012). However, commonly used techniques such as NMF are not currently utilised in a way which reveals neural drive to muscles. This is mostly because EMG data are subjected to pre-processing steps which obscure neural activity before analysis. Specifically, muscle activity is routinely smoothed to form an envelope and normalised in the time domain. Heavy filtering applied to smooth the signal removes all frequency domain activity which correlates with neural firing. Time normalisation alters the time scale of events in the EMG which depend on neural components (such as reflex related activity). Common drive to muscle pairs can be identified using intermuscular coherence (Farmer et al., 1993). This technique is usually only applied to a pair of muscles during an isometric task. However, by recording from muscles across the limb, we can monitor how common input to motoneurones varies depending on the task context and use this as a means to classify muscles into synergies.

2.3 Amplitude Matching, Evoked Responses and Time-Frequency Analysis during Arm Cycling and Tonic Contractions

Data for these experiments were collected at Memorial University, Newfoundland, Canada.

2.3.1 Frequency Analysis of TMS/TMES Response Reveals Task-Dependent Shift in Central Drive to Biceps Brachii

2.3.1.1 Data Collection

Data for this study were provided by Kevin Power and have been published previously using different analytical methods (Forman et al., 2014).

i. *Muscles*

BB – biceps brachii, LT – lateral triceps brachii.

ii. *Electromyography*

The skin over the midline of the right biceps and triceps brachii was prepared by removing dead epithelial cells by light abrasion using sand paper, and cleansed with an isopropyl alcohol swab. Surface electrodes (Medi-Trace 130 ECG conductive adhesive electrodes) were positioned longitudinally over the muscle belly using a bipolar configuration (Ag-AgCl, 2 cm inter-electrode distance) with the ground electrode on the lateral epicondyle. EMGs were sampled at 5 kHz using the CED 1401 interface and Signal 4 software [Cambridge Electronic Design (CED), Cambridge, United Kingdom]. Signals were amplified using a CED 1902 amplifier, and filtered with a three-pole Butterworth filter to give cut-off frequencies of 10-1,000 Hz.

iii. *Protocol*

Wrist braces were worn throughout the experiment. Subjects were asked to cycle for 1 minute at a workload of 25 W at a cadence of 60 RPM on an arm cycle ergometer (Monark Rehab Trainer, model 881E) mounted on a table (***figure 2.1A***). The crank positions relative to a clock face were used to represent different phases of the cycling (***figure 2.1B****)*: 6 o'clock (mid-flexion, maximum biceps brachii activity) and 12 o'clock (mid-extension, minimum biceps brachii activity). These points were used to trigger recording and stimulation for the cycling task (***figure 2.1C***) during the rest of the experiment with a magnet on the crank handle. For each phase of the cycling, the average background RMS EMG of the biceps brachii was measured from 50 ms before the stimulation artefact. Isometric tasks were then performed matching the contraction intensity at each phase. Participants tried to match biceps brachii RMS EMG to a horizontal line on the monitor indicating the desired intensity. Isometric contractions were produced with the arm crank locked in the corresponding position similar to previous studies (Carroll et al., 2006).

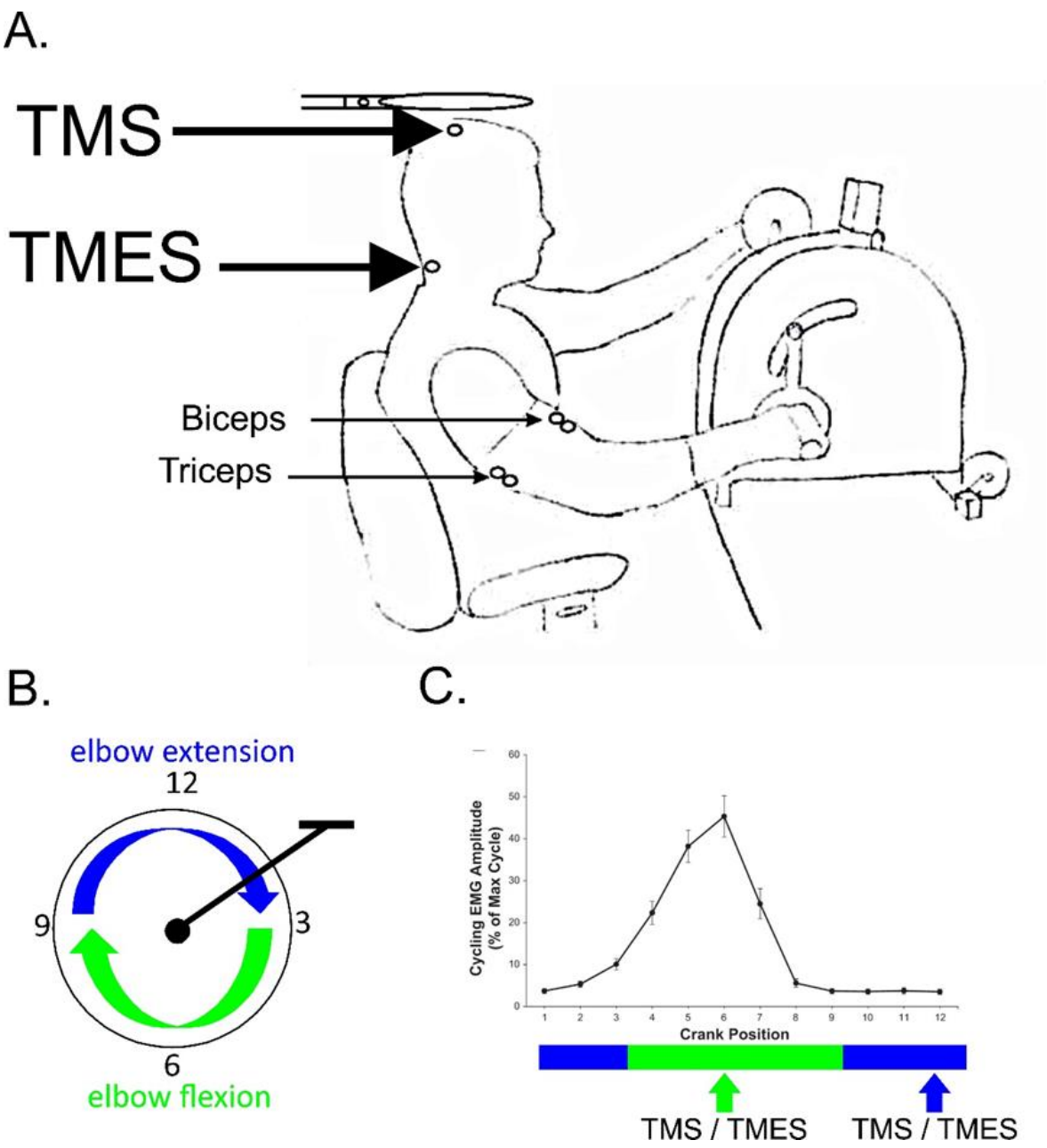

Figure 2.1. Data collection from Forman et al. (2014). **A.** EMGs were recorded from biceps and triceps. **B.** Flexion (biceps) and extension (triceps) and positions on clock face. **C.** Average biceps EMG throughout one revolution. **A.** and **C.** adapted from Forman et al. (2014).

iv. *Stimulation*

Erb's point brachial plexus stimulation was used to obtain the maximum amplitude of a compound muscle action potential (Mmax) in biceps brachii. Transcranial Magnetic Stimulation (TMS) and Trans-Mastoid Electrical Stimulation (TMES) intensities were then adjusted to give approximately 5-10% of Mmax peak-to-peak amplitude. These intensities were used for the

remainder of the study. TMS was applied over the vertex using a circular coil (13.5 cm outside diameter) attached to a Magstim 200 (Magstim, Dyfed, United Kingdom). TMES was applied via adhesive Ag-AgCl electrodes fixed to the skin slightly inferior to the mastoid processes and current passed between them (100 μs duration, 125-350 mA; model DS7AH; Digitimer). Stimulation was delivered either during cycling at the 6 or 12 o'clock position, or during a 5 s isometric contraction fixed at the equivalent position, where biceps brachii RMS EMG was matched to respective phase during cycling (***figure 2.1***). Both during cycling and tonic contractions at each position, and for both TMS and TMES, 10 trials were recorded (*n* = 10).

2.3.1.2 Data Analysis

See ***appendix 1*** for information about associated scripts.

i. Latency Analysis

Latency measurements

Latency to the peak of the motor-evoked potential (MEP) was measured for each condition from the rectified EMG within a 5-45 ms time window post-stimulus using custom-written scripts[1] for Spike 2 [Cambridge Electronic Design (CED), Cambridge, United Kingdom] (***figure 2.2***).

Statistics

Results were compared using a two-way ANOVA (subject and condition). Post-hoc tests were carried out using Tukey's honest significant difference test with Bonferroni correction for multiple comparisons. All statistical analysis were carried out using custom-written R scripts. The latency for the maximal response was the used to assess the power spectral density following wavelet transformation.

---

[1] These scripts are available, with permission, from the University of Leeds Data Repository at: https://doi.org/10.5518/592 (Richards et al., 2018).

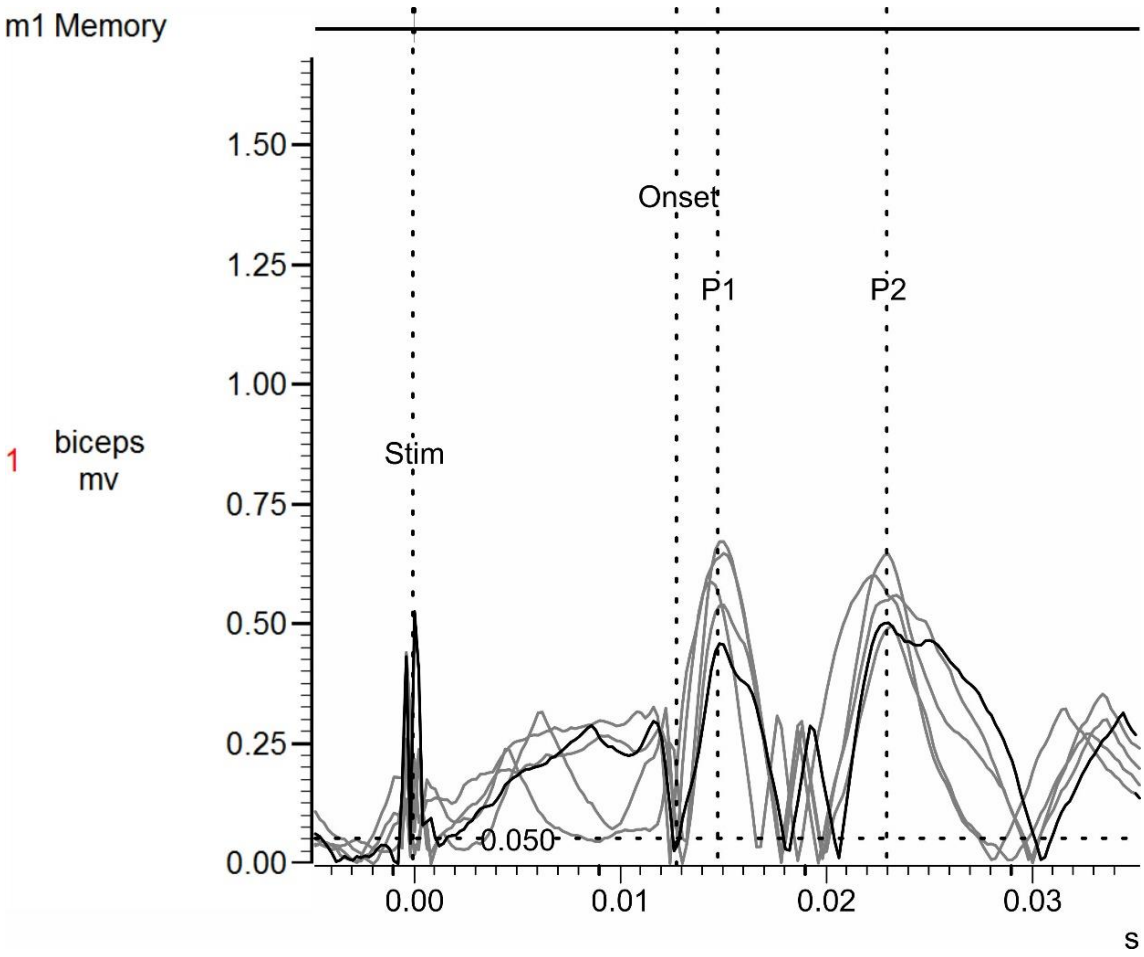

Figure 2.2. Screenshot of Spike 2 display during identification of events in evoked potentials. Scripts were written to record latency data relating to important events in evoked potentials, which was used in time-frequency analysis. Time points of relevant events were saved to a marker channel (top, labelled m1 Memory). Adjustments to the vertical cursors were made by the user if necessary.

ii. Time-frequency Analysis

Custom scripts[2] were written for submission to a high performance computer which perform pre-processing (DC offset removal with a 2 s time window), apply a wavelet transform, and extract power spectral density (PSD) at the relevant time point. This system utilised parallel processing routines and was submitted to a high performance computer for analysis (***appendix figure 1***).

[2] These scripts are available, with permission, from the University of Leeds Data Repository at: https://doi.org/10.5518/592 (Richards et al., 2018).

Time-frequency spectrograms were obtained using the Matlab® wsst() function (WSST - Wavelet Synchro-Squeezed Transform) using 48 voices per octave and L1 normalisation (***figure 2.3A***). We used the Amor wavelet (the analytical form of the Morlet wavelet) since it is well suited to detecting transient changes in frequency:

$$\psi(x) = ((\pi * F_b)^{-0.5}) * e^{2*\pi*i*F_c*x} * e^{-(x^2)/F_b}$$

Equation 1.

where $\psi(x)$ is the wavelet transform at time x, F_c is the centre frequency, F_b is the damping coefficient, and i is $\sqrt{-1}$. In usual circumstances, there is a significant spread around the centre frequency (***figure 2.3B***). To overcome this problem, we filtered around each frequency band measured and we performed a separate wavelet transform for each frequency band (***figure 2.3C***). Wavelet transforms were produced for each frequency band between 1-150 Hz in steps of 1 Hz using a 4th order Butterworth filter with cut-offs 1.5 Hz above and below the band of interest (or a low cut-off of 1 Hz for the 1-2 Hz bin):

$$H(s) = \frac{(1 - f_1) \dots (1 - f_{k1})}{(s - s_1) \dots (s - s_{k2})}$$

Equation 2.

where $H(s)$ is the filter transfer function, f is the zeros of the filter, s is the poles of the filter, and $k1$ and $k2$ are constants which depend on the filter design. For each 1 Hz band, the average amplitude of all bins within the range was calculated (the frequency distribution is logarithmic so the interval between frequency bins is smaller at lower frequencies). If there was no data point available within a frequency range (as with some frequencies above 60 Hz) then that bin was not included in further analysis. Power spectral density was assessed at time points corresponding to the MEP peak (***figure 2.2***) when stimulation was applied and equivalent points in the cycle when stimulation was not (10 per condition per subject). Statistics are described at the end of this section.

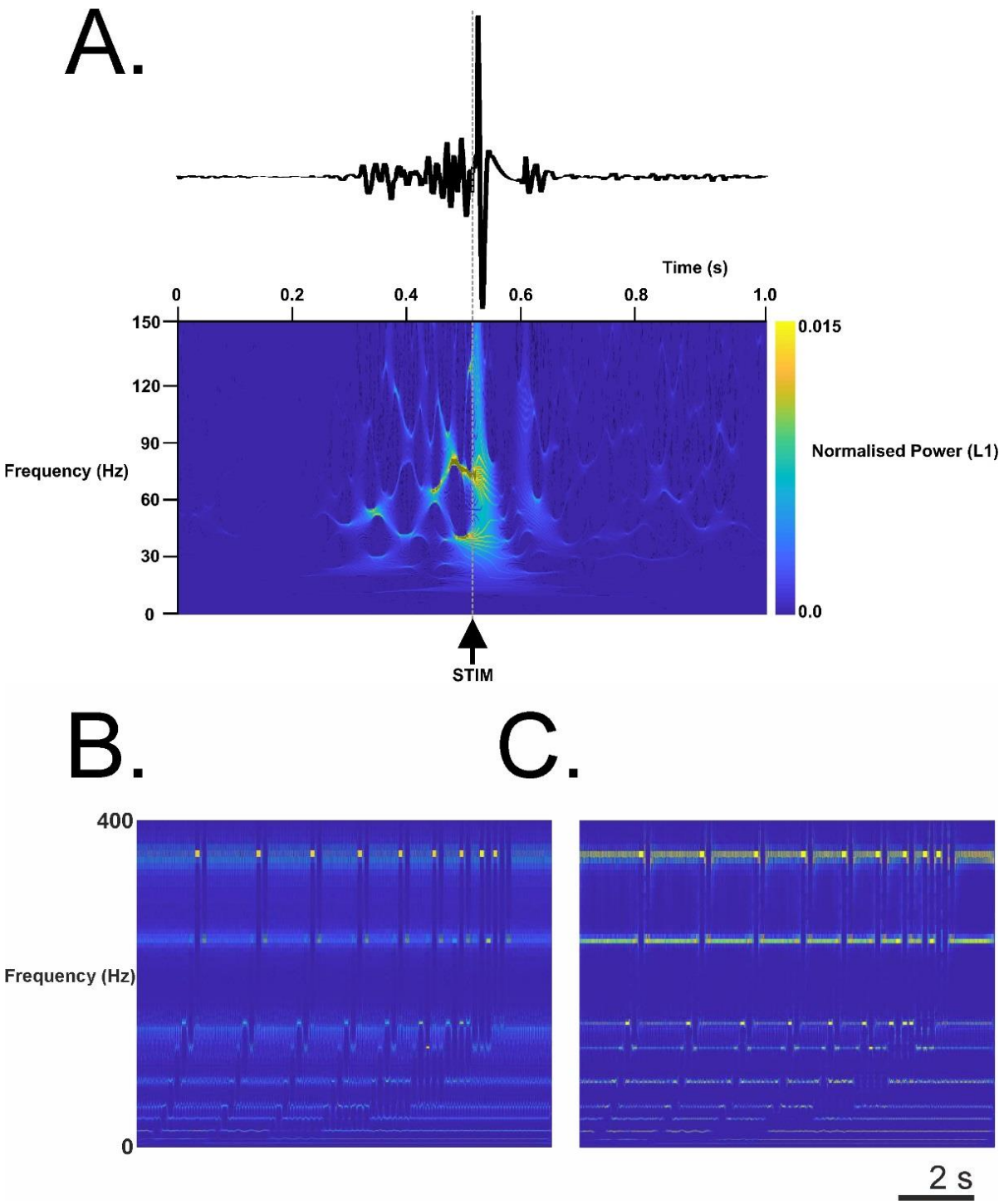

Figure 2.3. EMG data, Wavelet Synchro-squeezed Transform and examples of filtering process. **A.** Representative EMG trace of one biceps burst during cycling (top) showing stimulus artefact (dashed line) and TMS response, and corresponding wavelet synchro-squeezed transform (bottom). **B.** WSST of simulated data taken without filtering to show bleeding between frequency bands **C.** Visual reconstruction of filtered WSST. Note that the unfiltered WSST in **B.** shows bleeding between frequency bands but when the signal is filtered at each frequency before reconstruction (as in **C.**), the frequency resolution is improved.

iii. Wavelet Coherence Analysis

The scripts written for the time-frequency analysis were adapted to measure wavelet coherence between biceps and triceps brachii at a pre-determined time point[3]. The Matlab® wcoherence() function was used to obtain wavelet coherence spectra between the two signals, using 32 voices per octave (Matlab®, 2016). Similar to the time-frequency analysis, we used the Amor wavelet to calculate coherence using the equation:

$$C_{xy}(a,b) = \frac{|S(\psi_x^*(a,b)\psi_y(a,b))|^2}{S(|\psi_x(a,b)|)^2 S(|\psi_y(a,b)|)^2}$$

Equation 3.

where $C_{xy}(a,b)$ is the coherence of continuous wavelet transform of x and y at scales a and position b, $*$ denotes the complex conjugate, and S is the smoothing operator in time and scale. Signals were subjected to the same filtering procedure used in the time-frequency analysis, except instead of using steps of 1 Hz, signals were filtered based on frequency bands determined from the results of the time-frequency analysis. Coherence was measured at the same time points as time-frequency analysis.

Statistics

The time frequency analysis and wavelet coherence were analysed by performing ANOVAs for each muscle (two-way, subject and condition) at each frequency band to compare differences at that frequency between conditions. Post-hoc tests were carried out using Tukey's honest significance difference test with Bonferroni correction for multiple comparisons. All statistical analysis were carried out using custom-written scripts for R.

[3] These scripts are available, with permission, from the University of Leeds Data Repository at: https://doi.org/10.5518/592 (Richards et al., 2018).

2.3.2 Regulation of Group I and II Reflexes from Human Forearm and Hand to Upper Limb Muscles during Arm Cycling and Tonic Contractions

2.3.2.1 Data Collection

i. Muscles

PM – pectoralis major, MD – middle deltoid, UT – upper trapezius, BB – biceps brachii, LT – lateral triceps brachii, MT – medial triceps brachii, FR – flexor carpi radialis, ER – extensor carpi radialis, FDB – flexor digiti minimi brevis.

ii. Electromyography

The skin over each muscle was prepared by removing dead epithelial cells by light abrasion using sand paper, and cleansed with an isopropyl alcohol swab. Electrode gel was added to the each electrode for better conductivity and to increase SNR. Surface electrodes (Medi-Trace 130 ECG conductive adhesive electrodes) were positioned longitudinally over the muscles using a bipolar configuration (Ag-AgCl, 2 cm inter-electrode distance) with the ground electrode on the lateral epicondyle. EMGs were sampled at 5 kHz using the CED 1401 interface and Signal 4 software [Cambridge Electronic Design (CED), Cambridge, United Kingdom]. Signals were amplified using a CED 1902 amplifier, and filtered with a three-pole Butterworth filter to give cut-off frequencies of 10-1,000 Hz.

iii. Protocol

After stimulation points had been determined, wrist braces were worn throughout the experiment. Methods were similar to those described in section 2.3.1. Subjects were asked to cycle for 1 minute at a workload of 25 W at a cadence of 60 RPM on an arm cycle ergometer (Monark Rehab Trainer, model 881E) mounted on a table. The crank positions relative to a clock face were used to represent different phases of the cycling: 12 o'clock (mid-extension, minimum biceps brachii activity), 3 o'clock (extension-flexion transition/pre-maximum biceps brachii activity), and 6 o'clock (mid-flexion, maximum biceps brachii activity, ***figure 2.1***). These points were used to

trigger recording and stimulation for the cycling task during the rest of the experiment. For each phase of the cycling, the average background RMS EMG of the biceps brachii was measured from 50 ms before the stimulation artefact. An isometric task was then performed for each phase, matching the contraction intensity. Participants tried to match biceps brachii RMS EMG to a horizontal line on the monitor indicating the desired intensity. Isometric contractions were produced with the arm crank locked in the corresponding position similar to previous studies (Carroll et al., 2006).

iv. Stimulation

The stimulation procedure was similar to that of Lourenço et al., (2006). The ulnar nerve was stimulated at the wrist level, on the lateral aspect of the palmar side. A probe was used to locate the optimum position for the stimulating electrodes. Conductive gel was applied to two stimulating electrodes (Medi-Trace 130 ECG conductive adhesive electrodes) which were then were placed 2 cm apart and secured with medical tape, with the cathode proximal. Stimuli were delivered with a 1 ms square pulse. Threshold (T) was determined by gradually increasing current until there was a visible twitch in the FBD and a response was visible in the EMG. Intensity of stimulation was expressed as multiples of that used for threshold (e.g. 2T is twice the intensity for threshold). When the threshold had been ascertained, the FDB electrode was replaced for one of the shoulder muscles since there limited channels were available. The subject then sat with the hand pronated to collect responses at rest at 1T and 3T and additionally at 1.5T in one subject. One subject was collected at 2.5T rather than 3T since they reported nociceptive stimulus at 3T. For one subject, increments of 0.5T up to 3T were collected at rest in order to observe changes in response with increasing stimulus intensity. Wrist guards were then worn for the rest of the experiment. Stimuli were delivered either during cycling at the 3, 6, or 12 o'clock position, or during a 10 s isometric contraction in the 6 o'clock position where biceps brachii RMS EMG was matched to respective phase during cycling. During the isometric task, participants had 2 s to match the intensity, then stimuli were delivered at 1 s intervals for 10 s. For each phase of cycling and for intensity matched contractions at 6 o'clock, 100 stimulations were recorded.

2.3.2.2 Data Analysis

DC offset was removed, and EMG traces were rectified. Averages of responses to 100 stimulations were then taken. Averages were visually inspected for presence of a reflex within a 0-40, 40-100, and 100-200 ms time window which represented short, medium and long latency responses. Reflexes were defined as a deviation from the background EMG of the same muscle without stimulation (at the same phase during cycling).

2.4 Using Intermuscular Coherence to Identify Common Input to Muscles Activated During Shoulder Abduction and Adduction

Data for these experiments were collected at the University of Leeds, United Kingdom.

2.4.1 Data Collection

i. Participants

Experiments were performed under approval granted by the local ethical committee (University of Leeds BIOSCI 15-029). Twenty-one subjects were recruited to the study (12 male, 9 female, 2 left-handed), aged between 23 and 28 (mean ± SD, 25 ± 1.45). Inclusion criteria were healthy male or female individuals in between the ages of 18-30. Exclusion criteria were: 1) any active associated medical disorder 2) use of prescription medication or over the counter preparations that may alter results 3) a recent illness or viral infection (within the last two weeks) 4) use of recreational or performance enhancing drugs 5) ingestion of alcohol in the previous 24 hours 6) history of anaemia, asthma, diabetes, epilepsy, family history of sudden death, fainting, heart disease, high blood pressure, respiratory disease, muscle or joint injury 7) unable to provide informed consent or understand English 8) current pregnancy 9) recent intense exercise <48 hrs pre testing 10) any known neurological disorder 11) any musculoskeletal injury to the shoulder.

ii. Muscles

PM – pectoralis major, AD – anterior deltoid, MD – middle deltoid, PD – posterior deltoid, UT – upper trapezius, SA – serratus anterior, TM – teres major, LD – latissimus dorsi, IS – infraspinatus, BB – biceps brachii, LT – lateral triceps brachii, MT – medial triceps brachii, FR – flexor carpi radialis, ER – extensor carpi radialis, CD – contralateral middle deltoid.

iii. Electromyography

EMGs were captured at 1926 Hz (digitally up sampled to 2000 Hz) through Spike 2 [Cambridge Electronic Design (CED), Cambridge, United Kingdom] with a Delsys Trigno™ system, which filtered 20-450 Hz. Where available, EMGs were positioned with reference to SENIAM guidelines (Stegeman and Hermens, 2007). Muscles not covered by SENIAM were positioned with reference to other sources (Delagi et al., 2011; Kendall et al., 2013). Throughout this experiment, the contralateral middle deltoid acted as a negative control for different analysis types since it should not have been activated or share common drive with any other muscle.

iv. Protocol

Recordings were made on the participant's dominant side across 2 sessions which were at least 2 days apart. Participants were seated in an upright position in a Biodex Multi-joint System 3 Pro experimental chair (Biodex Medical Systems, Shirley, NY). The glenohumeral joint was used as reference to align to the centre of rotation for the dynamometer (***figure 2.4***). For each task, participants performed five contractions which were 5 s in length from the onset to the offset. Participants were asked to carry out three tasks: an isometric Maximum Voluntary Contraction in the direction of either shoulder abduction (ABD) or adduction (ADD), or a maximum voluntary effort (MVE). Each task was performed at 3 setting positions covering the normal range of motion (ROM) for horizontal shoulder abduction: close to the flank (30°) mid-range (75°), and arm above shoulder (120°). Prior to the onset of the trial, subjects sat with their arm rested in their lap. 30s before the task, the arm was positioned sideways away from the flank at the appropriate angle with the elbow fully extended. A prop was placed under the upper arm to support the

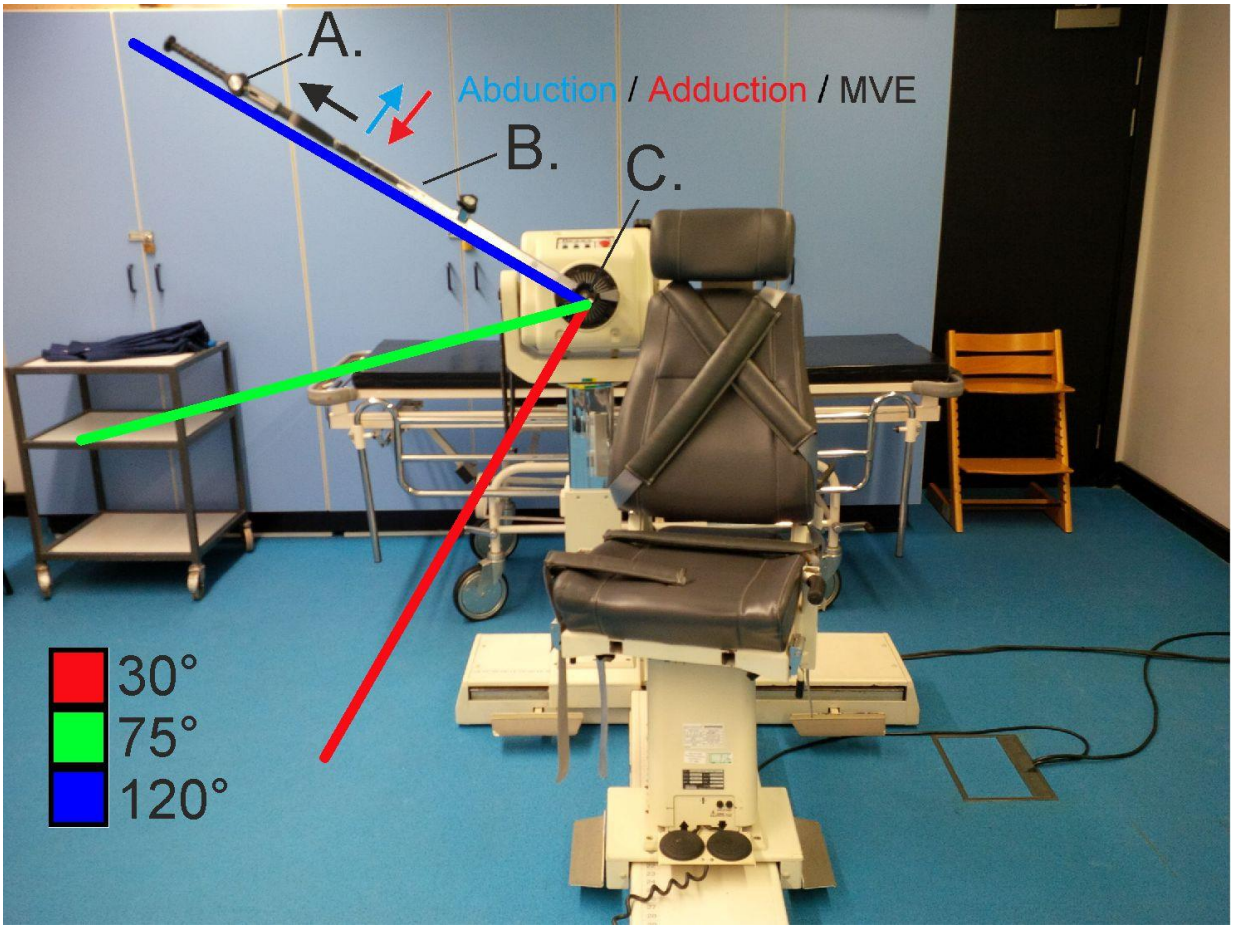

Figure 2.4. The Biodex System 3 Dynamometer. **A.** The handle which subjects grasped during the abduction (ABD) and adduction (ADD) MVC tasks. Coloured arrows indicate the direction of force that subjects applied to the handle during MVC tasks. The black arrow indicates that during the MVE task, the subject placed their hand over the handle and the weight of the limb was supported, but they did not apply a force to the handle. Coloured lines represent what the shoulder angle was during the task. **B.** the attachment for isometric shoulder abduction/adduction. **C.** The dynamometer shaft to which the attachment connects. This point served as the centre of rotation, and was aligned with the subject's glenohumeral joint.

weight of the limb at 75° and 120°. The hand was pronated at all times and kept level at all angles to avoid internal/external rotation of the shoulder joint. Instructions to "contract" and "relax" were given through a computerised voice with no verbal encouragement from the instructor. They remained fixed in position until 30 seconds following the task at which point they returned to the rest position. In total, recordings were made under 9 conditions (3 tasks at each of 3 angles). The order of collection was block randomised so that 5 conditions were collected in one session and 4 in another, and all trials for a given task collected consecutively. Five trials lasting 5s were collected, and subjects were given 3 min between trials to avoid muscle fatigue. Where EMG

amplitude was inconsistent between trials, subjects attempted up to 7 trials for each condition and the closest 5 trials were used for analysis.

v. Tasks

Maximum Voluntary Contraction (MVC) tasks

Subjects grasped the handle and produced MVCs of MD during ABD (a major shoulder abductor) or PM during ADD (a major shoulder adductor) by pushing up or down with their hand. Participants were shown RMS EMG traces of MD and PM. For the ABD task, participants were asked to produce the highest activation in MD whilst keeping PM minimal. For the ADD task, participants were asked to produce maximal PM amplitude whilst keeping MD minimal.

Maximum Voluntary Effort (MVE) task

During the maximum voluntary effort task, subjects' hands were rested across the handle but they were instructed not to grasp it. Participants produced the strongest possible voluntary contraction in MD based on the RMS amplitude, without movement of the joint or application of external force.

2.4.2 Data Analysis

See ***appendix 2*** for information about associated scripts.

i. Onset/Offset Marking and amplitude analysis

A series of Spike 2 scripts[4] were custom written to mark onsets and offsets on data files based on studies of gait analysis in the cat literature (***figure 2.5***). Several different measurements could be obtained using these scripts but its primary use was to mark burst onsets and offsets which allowed for coherence and cross-correlation analysis to be automated. EMG DC offset was removed (50 ms time window), were rectified, and then smoothed (20 ms time constant). Smoothing was minimal since we wanted to be sure to include short

[4] These scripts are available, with permission, from the University of Leeds Data Repository at: https://doi.org/10.5518/592 (Richards et al., 2018).

A.

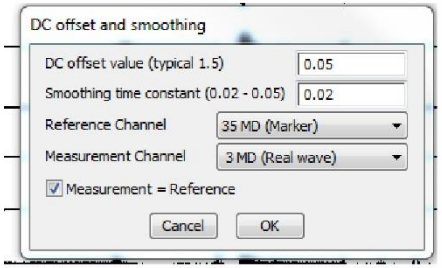
DC offset and smoothing
DC offset value (typical 1.5)
0.05
Smoothing time constant (0.02 - 0.05)
0.02
Reference Channel
35 MD (Marker)
Measurement Channel
3 MD (Real wave)
Measurement = Reference
Cancel
OK

B.

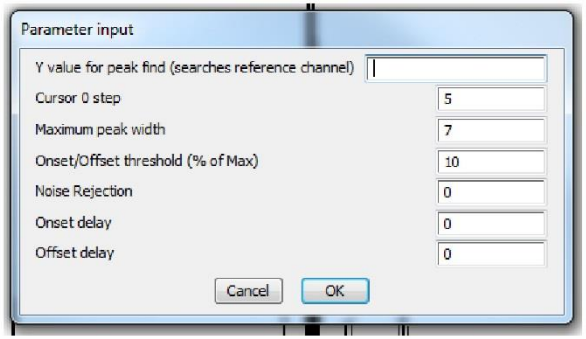
Parameter input
Y value for peak find (searches reference channel)
Cursor 0 step
5
Maximum peak width
7
Onset/Offset threshold (% of Max)
10
Noise Rejection
0
Onset delay
0
Offset delay
0
Cancel
OK

C.

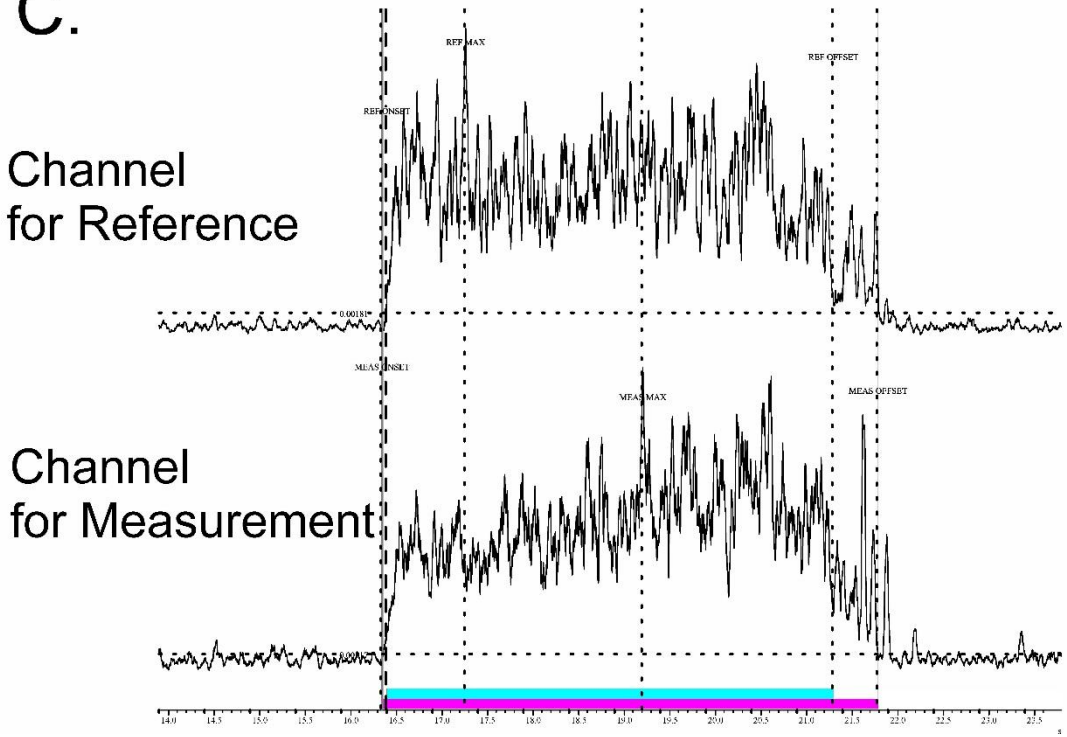
Channel
for Reference
Channel
for Measurement
REF MAX
REF OFFSET
REF ONSET
MEAS ONSET
MEAS MAX
MEAS OFFSET

D.

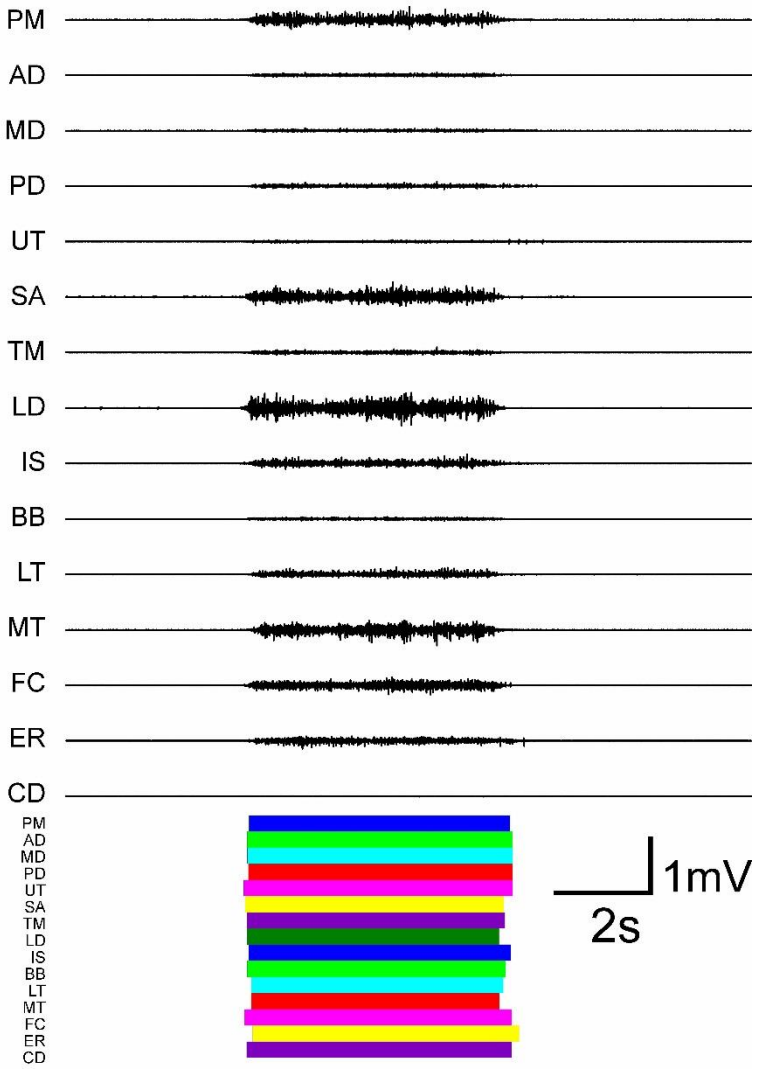
PM
AD
MD
PD
UT
SA
TM
LD
IS
BB
LT
MT
FC
ER
CD
1mV
2s

Figure 2.5. Screenshots showing Spike 2 user interface during demarcation of burst onsets and offsets. **A.** Dialogue box with options to apply DC offset, smoothing and to select channel. **B.** Dialogue box to determine parameters for the onset/offset percentage and delay. **C.** Example of the interface showing how bursts were identified. Coloured strips at bottom of panel represent burst profiles for respective muscles. **D.** Screenshot of raw EMG data (top) and after respective burst profiles have been demarcated (coloured strips, bottom).

latency events which contributed to the EMG at the start and end of the burst. Similar to the cat literature, to standardise as much as possible the onset of the EMG burst, the onset and offset were identified automatically as the point where EMG amplitude increased or decreased by a critical level (Duysens, 1977). We used 10% of the maximum rectified and smoothed EMG amplitude for that burst. This was then confirmed by the user and corrected if necessary. Overall around 1575 individual bursts were processed manually (5 trials x 15 muscles x 21 participants) to give a burst profile similar to those used in locomotion studies in cats (Drew and Rossignol, 1987). Group mean of mean RMS amplitude was calculated from the regions between cursors for each task at each angle for each muscle across subjects. Individual means from each muscle during each task at each angle were compared across angles using one-way ANOVA and Tukey HSD post-hoc test (n = 21).

ii. Coherence analysis

A script library[5] was generated which allowed data to be transferred between Matlab® and Spike 2 v8.13 [Cambridge Electronic Design (CED), Cambridge, United Kingdom] and to allow for batch processing for different analyses. We were mostly interested in correlating activity between muscles based on the pre-determined onset and offset times using coherence analysis and cross-correlation analysis. 30 s at the start of the data file whilst the subject was at rest was removed because there was significant baseline drift in this period. The mean of the signal was subtracted from the rest of the trace to remove the DC offset. A 4th order Butterworth filter was then applied following DC removal at 10-500 Hz (EMGs were filtered on collection at 20 ± 5 – 450 ± 50 Hz with no option to adjust them). Interference which was present in the EMG at a 75 Hz, and harmonics of this were removed using a spectrum estimation method. A custom-written script was run on each data file for each task for each subject. This totalled around 189 runs (21 subjects x 9 conditions). Using one muscle as a reference, this script calculated power spectrum, coherence,

[5] These scripts, or information on where to obtain them, are available with permission from the University of Leeds Data Repository at: https://doi.org/10.5518/592 (Richards et al., 2018).

and phase between the reference and every other muscle, before moving to the next channel to be used as a reference. The sections of data that were included were between the onsets and offsets of muscle activity for the reference muscle for each of the 5 trials. Onset and offset had been marked previously as 10% of peak RMS for that burst. Coherence and power spectrum were calculated using Bartlett's method, where FFT windows are overlapped by 50%. For each channel, the results files were automatically named based on the subject and reference channel for further analysis. Frequency coherence analysis allows comparison of the similarity of frequency content between two signals within a given time window. Frequency coherence (FFT size 1024) was calculated between all muscle pairs from the raw unrectified EMG (see section 2.2.5 for discussion) using the equation:

$$C(f) = \frac{|\Sigma csd_{xy}(f)|^2}{\Sigma psd_x(f)\ \Sigma psd_y(f)}$$

Equation 4.

where C is coherence, f is a given frequency, csd is the cross spectral density, psd is the power spectral density, and x and y each represent one of the two waveforms. Frequency is plotted on the X-axis and coherence is plotted on the Y-axis between 0 and 1 where 1 represents complete coherence between the two samples. Once the results files had been generated, batch-processing scripts were used to extract group data.

Group Mean Peak Coherence in Band

For each condition, a batch processing script was used to calculate group mean coherence based on the peak measurement within a band. This is one method to assess the magnitude of coherence though others can also be useful (Ushiyama et al., 2010). Bands were 20-35 Hz, 35-60 Hz and 60-100 Hz, which had been determined to be useful previously (see Chapter 3).

Number of Subjects over Confidence Interval

A separate batch processing script was used to calculate the number of subjects which were over the confidence interval across the sample within

(***figure 2.6A***). The confidence interval was defined using the equation (Rosenberg et al., 1989):

$$CL = 1 - \alpha^{\frac{1}{L-1}}$$

Equation 5.

where CL is the confidence level, L is the total number of segments used to calculate the coherence and α = 0.05 (above 95% confidence interval). L is dependent on the number FFT segments which are included in the analysis. For a single subject, there are 5 trials lasting 5 s for each condition. One FFT window at a sampling frequency of 2000 Hz requires 512 s of data. The data were analysed using Bartlett's method, whereby FFT windows were overlapped by 50%. This means that for each subject there are around 100 windows included (depending on the onset and offset times). Since there was a 50% overlap, this number is divided by 2 to give L (Welch, 1967).

iii. Cross-correlation analysis

Using a similar batch processing script[6] as described for the previous section, cross-correlations were calculated using each muscle as a reference against all others from sections of data previously defined by onset and offset of muscle bursts. This analysis was based around the in-built waveform correlation function in Spike2. This allowed examination of the similarity of the amplitude changes between the two EMGs relative to time. Correlation, plotted on the Y-axis is given within the range of 1 to -1, where 1 is a perfect correlation, -1 is an inverse correlation, and 0 indicates no correlation. Phase is on the X-axis, where 0 is in the centre of the plot representing no phase, while deviations from 0 represent either a positive or negative shift.

[6] These scripts are available, with permission, from the University of Leeds Data Repository at: https://doi.org/10.5518/592 (Richards et al., 2018).

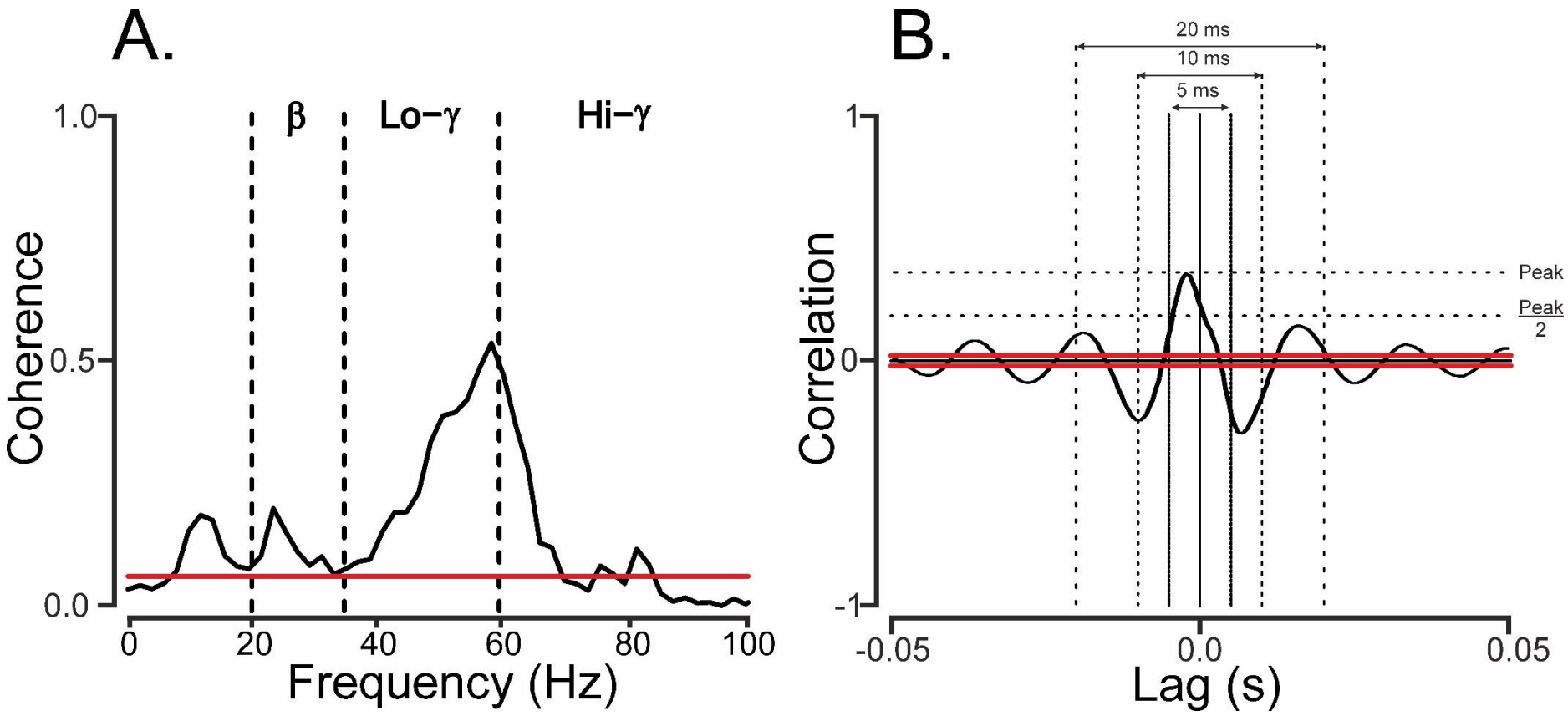

Figure 2.6. Example of the confidence intervals used for analysis. Figures show coherence (FFT size 1024, bin size 1.95 Hz, **A.**) or correlations (**B.**) between MD and LT at 30° during ABD from a representative subject. **A.** Vertical dashed lines indicate the different bands used for analysis (20-35, 35-60, 60-100 Hz). The beta band is measured at 20-35 instead of 15-35 Hz since the EMGs were filtered 20-450 Hz at time of collection. Red line indicates the 95% confidence interval. **B.** Representative cross-correlation plot. Solid vertical line at the centre indicates 0 lag. From the centre (0) out, subsequent vertical lines represent the 5, 10, and 20 ms time window. Horizontal Dashed lines indicate the peak cross correlation index and half of this. Horizontal red lines indicate the 95% confidence interval.

Group Mean Absolute Peak Correlation in Band

For each condition, a batch processing script was used to calculate group mean correlation index based on the absolute peak measurement. This was based on a 250 ms window either side of 0.

Half-width measurements and count of Number of Subjects over Confidence Interval

A separate batch processing script was used to calculate the number of subjects where the peak was over the confidence interval across the sample. We were also interested to know the correlation half-width since it can be used to identify polysynaptic inputs (Vaughan and Kirkwood, 1997). First, the peak was assessed. If it was over the confidence interval, the subject was counted into either a <5 ms, <10 ms, or <20 ms bin according to the half-width. The confidence interval was defined using the following equation based on the Matlab® help files and Halliday et al. (Halliday et al., 1996; Matlab®, 2018):

$$CL = 0 \pm \frac{2}{\sqrt{L}}$$

Equation 6.

where CL is the confidence level and L is the total number of data points included divided by the number of sections taken to give α = 0.05 (above 95% confidence interval, ***figure 2.6B***). Each 5 s includes around 10,000 data points when sampled at 2000 Hz. Since there were five 5 s trials for an individual subject, in this case this L was defined as (50,000 data points/5 trials per condition). The numerator 2 is the error function of an autocorrelation to give the 95 percentile point of the normal distribution. Matlab® help files and Halliday et al. give an error function as 1.96 which gives the 97.5 percentile point. In the present experiment, we corrected this to 2 since we used 95% confidence interval.

iv. Cluster Analysis

A cluster analysis[7] was performed on the group mean coherence values in order to identify networks of muscles which were activated depending on 1) different tasks and 2) different frequency bands. The data subjected to this analysis were from all tasks at 75°. This angle is mid-range of motion, and is therefore subject to less posture-dependent bias in the muscle activation patterns than at 30° or 120°. This analysis was similar to the analysis used by the Boonstra group to identify muscle networks (Boonstra et al., 2015; Kerkman et al., 2018). In short, muscles of networks are identified based on chosen factors (in this case task and frequency band) using a non-negative matrix factorisation (NMF) algorithm.

Thresholds are first applied to the mean coherence values in the form of 1) a proportional threshold, and 2) an absolute threshold. The proportional threshold defines what proportion of the muscles are included in the network. If the chosen threshold is too high, resultant networks will include too many muscles to distinguish between clusters; if it is too low, too few muscles are included to identify networks. We determined that a proportion of 0.1 gives networks which include enough muscles to discriminate between factors, but not so few that networks represent interactions between individual muscle pairs. The absolute threshold sets all coherence values below this to 0 and excludes them from the analysis. We used 0.06 based on the confidence interval for the amount of data included for a single subject. Next, the operator defines the number of clusters to be produced for the output. This was defined by using the residual from the NMF, which represents the approximation error accounted for during the clustering analysis. This was selected by running the analysis with different numbers of clusters and then plotting the number of clusters against the residual (***figure 2.7***). The number of clusters used for

[7] These scripts, or information on where to obtain them, are available with permission from the University of Leeds Data Repository at: https://doi.org/10.5518/592 (Richards et al., 2018).

analysis was the number beyond which no further decreases were seen in the residual, which was 5.

The mean values are then subjected to an NMF analysis (with 10,000 iterations) whereby muscle networks are identified based on a clustering coefficient which depends on how coherence values between muscle pairs are altered by the different factors. This analysis yields clusters represented by two outputs: a dependency matrix, which identifies which dependent variables (task, frequency band) produce the network, and an adjacency matrix, which identifies the muscles involved in the network. This adjacency matrix is then translated into a diagrammatic representation of the network where clusters are illustrated based on the connectivity between muscle pairs.

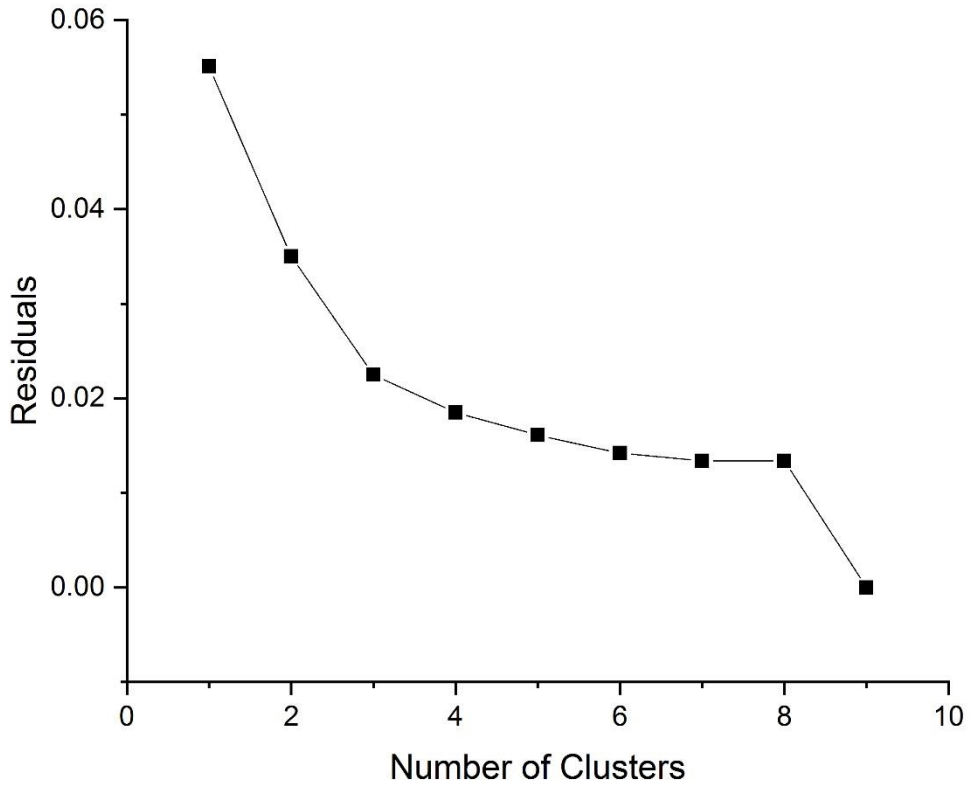

Figure 2.7. Number of clusters plotted against residual error. The residual error of NMF was calculated using different numbers of clusters in order to determine the optimum number of clusters to describe the dataset. Five clusters were used since this is where the error shows little decrease when the number of clusters is increased. Error drops to 0 with 9 clusters since this is where each cluster will result from a single factor, of which there were 9 (3 tasks x 3 frequency bands).

In this diagram, the line thickness reflects the coupling strength of each muscle pair.

Chapter 3: Frequency analysis of TMS/TMES response reveals task-dependent shift in central drive to Biceps Brachii

3.1 Abstract

Both Transcranial Magnetic Stimulation (TMS) and corticomuscular/intermuscular coherence (CMC/IMC) have been proposed as metrics able to gauge corticospinal connectivity following injury such as stroke. Pyramidal neurones of the primary motor cortex (M1 motoneurones) contact spinal motoneurones directly. However, collaterals from these M1 motoneurones also make indirect contact with spinal motoneurones through pathways such as the reticulospinal tract and spinal pathways. The outcome measures of TMS and CMC examinations are therefore unlikely to be completely corticospinal in origin. The contribution of a given pathway to motoneurone activity will vary depending on the motor task. For example, during a repetitive task such as arm cycling, reflexes are modulated depending on the phase of the cycle, and the movement is maintained by spinal or subcortical central pattern generator networks. However, a task such as an isometric contraction, where the muscle does not change length, is thought to be predominantly corticospinal in origin. To be able to effectively assess corticospinal excitability following insults such as stroke, it is important that we are able to identify these differences from non-invasive EMG recordings during natural behaviour.

CMC and IMC studies show coherence in three bands: alpha (α) at 8-12 Hz, beta (β) at 15-35 Hz, and gamma (γ) at 35-100 Hz. During sustained isometric contractions, corticomuscular coherence is reported to be in the β-band, but during dynamic movements it is often reported outside of this band. The presence of coherent frequencies outside of this band probably result from

task-dependent activation of different pathways. We can gain some insight into the activity of these pathways by stimulating these pathways differentially. The evoked response to TMS depends on the excitability of cortical and subcortical areas as well as spinal motoneurone pools. The corticospinal axons can be stimulated electrically using Trans-Mastoid Electrical Stimulation (TMES) thus directly reveals the excitability of the spinal motoneurone pool. It has recently been demonstrated that TMS responses, but not TMES responses are increased in a cycling task compared to an intensity-matched tonic contraction (Forman et al., 2014). With this dataset, we use the task specific (isometric/cycling), and stimulation specific (TMS/TMES) conditions to identify a causal relationship between specific pathways and candidate frequency bands. Our data suggest that the corticospinal pathway contributes primarily to 15-35 Hz EMG activity range but also probably contributes to frequencies up to 60 Hz. Subcortical pathways, probably reticular, contribute to the 35-100 Hz range, and activity between 60-100 Hz may result from activation of spinal CPG pathways.

3.2 Introduction

3.2.1 The clinical and research needs for a means to identify neural drive in humans

In cases such as stroke or spinal cord injury, currently used predictors of recovery are variable (Prabhakaran et al., 2007). Current practice focuses on connectivity of the direct corticospinal pathway from M1 motor cortex to spinal cord motoneurones. Whilst in primates this direct pathway is believed to be most important for fine motor control, there are many indirect pathways which also terminate on the spinal motoneurone, including the reticulospinal pathway (Kuypers, 1981). After injury to the CST, the primates reticulospinal pathway compensates for some functions, like distal hand movements, which are normally under corticospinal (Baker, 2011). The ability to test animal research clinically is restricted by the necessity for non-invasive study in humans. A method to quantify synaptic connectivity in alternative pathways capable of facilitating recovery would therefore be a valuable investigative and diagnostic tool.

Spinal motoneurones provide the ‘final common pathway’ to the muscle, and receive neural contacts from a wide range of sources of cortical, subcortical, spinal and peripheral origins. The corticospinal tract, which originates primarily in the upper motoneurones of M1, makes direct synaptic contact with spinal motoneurones, is considered the most important descending input for fine motor control. In the human upper limb, for example, motor pools for distal muscles involved in fine hand movements receive many corticospinal inputs while motor pools for more proximal muscles rely more heavily on a reticulospinal or corticoreticulospinal (corticobulbospinal) input (Dewald et al., 1995; Lemon, 2008). Maintenance of steady activity during isometric contractions is believed to originate from the motor cortex (Fetz and Finocchio, 1975; Gross et al., 2000). The reticulospinal tract is also found to be involved in muscle recruitment when high muscle force is necessary (Tazoe and Perez, 2017). Neuronal networks localised in the spinal cord, known as central pattern generators (CPG), can autonomously generate patterns of activity which maintain repetitive rhythmic movement across all species from fish and amphibians to primates (Grillner, 1981; McCrea and Rybak, 2008). In humans, evidence for the lower limb CPG is now well documented, and its existence is widely accepted (Dietz and Harkema, 2004; Zehr and Duysens, 2004). When the CPG is active, it can prevent incoming signals from the periphery from interfering with rhythmic activity (Perreault et al., 1999). However, Drew has shown that stimulation of descending tracts can powerfully influence EMGs of forelimb muscles during locomotion (Armstrong and Drew, 1985). Less work has gone into exploring the CPG of the human upper limb. Yamaguchi has showed evidence for forelimb CPG in the cat by showing the phase dependence of motoneuronal responses to stimulation of the lateral funiculus during locomotion (Yamaguchi, 2004). Zehr has provided the strongest evidence for the existence of a human upper limb CPG by showing presynaptic modulation of reflex pathways during arm cycling (Zehr et al., 2004).

3.2.2 Caveats and limitations of existing methods

EMG-EMG coherence analysis (intra- or intermuscular, IMC) (Farmer et al., 1993), and EEG (electroencephalography)/MEG (magnetoencephalography)-

EMG (corticomuscular, CMC) (Conway et al., 1995) coherence analysis are interesting tools for clinical assessment (Grosse et al., 2002), and for research (Kilner et al., 2000). CMC is suggested to reflect a neuro-muscular binding mechanism whereby oscillations in the sensorimotor cortex integrate afferent inflow (Kasuga et al., 2017), and are transmitted to the spinal motor pool in order to produce the appropriate muscular output. IMC indicates common drive to a muscle pair (Farmer et al., 1993; Salenius et al., 1997). During sustained low-level contractions, beta band (~15-30 Hz) corticomuscular coherence is thought to reflect transmission through the corticospinal pathway (Farmer et al., 1993; Salenius et al., 1997). Coherence in the alpha (8-12 Hz) (Budini et al., 2014; Mehrkanoon et al., 2014) and gamma (35-100 Hz) (Omlor et al., 2007; Patino et al., 2008) band has also been reported, and are most often reported to occur during dynamic movements and high force contractions respectively. Functionally, patterns of coherence have been studied over several parameters; force (Kristeva et al., 2007; Chakarov et al., 2009), finger dynamics (Riddle and Baker, 2006), and muscle selection (de Vries et al., 2016; Reyes et al., 2017).

Most coherence studies assume stationarity of the data. This effectively ignores the continuity of the activities during the event on the assumption that all frequencies are of equal variability within the selected window of data, which is inapplicable to physiological situation. Coherence also uses the Fourier transform function for these comparisons, which furthers the temporal issues, as this mathematical function has no time resolution. Similarly, commonly used waveform pre-processing steps such as rectification (Ward et al., 2013; McClelland et al., 2014) and filtering suppress the amplitude of higher frequencies, making investigations into frequencies above 60 Hz rare. Historically, analysis of signal amplitude was common, where the process of rectification can be useful. However, for more recently developed frequency domain analysis, the non-linear process of rectification irreversibly distorts the signal forcing power to the low end of the frequency spectrum. Despite these effects, this practice has continued to be used. It is possible that this may be obscuring valuable information about neural drive to spinal motoneurones.

For a meaningful correlation between EEG and EMG, the cortical activity recorded through the EEG must be transmitted linearly to the muscle. Although, M1 pyramidal neurones exhibit direct correlation with the endpoint (Georgopoulos and Stefanis, 2007), the signal transfer from cortex to the spinal circuits is not linearly correlated possibly owing to the existence of both direct and indirect pathways to the spinal motoneurone from M1, commonly via cortical, subcortical, and spinal relays (Isa et al., 2007). In sEMG recordings from the muscle, owing to morphological limitations, the input from these pathways to the muscle cannot be recorded through the skin surface, and therefore cannot be accounted for in coherence analysis. As far as we know it is unknown whether stimulation of specific pathways produce muscle output that relates to the frequency bands identified in coherence studies.

3.2.3 Wavelet Synchro-Squeezed Transform (WSST) as a high resolution time-frequency analysis to identify transient of physiological events

Owing to the fact that the FFT methods of coherence analysis have no time resolution, we cannot use them to identify transient shifts in the frequency content of an EMG signal. This is significant because local loops have short latencies and may have transient effects on the EMG. For example, responses in the biceps brachii to stimulation of low threshold fibres in median nerve in the cubital fossa have a latency of around 14 ms (Miller et al., 1995), and biceps brachii responses to TMS are around 12 ms (Taylor, 2006). The standard FFT window size used for coherence analysis is usually lower than 2048 samples, which corresponds to 819.2 ms when sampled at 2500 Hz. This window size is then too large for detecting changes in EMG activity which occur during such a short time window. One way around this is to apply a wavelet transform. Neto et al. (2010) have used wavelet coherence of EMGs to identify common drive to hand muscles with improved time-frequency localization (Neto et al., 2010). The wavelet transform can achieve this by breaking down the signal into finite-time ‘wavelets’ instead of infinite sinusoidal harmonics. The wavelet represents a set of functions with the form of small waves created by dilations and translations from a simple generator function, which is called the mother wavelet. The Matlab® wsst() function, which applies

a Wavelet Synchro-Squeezed Transform, can achieve maximal resolution in both the time and frequency domain (see Chapter 2 for more details). This allows us to examine transient changes in the frequency content of EMG signals, for example in response to stimulation or due to activation of local pathways.

3.2.4 Corticospinal Excitability of the Biceps Brachii is higher during Arm Cycling than an Intensity-Matched Tonic Contraction (Forman 2014)

Data used for the current study was sourced from the laboratory of Kevin Power, where differences in cortical and spinal motoneurone excitability are addressed by delivering stimulation to descending pathways whilst human participants are engaged in behavioural tasks. Stimulation is delivered using transcranial magnetic stimulation (TMS) of the motor cortex, or trans-mastoid electrical stimulation (TMES) to electrically stimulate the pyramidal tract at the level of the cervicomedullary junction (***figure 2.1***). The motor evoked potentials (MEPs) and cervicomedullary evoked potentials (CMEPs) from these technique are useful because they correspond to slightly different neural activation (***figure 3.1D***). The amplitude of the response to motor cortical stimulation depends on the excitability of cortical neurones as well as everything caudal to this. The response is primarily due to action potentials in cortical motoneurones travelling contralaterally through the pyramidal tract to the target muscle. Cervicomedullary evoked potentials also travel through the pyramidal pathway. However, since the stimulation point is below the level of the hindbrain, the size of the evoked response is more dependent on the excitability of spinal pathways than cortical pathways (Taylor, 2006). Contrasting response amplitude between these two techniques is a way to assess differences in spinal compared to cortical excitability.

The behavioural context in which these stimulation techniques are applied is also important. By using an arm cycling task, we are able to engage spinal CPG pathways. Regulation of descending (Armstrong and Drew, 1985) and sensory (Zehr et al., 2004) pathways occurs whilst the CPG is active. In

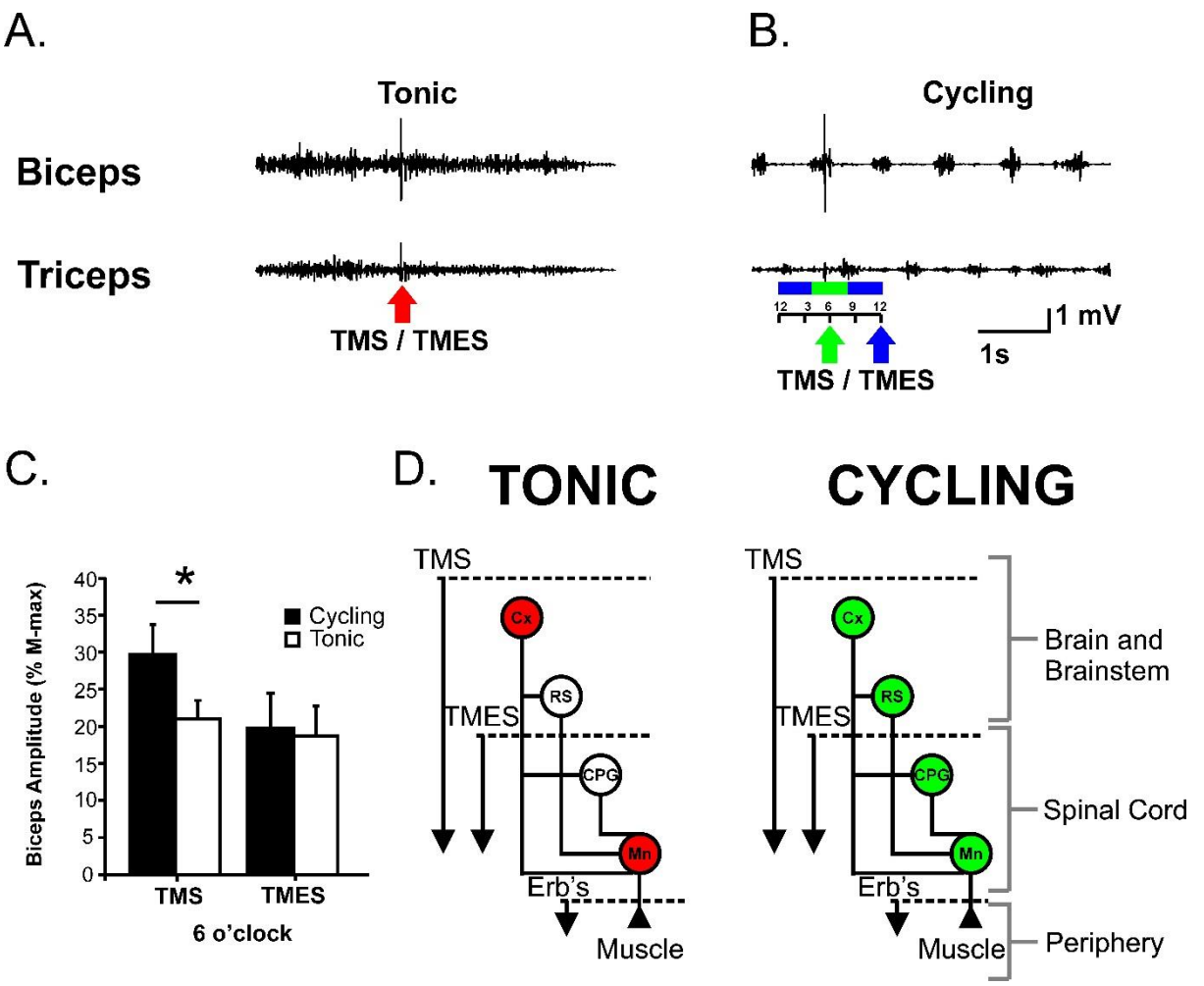

Figure 3.1. Data collection and findings from Forman et al. (2014). **A.** EMGs were recorded from biceps triceps brachii (sampled at 5 kHz). Subjects matched the amplitude during tonic contractions (**A.**) to either 12 or 6 o'clock during cycling (**B.**). **A.** is matched to 6 o'clock in **B.** Arrows indicate when stimulation was delivered. **C.** Forman et al. (2014) showed that responses in biceps brachii were larger during the flexion phase of cycling than in the tonic condition **with TMS but not TMES** ($p < 0.001$, $n = 10$). **D.** This effect was attributed to recruitment of additional pathways which were active during cycling. Cx = Cortex, RS = Reticulospinal tract, CPG = Central Pattern Generator, Mn = Spinal Motoneurone. Coloured circles indicate that the pathway was active during the task. Dashed horizontal lines show the level at which stimulation was delivered. **C.** was adapted from Forman et al. (2014).

humans, this can be observed by monitoring how responses to stimulation vary throughout the phase of a cycle (Zehr et al., 2004). The Power lab exploit this to reveal interesting differences between the excitability of cortical and spinal neurones (Forman et al., 2014). The crank positions of the arm cycle ergometer relative to a clock face are used to represent different phases of the cycling: 6 o'clock (mid-flexion, maximum biceps brachii activity) and 12 o'clock (mid-extension, minimum biceps brachii activity, ***figure 2.1***). These points can then be used to trigger recording and stimulation for the cycling task with a magnet on the crank handle. In their 2014 paper, the Power lab

applied stimulation at these positions during cycling (Forman et al., 2014). They also included another task in the experiment where isometric contractions were performed with the cranks in the equivalent positions, and the amplitude matched to the equivalent phase during cycling (***figure 3.1***). This is useful because it allows us to compare between a task where the CPG is active (cycling) and a task which is primarily driven by the motor cortex and brain (Fetz and Finocchio, 1975; Gross et al., 2000). Forman et al. (2014) showed that responses to TMS, but not TMES were increased during cycling compared to an amplitude matched isometric contraction at the 6 o'clock position (Forman et al. 2014, and ***figure 3.1C***). They concluded from this that increased cortical excitability during the cycling task recruits additional subcortical pathways which are not active during the isometric task which produce the higher response amplitude with TMS. We subjected data from this study to a WSST frequency analysis in order to identify pathway specific differences in the frequency content of the EMG.

3.2.5 Experimental rationale

Using data from Forman (2014), the current study uses *combinations* of tasks and stimulation to target the previously discussed pathways in an attempt to identify them using non-invasive sEMG (surface electromyography) measures. We apply a sensitive time-frequency analysis (wavelet synchro-squeezed transform) to look at short latency responses to stimulation of the motor cortex and pyramidal tract in biceps brachii in a task-specific context. TMS is a tool which is used for probing corticomotoneuronal excitability by observing motor evoked potentials (MEPs) in the muscle. Short latency responses (around 13.5 ms to the biceps brachii (Taylor, 2006)) to TMS are consistent with calculations using conduction velocity of the fast corticospinal pathway. However, polysynaptic responses via the pontomedullary reticular formation can contribute at similar latencies (Fisher et al., 2012). Due to the level of stimulation, by comparing TMS to TMES, we can infer contributions of subcortical but supraspinal centres on the muscle output.

The original paper (Forman et al., 2014) showed that biceps brachii responses to motor-cortical TMS, but **not** transcutaneous stimulation of the pyramidal

tract (***figure 3.1C***), are increased during arm cycling compared to a tonic contraction. This effect was attributed to higher excitability of cortical motoneurones having downstream effects on recruitment of spinal motoneurones (***figure 3.1D***). Since this effect can be seen in the amplitude of the response, we hypothesised that it may also be detected in the frequency domain, and that this could act as a marker of task-dependent drive to muscles. Our goals were: *i.* To characterise the previously described amplitude modulations within the frequency domain. *ii.* An exploratory study to use the pathway-specific tasks and stimulus evoked responses to identify candidate frequency bands associated with spinal and subcortical pathways across a broad frequency spectrum. *iii.* To determine whether distinct frequency bands in the muscle output were associated with corticospinal activity. Since it should reflect the time point for highest synchrony and recruitment within the spinal motor pool, we assessed the time of peak response to stimulation in order to isolate drive to motoneurones. We show for the first time that frequency analysis of response to stimulation may serve as a valuable clinical tool for assessing neural drive to muscle.

3.3 Hypothesis

We hypothesized that altered neural drive between the cycling and tonic task will reveal a different frequency distribution of the EMG when no stimulus is applied. Frequencies with high amplitude during the tonic task will reflect corticospinal inputs, and during the cycling task will be subcortical or spinal in origin. Stimulation with TMS will reveal cortical pathways and divergent systems which are contacted by it and active during the task. TMES will reveal the spinal contacts of the corticospinal tract. Based on coherence studies, we expect that the frequencies associated with corticospinal activity will be in the range of 15-60 Hz.

3.4 Methods

Methods are described in the General Methods Chapter.

3.5 Results

3.5.1 Time to peak Measurements

Time to peak was shorter by 2-4 ms with CMEPs than with MEPs. We compared biceps and triceps brachii in each condition. For both TMS and TMES, patterns between conditions were similar (***figure 3.2***). Except at the 12 o'clock position with TMS (*NS*), during the cycling task, the peak response time was shorter for the agonist (biceps brachii during flexion at 6 o'clock, triceps brachii during extension at 12 o'clock, $p < 0.01$, ***figure 3.2***). During the isometric task matched to 6 o'clock, the latency to peak was shorter in biceps brachii than triceps brachii with TMES ($p < 0.01$), though they were similar with TMS (*NS*, ***figure 3.2***). Matched to 12 o'clock, the latency to peak was shorter in triceps brachii than biceps brachii with TMS ($p < 0.01$), though there was no significant difference with TMES (*NS,* ***figure 3.2***).

3.5.2 Time-Frequency Analysis

At the time of collection, signals were filtered 10-1000 Hz. Differences at frequencies below 10 Hz will not be discussed for this reason. Comparisons will primarily be made between cycling and matched tonic positions in the biceps brachii, since amplitude matching of muscle activity and response amplitude was performed with this muscle. EMGs were transformed using a WSST (***figure 3.3B***). Wavelet coherence was also calculated between the biceps and triceps brachii (***figure 3.3C***). The Erb's point stimulation, which was used to obtain the Mmax (the maximal direct muscle response to electrical stimulation), was higher than all other conditions across the frequency spectrum due to the increased amplitude of the response (***figure 3.4*** and ***3.5***). Likewise, between control and stimulation, increases were seen across the frequency spectrum for both cycling and tonic tasks due to the increased amplitude of the response (***figure 3.5***). However, differences in the frequency distribution due to alterations at specific frequencies rather than a general increase in amplitude were apparent between tasks, and between TMS and TMES.

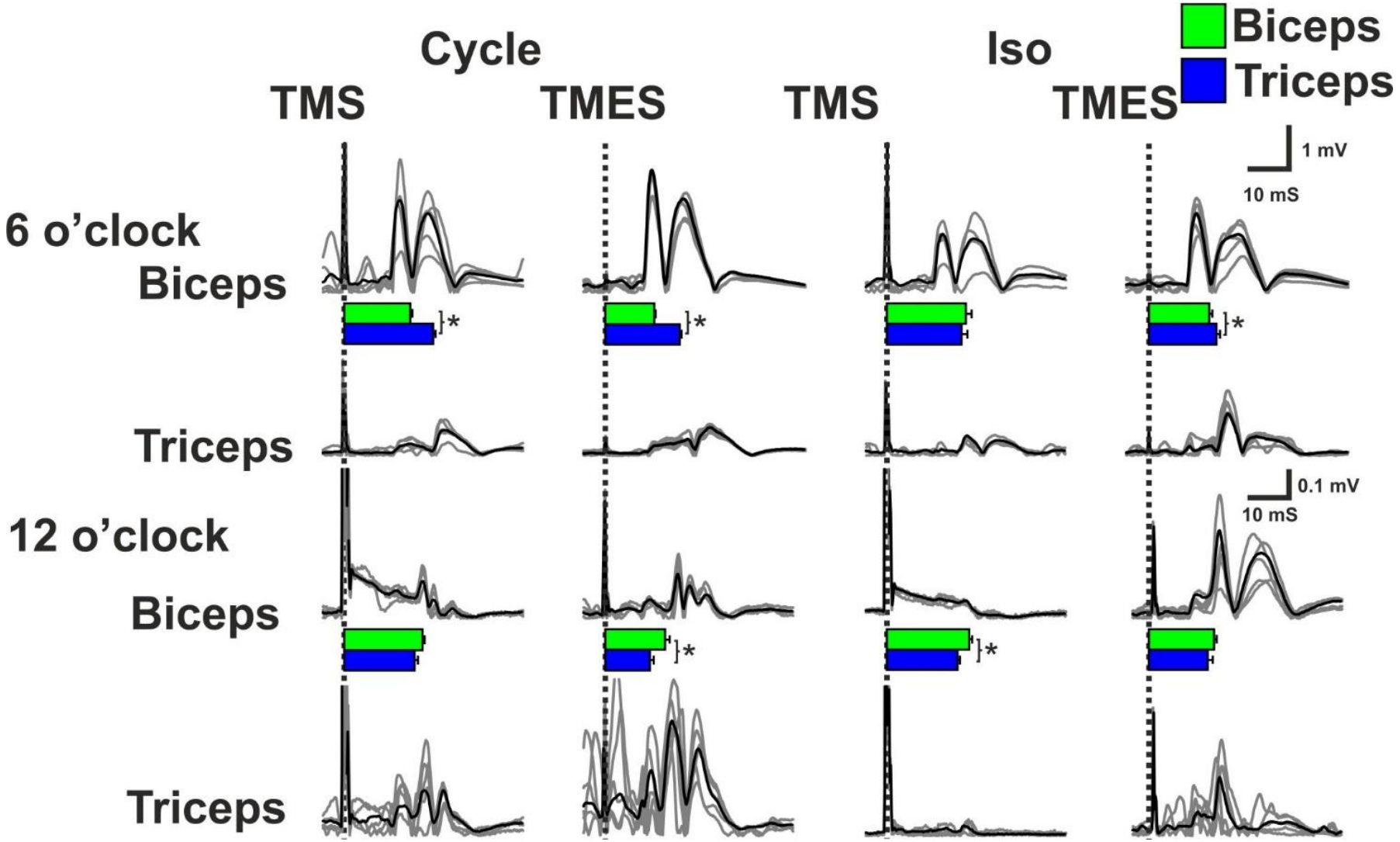
Cycle
Iso
Biceps
Triceps
TMS
TMES
TMS
TMES
1 mV
10 mS
6 o'clock
Biceps
}*
}*
}*
}*
Triceps
0.1 mV
10 mS
12 o'clock
Biceps
}*
}*
Triceps

Figure 3.2. Task-dependent change in corticospinal drive to arm muscles. Representative traces from one subject to show shifts in time to peak in response to stimulation. Traces show average (black) and individual (grey) rectified EMG from a representative subject. Bars show group mean of means. Individual means were compared between biceps and triceps across the group (two-factor ANOVA, Tukey's HSD post-hoc with Bonferroni correction, $p < 0.01$, $n = 10$). Vertical dashed line indicates stimulation time. Note separate scale bars for 6 o'clock and 12 o'clock.

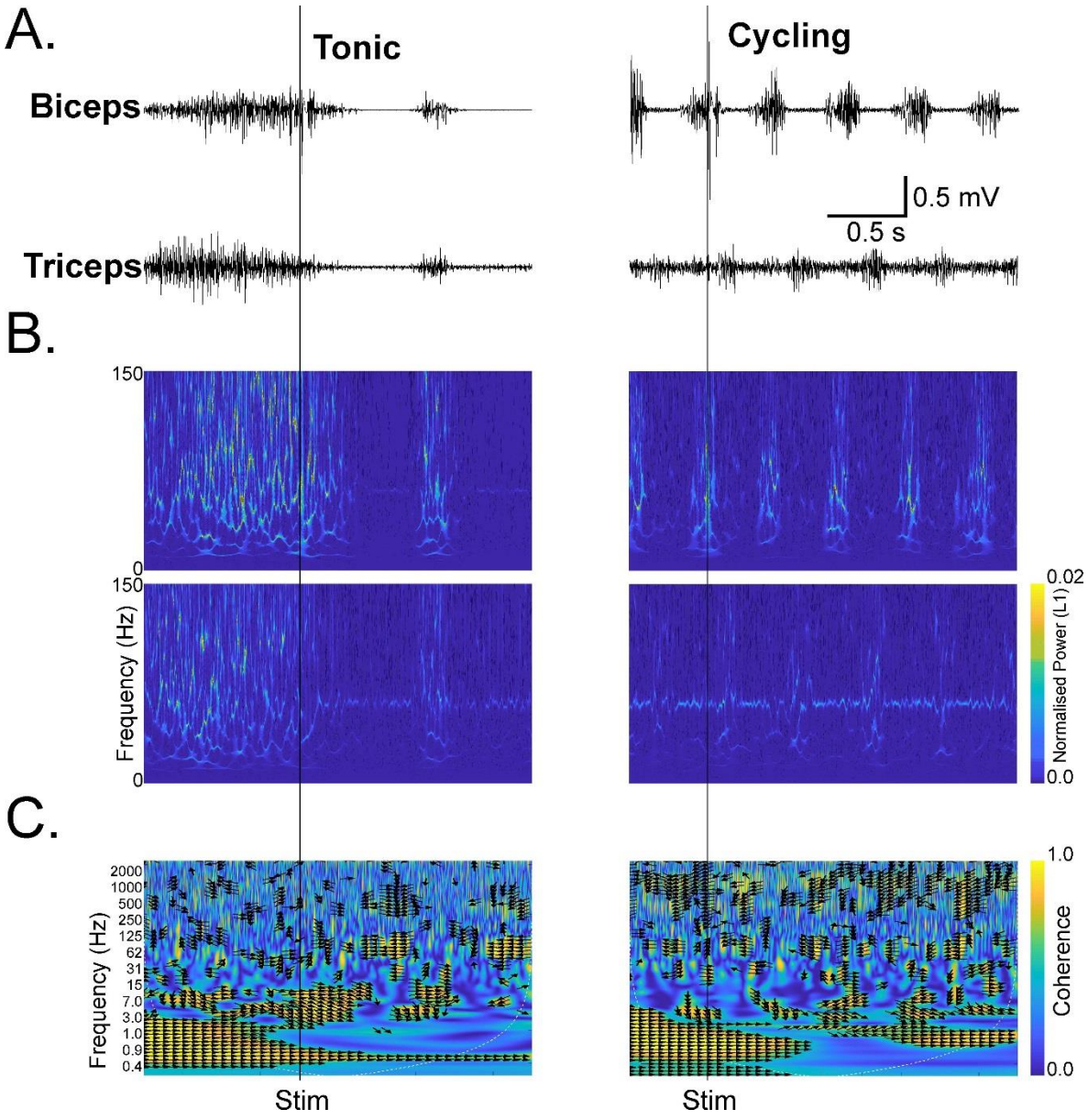

Figure 3.3. Raw EMG, and corresponding WSST and wavelet coherence Spectrograms for biceps and triceps brachii during the cycling and tonic tasks. **A.** Example raw EMG (sampled at 5 kHz) from biceps and triceps brachii during the tonic and cycling task. The cycling task shows several bursts. Vertical line shows stimulus time across all figures. All figures are on the same time scale. **B.** Corresponding WSST spectrograms generated using the Amor wavelet and 48 voices per octave. Top – biceps, bottom – triceps. **C.** Wavelet coherence spectrograms showing coherence between the biceps and triceps brachii EMG signals in **A.** Coherence was generated using the Amor wavelet and 32 voices per octave. Black arrows show phase direction. Note that the y-axis is displayed on a linear scale for the WSST spectrograms but on a log scale for the coherence spectrograms.

3.5.2.1 12 o'clock position

Since the 12 o'clock position during cycling is the point with least activity in the biceps brachii, when matching for tonic contractions EMG activity is minimal. At baseline (no stimulation), at the 12 o'clock position, there was no

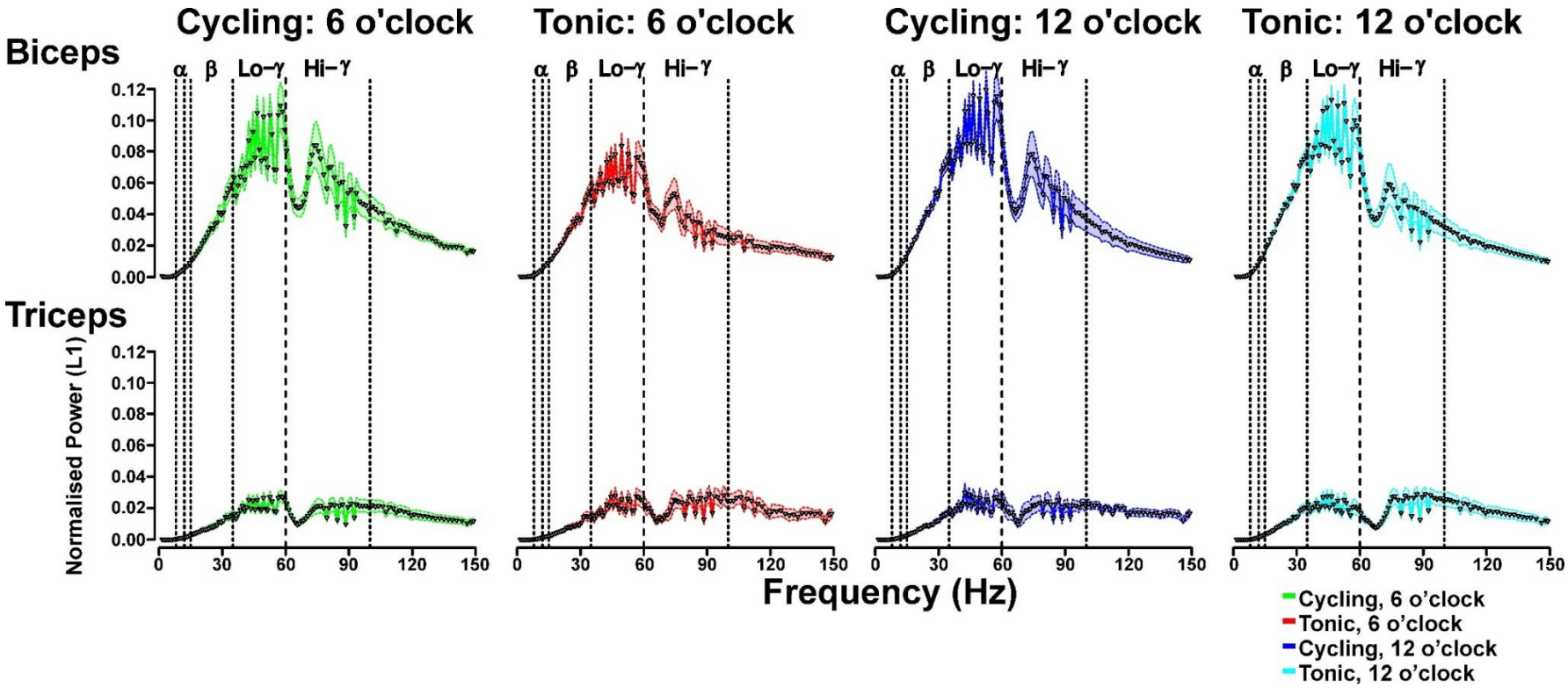

***Figure 3.4. Power spectral density measured from WSST at the time of response to Erb's point stimulation*.** Power spectral density was measured from the WSST at the time of the peak of the response to Erb's point stimulation for each condition. Data shows mean of mean ± SEM (5 per subject, *n* = 10). Power is binned into 1 Hz bands from 1-150 Hz. Each point is the mean of mean of all rows in the WSST that fell between one frequency band and the next. The frequency domain is logarithmic in the WSST, so whilst low frequencies include several rows, for higher frequencies there may have only been a single row over several frequencies. Therefore, at higher frequencies there is only a point for every other frequency. The dip around 60 Hz is probably due to a notch filter applied at the time of recording.

difference between tonic and cycling at any frequency between 1-150 Hz in biceps brachii. No differences were present between cycling and tonic conditions with TMS or TMES. In the triceps brachii, there was a general increase in cycling compared to tonic up to 100 Hz. This data was not included in some figures since the focus of the study is on the biceps brachii and the only significant results were in the triceps brachii.

3.5.2.2 6 o'clock position

In biceps brachii at baseline, beta band activity was similar between the cycling and tonic tasks, though two points were increased during cycling (***figure 3.5A***). The largest increase was in the high gamma band (> 60 Hz) during cycling compared to the tonic task. With TMS, responses were increased in both the low and high gamma range during cycling compared to tonic. Responses to TMES were increased during cycling compared to tonic within only the high gamma range, similar to the control condition. In triceps brachii, the tonic condition was increased compared to the cycling across the board, due to co-contraction with biceps brachii in this task compared to antagonist interactions during cycling. However, with both TMS and TMES, the tonic task was only increased above 60 Hz compared to cycling.

3.5.3 Wavelet Coherence Analysis

In the control condition, at 6 o'clock, there was increased coherence between the biceps and triceps brachii in the beta band during cycling compared to tonic (***figure 3.6***, $n = 10$, $p < 0.01$). At 12 o'clock, there were no significant differences in the beta, low, or high gamma band between cycling and tonic tasks. The coherence levels during the tonic task at 6 o'clock were notably similar to both cycling and tonic at 12 o'clock in all bands. They were also similar in the low and high gamma during cycling at 6 o'clock. With TMS at 6 o'clock, coherence levels were higher in the beta, low and high gamma bands during cycling compared to the tonic task (***figure 3.6***, $n = 10$, $p < 0.01$). With TMES, coherence was higher only in the beta band during cycling compared to tonic (***figure 3.6***, $n = 10$, $p < 0.01$). With TMES at 12 o'clock, coherence levels were higher in the beta band during the tonic task

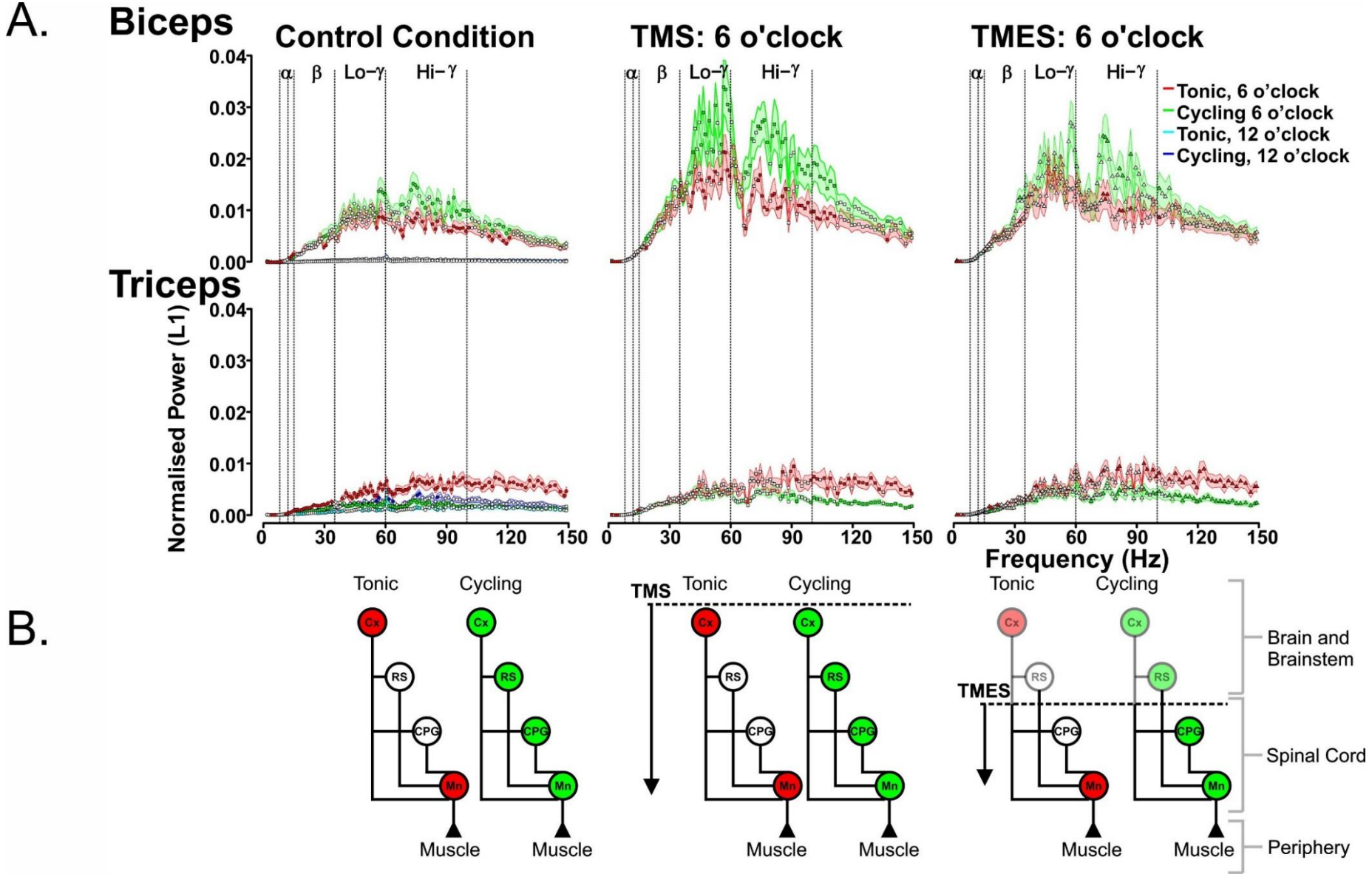
A.
Biceps
Triceps
Control Condition
TMS: 6 o'clock
TMES: 6 o'clock
α
β
Lo–γ
Hi–γ
Tonic, 6 o'clock
Cycling 6 o'clock
Tonic, 12 o'clock
Cycling, 12 o'clock
Normalised Power (L1)
0.04
0.03
0.02
0.01
0.00
0
30
60
90
120
150
Frequency (Hz)
B.
Tonic
Cycling
TMS
TMES
Cx
RS
CPG
Mn
Muscle
Brain and Brainstem
Spinal Cord
Periphery

Figure 3.5. Power spectral density measured from WSST results. **A.** Power spectral density was measured from the WSST for control (no stimulation), and with TMS and TMES. Measurements were made mid-flexion (6 o'clock) and mid-extension (12 o'clock) during cycling, or during an amplitude matched tonic contraction. With stimulation, the time points which were extracted from the WSST correspond to the peak of the MEP. Data shows mean of mean ± SEM (up to 10 measures per subject, $n = 10$). Power is binned into 1 Hz bands from 1-150 Hz (there are some gaps at higher frequencies – see legend of ***figure 3.4***). Filled points indicate significance between Cycling and Tonic for a given position (Two-factor ANOVA, Tukey's HSD post-hoc, $p < 0.01$). Vertical lines indicate different frequency bands. **B.** Schematics of likely circuits. Filled circles show pathways which are active as a result of the task. Horizontal dotted lines indicate the level of stimulation. Pathways affected by the simulation are translucent. Cx = Cortex, RS = Reticulospinal tract, CPG = Central Pattern Generator, Mn = Spinal Motoneurone.

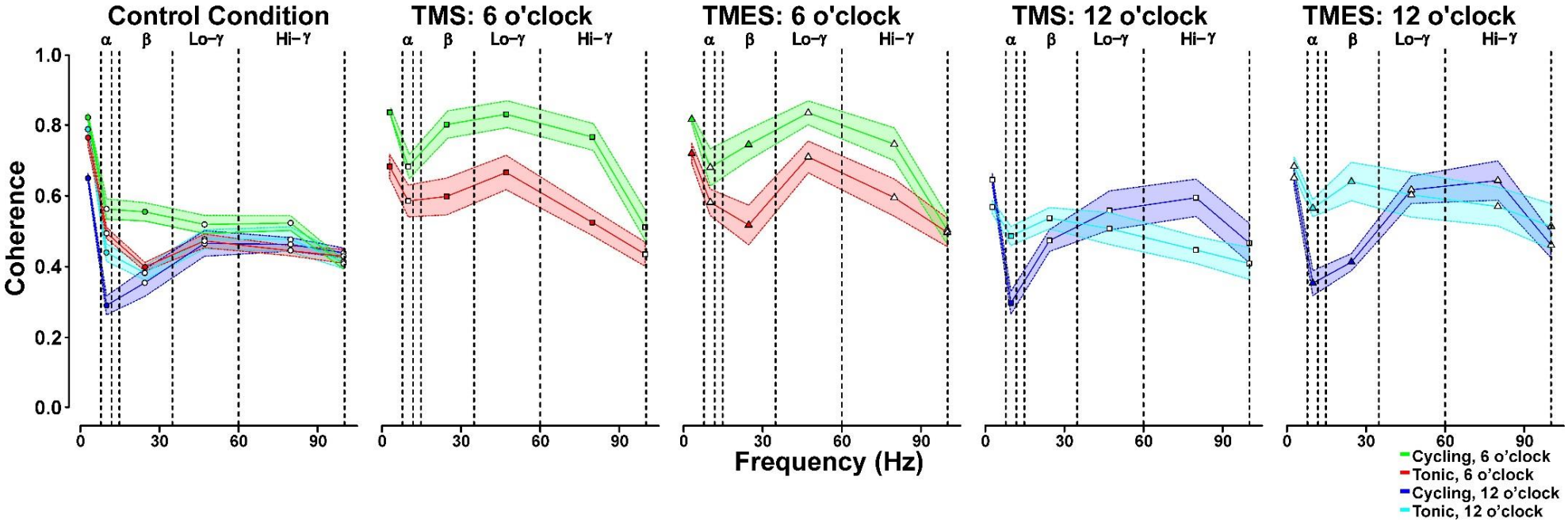

Figure 3.6. Biceps-triceps coherence measured from wavelet coherence. Coherence was measured from the wavelet coherence spectrogram for control (no stimulation), and with TMS and TMES. Measurements were made mid-flexion (6 o'clock) and mid-extension (12 o'clock) during cycling, or during an amplitude matched tonic contraction. With stimulation, the time points which were extracted from the WSST correspond to the peak of the MEP. Data shows mean of mean ± SEM (up to 10 measures per subject, $n = 10$). Points represent frequency bands which were 1-6, 6-15, 15-35, 35-60, 60-100, 100-200 Hz. The signals were filtered at the limits of each band before coherence was measured. Filled points indicate significance between Cycling and Tonic for a given position (two-factor ANOVA, Tukey's HSD post-hoc, $p < 0.01$). Vertical lines indicate different frequency bands.

compared to cycling. Apart from this, there were no statistical differences between the cycling and tonic tasks at 12 o'clock in any band, with TMS or with TMES.

3.6 Discussion

Human neurophysiology is often biased towards the brain and the cortex for control of movement and for use as prediction for recovery. However, subcortical pathways such as the reticulospinal pathway could provide some compensation following loss of the corticospinal pathway (Baker, 2011). There are also networks of cells in the spinal cord known as central pattern generators which can autonomously sustain muscle activity, and regulate sensory and descending inputs during repetitive movements (Grillner, 1981). It widely accepted that there is a CPGs which can regulate activity in the lower limb in humans (Dietz and Harkema, 2004; Zehr and Duysens, 2004), and there is evidence for a human upper limb CPG (Zehr et al., 2004). In humans, it is difficult to study these pathways since experiments must be non-invasive and we can only obtain indirect evidence by recording EMGs. For these reasons, we do not currently have a good measure for quantifying reticulospinal or spinal contributions to movement. A common method to study the CPG in the upper limb is to record EMGs during a rhythmic movement such as arm cycling, and observe differences in response to stimulation throughout different phases of the movement. This was the approach taken by Forman (2014) who applied TMS and TMES during an arm cycling task and an intensity matched tonic contraction (***figure 3.1C***). We used this dataset to identify subcortical pathways in the EMG.

Analysis of the frequency domain of EMG signals can be used to identify common neural drive to muscles using intermuscular coherence (Farmer et al., 1993). This is a technique which has promising clinical and research applications. Coherence between 5-60 Hz has been cited as having a cortical origin. However, since other pathways contribute to the generation of muscle activity depending on the task, we hypothesized that we could identify frequency bands associated with other circuits in the EMG. Definition of which

frequencies within this band actually constitute the corticospinal pathway is also in need of clarification. Commonly used frequency analysis techniques such as the fast Fourier transform have no time resolution so we cannot pin down short latency fluctuations in the frequency content of EMG. To overcome this problem, we applied a wavelet synchro-squeezed transform, a time-frequency analysis with maximal resolution in both the time and frequency domain. This technique gives us the time resolution to be able to assess changes in frequency content over a short enough time frame to be comparable to standard physiological measures such as response to TMS.

3.6.1 Time to peak

We began by trying to identify task related changes in time to peak in response to stimulation to establish if there was any changes in neural drive which could be identified in the time domain. We found that during cycling, the time to peak was dependent on the phase, and during tonic contractions, this depends on the background muscle activity.

3.6.1.1 Time to peak suggests regulation of descending drive is altered depending on phase (cycling) and prior muscle activity (tonic)

Time to peak was shorter by 2-4 ms with CMEPs than with MEPs (***figure 3.2***). This confirms the expected outcome since CMEPs are known to have shorter response latencies than MEPs (Taylor, 2006). The novelty of this study is the finding that during cycling, the muscle acting as an agonist is maximally active earlier than the antagonist in response to stimulation (***figure 3.2***). The difference in time to peak of evoked response in biceps and triceps brachii with either pyramidal tract or motor cortex stimulation was similar, suggesting that the delay is not due to these supraspinal structures.

However, during the tonic task, differences in time to peak between biceps and triceps brachii were not similar. At the 6 o'clock position (matched to mid-flexion during cycling), with TMS, the time to peak in biceps brachii is shorter than in triceps brachii (*NS*), though with TMES, it was shorter for triceps brachii (***figure 3.2***). This can be explained because during a tonic contraction, there is a shift in excitability in a polysynaptic pathway caudal to the cortex but

rostral to the brainstem. Since the muscle is not contracting, there is little EMG activity at the 12 o'clock position, resulting in MEP amplitudes as much as 10 fold lower than at the 6 o'clock positions. In this scenario, the triceps brachii latency is shorter than biceps brachii with TMS ($p < 0.001$) and TMES (*NS*, ***figure 3.2***).

Shifts in time to peak may be due to multiple factors. During cycling, CPG activity at a spinal level could inhibit the antagonist response through reciprocal Ia pathways from the agonist. During the tonic tasks, the low muscle activity in the 12 o'clock position compared to when the muscle is active in the 6 o'clock position is likely a factor. The tonic task is primarily driven by supraspinal pathways. Therefore when there is no contraction and the muscles are inactive (12 o'clock), the excitability of both biceps and triceps brachii motoneurones will be low. During an active tonic contraction (6 o'clock), both muscles are co-activated by supraspinal pathways but since the biceps brachii is the prime mover, the biceps brachii motor pool may be more excitable. Arm position can also affect the size of evoked responses (Nuzzo et al., 2016), so the difference in posture between 12 and 6 o'clock could also be a factor.

3.6.2 Frequency domain

Forman et al. (2014) set out to identify differences in response amplitude to compare the excitability of cortical circuits and their terminations on to spinal motoneurones between tasks. The current study is an attempt to identify an analogous response for these events in the frequency domain. Whilst both tasks involve the corticospinal pathway, the cycling task also involves the spinal CPG activation (Zehr and Kido, 2001). Our goals were: *i.* To characterise the previously described amplitude modulations within the frequency domain. *ii.* An exploratory study to use the pathway-specific tasks and stimulus evoked responses to identify candidate frequency bands associated with spinal and subcortical pathways across a broad frequency spectrum. *iii.* To determine whether distinct frequency bands in the muscle output were associated with corticospinal activity. The following results show for the first time that is it possible not only to identify frequencies associated

with brainstem circuits, but also frequencies associated with spinal activation. This is possible by combining anatomical and neurophysiological knowledge about pathways activated with TMS compared to TMES, and those which are active during the cycling compared to the tonic task.

3.6.2.1 i. Frequency domain characterisation of Forman 2014 findings

Forman reported that responses to TMS, but not TMES, are increased in amplitude during cycling compared to tonic tasks (***figure 3.1C***). This implies that additional pathways beyond the corticospinal pathway, located rostral to the brainstem are recruited during the cycling task (***figure 3.1D***). A likely candidate for this effect is the reticulospinal pathway, since brainstem areas such as the mesencephalic locomotor region (MLR) are known to be recruited during repetitive rhythmic actions such as locomotion making it both physiologically and anatomically plausible (Perreault et al., 1999). In the frequency domain, TMS causes an increase in both low and high gamma in cycling compared to tonic (***figure 3.5A***). This differs from the control condition (6 o'clock, cycling, no stimulation) and TMES (***figure 3.5A***), where increases are only in the high gamma range in cycling compared to tonic. Similar results were seen in the coherence measures, whereby with TMS, coherence is increased during cycling compared to tonic at 6 o'clock in the beta, low and high gamma bands, though with TMES only the beta band is increased (***figure 3.6***). In the following sections, we will argue that the variation in responses to stimulation in the low and high gamma range can be used to differentiate between spinal as well as reticulospinal pathways.

3.6.2.2 ii. Low-gamma (35-60 Hz) is probably reticulospinal in origin, and high-gamma (60-100 Hz) is probably spinal

In the control condition, power in high gamma is increased during cycling compared to a tonic contraction (***figure 3.5A***). This could reflect both reticular and spinal activation since both are expected to be active during the cycling but not the tonic task (***figure 3.5B***). With TMS, both low and high gamma show an increase during cycling compared to tonic contraction (***figure 3.5A***). TMS excites the motor cortex and collaterals anatomically and hierarchically caudal to the motor cortex so both the reticulospinal and the spinal CPG could be

involved (***figure 3.5B***). However, TMES preferentially activates the pyramidal tract and spinal pathways over other pathways from the brain and brainstem (***figure 3.5B***). With TMES, only the high gamma is increased during cycling compared to a tonic contraction, similar to control (***figure 3.5A***). The high gamma range is most likely to result from spinal CPG activity since they are increased with all cycling tasks compared to the tonic task, and also with both TMS and TMES. The reticulospinal seems to affect the low gamma range as it is increased with cycling compared to tonic with TMS, but not TMES, which would stimulate below the brainstem. During cycling, the high gamma range also appears to be increased with TMS compared to TMES, suggesting that it probably has some effects in this window as well. During cycling, drive to muscles is phasic. If pathways providing the drive to muscles act at different frequencies, they will produce muscle firing which corresponds to the frequency of neuronal firing. If these pathways are then stimulated, the activity in the pathway will increase, and will therefore increase the muscle activity and the frequency of the frequency will correspond to the activity of the pathway which is stimulated. This is why looking at the wavelet transform of muscle activity during the response reveals these pathways.

3.6.2.3 iii. Corticospinal frequencies

Since the corticospinal pathway cannot be activated in isolation either by task or by method of stimulation, identifying a frequency associated with the corticospinal pathway is complex. Pathways contributing to muscle activity may have either supplementary or complimentary effects on the frequency domain to those frequencies affected by the corticospinal pathway. The outcomes are not mutually exclusive. If the effects are complementary, then the same frequencies as the corticospinals will be affected. If the effect is supplementary, then frequencies outside of the corticospinal range will be affected.

Compared to control, there is an increase in amplitude across all frequencies with both TMS and TMES (***figure 3.5A***). This is probably due to the increased amplitude of the EMG signal at the time point measured (peak of response) compared to the amplitude of the EMG in the control condition. One interpretation of this is that the corticospinal pathway increases muscle firing

at every frequency, which is supportive of additional pathways having a complementary effect. Since this is also the case with Erb's point stimulation, which activates all motoneurone efferents innervating the muscle, it is likely that the change in amplitude at all frequencies relates to a change in amplitude of the signal. Instead, we should examine how the frequency distribution of responses changes between tasks where the amplitude is the same.

A better explanation is that the corticospinal TMS and TMES response is similar in frequency content, but additional pathways affect different frequency bands. This is possible since the corticospinal pathway is involved in both tasks. TMS may activate descending neurones and TMES their axons coursing through the brainstem and spinal cord causing a similar effect between tasks. In this case, the beta band could be corticospinal since it is the same with both TMS and TMES between cycling compared to tonic, supporting the supplementary role. Wavelet coherence was higher in the beta band was higher during cycling compared to tonic at 6 o'clock in control, TMS, and TMES conditions (***figure 3.6***). This suggests that shared drive in the beta band is different between the two conditions whilst drive in higher frequencies remains unchanged. This is likely to do with the phasicty of pathways active at higher frequencies (see next section). If descending drive is higher at 6 o'clock than at 12 o'clock or during tonic tasks, beta band coherence reflecting descending drive is consistent with our results. Our temporal analysis of responses also supports this since we have shown altered descending drive throughout the cycle.

3.6.3 Wavelet Transform and Wavelet Coherence taken together

Analysis of wavelet transform (***figure 3.3B, 3.4*** **and** ***3.5***) and of wavelet coherence (***figure 3.3C and 3.6***) inform us of different parameters of the data. The wavelet transform informs us of the frequency distribution of the signal as a function of time. With EMG data, this reflects the frequency components of firing of an individual muscle. However, wavelet coherence between a muscle pair can inform us about common drive to the motoneurones of the muscles. This means that coherence is high only in frequencies which are common to the muscle pair. In the control condition at 6 o'clock, EMG power is higher in

the high gamma band during cycling compared to tonic. However, coherence is higher in the beta band during cycling compared to tonic, but the same in the gamma band. Coherence during cycling and tonic at 12 o'clock was similar to cycling at 6 o'clock in all bands. This shows us that the common drive to muscles is altered at 6 o'clock during cycling compared to other conditions. It is especially interesting that the drive is different between 6 o'clock and 12 o'clock during cycling, since this suggests that there is a different drive for contraction of the triceps brachii compared to contraction of the biceps brachii. This is supported by the response latency analysis. Since beta band coherence is increased during biceps brachii contraction, this suggests that this frequency is due to increased corticospinal drive. However, gamma coherence is unchanged by the task at control. If high frequency components come from CPG circuits, this could be because CPG drive is to muscles is phasic, and therefore not shared between biceps and triceps brachii at any phase in the cycle.

The results with stimulation at 6 o'clock were similar between the wavelet transform and with wavelet coherence. However, with TMES, the beta band is similar between cycling and tonic in the wavelet, whereas coherence is higher during cycling. There is also no significant difference between cycling and tonic in high gamma coherence at 6 o'clock, whilst there are differences in the frequency spectra. Both of these discrepancies can probably be explained by differences in shared drive between the conditions, and different drive depending on the phasicity of the cycle.

3.6.4 Comparison of our results to those within the literature

In the literature, coherence within the beta band (15-35 Hz) between cortex and muscle, and muscle-muscle is thought to originate in the motor cortex and be transmitted through the direct corticospinal pathway to the muscle (Farmer et al., 1993; Conway et al., 1995; Kilner et al., 1999). In primates, this correlates with oscillations around 25 Hz in the sensorimotor cortex (Murthy and Fetz, 1992) and during development, appearance of corticomuscular coherence coincides the synapsing of corticospinal fibres with neurones in the spinal cord in human infants (Ritterband-Rosenbaum et al., 2016). However,

in the literature, the definition for frequency bands is erratic. Some studies cite coherence around 10 Hz, 20 Hz, and 40 Hz (McAuley et al., 1997; Riddle et al., 2004), monkey motor cortex oscillations are cited around 25-35 Hz (Murthy and Fetz, 1992), and boundaries of the beta band vary between 13-30 Hz (Neto et al., 2010) and 15-33 Hz (Salenius et al., 1997). Raethjen et al. (2002) has suggested that 6-15 Hz is also corticospinal in origin (Raethjen et al., 2002). One reason for the range in the boundaries for the band may be the window size used for the FFT, which can vary between 512 and 2048. This gives different frequency resolution so coherence may be present in different frequencies depending on the bin size. We decided to better define this band so that it could be confined to a reliable and consistent range. To do this we used a bin size of 1 Hz so that we could determine whether there was changes in discreet frequency bands across the population as a whole. Surprisingly, our results do not show the beta band as being the band which shows the most significant changes between tasks and stimulation methods. There are several possible explanations for this. As previously discussed, this could be because there is no difference between tasks and stimulation methods in the beta band because the recruitment from the pyramidal tract is similar. Another reason may the pre-processing step of rectification which is routinely applied during most studies applying a frequency analysis but was not applied here. A final reason could be that the biceps brachii motoneurone pool receives proportionately less descending input from the corticospinal pathway than an alternative pathway. Based on our results, it seems most likely that the corticospinal system affects EMG power between 15-60 Hz. However, there was interesting alterations in the frequency domain in frequencies above 35 Hz.

We have proposed that subcortical pathways are involved in gamma band EMG activity. This is in agreement with the hypotheses of Nishimura (Nishimura et al., 2009) who report muscle coherence between 30-46 Hz one month post CST lesion in primates and no beta or gamma band cortical coherence post lesion. They suggested a subcortical source for gamma band coherence. Rossiter et al. (2013) have reported variable outcomes in corticomuscular coherence from stroke patients but a common trend was a reduction of beta band coherence and an increase in gamma band coherence.

Although corticomuscular coherence is an inherently variable measure (Ushiyama et al., 2016) and variability in the nature and extent of the injury is inevitable in stroke patients, Rossiter's findings point towards cortical reorganisation and an increased reliance on gamma activity which probably involves subcortical pathways. We have also proposed that spinal CPG networks contribute to EMG activity in the 60-100 Hz range, based on the finding that these frequencies are still present during cycling with TMES. Whilst this is difficult to confirm, high oscillations (60-110 Hz) are present in EMGs recorded from other systems which receive input from a CPG such as respiratory and masticatory muscles (Bruce and Ackerson, 1986; Smith and Denny, 1990). This is in agreement with our findings and it may be that high frequency oscillations are a functionally important phenomenon in CPG networks. Indeed in the cat, high frequency coherence has been seen in motoneurones between 100 and 300 Hz during CPG activity and was thought to relate to the short term synchrony between two closely synergistic muscles (Nielsen et al., 2005). However, it is very uncommon for frequencies above 60 Hz to be measured in the literature.

3.6.5 High Resolution Benefits of Application of WSST to EMG data

We used the Matlab® wsst() function to apply a Wavelet Synchro-Squeezed Transform to EMG data. This has the joint benefits of both optimal time and optimal frequency resolution. In this study, both points are of interest to us. Firstly, we wanted to clearly define frequency bands as clearly as is possible in an attempt to define distinct frequency bands as accurately as possible, and to test whether different pathways would affect specific frequencies within bands. To this end, we used 1 Hz bands to identify localised frequency differences across the population. Whilst our results did not show localised intra-band peaks which correlated with activation of specific pathways, they do show that the commonly used definition for beta and gamma band coherence are generally applicable. Broad definitions for the beta band between 15-35 Hz and the low gamma band at 35-60 Hz show a good fit with our data. However, we also show that frequencies above 60 Hz show interesting task and stimulation dependent changes. Frequencies this high are

rarely taken into account in the literature and we suggest that we may be missing valuable information by not taking this into account. We also applied a filter to the signal of each band before applying the transform. This was necessary in order to mitigate side lobes and bleeding between bands. Without applying this step, activity appears smeared, or clumped into pockets spectrogram rather than being in distinct bands.

The second advantage of using a wavelet synchro-squeezed transform was the time resolution it allowed. This was important to us since we were seeking to identify the shortest latency events following stimulation of descending pathways. Commonly used frequency analysis methods such as the FFT are based on windowed sections of data, and hence have no time resolution. We therefore we cannot use them to identify transient shifts in the frequency content of an EMG signal. Using a WSST allows us to examine the frequency content of signals in a similar time window to standard physiological measures such as the MEP peak. Transient changes in the frequency content of EMG signals at these latencies are representative of the pathways which were stimulated. We used this to show that corticospinal and reticulospinal pathways probably overlap with the corticospinal pathway acting at 15-60 and the reticulospinal pathway at 35-100 Hz.

3.6.6 High frequency components of EMG should be studied more closely

For a number of reasons, it is common in the field for alpha, beta and gamma band coherence to be studied, but not higher frequencies. One reason is that there is little evidence to suggest that motor units firing above 25 Hz, though this is mostly to do with restrictive conditions which are required for data on single MU’s to be collected, including restricting movement, using low force contractions, and recording from anaesthetised animal preparations (Johnson et al., 2017). In studies investigating motor unit activation patterns in isometric, eccentric, and concentric conditions, 25 Hz is usually the ceiling for discharge rates (Linnamo, 2002; Kallio et al., 2013). Such studies tend to report the mean firing rate so this probably not an accurate representation of the overall range. More research is needed to clarify the relationship between the

frequency content of the surface EMG and firing of individual motor units. It is possible that changes in the spectral properties of the EMG may relate to task-related differences intrinsic to the muscle such as type of contraction (isometric contraction in the tonic condition, concentric in the cycling condition), type of motor unit recruited, or muscle fibre conduction velocity (Poosapadi Arjunan et al., 2016). However, since the tasks and the stimulation in this study selectively activate discreet pathways, the most likely explanation is a different presynaptic drive between conditions.

3.6.7 Clinical Applications

The findings presented here have significant clinical implications. Importantly, they offer a potential means by which we can non-invasively examine fidelity of cortical and subcortical circuits by observing the frequency content of EMG signals in response to TMS. This is significant since at present we have no way to do this. Following an injury such as stroke or spinal cord injury, we believe that this will be a useful means by which to assess remaining pathways which is economical financially, in terms of time, and level of expertise needed to carry out the examination. We have also outlined that EMG frequencies correlate with specific pathways. This could be useful for assessing neural drive to EMGs without stimulation. The tasks used here also have potentially useful clinically applications. Hemiplegic patients may have residual movement on the affected side and still have capacity for movement on the other side. An arm cycling related therapy coupled with appropriately timed stimulation could be a good means to encourage neural plasticity in remaining pathways to facilitate recovery. Future studies should seek to confirm the findings presented here in a clinical population.

3.6.8 Considerations

For These experiments hold a bias towards the biceps brachii muscle since this was the muscle primarily being explored. No amplitude matching was carried out for the triceps brachii so there are no data to corroborate our findings during an isometric elbow extension. Also, the magnetic stimulation and hotspot was adjusted primarily for the biceps brachii responses rather

than triceps brachii so evoked potentials were larger when recorded from biceps brachii.

Chapter 4: Using Intermuscular Coherence to Identify Common Input to Muscles Activated During Shoulder Abduction and Adduction

4.1 Abstract

Shoulder muscle synergies have been identified during isometric abduction/extension and adduction/flexion (Roh et al., 2013), and during point-to-point reaching tasks to study activation of temporal synergies (Cheung et al., 2012). These studies applied a non-negative matrix factorization analysis which does not reveal the neural drive to the muscles. Most shoulder muscles serve multiple functions so details of muscles sharing common neural input are probably complex. Interactions between muscle pairs at the shoulder or between shoulder and arm are rarely studied, leading to significant gaps in our understanding of these common pathways and the recruitment of muscles to produce functional output. Cross-correlation and frequency coherence analysis have previously been used to identify common neural input to muscle pairs (Kirkwood and Sears, 1978; Kirkwood et al., 1982; Farmer et al., 1993; Vaughan and Kirkwood, 1997; Neto et al., 2010). Here, sEMG recordings were made from 15 shoulder and arm muscles including those which are prime movers for shoulder abduction (deltoids, trapezius, triceps brachii) or adduction (pec. major, serratus anterior, lattisimus dorsi). We investigated muscle interactions during three tasks: an isometric maximum voluntary contraction in the direction of either (1) abduction or (2) adduction, and (3) a novel maximum voluntary effort task. Each task was observed at three angles within the range of motion of shoulder abduction. For all tasks and angles, we identified common input and the likely source between pairs of muscles. We show how muscle interactions are altered with

biomechanical adjustments and other inputs like the central and peripheral neural drive.

4.2 Introduction

4.2.1 Pathways for Control of the Upper Limb

Any force exerted on a distal joint of the upper limb must be counteracted with an increase in activity of muscles which stabilise more proximal joints (Rothwell, 1987). For example, when picking up a full wine bottle which was expected to be empty, muscles acting at the wrist and elbow must communicate with muscles at the shoulder to ensure the unexpected weight can be countered efficiently. However, examination of the pathways or mechanisms meeting this need are rare. Descending and sensory pathways must adjust to postural changes and produce the appropriate output through the 'final common path' - the spinal motoneurone to the muscle, as defined by Sherrington (Sherrington, 1906). The corticospinal tract is the most important descending pathway for fine control of the distal musculature (Lemon, 2008). In monkeys, motoneurones of distal muscles receive a higher proportion of direct synaptic contacts from the corticospinal tract than proximal muscles. Until recently, the reticulospinal tract was thought to be predominantly involved in gross control of proximal muscle groups (Baker, 2011). However, distributed monosynaptic reticulospinal contacts in monkeys can also compensate for several aspects of hand function following damage to the pyramidal tract (Zaaimi et al., 2012). In the baboon, studies have catalogued Ia afferent pathways between muscles at different joints of the upper limb (Hongo et al., 1984). Only recently have studies begun to uncover interactions of muscles acting at different joints in people (Miller and Dewald, 2012). Reciprocal inhibition at the human wrist is mediated predominantly by Ib inputs though it is not known if these inputs extend to the shoulder (Wargon et al., 2006). Monosynaptic Ia and recurrent pathways have been studied in the upper limb in man but are also incomplete at the shoulder (Pierrot-Deseilligny and Burke, 2012). These pathways contribute to coordinated muscle activation during natural movement. Muscle co-activation patterns can be used to identify muscles synergies. A commonly used technique for this is

Non-Negative Matrix Factorisation (NMF), as applied by Roh et al. (2013) to shoulder and elbow muscles. However, current muscle synergy analysis techniques cannot reveal neural drive between muscles.

4.2.2 Muscle Synergy Analysis and Clinical Applications

Bernshteĭn's muscle synergy theory states that the CNS overcomes redundancy by grouping activation of individual units (muscles) into functional modules (synergies). Whilst it has recently been shown that biomechanical factors can cause synergistic muscle activation even if muscles are not activated in groups (Kutch and Valero-Cuevas, 2012), the muscle synergy hypothesis may explain how the CNS may reduce dimensions of control during movement. One view is that motor modules, or motor primitives within the CNS may encode simple activation patterns which can be combined to produce more complex movements (Flash and Hochner, 2005). Motor primitives have been activated to produce defined outputs in the spinal cord and medulla (Schepens, 2004; Roh et al., 2011). This fits with the view that muscle synergies are centrally organised and may be selectively activated by supraspinal (Yakovenko et al., 2011) or spinal inputs (McCrea and Rybak, 2008). Overduin et. al (2012) recently used a non-negative matrix factorisation to identify both spatial and spatiotemporal synergies in primates during a reaching task, correlating field recordings from cortical neurones with EMG activity. Though the cortex is important for muscle selection, recruitment of muscles into synergies is also affected by afferent information (Ting and Macpherson, 2005; Cheung et al., 2005). In humans, after a cortical stroke, muscle synergies are fractionated or merged (Cheung et al., 2012). This shows how selection of spatial muscle synergies can be disrupted in absence of effective descending motor command. Consequently, muscle synergy analysis has the potential for applications like clinical assessment of damage to descending pathways. However, for a clinical analysis, this is a complex technique to perform since it is time consuming and requires technical knowledge. At current, analytical methods cannot tell us where in the sensorimotor loops synergies are formed and how different areas interact to form spatial or spatiotemporal muscle synergies. Better clarification of muscle interactions and the corresponding pathways would therefore improve our

understanding of the influence of peripheral afferents and spinal circuits on formation of muscle synergies. This may be achievable using intermuscular frequency coherence analysis.

4.2.3 Intermuscular Coherence Analysis

Intermuscular coherence analysis is a technique which has been used to identify common synaptic drive to motoneurones of a pair of muscles (Farmer et al., 1993; Laine et al., 2015). Coherence represents oscillatory synchrony between two signals, specifically with reference to the source. Beta band coherence originates from the sensorimotor cortex (Murthy and Fetz, 1992) and the activity recorded from the muscle is thought to represent binding of sensory and motor pathways to create a central-peripheral feedback loop (Farmer, 1998; Baker, 2007). Beta band corticomuscular coherence increases as a function of force during a sustained contraction (Kilner et al., 2000), and disappears to be replaced by gamma band coherence during dynamic tasks (Mehrkanoon et al., 2014). Both gamma and beta band corticomuscular coherence are seen to be sensitive to changes in peripheral activity (McClelland et al., 2012a; Schmied et al., 2014). This is usually attributed to long sensory loops involving the brain (Kasuga et al., 2017). Studies which measure corticomuscular coherence have a bias towards circuits at a cortical level. Local spinal circuits are rarely considered to be a factor. The current study shows that it is possible to identify spinal involvement in muscle interactions by analysing coherence across multiple muscles during an appropriate motor task.

4.2.4 Maximum Voluntary Contractions (MVCs) are unreliable as a Normalisation Factor and for Corticospinal Assessment

Maximum Voluntary Contractions (MVCs) are recorded as a means to determine EMG amplitude during recruitment of the whole motoneurone pool for use as a normalisation factor, and to quantify corticospinal drive. There are 4 issues with the collection of MVCs to measure corticospinal drive. Firstly, joint angles and limb positions are not always specified in the literature, and not always standardised between studies which are investigating the same pathway. This is significant since corticospinal excitability is altered by

pathways at a spinal level depending on limb position (Nuzzo et al., 2016). Inflow of afferent information from the periphery to the spinal cord is likely to be a factor in this, since it can affect the recruitment of spinal motoneurones through excitatory or inhibitory reflex pathways or presynaptic inhibition (Pierrot-Deseilligny and Burke, 2012). This, coupled with involvement of divergent corticospinal (Iles and Pisini, 1992) and subcortical pathways (Tazoe and Perez, 2017) mean that EMG amplitude is therefore not a direct measure of corticospinal input to motoneurones. Secondly, MVCs are routinely only recorded from the muscle of interest. Theoretically, if it were possible to activate a single muscle in isolation, this approach would be appropriate. However, it is more common that multiple muscles are co-activated (Lee et al., 2014). Since production of muscle activity during an MVC may in fact involve a number of sources, muscles which are recruited by additional pathways are therefore overlooked when only a single muscle is recorded. Hence the interactions between muscles are not accounted for, and MVCs present an incomplete representation of pathways involved in neuromuscular control. Thirdly, it is common that too few MVCs are collected to ensure the subject can obtain 100%. When MVCs are performed properly, the limb is secured into position and the subjects apply the maximum possible force against a resistance which gives little or no tolerance. However, even when joint angles are controlled and the limb is properly secured, if too few measurements are taken, the participant may not achieve 100%. Subsequent measures normalised to this are therefore misleading. Fourthly, MVC amplitude can be very variable. This can change from day to day, even from trial to trial, and depend on various factors including fatigue (Gandevia, 2001). We have observed that muscle interactions can be variable from trial to trial, showing that muscle groupings shift when the subject attempts an MVC (unpublished data). One factor for this is probably slightly different muscle tendon and spindle receptors afferent inflow producing different patterns of motoneurone recruitment depending on the synaptic distribution of reflex pathways involved. MVCs are routinely used in clinical practice. However, the complications outlined here highlight the need for a more appropriate test where these factors could be accounted for depending on the scenario.

4.2.5 Maximum Voluntary Effort (MVE) Task for Identifying Muscle Pairs activated by Common Descending Pathways

In this study we approach these problems by using a Maximum Voluntary Effort (MVE) task of a prime mover whilst recording from additional muscles of the upper limb. During an MVE, the limb is secured as with an MVC, but subjects attempt to contract the muscle of interest in isolation without applying a force against a resistance. The purpose of this is to reduce the effects of reflex and spinal pathways on the recruitment patterns of muscles which would be present during an MVC. In this situation, the drive to the primary muscle should be primarily descending in origin, having eliminated the propriospinal inputs from the periphery. During an MVE, the amplitude of the primary muscle is greatly reduced compared to during an MVC. This supports the theory that multiple pathways are involved in, or are necessary for motoneurone recruitment during an MVC to allow all of the motor pool to be recruited for the task. Muscle synergies identified from such muscle activation patterns can then be used as a marker for cortical damage after stroke in humans (Cheung et al., 2012). Here, we provide a profile for muscles sharing common input from descending pathways in healthy humans.

These data were generated for use as a catalogue to compare clinical data from patients who have suffered damage to descending pathways or peripheral nerve damage. This is towards providing a less complex clinical analysis which will yield more information by identifying key interactions which are of clinical relevance. Since muscle interactions during an MVE can vary greatly from subject to subject, one outcome of this study is to identify the interactions which are most common across the sample during an MVE. In future studies we can reduce the number of muscles recorded to only those relevant for the test. With similar studies in patients, we can then use interactions identified here as makers for variability in the remnants of descending pathways in clinical populations, along with their viability towards restoration of function. We recorded MVEs and MVCs of muscles activated during abduction (ABD) and adduction (ADD) at 3 different angles throughout the range of motion of shoulder abduction, to precisely identify the role of

descending versus the peripheral inputs in shaping the motor output from the muscle across multiple subjects but under identical restrictions to movement.

4.2.6 Outcome Measures

To catalogue these interactions, we are using 4 outcome measures. The first is peak coherence index, which gives a measure of correlation between muscle activity in the frequency domain. Coherence between muscles reflects presynaptic branching of common pathways onto the spinal motoneurone. This is measured in the beta, low-gamma, and high-gamma band since we have previously suggested (see Chapter 3) that different frequency bands could correlate with contributions of different pathways within the EMG. The second is the number of subjects in which coherence exceeds a confidence interval defined by an existing statistical framework (Halliday et al., 1996; Amjad et al., 1997) to measure variability from subject to subject. The third is the peak correlation index, which gives a measure of correlation of muscle activity in the time domain. The final measure is the correlation half-width. This measure was used by Kirkwood and Sears to show that a half-width of <5 ms is due to common pre-synaptic branching directly to pairs of motoneurones, and broader half-widths reflect common input through a di- or poly-synaptic pathway (Kirkwood and Sears, 1978; Vaughan and Kirkwood, 1997). We catalogue these interactions towards the identification of motor primitives in the brain compared to those in the spinal cord. Muscle interactions present during an MVC task may include those present during an MVE as well as those induced by the increased peripheral activity. We can begin to identify and compare spinal and cortical motor primitives by those which are activated differentially or to supplement between tasks. We stand to learn more by looking at the patterns of shared drive to motoneurones of multiple muscles than we do by looking only at amplitude or corticomuscular coherence with a single muscle.

4.3 Methods

Methods are described in the General Methods Chapter.

4.4 Results

4.4.1 Amplitude analysis

EMGs were recorded from 14 muscles of the dominant shoulder and upper limb of each subject (*n* = 21). One contralateral muscle was recorded (contralateral deltoid). This was included 1. to insure there was no contralateral activity during tasks, and 2. to act as a negative control for coherence, correlations, and cluster analysis to see what would happen in a muscle with no signal. Patterns of muscle activity varied most between tasks, but also some muscles showed changes in amplitude at different angles (***figure 4.1, 4.2,*** **and** ***4.3***). RMS values were calculated to show amplitude shifts across tasks and angles, and also to use as a reference for the coherence analysis. Amplitude varied depending on the task – abductors (AD, MD, PD, UT ***figure 4.4***) were highest amplitude during ABD, adductors were highest during ADD (PM, LD, ***figure 4.4***). Between different muscle groups, muscle amplitude was most similar during the MVE task (***figure 4.4***).

4.4.2 Power spectrum

For each muscle during each task, at each angle, for each subject, power spectrum were normalized to the highest value. The average across the sample was calculated (***figure 4.5***). The average frequency distribution varied somewhat from muscle to muscle, but was most often highest around 50 Hz (***figure 4.5***).

4.4.3 Cross correlations and coherence

Cross-correlations index varied from muscle to muscle and depending on task and angle (see ***figure 4.6*** for a representative subject). The peak of the correlation almost always centered around 0. Coherence between muscle pairs also varied depending on the muscle pair being examined, as well as the task and angle (see ***figure 4.7*** for a representative subject). The grouped results are discussed in full in the next section.

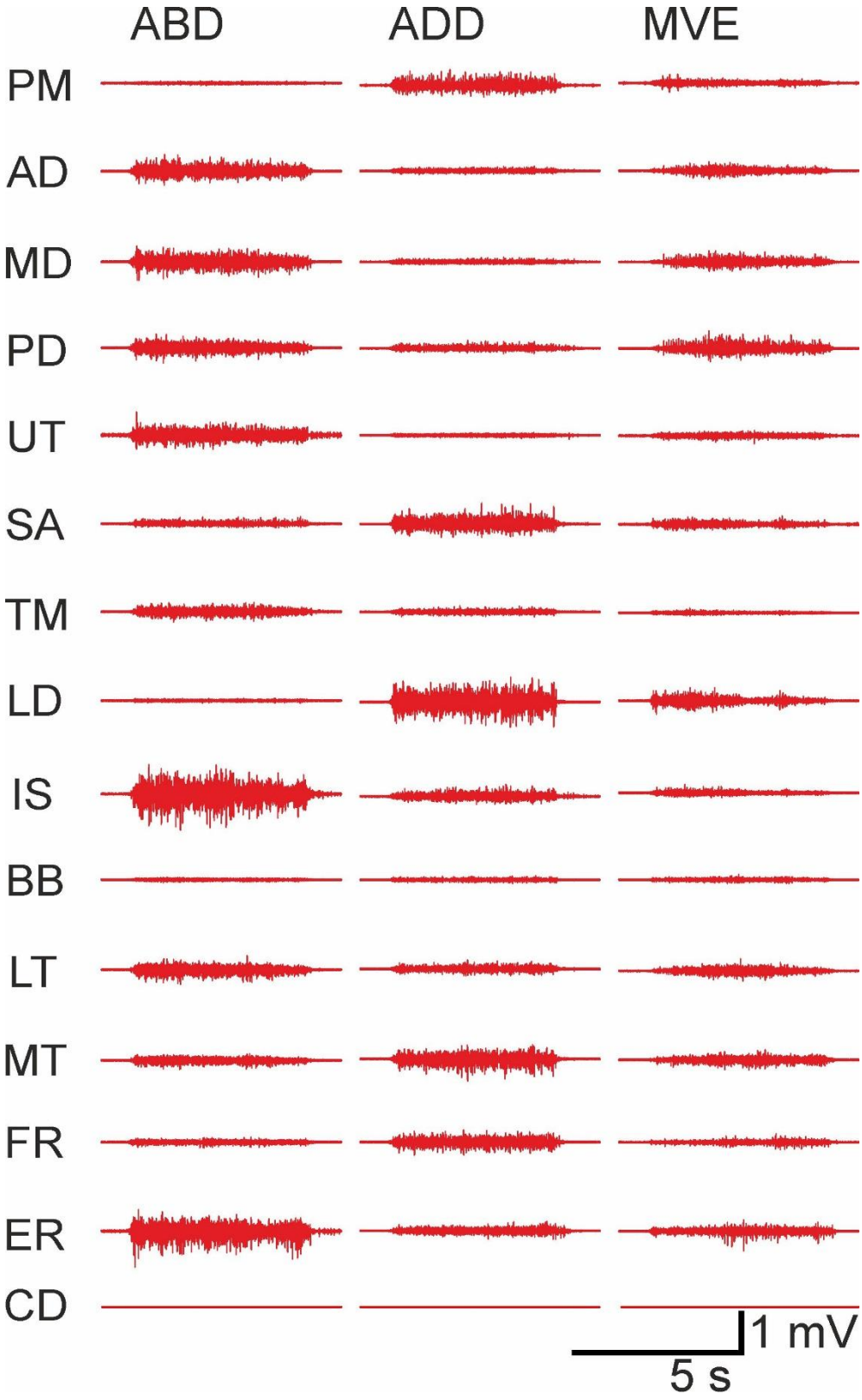

Figure 4.1. Raw EMG for ABD, ADD and MVE task recorded at 30° from a representative subject. Raw EMG (sampled at 2 kHz) from muscles across the shoulder and upper limb recorded during MVC and MVE experiments from a representative subject. Each shows one of five 5 s trials recorded for each condition.

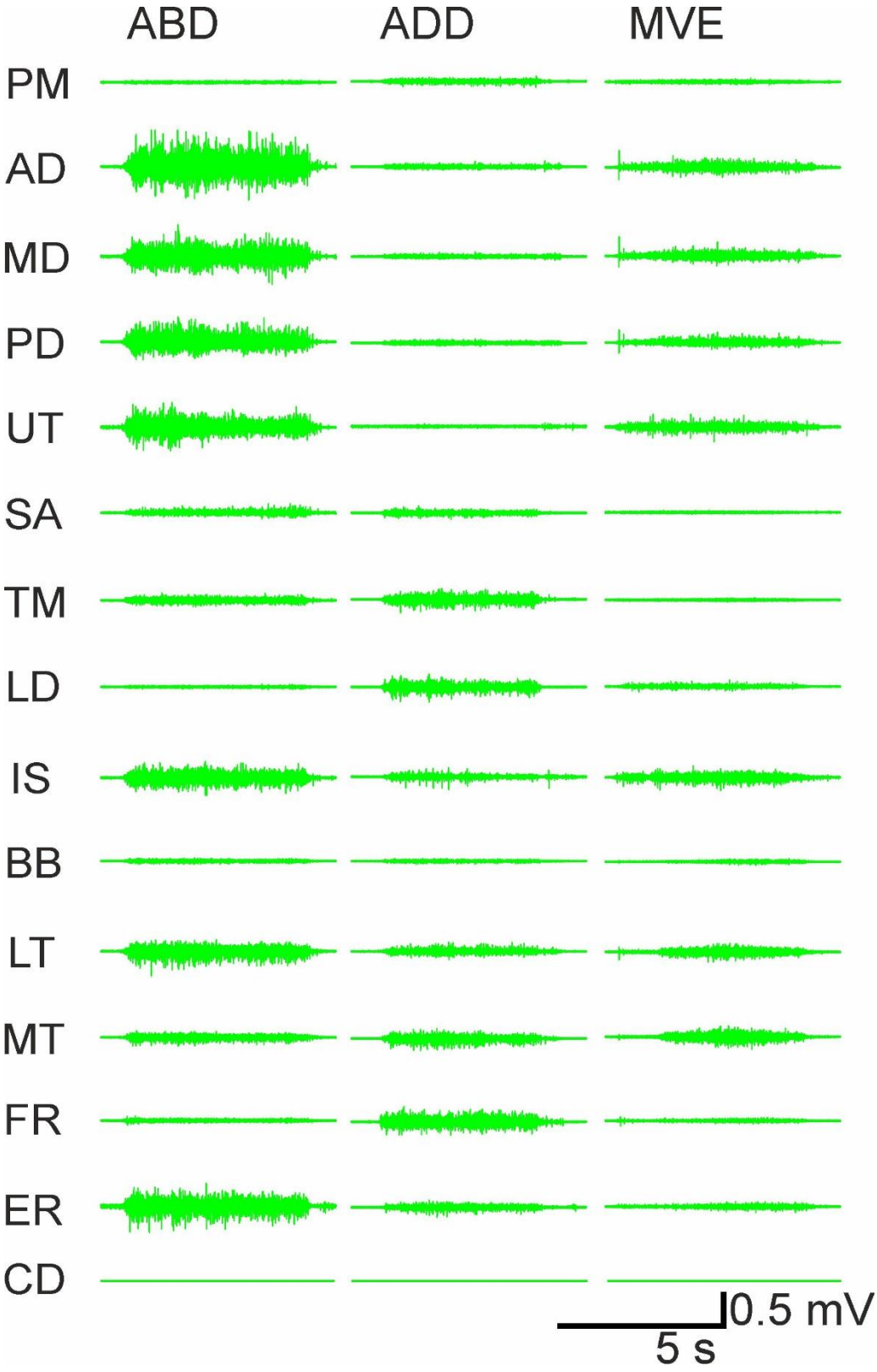

Figure 4.2. Raw EMG for ABD, ADD and MVE task recorded at 75° from a representative subject. Raw EMG (sampled at 2 kHz) from muscles across the shoulder and upper limb recorded during MVC and MVE experiments from a representative subject. Each shows one of five 5 s trials recorded for each condition.

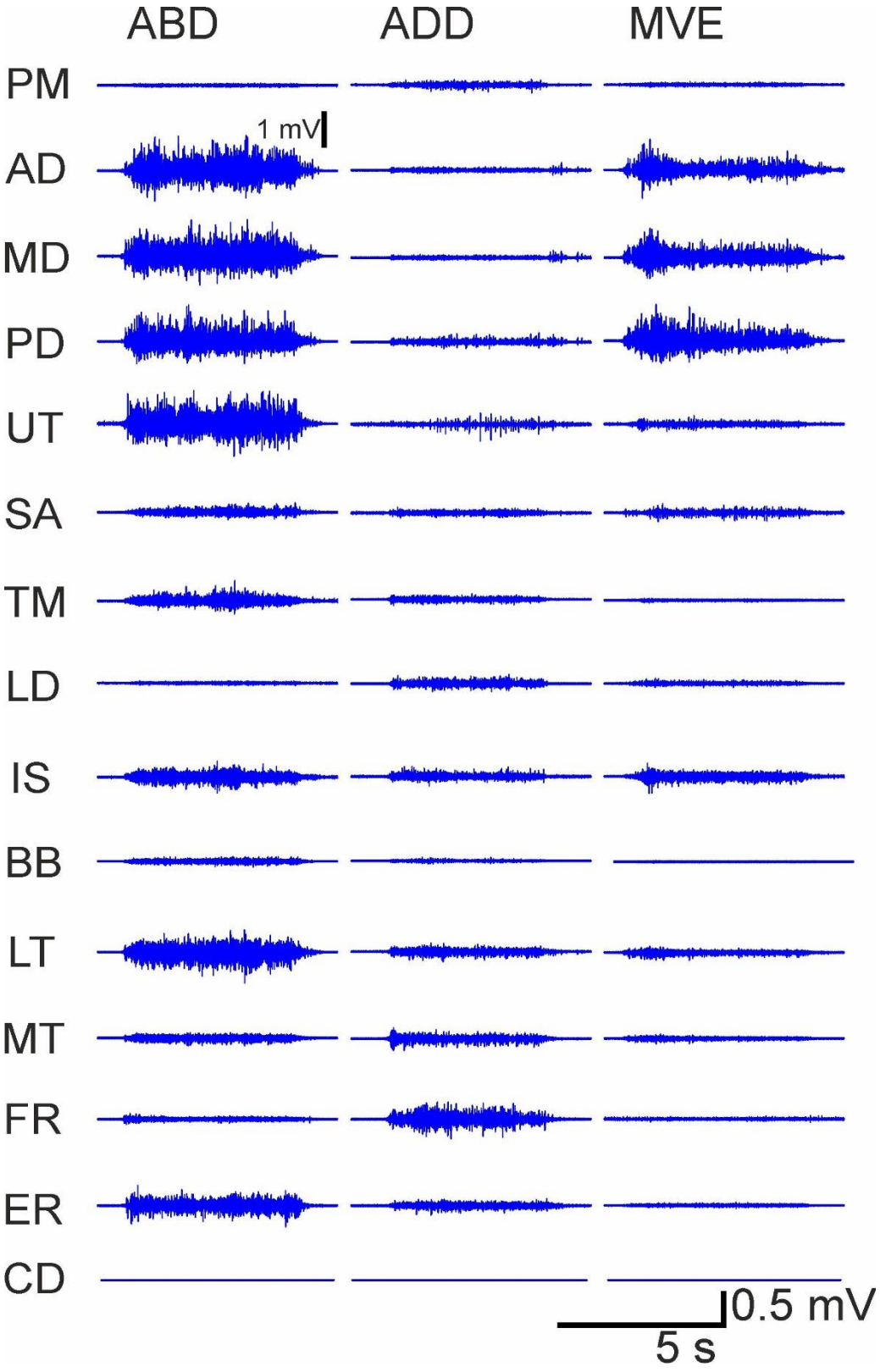

Figure 4.3. Raw EMG for ABD, ADD and MVE task recorded at 120° from a representative subject. Raw EMG (sampled at 2 kHz) from muscles across the shoulder and upper limb recorded during MVC and MVE experiments from a representative subject. Each shows one of five 5 s trials recorded for each condition. AD during ADD has a separate scale bar.

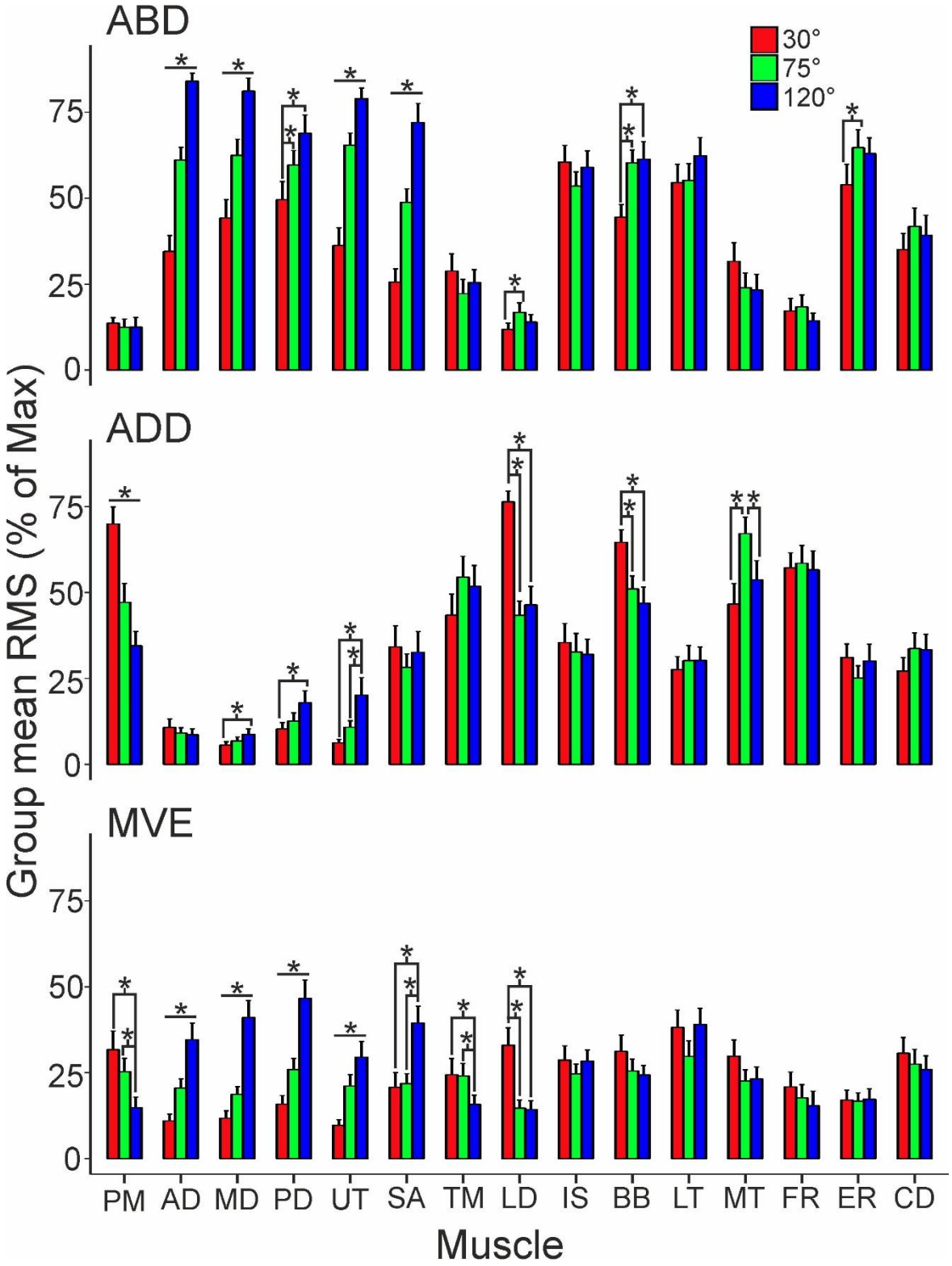

Figure 4.4. Group mean of mean RMS amplitude from EMG recorded during ABD, ADD and MVE tasks. Data were normalised to the maximum RMS values across all experiments prior to analysis (five 5 s trials per subject). Individual means from each muscle during a given task were compared across angles using one-way ANOVA and Tukey HSD post-hoc test (* = $p < 0.01$, $n = 21$).

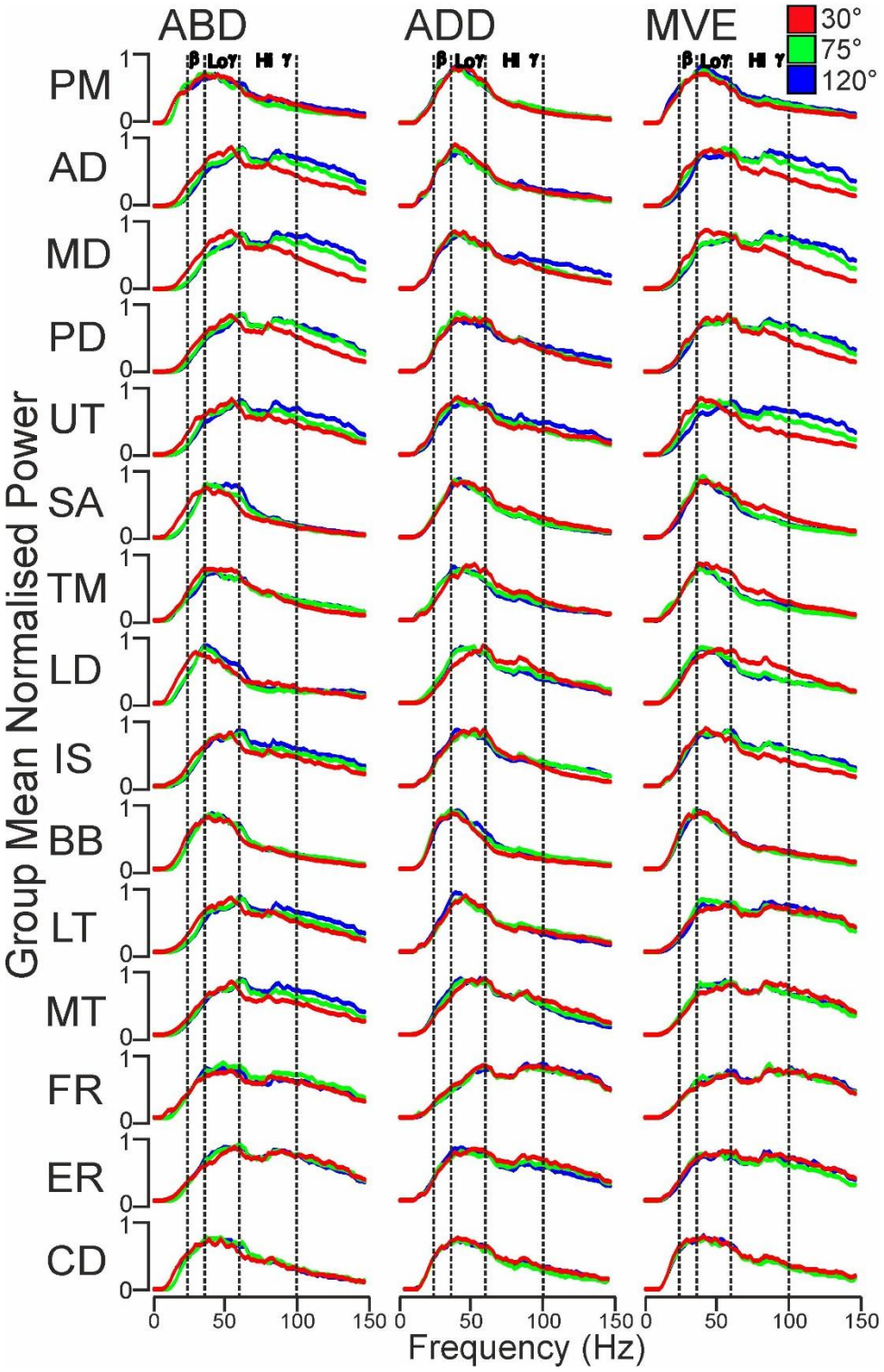

Figure 4.5. Group mean of mean normalised power spectrum for ABD ADD and MVE tasks. Data were normalised to the frequency for each muscle at each angle during each task for each subject prior to calculating the mean, and includes five 5 s trials from each subject (n = 21). Data were normalised to obtain an estimate of the frequency distribution of power spectrum across the group. Vertical dashed lines indicate the different bands used for coherence analysis (20-35, 35-60, 60-100 Hz).

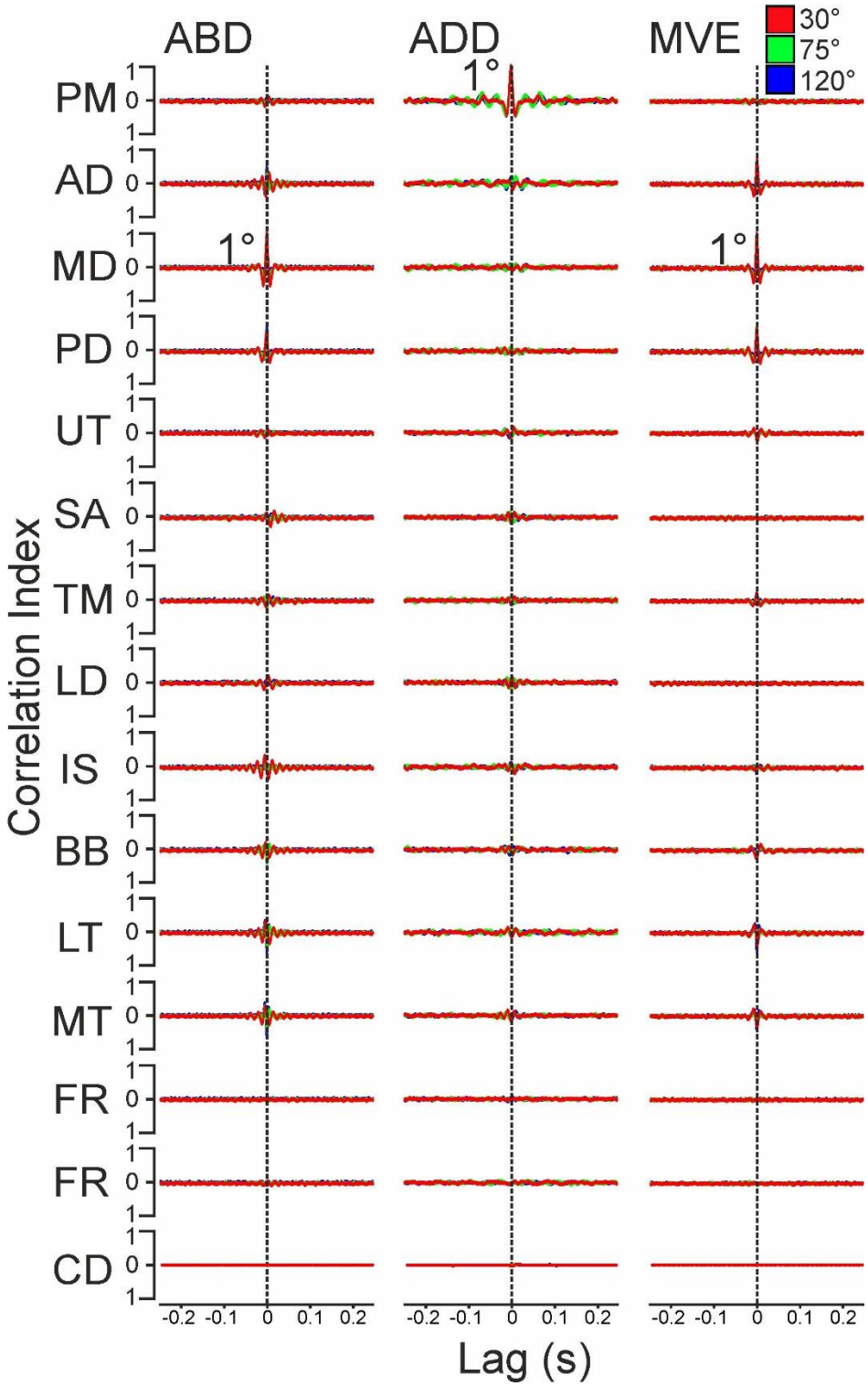

Figure 4.6. Cross-correlations from ABD, ADD and MVE tasks for a representative subject. Examples of results of cross-correlation analysis during MVC or MVE tasks shown in a 500 ms time window, from -250 to 250 ms. Results are from five 5 s trials. Dashed vertical lines indicate 0 lag. All correlations are shown between the primary muscle for each task (MD during ABD and MVE, PM during ADD), labelled 1°.

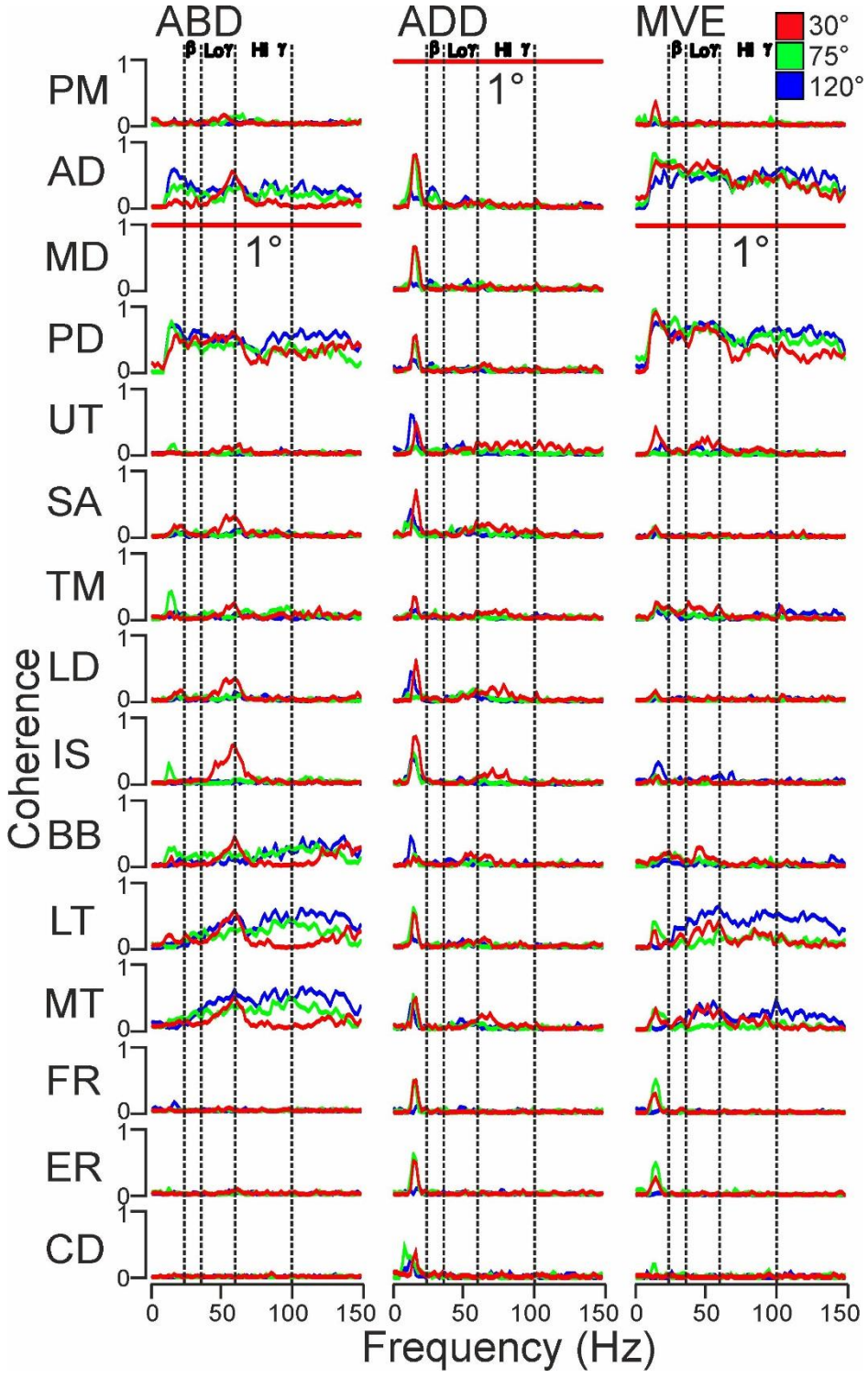

Figure 4.7. Coherence spectra from ABD, ADD and MVE tasks for a representative subject. Examples of results of coherence analysis during MVC or MVE tasks from five 5 s trials (FFT size 1024, bin size 1.95 Hz). Vertical dashed lines indicate the different bands used for analysis (20-35, 35-60, 60-100 Hz). The beta band is measured at 20-35 instead of 15-35 Hz since the EMGs were filtered 20-450 Hz at time of collection. Coherence was calculated between the primary muscle for each task (MD during ABD and MVE, PM during ADD), labelled 1°.

4.4.4 Muscle interactions - Postural Differences

4.4.4.1 Abduction, Change with Posture (*figure 4.8* and *4.9*)

i. Shoulder-Shoulder interactions

Coherence

Abductor-abductor coherence (AD, MD, PD) was high across angles and frequency bands with the exception of AD-PD, which was low in the beta band (***figure 4.8A***). More than 90% of subjects showed significant coherence, though only approximately 60% in the beta band for AD-PD (***figure 4.8B***).

Adductor-Abductor coherence (PM to deltoids) was low with the exception of the low gamma PM-AD coherence at 75° (***figure 4.8A***). Significant low and high gamma PM-deltoids coherence was present in most subjects with AD (min 75%) then MD (min 55%) then MD (min 50%, ***figure 4.8B***).

Adductor-adductor coherence (PM to -SA and -LD) was high in the low gamma band at 75° and 120° (***figure 4.8A***). At 75° and 120°, at least 60% of subjects showed significant coherence regardless of angle or frequency band (***figure 4.8B***).

Abductor-axial coherence (MD to -UT and -IS) in the low gamma band (***figure 4.8A***). Deltoids-IS and -UT coherence was highest at 30° with the exception of AD-UT interactions which were highest at 75° (***figure 4.8A***). At least 70% subjects showed significant coherence in low gamma in these muscles in all cases (***figure 4.8B***).

Cross-Correlation

Abductor-abductor correlations (AD, MD, PD) were high across angles (***figure 4.9A***). In at least 85% of subjects, the half-width of the correlations was <5 ms (***figure 4.9B***).

Adductor-abductor correlations (PM to deltoids) were low across angles (***figure 4.9A***). Correlation half-widths were <5 ms for PM-MD and -PD for most subjects (at least 60%), but increasingly more subjects (at least 25%) were in the 10 ms window for PM-AD (***figure 4.9B***).

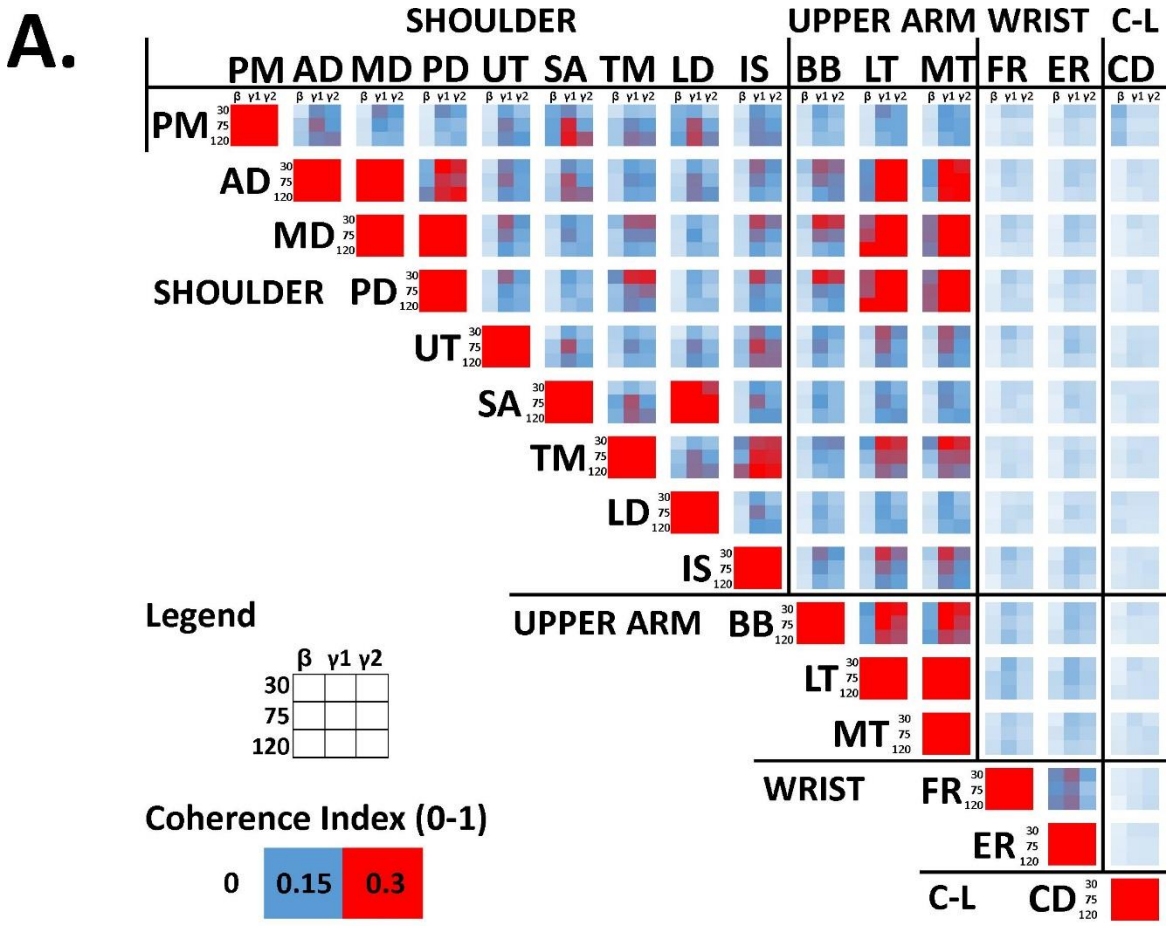
A.
SHOULDER
UPPER ARM
WRIST
C-L
PM AD MD PD UT SA TM LD IS
BB LT MT
FR ER
CD
β γ1 γ2
30 75 120
Legend
Coherence Index (0-1)
0 0.15 0.3

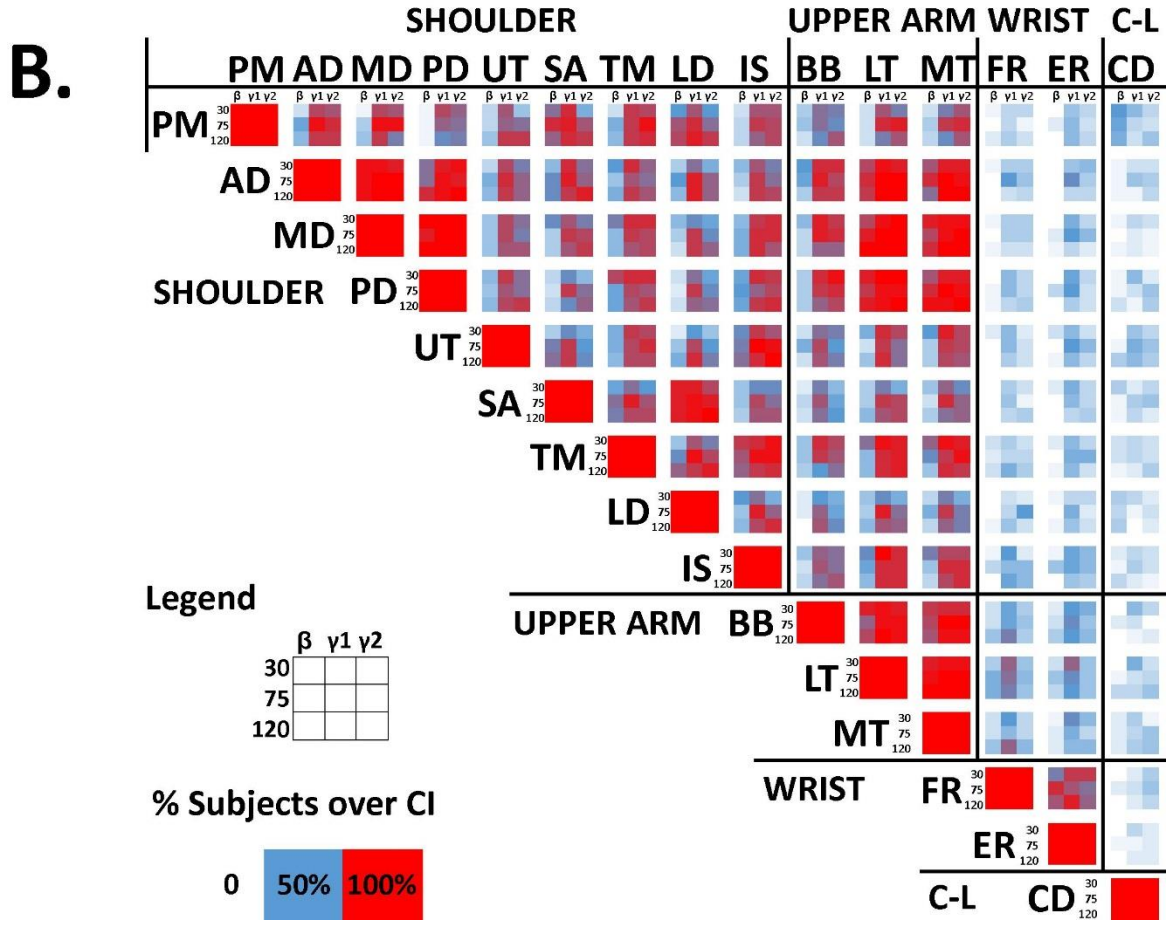
B.
SHOULDER
UPPER ARM
WRIST
C-L
PM AD MD PD UT SA TM LD IS
BB LT MT
FR ER
CD
β γ1 γ2
30 75 120
Legend
% Subjects over CI
0 50% 100%

Figure 4.8. Matrices of coherence between muscle pairs during ABD task, compared across angles. **A.** Group mean peak coherence measured between 20-35, 35-60 and 60-100 Hz (FFT size 1024). Data are from five 5 s trials per subject (*n* = 21). **B.** Percentage of subjects (*n* = 21) where the peak was above the 95% confidence interval as defined by Halliday et al. (1989). For each muscle pair there are 9 squares. As shown in the legends, columns correspond to different frequency bands and rows correspond to different angles. References for the colour intensity are shown in the legends. C-L – contralateral.

Adductor-adductor correlations (PM to -SA and -LD) were highest at 120° (***figure 4.9A***). At least 70% of subjects had half-widths within the 10 ms window (***figure 4.9B***).

Abductor-axial muscle correlations (MD to -UT and -IS) were highest at 30° (***figure 4.9A***). Half-widths in most subjects (at least 55%) were within the 5 ms window (***figure 4.9B***).

ii. Shoulder-Upper arm interactions

Coherence

Shoulder abductor-elbow flexor coherence (deltoids-BB) was low at most angles except at 30° where low and high gamma coherence was present (***figure 4.8A***). Significant coherence was present in at least 65% of subjects in the low and high gamma bands (***figure 4.8B***).

Shoulder abductor-elbow extensor coherence (deltoids to triceps brachii) was high in both the low and high gamma band across angles (***figure 4.8A***). Significant gamma band coherence was universally present across subjects and angles. Beta band coherence was present in at least 75% subjects (***figure 4.8B***).

Axial-elbow extensor coherence (UT, TM, IS to -LT and -MT) was present commonly in the low gamma band at 30° and 75° (***figure 4.8A***). With the exception of UT-LT, at least 80% subjects show significant coherence in low, and high gamma bands across angles (***figure 4.8B***).

Cross-Correlation

Shoulder abductor-elbow flexor correlations (deltoids-BB) were high at 30° (***figure 4.9A***). Correlation half-widths were in the 5 ms window across angles in at least 60% of subjects, with the exception of AD-BB at 30° where

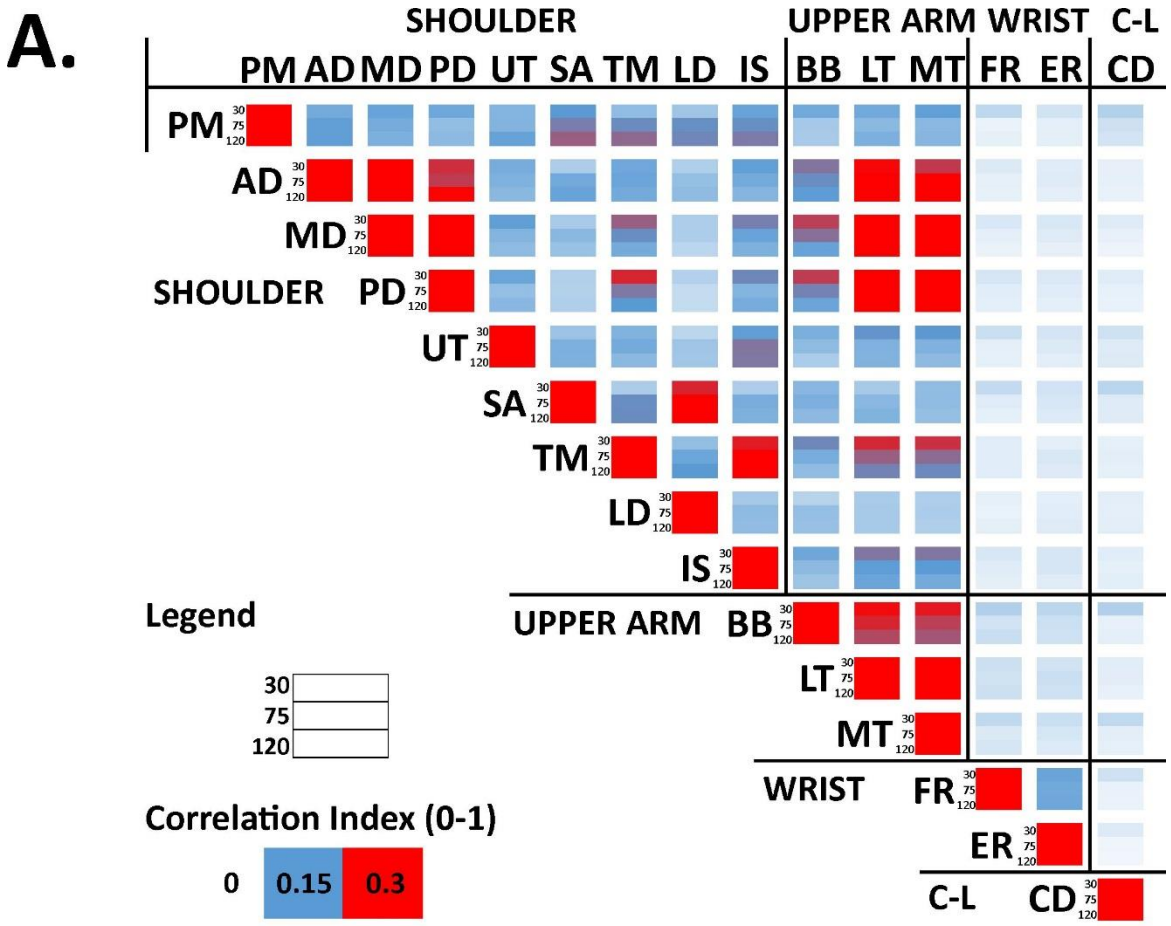
A.
SHOULDER
UPPER ARM
WRIST
C-L
PM AD MD PD UT SA TM LD IS
BB LT MT
FR ER
CD
SHOULDER
UPPER ARM
WRIST
C-L
Legend
30
75
120
Correlation Index (0-1)
0
0.15
0.3

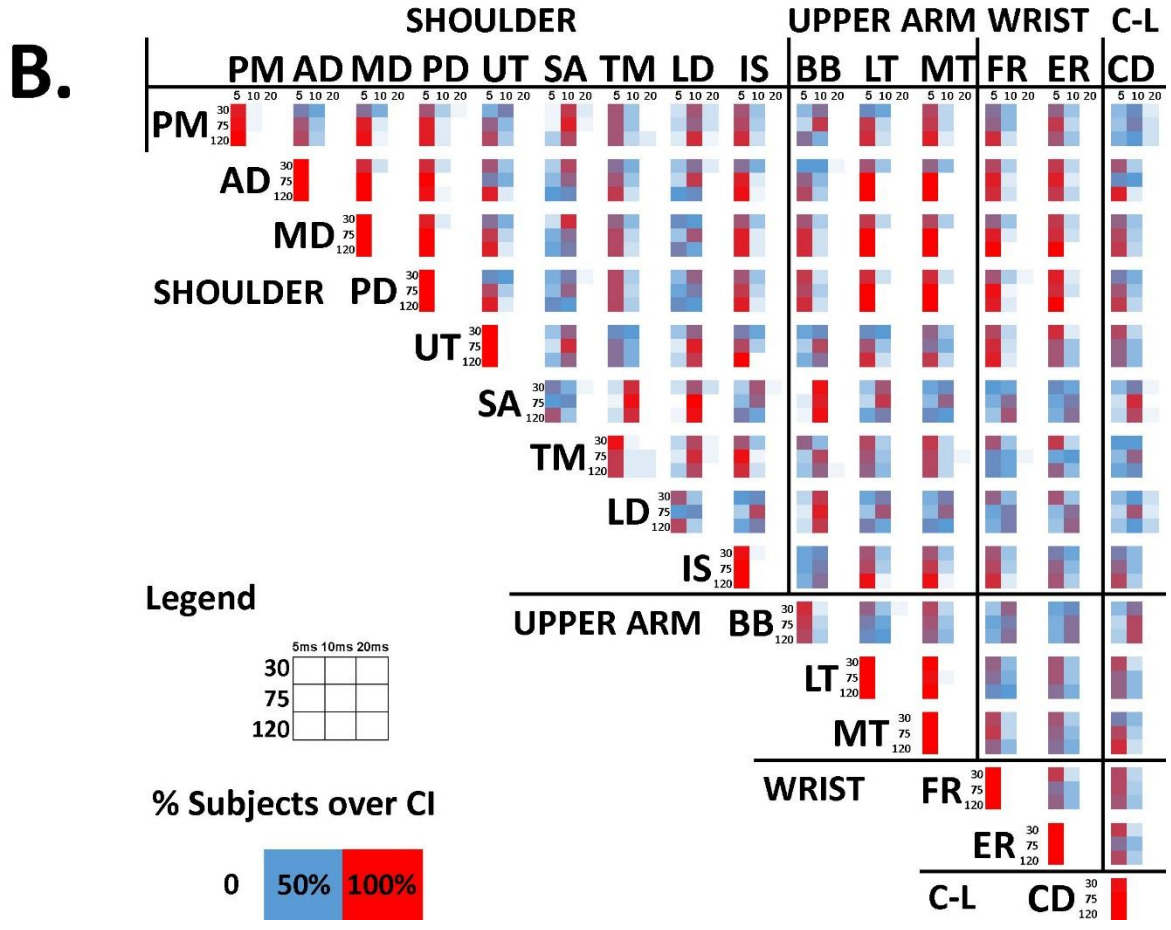
B.
SHOULDER
UPPER ARM
WRIST
C-L
PM AD MD PD UT SA TM LD IS
BB LT MT
FR ER
CD
5 10 20
SHOULDER
UPPER ARM
WRIST
C-L
Legend
5ms 10ms 20ms
30
75
120
% Subjects over CI
0
50%
100%

Figure 4.9. Matrices of cross-correlations between muscle pairs during ABD task, compared across angles. **A.** Group mean absolute peak correlation index. Data are from five 5 s trials per subject (*n* = 21). Legend shows rows corresponding to different angles and references for colour intensity **B.** Correlation half-widths. For each muscle pair there are 9 squares. Columns correspond to different half-widths (< 5 ms, 5-10 ms and 10-20 ms), and rows correspond to different angles. Colour intensity relates to the percentage of subjects (*n* = 21) where the half-width falls within that window. C-L – contralateral.

equal numbers were in the 5 and 10 ms window for around 65% subjects (***figure 4.9B***).

Shoulder abductor-elbow extensor correlations (deltoids to triceps brachii) were high across angles (***figure 4.9A***). Correlation half-widths were within the 5 ms window in at least 60% of subjects (***figure 4.9B***).

Axial-elbow extensor correlations (TM to -LT and -MT) were high at 30° (***figure 4.9A***). Across angles, half-widths were at least 65% in the 5 ms window with the rest in the 10 ms window (***figure 4.9B***).

iii. Shoulder-Wrist interactions

Coherence

Shoulder abductor-wrist extensor coherence (MD-ER) was moderate in both the low and high gamma band at 30° and 75° (***figure 4.8A***). Significant coherence was present in up to 50% of the sample (***figure 4.8B***).

Cross-Correlation

Shoulder abductor-wrist extensor correlations (MD-ER) were low across angles (***figure 4.9A***). Half-widths were in the 5 ms window for around 80% of the sample (***figure 4.9B***).

iv. Shoulder-Contralateral interactions

Coherence

Low adductor-contralateral deltoid coherence (PM-CD) was present in the beta band across angles (***figure 4.8A***). This was significant in around 50% of the sample (***figure 4.8B***).

Cross-Correlation

Low adductor-contralateral deltoid correlations (PM and SA to -CD) were present (***figure 4.9A***). Half-widths for PM-CD were split approximately 50/50 across the sample in the 5 ms and 10 ms windows (***figure 4.9A***). SA-CD half-widths were predominantly in the 10 ms window (***figure 4.9A***).

v. Upper arm-Upper arm interactions

Coherence

Elbow flexor-extensor coherence (BB to triceps brachii) was low in the beta band (***figure 4.8A***). In the low and high gamma band, coherence was high but decreased as angle increased (***figure 4.8A***). All interactions were significant across bands and angles in at least 65% of the sample (***figure 4.8B***).

Cross-Correlation

Correlations between upper arm muscles were high. Flexor-extensor correlations were highest at 30° and decreased as angle increased (***figure 4.9A***). BB-LT correlations were higher than BB-MT correlations (***figure 4.9A***). BB-LT half-widths were split between the 5 and 10 ms time window (***figure 4.9B***). Around 60% of subjects had BB-MT half-widths in the 5 ms time window (***figure 4.9B***).

vi. Upper arm-Wrist interactions

Coherence

Upper arm-wrist coherence (BB, LT and MT to -ER and -FR) was present in the low gamma band (***figure 4.8A***). This was present in all cases; flexor-flexor (BB-FR), flexor-extensor (BB-ER, FR-LT, FR-MT), and extensor-extensor (LT-ER, MT-ER, ***figure 4.8A***). Coherence was significant in 35-65% of the sample (***figure 4.8B***).

Cross-Correlation

Upper arm-wrist correlations were low (***figure 4.9A***). Elbow flexor-wrist muscle half-widths were mostly in the 10 ms window (***figure 4.9B***). Elbow

extensor-wrist muscle half-widths were mostly in the 5 ms window (***figure 4.9B***).

vii. Upper arm-Contralateral interactions

Coherence

Upper arm-contralateral coherence was minimal (***figure 4.8A***).

Cross-Correlation

Upper arm-contralateral correlations were low minimal (***figure 4.9A***).

viii. Wrist-Wrist interactions

Coherence

Wrist flexor-extensor coherence (FR-ER) was highest in the low gamma band at 30° and 120° (***figure 4.8A***). At least 65% of subjects showed significant coherence in the gamma band at these angles (***figure 4.8B***). Beta band coherence was present at all angles and was highest at 75°. At least 55% of subjects at 30° and 120°, and around 85% at 75° showed significant coherence in the beta band (***figure 4.8B***).

Cross-Correlation

Moderate wrist flexor-extensor correlations were present across angles (***figure 4.9A***). At 30°, half-widths were in the 5 ms window in around 80% subjects (***figure 4.9B***). At 75° and 120°, half-widths were around 2:1 in the 5 to 10 ms window across subjects (***figure 4.9B***).

ix. Wrist-Contralateral interactions

Coherence

Wrist-contralateral coherence was minimal (***figure 4.8A***).

Cross-Correlation

Wrist-contralateral correlations were minimal (***figure 4.9A***).

4.4.4.2 Adduction, Change with Posture (*figure 4.10* and *4.11*)

i. Shoulder-Shoulder interactions

Coherence

Abductor-abductor coherence (AD, MD, PD) was high across bands and angles (***figure 4.10A***). At least 90% of the subjects showed significant coherence at all angles and in all bands (***figure 4.10B***).

Abductor-adductor (PM-AD) coherence was present in the beta band (***figure 4.10A***). At all angles, PM-deltoids coherence was present in the low gamma band (***figure 4.10A***). Around 70% subjects showed significant coherence in the low gamma band (***figure 4.10B***).

Abductor-axial coherence (deltoids-TM) was highest in the low gamma band (***figure 4.10A***). This was maintained across the sample (at least 70% of subjects) across angles (***figure 4.10B***).

Axial-axial coherence (TM-IS) was high across bands and angles, except the beta band at 30° (***figure 4.10A***). At least 75% of subjects showed significant coherence across angles and bands (***figure 4.10B***).

Cross-Correlation

Abductor-abductor correlations (AD, MD, PD) were high across angles (***figure 4.11A***). In at least 65% of subjects the half-width of the correlations was in the 5 ms window between MD-PD (***figure 4.11B***). AD-MD and PD half-widths varied between 5 ms and 10 ms.

Abductor-adductor correlations (PM-deltoids) were highest between PM-AD (***figure 4.11A***). At all angles, PM-deltoids half-widths were in the 10 ms window for at least 80% of the sample (***figure 4.11B***).

Abductor-axial correlations (deltoids to TM) varied across angles and muscles. Whilst AD-TM interactions correlations were moderate, MD-TM correlations were highest at 30°, and PD-TM correlations were highest at 75° (***figure 4.11A***). Half-widths varied between 5 ms and 10 ms across angles (***figure 4.11B***).

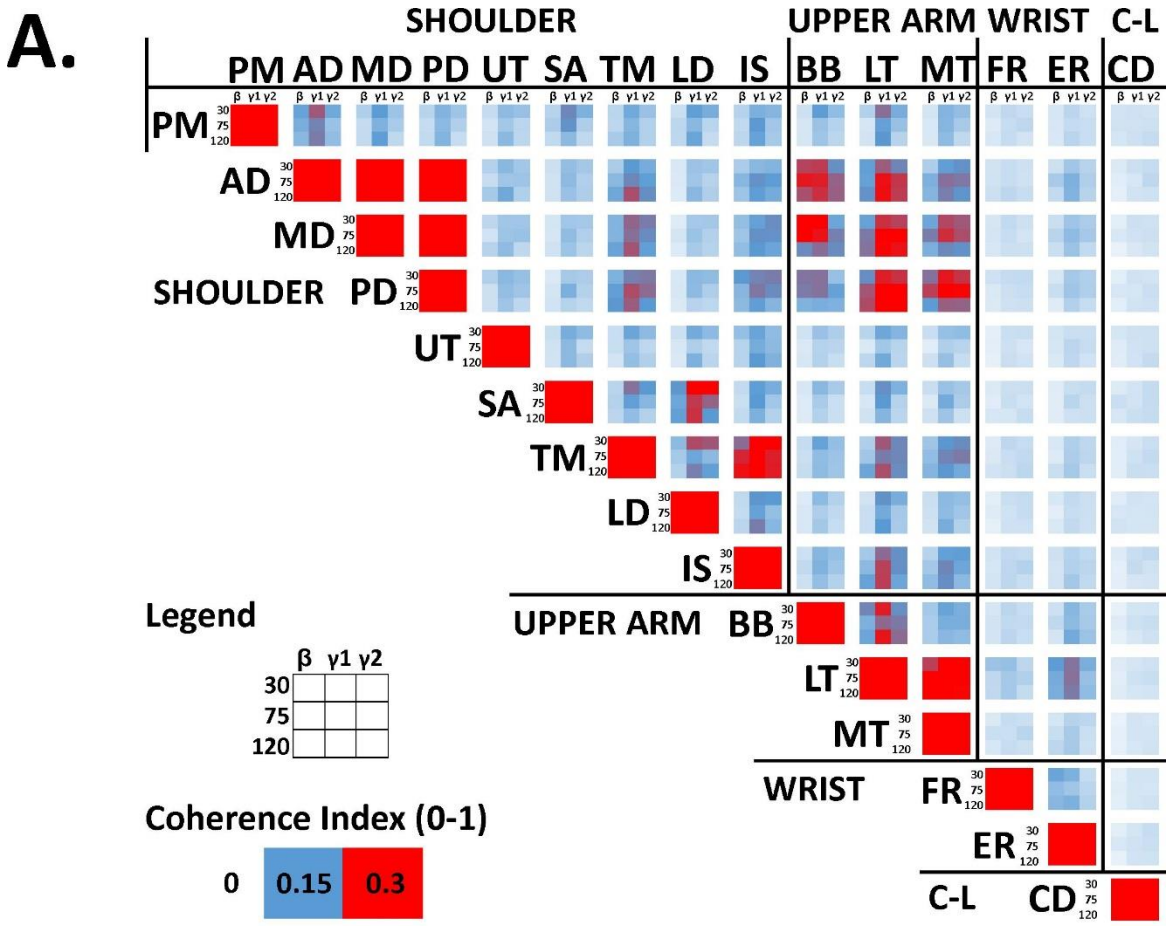
A.
SHOULDER
UPPER ARM
WRIST
C-L
PM AD MD PD UT SA TM LD IS
BB LT MT
FR ER
CD
β γ1 γ2
30 75 120
SHOULDER
UPPER ARM
WRIST
C-L
Legend
β γ1 γ2
30
75
120
Coherence Index (0-1)
0
0.15
0.3

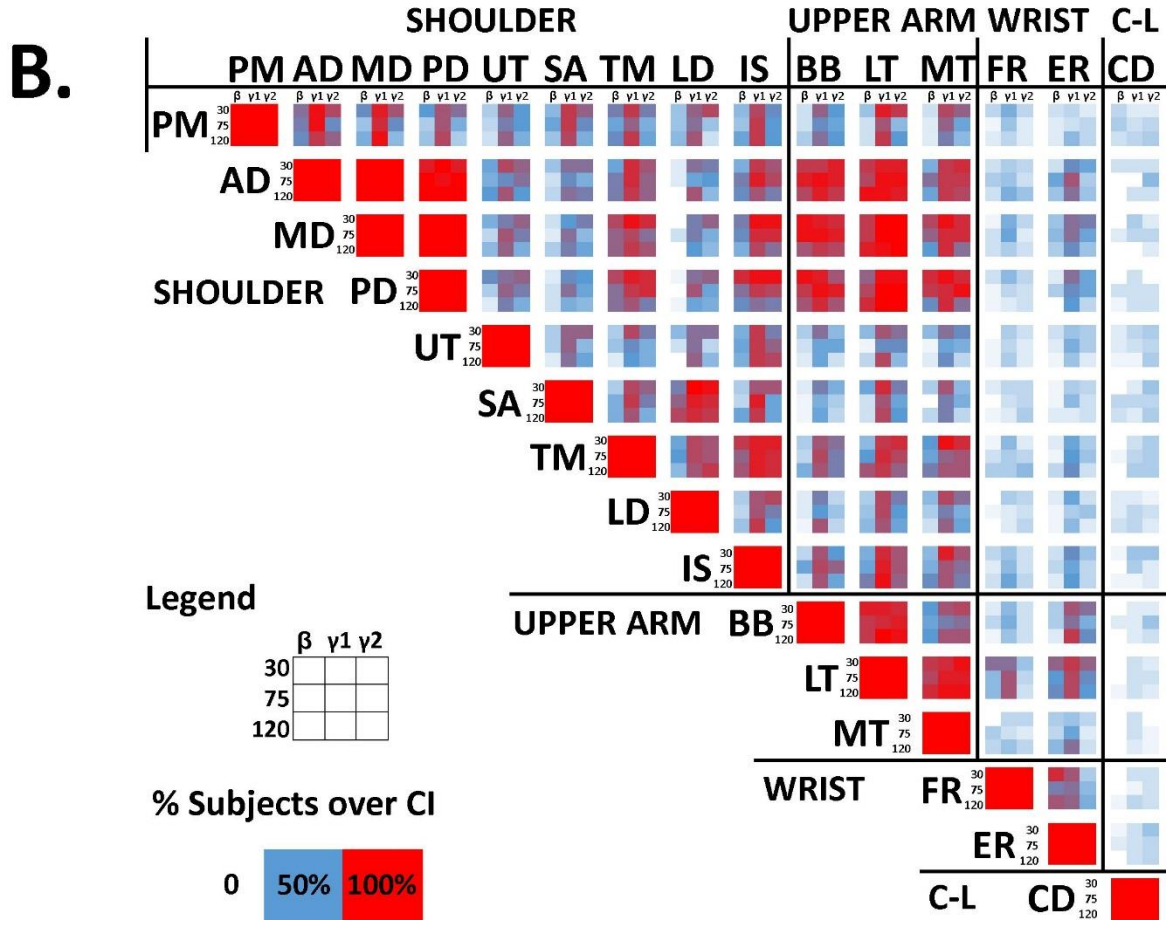
B.
SHOULDER
UPPER ARM
WRIST
C-L
PM AD MD PD UT SA TM LD IS
BB LT MT
FR ER
CD
β γ1 γ2
30 75 120
SHOULDER
UPPER ARM
WRIST
C-L
Legend
β γ1 γ2
30
75
120
% Subjects over CI
0
50%
100%

Figure 4.10. Matrices of coherence between muscle pairs during ADD task, compared across angles. **A.** Group mean peak coherence measured between 20-35, 35-60 and 60-100 Hz (FFT size 1024). Data are from five 5 s trials per subject (*n* = 21). **B.** Percentage of subjects (*n* = 21) where the peak was above the 95% confidence interval as defined by Halliday et al. (1989). For each muscle pair there are 9 squares. As shown in the legends, columns correspond to different frequency bands and rows correspond to different angles. References for the colour intensity are shown in the legends. C-L – contralateral.

Axial-axial correlations (TM-IS) were high across angles (***figure 4.11A***). Half-widths varied between 5 ms and 10 ms across angles (***figure 4.11B***).

ii. Shoulder-Upper arm interactions

Coherence

Shoulder abductor-elbow flexor coherence (AD and MD to -BB) was highest in the beta and low gamma band, especially at 30° and 75° (***figure 4.10A***). At least 70% of subjects showed significant coherence across angles and bands (***figure 4.10B***).

Shoulder abductor-elbow extensor coherence (AD, MD, and PD to -LT) was mainly in the low and high gamma band (***figure 4.10A***). At least 90% of subjects showed significant coherence across angles and bands (***figure 4.10B***).

Axial-elbow extensor coherence (IS-LT) was mainly in the low gamma band (***figure 4.10A***). At least 85% of subjects showed significant coherence in the low and high gamma band across angles (***figure 4.10B***).

Cross-Correlation

Shoulder abductor-elbow flexor correlations (AD and MD to -BB) were high at 75° and 120° (AD-BB) and 30° and 75° (MD-BB, ***figure 4.11A***). Half-widths were in the 10 ms window for at least 75% subjects (***figure 4.11B***).

Shoulder abductor-elbow extensor correlations (deltoids-LT) were high across angles (***figure 4.11A***). Half-widths varied between 5 ms and 10 ms across angles (***figure 4.11B***).

Axial-elbow extensor correlations (IS-LT) were moderate and unchanged across angles (***figure 4.11A***). At 30°, half-widths were in between 5 and 10

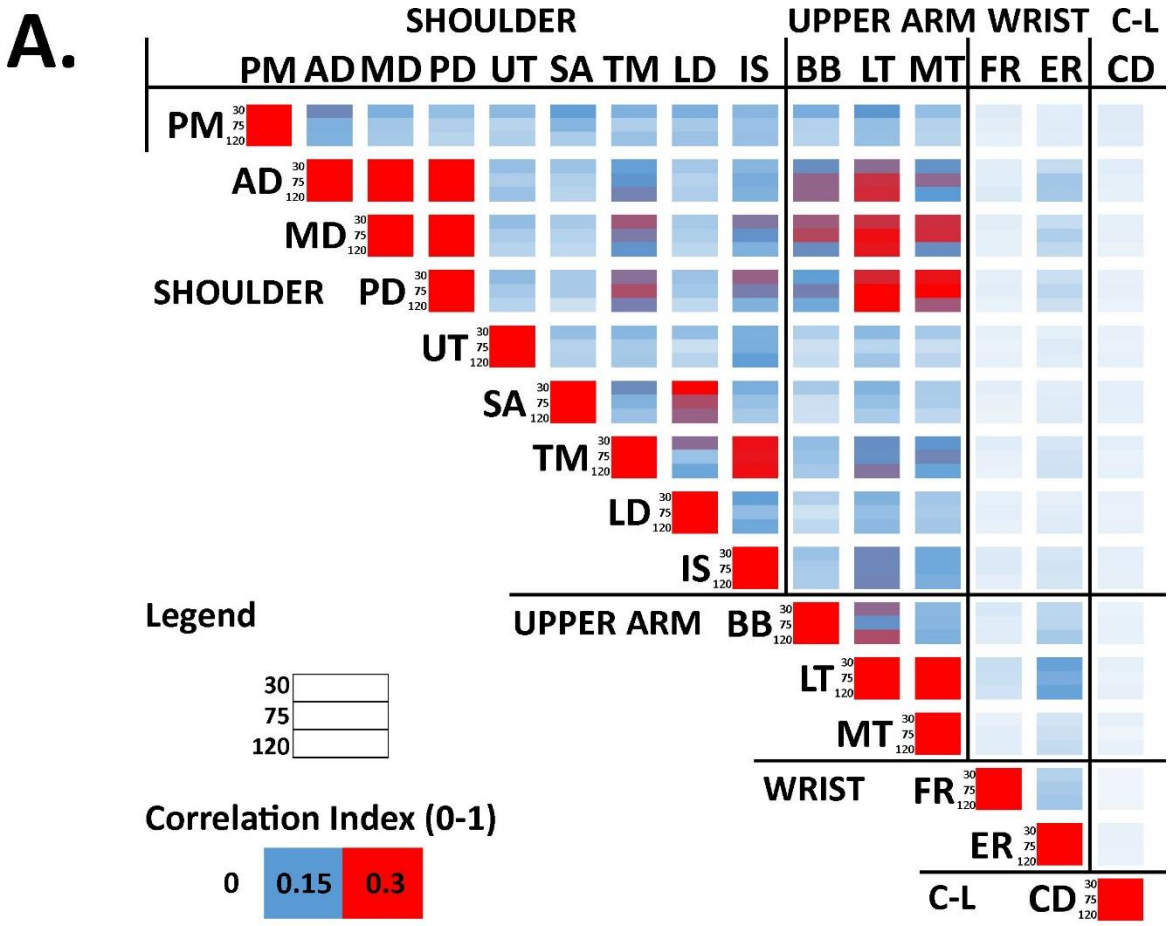
A.
SHOULDER
UPPER ARM
WRIST
C-L
PM AD MD PD UT SA TM LD IS
BB LT MT
FR ER
CD
SHOULDER
UPPER ARM
WRIST
C-L
Legend
30
75
120
Correlation Index (0-1)
0
0.15
0.3

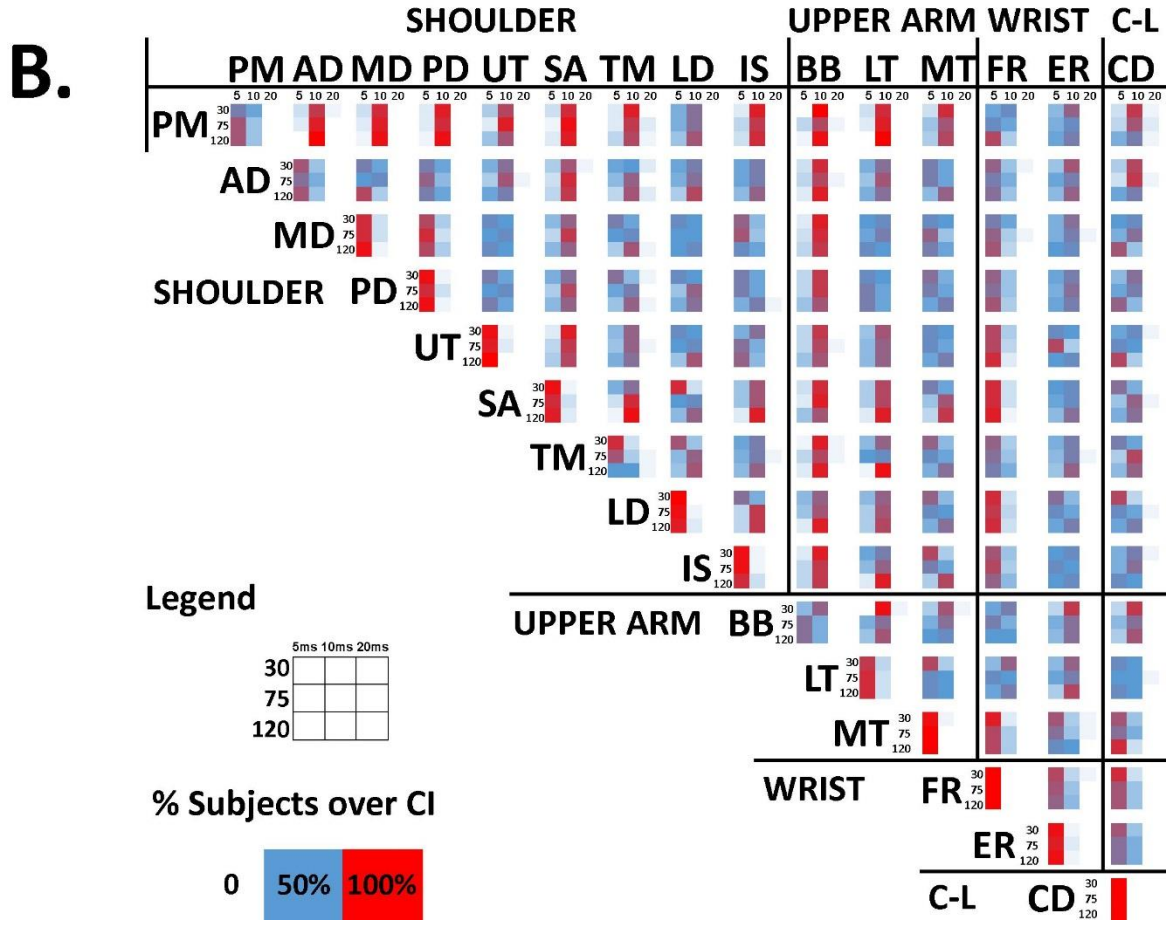
B.
SHOULDER
UPPER ARM
WRIST
C-L
PM AD MD PD UT SA TM LD IS
BB LT MT
FR ER
CD
5 10 20
SHOULDER
UPPER ARM
WRIST
C-L
Legend
5ms 10ms 20ms
30
75
120
% Subjects over CI
0
50%
100%

Figure 4.11. Matrices of cross-correlations between muscle pairs during ADD task, compared across angles. **A.** Group mean absolute peak correlation index. Data are from five 5 s trials per subject (*n* = 21). Legend shows rows corresponding to different angles and references for colour intensity **B.** Correlation half-widths. For each muscle pair there are 9 squares. Columns correspond to different half-widths (< 5 ms, 5-10 ms and 10-20 ms), and rows correspond to different angles. Colour intensity relates to the percentage of subjects (*n* = 21) where the half-width falls within that window. C-L – contralateral.

ms. At 75° and 120°, around 60% and 90% are in the 10 ms window respectively (***figure 4.11B***).

iii. Shoulder-Wrist interactions

Coherence

Moderate shoulder abductor-wrist extensor coherence (AD, MD, and PD to ER) was present in the low gamma band (***figure 4.10A***). Low gamma coherence was significant in 50-70% of the sample (***figure 4.10B***).

Cross-Correlation

Moderate shoulder abductor-wrist extensor correlations (AD, MD, and PD to ER) were present (***figure 4.11A***). Half-widths varied between 5 ms and 10 ms across angles (***figure 4.11B***).

iv. Shoulder-Contralateral interactions

Coherence

Shoulder-contralateral coherence was minimal (***figure 4.10A***).

Cross-Correlation

Shoulder-contralateral correlations were minimal (***figure 4.11A***).

v. Upper arm-Upper arm interactions

Coherence

Elbow flexor-elbow extensor coherence (BB-LT) was high in the gamma band across angles (***figure 4.10A***). Around 85% showed significant coherence across angles and bands (***figure 4.10B***).

Cross-Correlation

Elbow flexor-elbow extensor correlations (BB-LT) were highest at 30° and 120° (***figure 4.11A***). 50-95% of subjects had half-widths in the 10 ms window (***figure 4.11B***).

vi. Upper arm-Wrist interactions

Coherence

Elbow extensor-wrist extensor coherence (LT-ER) was high in the beta band (particularly at 30°) and low gamma band (***figure 4.10A***). At least 75% subjects showed significant coherence in the low gamma band across angles (***figure 4.10B***). At 30°, around 65% subjects showed significant coherence in the beta band (***figure 4.10B***).

Cross-Correlation

Elbow extensor-wrist extensor correlations (LT-ER) were highest at 30° and 120° (***figure 4.11A***). At 30° and 120°, at least 65% half-widths were in the 10 ms window. At 75°, half-widths varied between 5 ms and 10 ms (***figure 4.11B***).

vii. Upper arm-Contralateral interactions

Coherence

Upper arm-contralateral coherence was minimal (***figure 4.10A***).

Cross-Correlation

Upper arm-contralateral correlations were minimal (***figure 4.11A***).

viii. Wrist-Wrist interactions

Coherence

Wrist flexor-extensor coherence (FR-ER) was high in both the beta and low gamma band (***figure 4.10A***). At 30° and 120°, at least 70% subjects showed significant coherence in the beta and low gamma band (***figure 4.10B***). At 75°,

at least 55% of subjects showed significant coherence in the beta and low gamma band (***figure 4.10B***).

Cross-Correlation

Wrist flexor-extensor correlations (FR-ER) were moderate across angles (***figure 4.11A***). At least 65% subjects had half-widths in the 5 ms window (***figure 4.11B***).

ix. Wrist-Contralateral interactions

Coherence

Wrist-contralateral coherence was minimal (***figure 4.10A***).

Cross-Correlation

Wrist-contralateral correlations were minimal (***figure 4.11A***).

4.4.4.3 Maximum Voluntary Effort, Change with Posture (*figure 4.12* and *4.13*)

i. Shoulder-Shoulder interactions

Coherence

Abductor-abductor (AD, MD, PD) coherence was high across bands and angles except for AD-PD which was lower in the beta and high gamma band at 75° (***figure 4.12A***). Except for AD-PD at 75°, at least 90% of subjects showed significant coherence across angles and bands (***figure 4.12B***).

Adductor-abductor (PM to -AD, -MD and -PD) coherence was high across angles in the low gamma band (***figure 4.12A***). 60-90% of subjects showed significant coherence in the low gamma band across angles (***figure 4.12B***).

Adductor-adductor (SA-LD) coherence was high in the low gamma band across angles, and in the beta band at 75° (***figure 4.12A***). At least 65% subjects showed significant coherence across bands and angles (***figure 4.12B***).

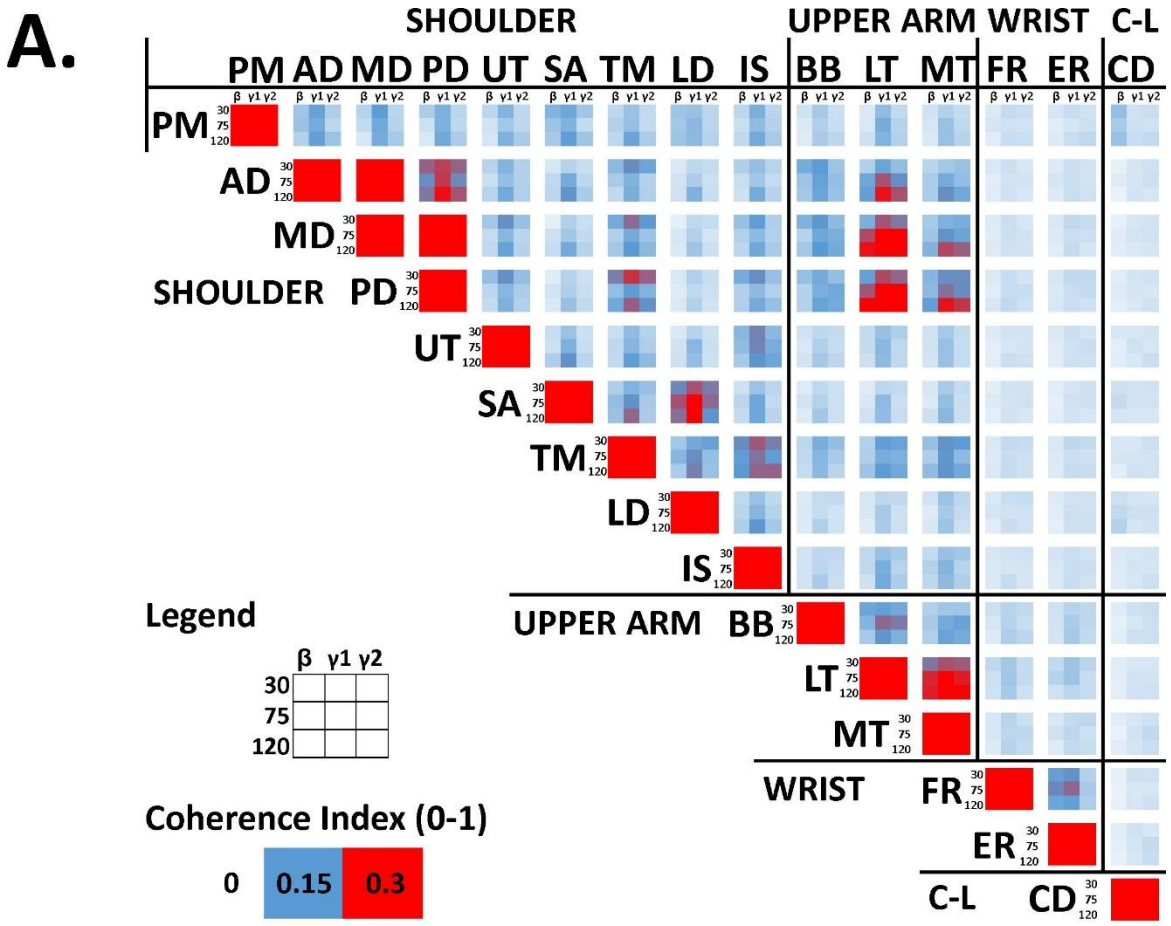
A.
SHOULDER
UPPER ARM
WRIST
C-L
PM AD MD PD UT SA TM LD IS
BB LT MT
FR ER
CD
β γ1 γ2
30 75 120
SHOULDER
UPPER ARM
WRIST
C-L
Legend
β γ1 γ2
30
75
120
Coherence Index (0-1)
0
0.15
0.3

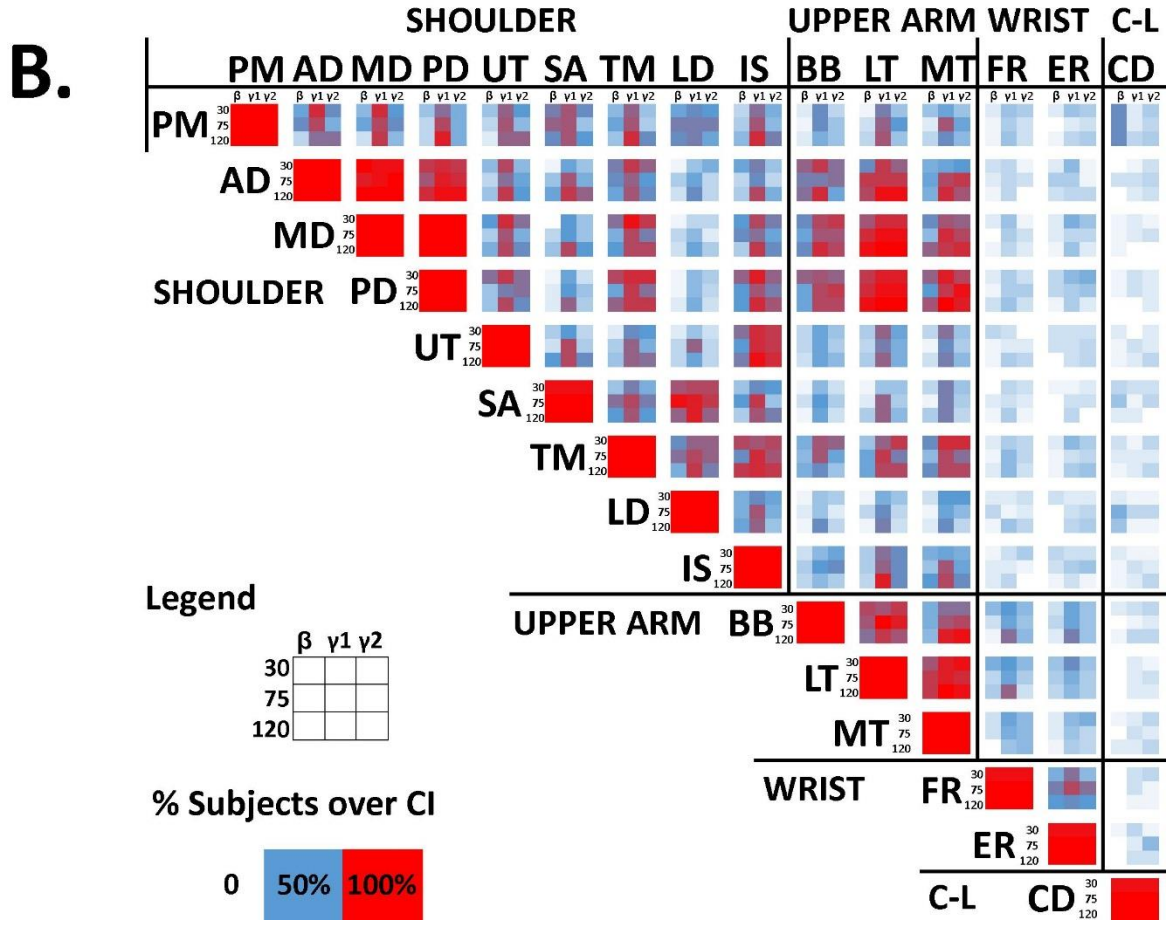
B.
SHOULDER
UPPER ARM
WRIST
C-L
PM AD MD PD UT SA TM LD IS
BB LT MT
FR ER
CD
β γ1 γ2
30 75 120
SHOULDER
UPPER ARM
WRIST
C-L
Legend
β γ1 γ2
30
75
120
% Subjects over CI
0
50%
100%

Figure 4.12. Matrices of coherence between muscle pairs during MVE task, compared across angles. **A.** Group mean peak coherence measured between 20-35, 35-60 and 60-100 Hz (FFT size 1024). Data are from five 5 s trials per subject (*n* = 21). **B.** Percentage of subjects (*n* = 21) where the peak was above the 95% confidence interval as defined by Halliday et al. (1989). For each muscle pair there are 9 squares. As shown in the legends, columns correspond to different frequency bands and rows correspond to different angles. References for the colour intensity are shown in the legends. C-L – contralateral.

Axial-axial coherence (TM-IS) coherence was present in the low gamma band at 30° and the low and high gamma band at 120° (***figure 4.12A***). With the exception of the beta band at 75°, at least 75% subjects showed significant coherence across bands and angles (***figure 4.12B***).

Cross-Correlation

Abductor-abductor correlations (AD, MD, PD) between all muscles (***figure 4.13A***). Half-widths for at least 85% of subjects were in the 5 ms window (***figure 4.13B***).

Adductor-abductor correlations (PM to -AD, -MD and -PD) were moderate across angles (***figure 4.13A***). At 30°, half-width was in the 10 ms window in around 75% of subjects. At 75° and 120°, half-widths varied between the 5 ms and 10 ms window (***figure 4.13B***).

Adductor-adductor correlations (SA-LD) were high across angles (f***igure 4.13A***). Half-widths were in the 10 ms window in around 85% subjects at 75° and 120° and 50/50 in the 5 and 10 ms window at 30°(***figure 4.13B***).

Axial-axial correlations (TM-IS) were high at 30° and 120° (***figure 4.13A***). At 30° and 75°, half-widths varied between the 5 ms and 10 ms window (***figure 4.13B***). At 120°, half-widths were in the 5 ms window in around 80% subjects (***figure 4.13B***).

ii. Shoulder-Upper arm interactions

Coherence

Shoulder abductor-elbow extensor coherence (deltoids-LT) increased in the low and high gamma band as angle increased (***figure 4.12A***). With the exception of the beta band at 30° for AD-LT, at least 65% subjects showed significant deltoids-LT coherence (***figure 4.12B***). MD and PD-MT coherence

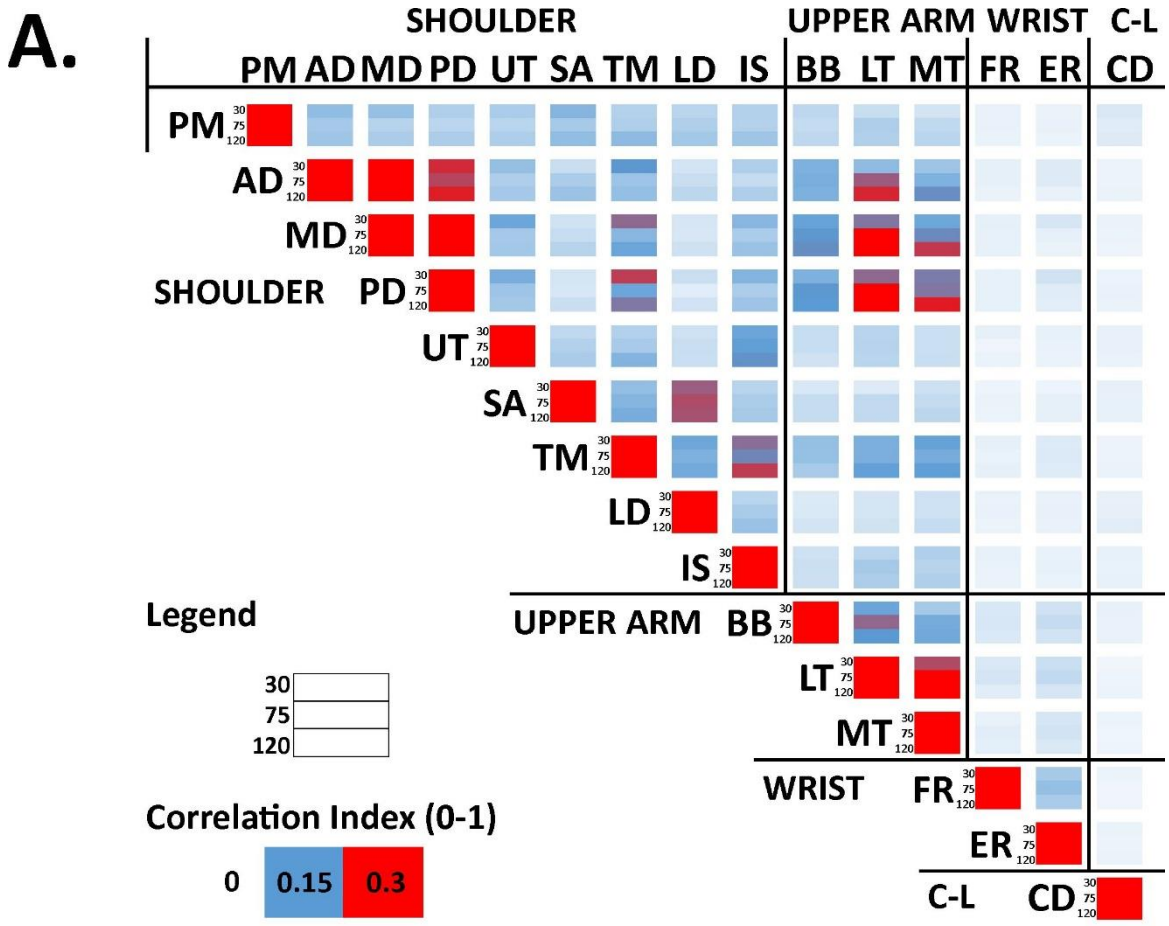
A.
SHOULDER
UPPER ARM
WRIST
C-L
PM AD MD PD UT SA TM LD IS
BB LT MT
FR ER
CD
Legend
30
75
120
Correlation Index (0-1)
0
0.15
0.3

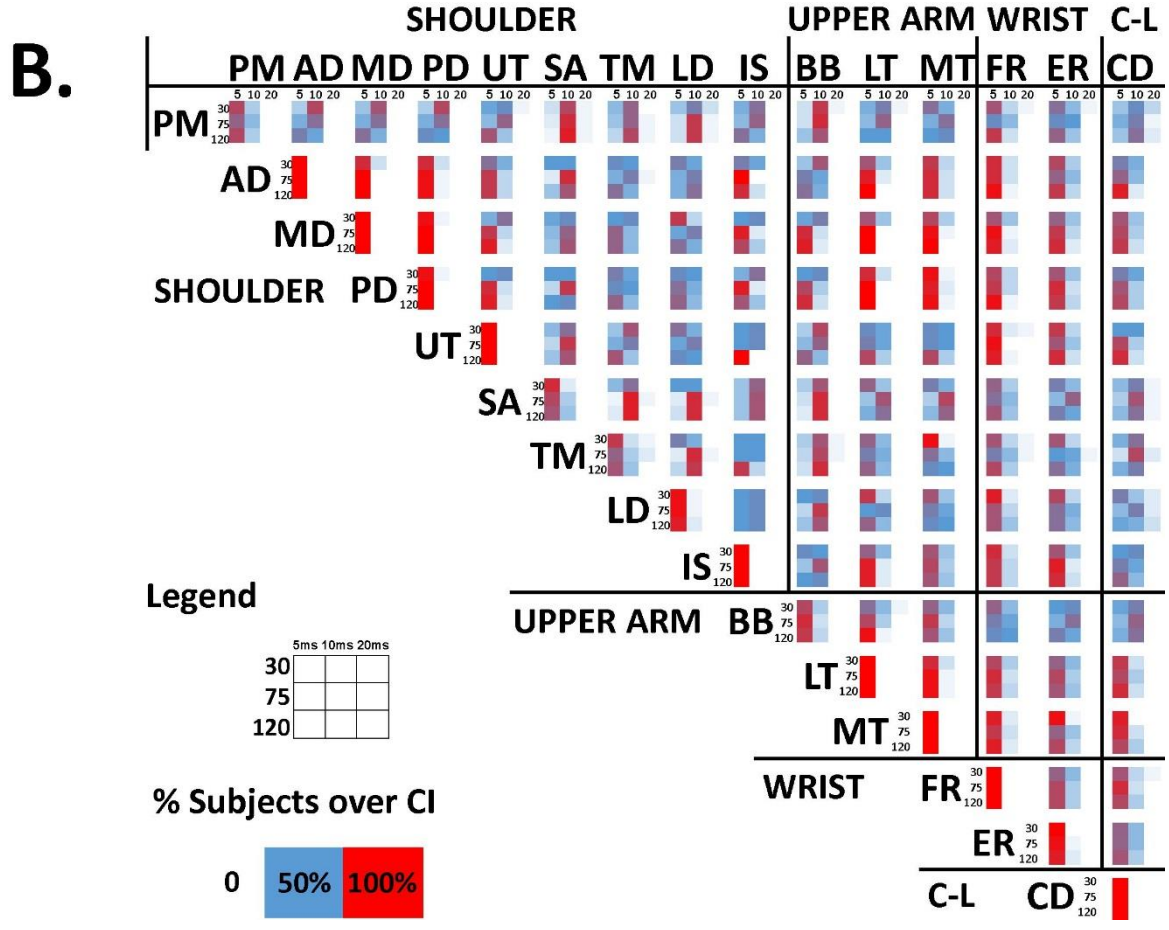
B.
SHOULDER
UPPER ARM
WRIST
C-L
PM AD MD PD UT SA TM LD IS
BB LT MT
FR ER
CD
Legend
5ms 10ms 20ms
30
75
120
% Subjects over CI
0
50%
100%

Figure 4.13. Matrices of cross-correlations between muscle pairs during MVE task, compared across angles. **A.** Group mean absolute peak correlation index. Data are from five 5 s trials per subject (*n* = 21). Legend shows rows corresponding to different angles and references for colour intensity **B.** Correlation half-widths. For each muscle pair there are 9 squares. Columns correspond to different half-widths (< 5 ms, 5-10 ms and 10-20 ms), and rows correspond to different angles. Colour intensity relates to the percentage of subjects (*n* = 21) where the half-width falls within that window. C-L – contralateral.

was high in both the low and high gamma band at 120° (***figure 4.12A***). At least 65% subjects showed significant coherence in the low and high gamma bands across angles (***figure 4.12B***).

Cross-Correlation

Shoulder abductor-elbow extensor correlations (deltoids-triceps brachii) increased as angle increased (***figure 4.13A***). Across angles, half-widths were in the 5 ms window for at least 70% subjects (***figure 4.13B***).

iii. Shoulder-Wrist interactions

Coherence

Shoulder-wrist coherence was minimal (***figure 4.12A***).

Cross-Correlation

Shoulder-wrist correlations were minimal (***figure 4.13A***).

iv. Shoulder-Contralateral interactions

Coherence

Shoulder-contralateral coherence was minimal (***figure 4.12A***).

Cross-Correlation

Shoulder-contralateral correlations were minimal (***figure 4.13A***).

v. Upper arm-Upper arm interactions

Coherence

Elbow flexor-extensor coherence (BB to -LT and -MT) was low except BB-LT at 75° in the low and high gamma bands (***figure 4.12A***). At least 60% subjects showed significant BB-LT coherence across bands and angles (***figure 4.12B***).

Elbow extensor-extensor coherence (LT-MT) was high except in the beta band at 30° (***figure 4.12A***). At least 60% of subjects showed significant coherence across bands and angles (***figure 4.12B***).

Cross-Correlation

Elbow flexor-extensor correlations were low except BB-LT at 75° (***figure 4.13A***). Half-widths varied between the 5 ms and 10 ms window (***figure 4.13B***), except at 120° where around 95% were in the 5 ms window.

Elbow extensor-extensor correlations were high across angles (***figure 4.13A***). Half-widths were in the 5 ms window in at least 85% of subjects.

vi. Upper arm-Wrist interactions

Coherence

Upper arm-wrist coherence (BB, LT, MT to -FR and -ER) was minimally present, mainly in the low gamma band (***figure 4.12A***). 30-60% subjects showed significance in the low gamma band between upper arm and wrist muscles (***figure 4.12B***).

Cross-Correlation

Upper arm-wrist correlations were low (***figure 4.13A***). Upper arm flexor-wrist half-widths were divided between the 5 and 10 ms time window. Upper arm extensor-wrist half-widths were in the 5 ms time window for at least 65% subjects (***figure 4.13B***).

vii. Upper arm-Contralateral interactions

Coherence

Upper arm-contralateral coherence was minimal (***figure 4.12A***).

Cross-Correlation

Upper arm-contralateral correlations were minimal (***figure 4.13A***).

viii. Wrist-Wrist interactions

Coherence

Wrist flexor-extensor coherence was mainly in the beta and low gamma band (***figure 4.12A***). At least 55% subjects showed significant coherence in the low gamma band at 30° and all bands at 75° (***figure 4.12B***).

Cross-Correlation

Wrist flexor-extensor correlations were moderate across angles (***figure 4.13A***). Half-widths were 5 ms for at least 65% subjects (***figure 4.13B***).

ix. Wrist-Contralateral interactions

Coherence

Wrist-contralateral coherence was minimal (***figure 4.12A***).

Cross-Correlation

Wrist-contralateral correlations were minimal (***figure 4.13A***).

4.4.5 Muscle interactions - Task Differences

4.4.5.1 30°, Change with Task (*figure 4.14* and *4.15*)

i. Shoulder-Shoulder interactions

Coherence

Abductor-abductor coherence (AD, MD, PD) was high in all bands across tasks except for AD-PD during ABD in the beta band (***figure 4.14A***). Except

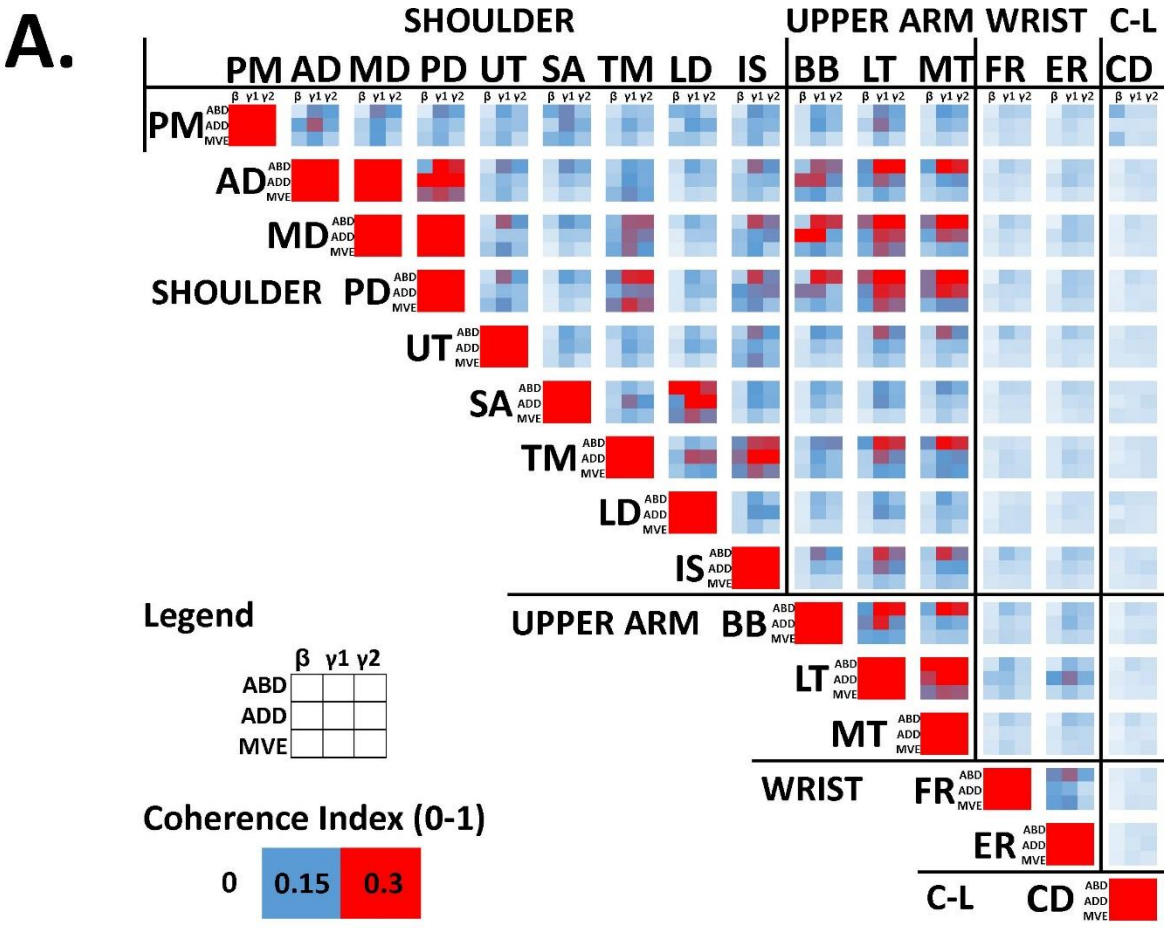
A.
SHOULDER
UPPER ARM
WRIST
C-L
PM AD MD PD UT SA TM LD IS
BB LT MT
FR ER
CD
β γ1 γ2
ABD
ADD
MVE
Legend
Coherence Index (0-1)
0
0.15
0.3

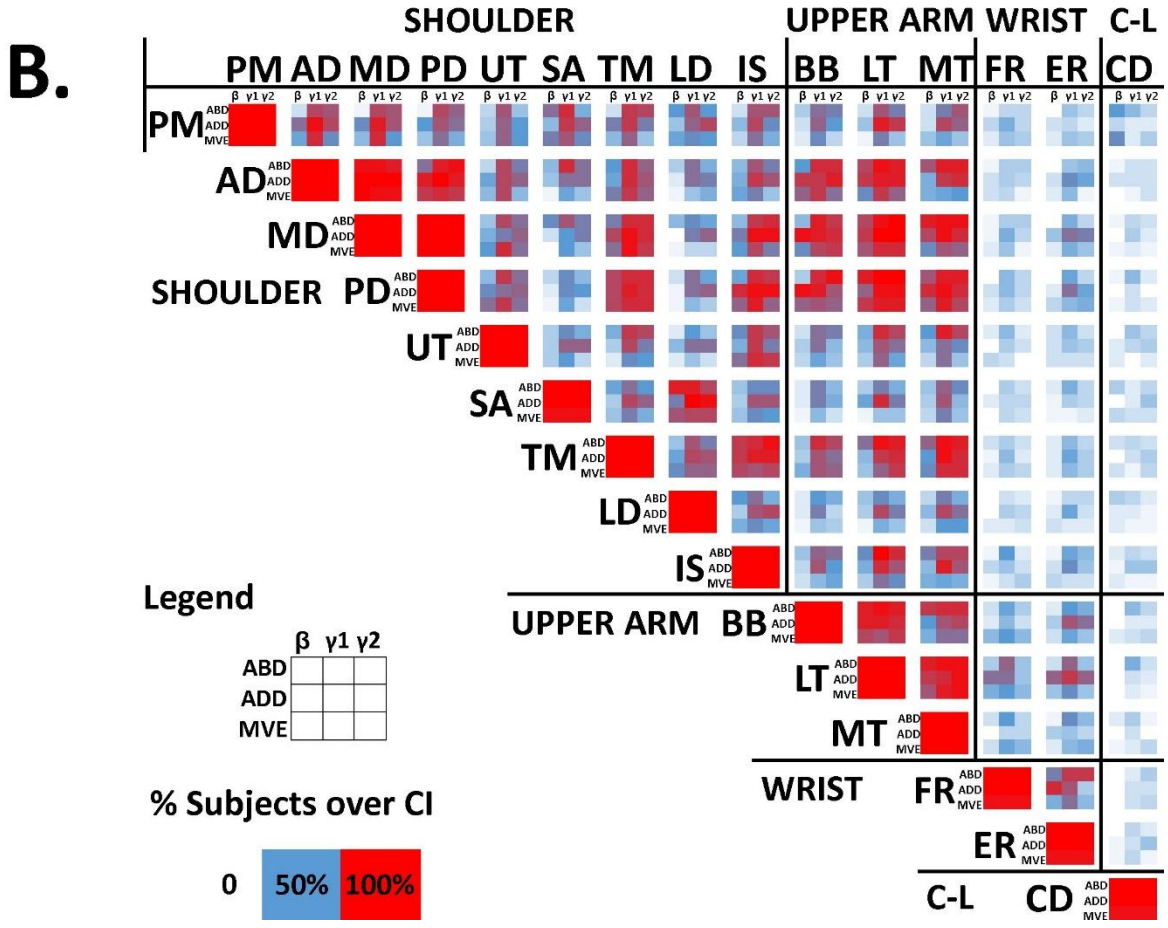
B.
SHOULDER
UPPER ARM
WRIST
C-L
PM AD MD PD UT SA TM LD IS
BB LT MT
FR ER
CD
β γ1 γ2
ABD
ADD
MVE
Legend
% Subjects over CI
0
50%
100%

Figure 4.14. Matrices of coherence between muscle pairs at 30°, compared across tasks. **A.** Group mean peak coherence measured between 20-35, 35-60 and 60-100 Hz (FFT size 1024). Data are from five 5 s trials per subject (*n* = 21). **B.** Percentage of subjects (*n* = 21) where the peak was above the 95% confidence interval as defined by Halliday et al. (1989). For each muscle pair there are 9 squares. As shown in the legends, columns correspond to different frequency bands and rows correspond to different tasks. References for the colour intensity are shown in the legends. C-L – contralateral.

for the beta band during ABD, at least 80% subjects showed significant coherence across tasks and bands (***figure 4.14B***).

Adductor-abductor coherence (PM-AD) was high in both the high and low gamma band across all tasks. Beta band coherence was only present during ADD (***figure 4.14A***). At least 75% of subjects showed significant coherence in the low gamma band during MVE and ABD, and high gamma during ABD. During ADD, approximately 60% subjects showed significant coherence in the beta band (***figure 4.14B***).

Adductor-adductor coherence (SA-LD) was high across bands during ABD but only in the low gamma during MVE, and both low and high gamma during ADD (***figure 4.14A***). Except for the beta band during ADD, at least 70% of subjects showed significant coherence in across bands and tasks (***figure 4.14B***).

Abductor-axial coherence (PD-TM) was present in the high and low gamma bands during ABD and MVE but not ADD (***figure 4.14A***). At least 75% subjects showed significant PD-TM coherence in the beta band, and at least 85% in the low high gamma band in all tasks (***figure 4.14B***).

Cross-Correlation

Abductor-abductor correlations (MD, AD, PD) were high across tasks (***figure 4.15A***). During ABD and MVE, half widths were in the 5 ms window for at least 85% of subjects (***figure 4.15B***). During ADD, half-widths were divided between 5 ms and 10 ms (***figure 4.15B***).

Adductor-abductor correlations (PM-AD) were highest during ADD (***figure 4.15A***). During ADD and MVE, half-widths were in the 10 ms window in at least 75% of subjects. During ABD, half-widths were divided between the 5 and 10 ms window across subjects (***figure 4.15B***).

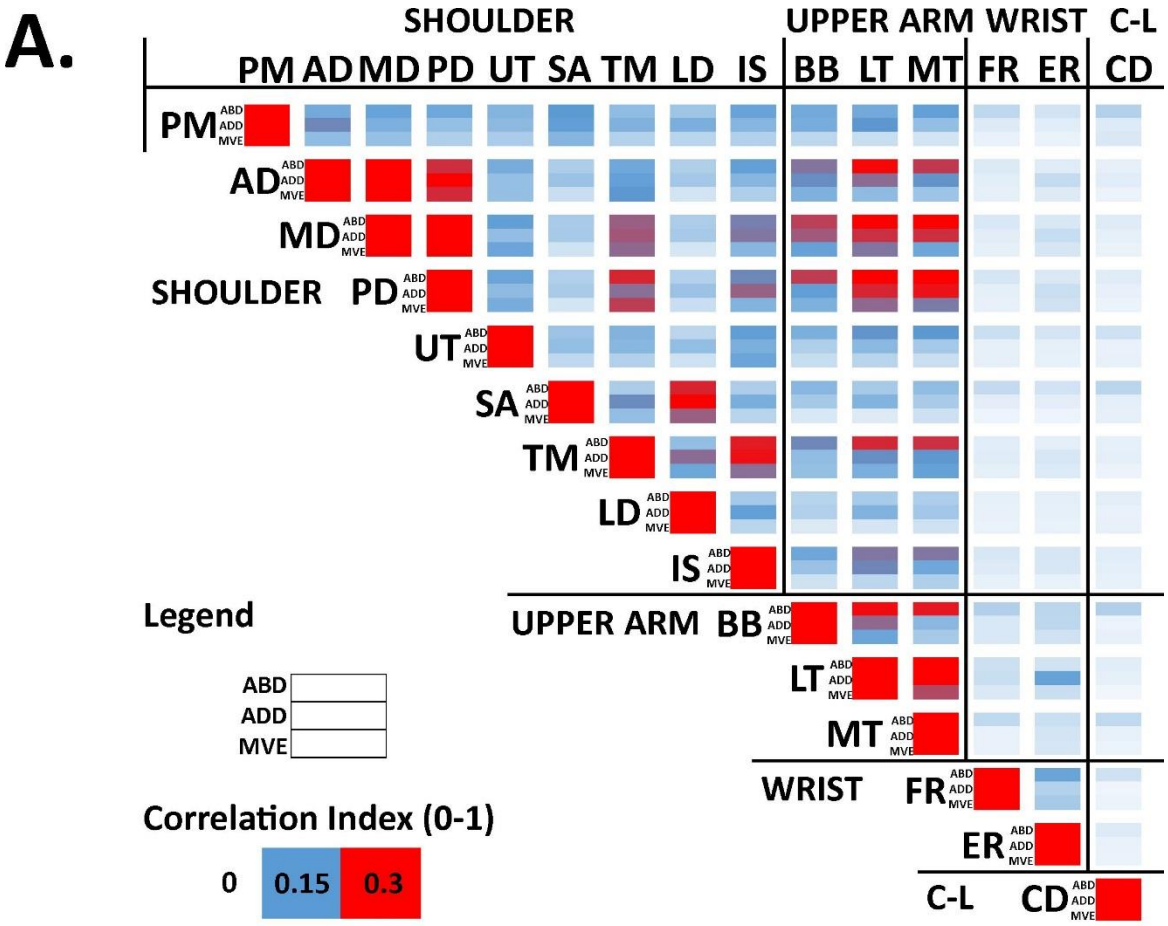
A.
SHOULDER
UPPER ARM
WRIST
C-L
PM AD MD PD UT SA TM LD IS
BB LT MT
FR ER
CD
ABD
ADD
MVE
Legend
ABD
ADD
MVE
Correlation Index (0-1)
0
0.15
0.3

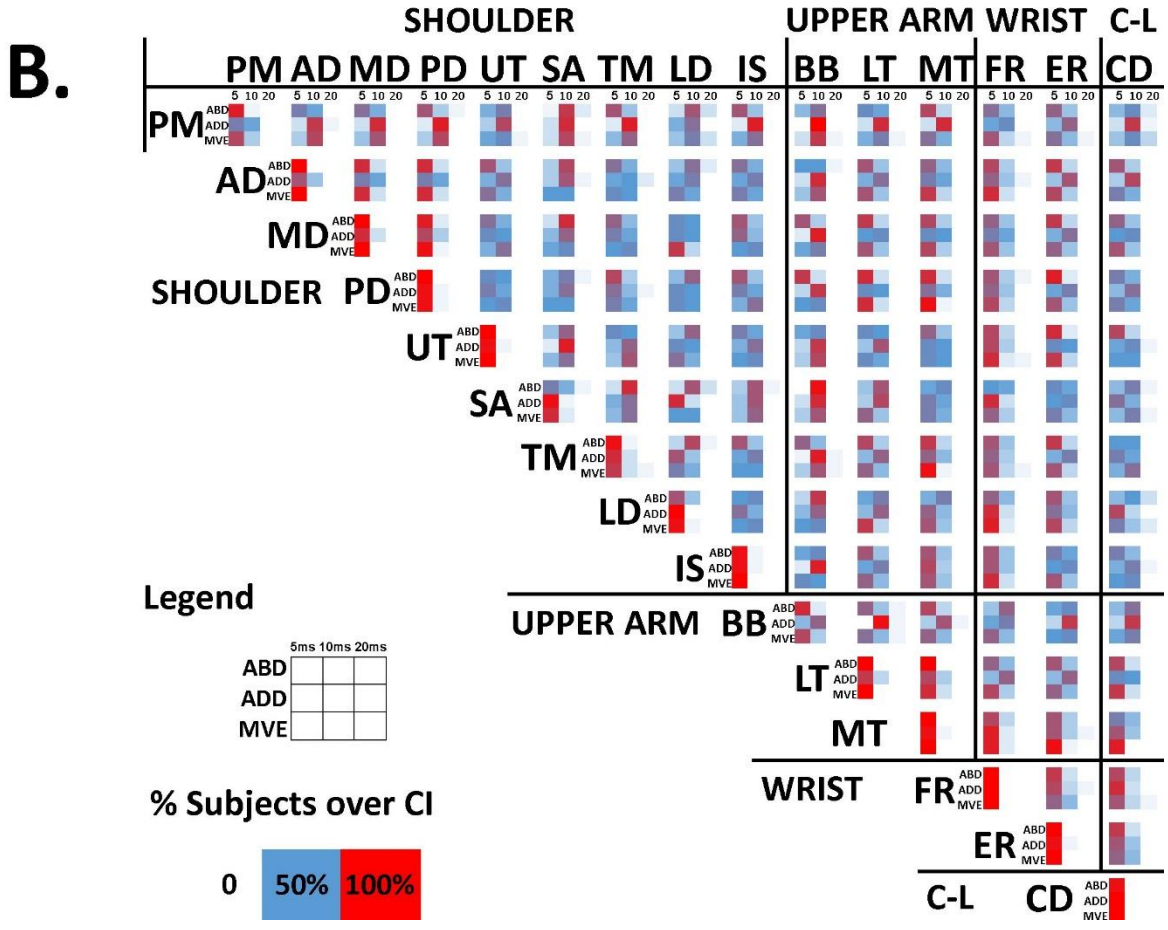
B.
SHOULDER
UPPER ARM
WRIST
C-L
PM AD MD PD UT SA TM LD IS
BB LT MT
FR ER
CD
5 10 20
ABD
ADD
MVE
Legend
5ms 10ms 20ms
ABD
ADD
MVE
% Subjects over CI
0
50%
100%

Figure 4.15. Matrices of cross-correlations between muscle pairs at 30°, compared across tasks. **A.** Group mean absolute peak correlation index. Data are from five 5 s trials per subject (*n* = 21). Legend shows rows corresponding to different tasks and references for colour intensity **B.** Correlation half-widths. For each muscle pair there are 9 squares. Columns correspond to different half-widths (< 5 ms, 5-10 ms and 10-20 ms), and rows correspond to different tasks. Colour intensity relates to the percentage of subjects (*n* = 21) where the half-width falls within that window. C-L – contralateral.

Adductor-adductor correlations (SA-LD) were high across tasks. Half-widths were in the 10 ms window during ABD for around 70% of subjects, 5 ms window during ADD for around 85% of subjects, and subjects were divided between 5 and 10 ms during MVE (***figure 4.15B***).

Abductor-axial correlations (PD-TM) were high during ABD and MVE but not ADD (***figure 4.15A***). Half-widths were in the 5 ms window during ABD for around 75% of subjects, and divided between 5 and 10 ms during ADD and MVE (***figure 4.15B***).

ii. Shoulder-Upper arm interactions

Coherence

Shoulder abductor-elbow flexor coherence (MD-BB) was high in both the low and high gamma band during ABD, the beta and low gamma band during ADD, and minimal during MVE (***figure 4.14A***). At least 65% subjects showed significant coherence in the low and high gamma bands during ABD and MVE, and across all bands during ADD (***figure 4.14B***).

Axial-elbow extensor coherence (TM-MT) was high across bands during ABD, and in low and high gamma bands during ADD and MVE (***figure 4.14A***). At least 85% subjects showed significant coherence in the low and high gamma band during ADD and MVE, and around 65% beta band during ABD (***figure 4.14B***).

Cross-Correlation

Shoulder abductor-elbow flexor (MD-BB) correlations were high during ABD and ADD but not MVE (***figure 4.15A***). Half-widths were in the 5 ms window for around 70% subjects during ABD, 10 ms window for around 90% subjects

during ADD, and divided between the 5 and 10 ms window during MVE (***figure 4.15B***).

Axial-elbow extensor correlations (TM-MT) were high during ABD and moderate during ADD and MVE (***figure 4.15A***). Half-widths were in the 5 ms window for around 80% of subjects during ABD, in the 10 ms window in around 65% during ABD and over 90% in the 5 ms window during MVE.

iii. Shoulder-Wrist interactions

Coherence

Shoulder abductor-wrist extensor coherence (MD-ER) was moderate in the low and high gamma during ABD and ADD (***figure 4.14A***). Around 50% of subjects showed significant coherence in the low gamma band during ABD, and 25-60% subjects showed significant coherence across bands during ADD (***figure 4.14B***).

Cross-Correlation

Shoulder abductor-wrist extensor correlations (MD-ER) were moderate during ADD (***figure 4.15A***). Half-widths were in the 5 ms time window during ABD and MVE in at least 65% subjects, and divided between the 5 and 10 ms time window during ADD (***figure 4.15B***).

iv. Shoulder-Contralateral interactions

Coherence

Shoulder adductor-contralateral abductor coherence (PM-CD) was present in the beta band during ABD and MVE (***figure 4.14A***). This was significant in around 50% subjects (***figure 4.14B***)

Cross-Correlation

Shoulder adductor-contralateral abductor correlations were present but low during ABD (***figure 4.15A***). Half-widths were divided between 5 and 10 ms time windows (***figure 4.15B***).

v. Upper arm-Upper arm interactions

Coherence

Elbow flexor-extensor coherence (BB-MT) was present across bands during ABD but only in the low and high gamma during ADD and MVE (***figure 4.14A***). At least 80% of subjects showed significant coherence in all bands during ABD, at least 70% in low and high gamma during ADD, and at least 60% in the low and high gamma during MVE (***figure 4.14B***).

Cross-Correlation

Elbow flexor-extensor correlations (BB-MT) were highest in ABD then ADD then MVE (***figure 4.15A***). Half-widths were in the 5 ms time window during ABD and MVE, and the 10 ms time window during ADD for at least 65% participants (***figure 4.15B***).

vi. Upper arm-Wrist interactions

Coherence

Elbow-wrist extensor coherence (LT-ER) was high across all bands during ADD, and in the low gamma band during ABD and MVE and (***figure 4.14A***). Significant coherence was present in at least 65% subjects in the low gamma band during ABD and at least 65% of subjects across all bands during ADD (***figure 4.14B***). Significant coherence was seen in around 50% of subjects in the low gamma band during MVE (***figure 4.14B***).

Cross-Correlation

Elbow-wrist extensor correlations (LT-ER) were high during ADD (***figure 4.15A***). For at least 65% of subjects, half-widths were in the 5 ms time window during ABD and MVE, and the 10 ms time window during ADD (***figure 4.15B***).

vii. Upper arm-Contralateral interactions

Coherence

Upper arm-contralateral coherence was minimal (***figure 4.14A***).

Cross-Correlation

Upper arm-contralateral correlations were minimal (***figure 4.15A***).

viii. Wrist-Wrist interactions

Coherence

Wrist flexor-extensor coherence (FR-ER) was high in all bands during ABD and in the beta and low gamma band during ADD and MVE (***figure 4.14A***). Around 80% subjects showed significant coherence in the low and high gamma band during ABD, at least 70% of subjects in the beta and low gamma band during ADD, and at least 60% in the low gamma band during MVE (***figure 4.14B***).

Cross-Correlation

Wrist flexor-extensor correlations (FR-ER) were highest during ABD (***figure 4.15A***). Half-widths were in the 5 ms time window across tasks for at least 65% of subjects (***figure 4.15B***).

ix. Wrist-Contralateral interactions

Coherence

Wrist-contralateral coherence was minimal (***figure 4.14A***).

Cross-Correlation

Wrist-contralateral correlations were minimal (***figure 4.15A***).

4.4.5.2 75°, Change with Task (*figure 4.16* and *4.17*)

i. Shoulder-Shoulder interactions

Coherence

Abductor-abductor coherence (AD, MD, PD) was high across bands and tasks, except AD-PD. AD-PD coherence was high both the low and high gamma band during ABD, in all bands during ADD, and the low gamma band during MVE (***figure 4.16A***). At least 60% of subjects showed significant

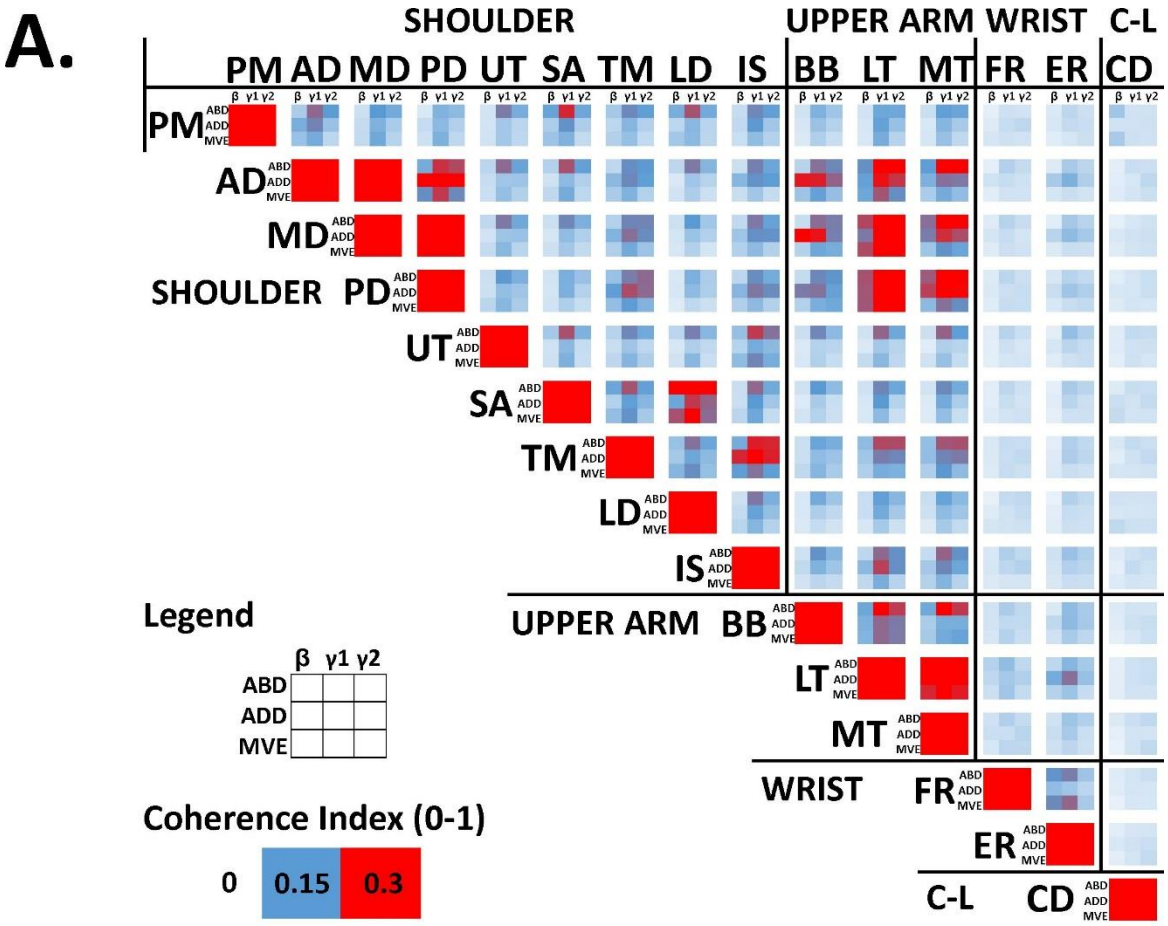
A.
SHOULDER
UPPER ARM
WRIST
C-L
PM AD MD PD UT SA TM LD IS
BB LT MT
FR ER
CD
β γ1 γ2
ABD
ADD
MVE
Legend
Coherence Index (0-1)
0
0.15
0.3

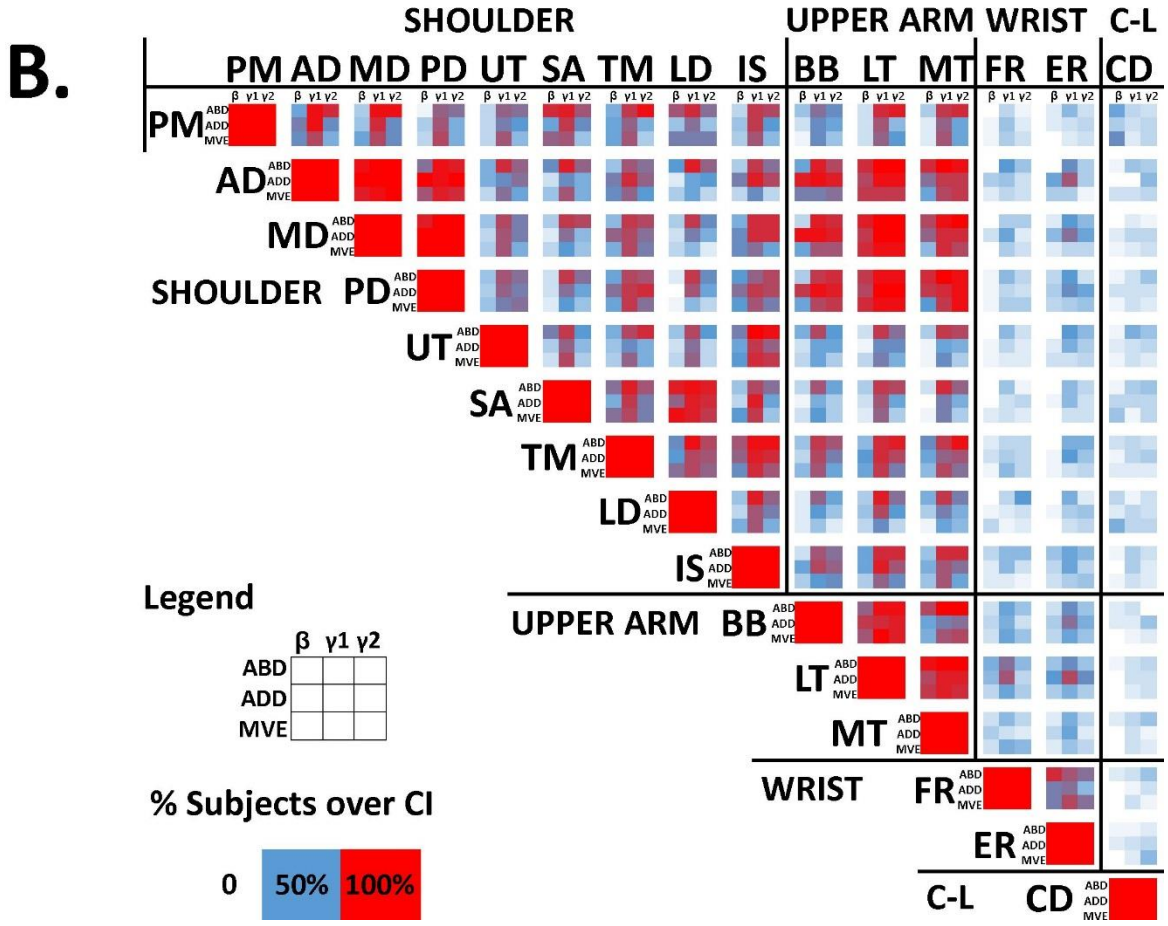
B.
SHOULDER
UPPER ARM
WRIST
C-L
PM AD MD PD UT SA TM LD IS
BB LT MT
FR ER
CD
β γ1 γ2
ABD
ADD
MVE
Legend
% Subjects over CI
0
50%
100%

Figure 4.16. Matrices of coherence between muscle pairs at 75°, compared across tasks. **A.** Group mean peak coherence measured between 20-35, 35-60 and 60-100 Hz (FFT size 1024). Data are from five 5 s trials per subject (*n* = 21). **B.** Percentage of subjects (*n* = 21) where the peak was above the 95% confidence interval as defined by Halliday et al. (1989). For each muscle pair there are 9 squares. As shown in the legends, columns correspond to different frequency bands and rows correspond to different tasks. References for the colour intensity are shown in the legends. C-L – contralateral.

coherence in the beta band during ADD and MVE. In all other tasks and bands, at least 85% of subjects showed significant coherence (***figure 4.16B***).

Adductor-abductor coherence (PM-AD) was high in both the low and high gamma band during ABD, the beta and low gamma band during ADD, and the low gamma band during MVE (***figure 4.16A***). At least 85% of subjects showed significant PM-AD coherence in the low and high gamma band during ABD and at least 65% the low gamma band during ADD and MVE (***figure 4.16B***).

Adductor-adductor coherence (SA-LD) was high in all bands during ABD and MVE and during the low and high gamma during ADD (***figure 4.16A***). At least 65% subjects showed significant coherence across all tasks and bands (***figure 4.16B***).

Cross-Correlation

Abductor-abductor correlations (AD, MD, PD) were high across tasks (***figure 4.17A***). During ABD and MVE, half-widths were in the 5 ms window in all subjects. During ADD, half-widths were divided between the 5 and 10 ms window (***figure 4.17B***).

Adductor-abductor correlations (PM-AD) were highest during the ABD, then ADD, then MVE (***figure 4.17A***). During the ABD, at least 70% of half-widths were in the 5 ms time window. During ADD and MVE, at least 60% half-widths were in the 10 ms time window (***figure 4.17B***).

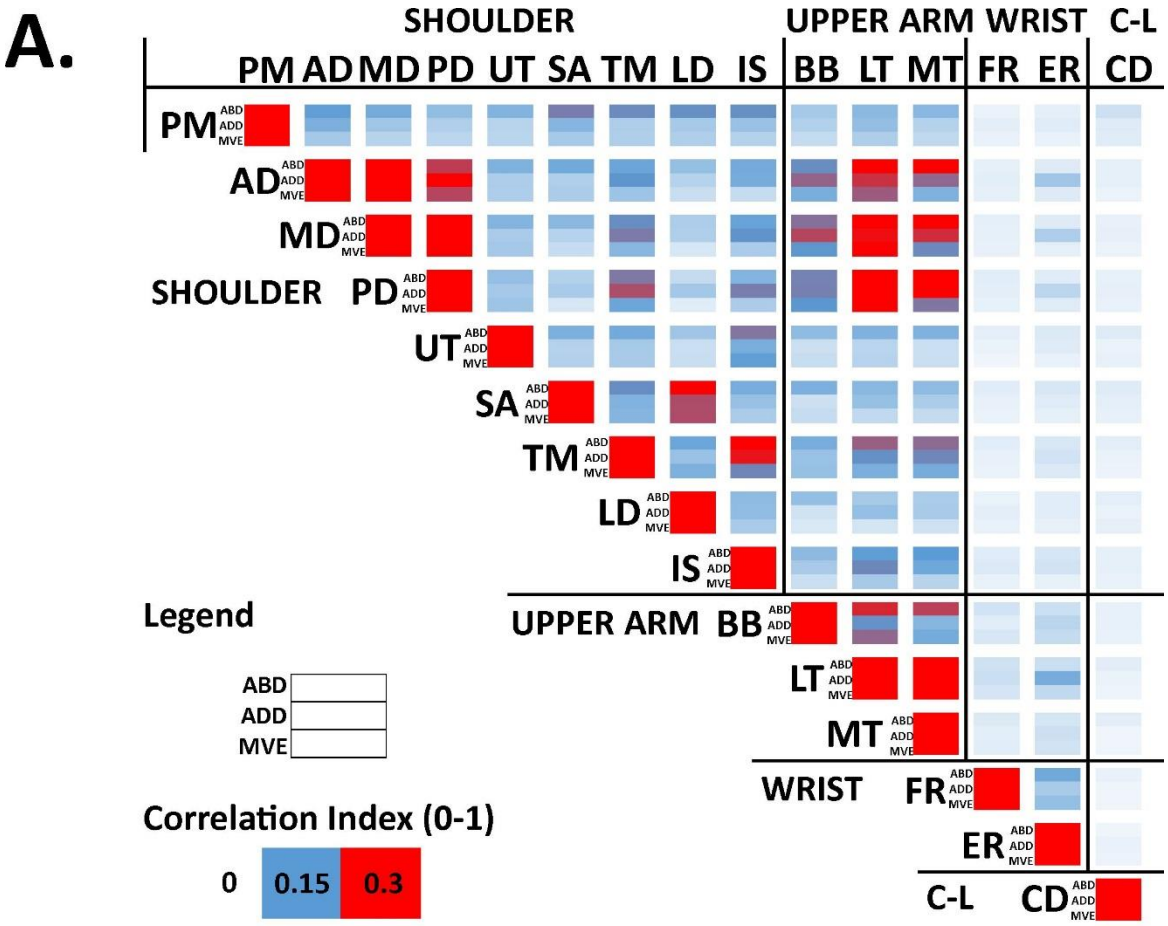
A.
SHOULDER
UPPER ARM
WRIST
C-L
PM AD MD PD UT SA TM LD IS
BB LT MT
FR ER
CD
ABD
ADD
MVE
Legend
Correlation Index (0-1)
0
0.15
0.3

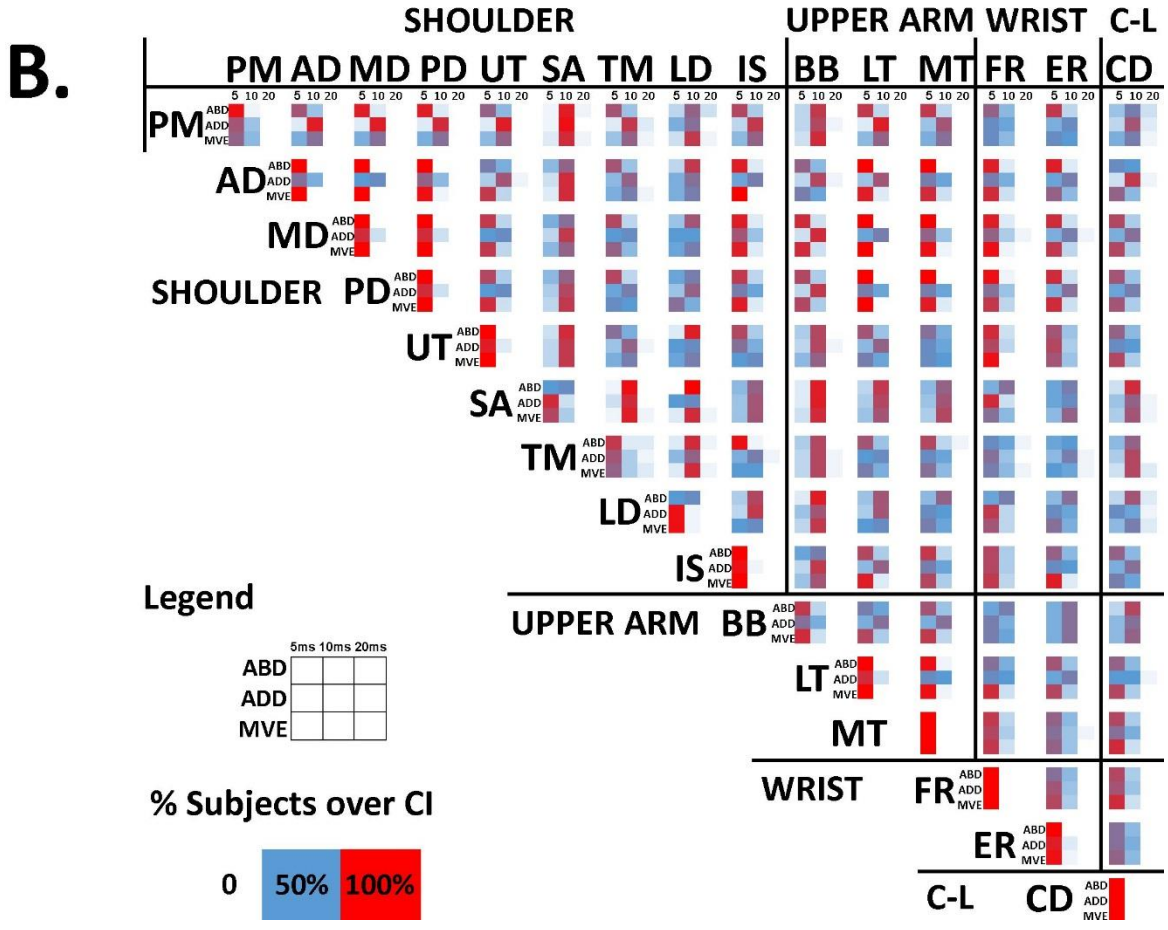
B.
SHOULDER
UPPER ARM
WRIST
C-L
PM AD MD PD UT SA TM LD IS
BB LT MT
FR ER
CD
5 10 20
5ms 10ms 20ms
ABD
ADD
MVE
Legend
% Subjects over CI
0
50%
100%

Figure 4.17. Matrices of cross-correlations between muscle pairs at 75°, compared across tasks. **A.** Group mean absolute peak correlation index. Data are from five 5 s trials per subject (*n* = 21). Legend shows rows corresponding to different tasks and references for colour intensity **B**. Correlation half-widths. For each muscle pair there are 9 squares. Columns correspond to different half-widths (< 5 ms, 5-10 ms and 10-20 ms), and rows correspond to different tasks. Colour intensity relates to the percentage of subjects (*n* = 21) where the half-width falls within that window. C-L – contralateral.

ii. Shoulder-Upper arm interactions

Coherence

Shoulder abductor-elbow flexor coherence (MD-BB) is high in both the low and high gamma band during ABD and MVE and the beta and low gamma band during ADD (***figure 4.16A***). Significant coherence was present in the low and high gamma bands in at least 75% subjects during ABD, at least 55% of subjects during MVE. At least 90% of subjects were significant for all bands during ADD (***figure 4.16B***).

Shoulder abductor-elbow extensor coherence (MD-LT) is high across tasks and bands with the exception the beta band during ADD (***figure 4.16A***). At least 90% of subjects show significant coherence in all bands and tasks (***figure 4.16B***).

Cross-Correlation

Shoulder abductor-elbow flexor correlations (MD-BB) were high during ADD (***figure 4.17A***). Half-widths were in the 5 ms window during ABD and MVE and in the 10 ms time window during ADD in around 85% subjects (***figure 4.17B***).

Shoulder abductor-elbow extensor correlations (MD-LT) were high during all tasks (***figure 4.17A***). Half-widths were in the 5 ms window during ABD and MVE in all subjects and divided between the 5 and 10 ms time window during ADD (***figure 4.17B***).

iii. Shoulder-Wrist interactions

Coherence

Shoulder abductor-wrist extensor coherence (MD-ER) was present in the low and high gamma bands during ABD and across all bands during ADD (***figure 4.16A***). Around 50% of subjects showed significant coherence in the low gamma band during ABD and the beta during ADD. Around 70% of subjects showed significant low gamma coherence during ADD (***figure 4.16B***).

Cross-Correlation

Shoulder abductor-wrist extensor correlations (MD-ER) was highest during ADD (***figure 4.17A***). Half-widths were in the 5 ms window during ABD and MVE in around 80% of subjects and divided between the 5 and 10 ms time window during ADD (***figure 4.17B***).

iv. Shoulder-Contralateral interactions

Coherence

Shoulder-contralateral coherence was minimal (***figure 4.16A***).

Cross-Correlation

Shoulder-contralateral correlations were minimal (***figure 4.17A***).

v. Upper arm-Upper arm interactions

Coherence

Elbow flexor-extensor coherence (BB-MT) was high in both the low and high gamma bands, and moderate in the beta band during ABD (***figure 4.16A***). During ADD and MVE BB-MT coherence was moderate in the low and high gamma bands (***figure 4.16A***). At least 80% of subjects showed significant coherence across all bands during ABD, and 55-75% in the low and high gamma bands during ADD and MVE (***figure 4.16A***).

Cross-Correlation

Elbow flexor-extensor correlations (BB-MT) were highest during ABD (***figure 4.17A***). Half-widths were in the 5 ms window during ABD and MVE in at least 70% subjects and were divided between the 5 and 10 ms time window during ADD (***figure 4.17B***).

vi. Upper arm-Wrist interactions

Coherence

Elbow-wrist extensor coherence (LT-ER) was present in the low gamma band during ABD and MVE and the beta and low gamma band during ADD (***figure 4.16A***). Around 50% of subjects show significant coherence in the low gamma band during ABD and MVE, and the beta and high gamma band during ADD (***figure 4.16B***). Around 75% of subjects showed significant coherence in the low gamma band during ADD (***figure 4.16B***).

Cross-Correlation

Elbow-wrist extensor correlations (LT-ER) were high during ADD (***figure 4.17A***). Half-widths were in the 5 ms window during ABD and MVE at least 70% of subjects and were divided between the 5 and 10 ms time window during ADD (***figure 4.17B***).

vii. Upper arm-Contralateral interactions

Coherence

Upper arm-contralateral coherence was minimal (***figure 4.16A***).

Cross-Correlation

Upper arm-contralateral correlations were minimal (***figure 4.17A***).

viii. Wrist-Wrist interactions

Coherence

Wrist flexor-extensor coherence (FR-ER) was present in the beta and low gamma band during ABD and MVE (figure 4.16A). At least 60% of subjects

showed significant coherence in all bands during ABD, in the low gamma during ADD, and in the high and low gamma during MVE (***figure 4.16B***).

Cross-Correlation

Wrist flexor-extensor correlations (FR-ER) were highest during ABD (***figure 4.17A***). Half-widths were in the 5 ms time window for at least 60% subjects during all tasks (***figure 4.17B***).

ix. Wrist-Contralateral interactions

Coherence

Wrist-contralateral coherence was minimal (***figure 4.16A***).

Cross-Correlation

Wrist-contralateral correlations were minimal (***figure 4.17A***).

4.4.5.3 120°, Change with Task (*figure 4.18* and *4.19*)

i. Shoulder-Shoulder interactions

Coherence

Abductor-abductor coherence (AD, MD, PD) was consistently high across bands and conditions with the exception of AD-PD. AD-PD was high in both the low and high gamma band during ABD, across bands during ADD, and in the low-gamma band during MVE (***figure 4.18A***). With the exception of AD-PD, which was at least 60%, significant coherence was present in 90% of subjects across all bands and tasks (***figure 4.18B***).

Adductor-abductor coherence (PM-MD) was present in the low and high gamma band during ABD and the low gamma band during ADD and MVE (***figure 4.18A***). At least 75% of subjects showed significant coherence in the low gamma band during all tasks, and the high gamma band during ABD (***figure 4.18B***).

Adductor-adductor coherence (PM-SA) was high in the low and high gamma band during ABD (***figure 4.18A***). At least 70% of subjects showed significant

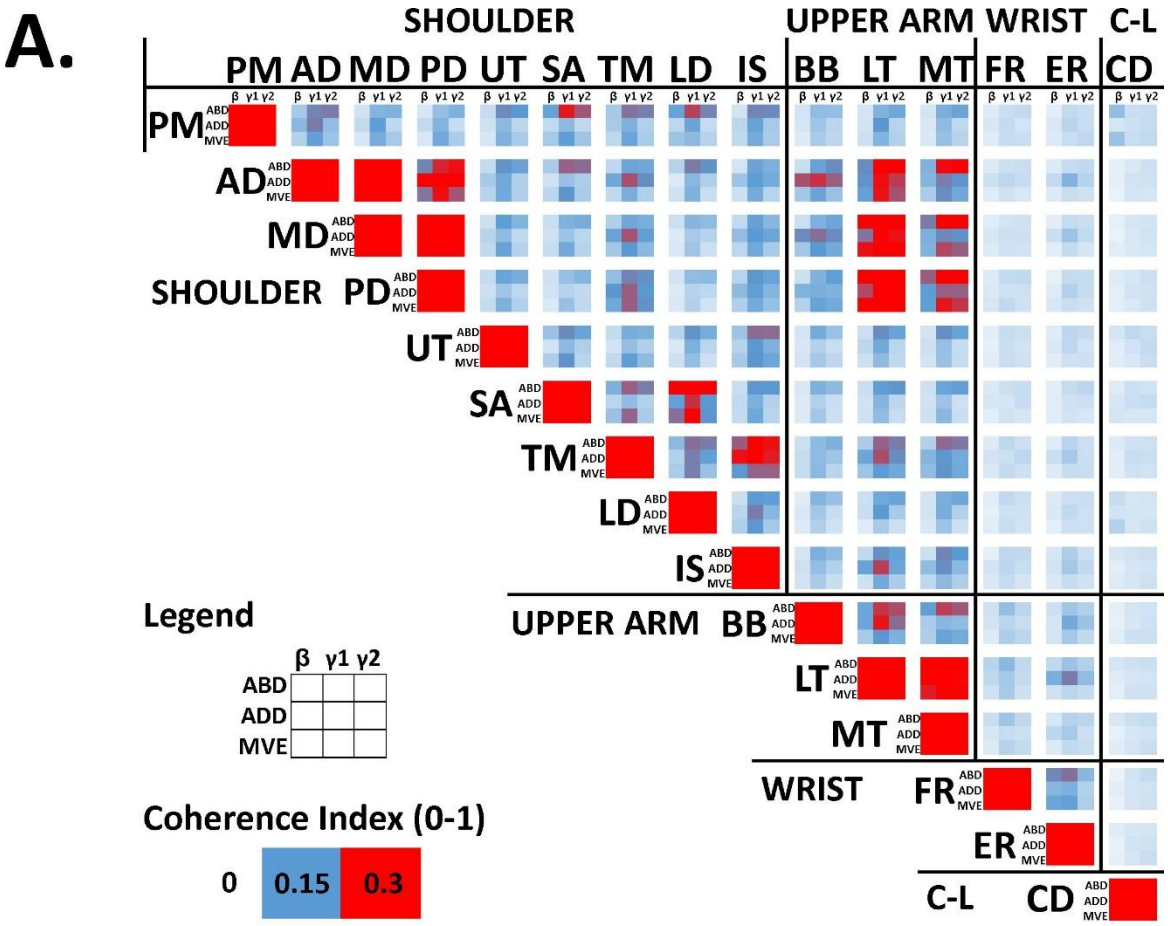
A.
SHOULDER
UPPER ARM
WRIST
C-L
PM AD MD PD UT SA TM LD IS
BB LT MT
FR ER
CD
β γ1 γ2
ABD
ADD
MVE
Legend
Coherence Index (0-1)
0
0.15
0.3

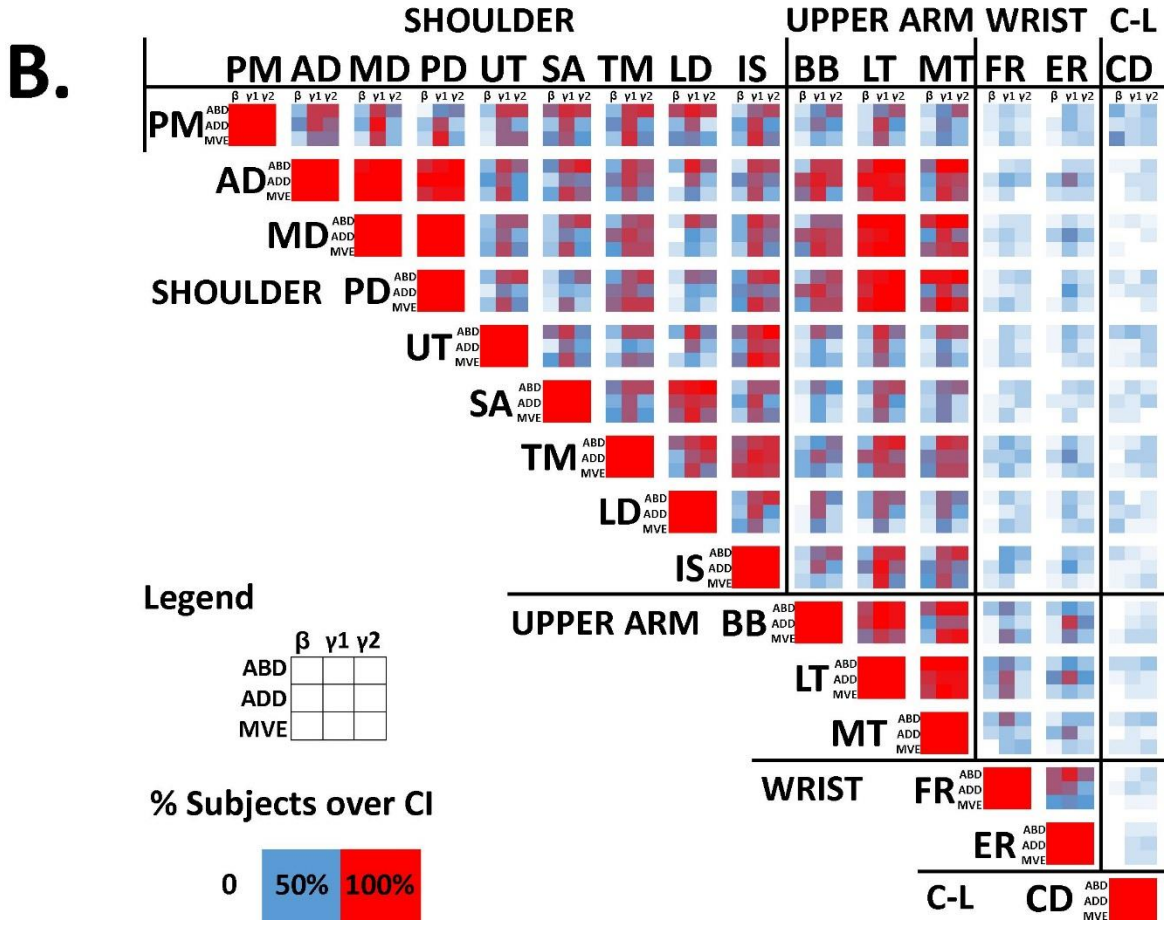
B.
SHOULDER
UPPER ARM
WRIST
C-L
PM AD MD PD UT SA TM LD IS
BB LT MT
FR ER
CD
β γ1 γ2
ABD
ADD
MVE
Legend
% Subjects over CI
0
50%
100%

Figure 4.18. Matrices of coherence between muscle pairs at 120°, compared across tasks. **A.** Group mean peak coherence measured between 20-35, 35-60 and 60-100 Hz (FFT size 1024). Data are from five 5 s trials per subject (*n* = 21). **B.** Percentage of subjects (*n* = 21) where the peak was above the 95% confidence interval as defined by Halliday et al. (1989). For each muscle pair there are 9 squares. As shown in the legends, columns correspond to different frequency bands and rows correspond to different tasks. References for the colour intensity are shown in the legends. C-L – contralateral.

coherence across all bands during ABD, and the low gamma band during ADD and MVE (***figure 4.18B***).

Cross-Correlation

Abductor-abductor correlations (AD, MD, PD) were high across all tasks (***figure 4.19A***). During ABD and MVE, half widths were in the 5 ms window in 90% subjects (figure 4.19b). During ADD, half-widths were divided between 5 ms and 10 ms (***figure 4.19B***).

Adductor-abductor correlations (PM-MD) were highest in ABD, then ADD, then MVE (***figure 4.19A***). During ABD half widths were in the 5 ms window in around 90% subjects (***figure 4.1B***). During ADD, half-widths were in the 10 ms window for around 90% subjects (***figure 4.19B***). During MVE, half-widths were divided between 5 ms and 10 ms (***figure 4.19B***).

Adductor-adductor correlations (PM-SA) were high during ABD (***figure 4.19A***). Half-widths were in the 10 ms window for around 90% subjects in all tasks (***figure 4.19B***).

ii. Shoulder-Upper arm interactions

Coherence

Shoulder abductor-elbow flexor coherence (AD-BB) was high in all bands during ADD, moderate in low and high gamma during ABD, and moderate in low gamma during MVE (***figure 4.18A***). At least 75% of subjects showed significant coherence in the low and high gamma band during ABD, all bands during ADD, and 55% in all bands during MVE (***figure 4.18B***).

Shoulder abductor-elbow extensor coherence (PD-MT) was high in all bands during ABD and in low and high gamma during ADD and MVE (***figure 4.18A***).

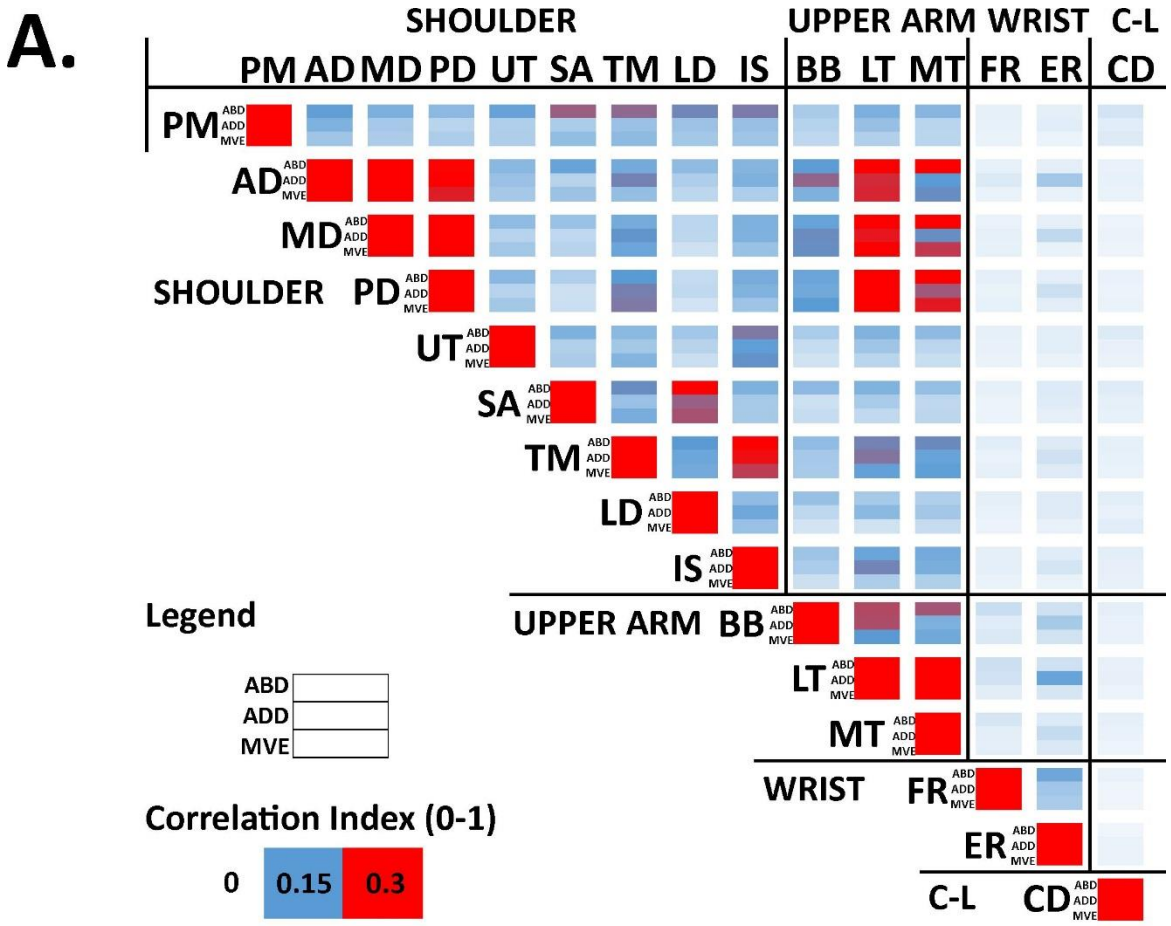
A.
SHOULDER
UPPER ARM
WRIST
C-L
PM AD MD PD UT SA TM LD IS
BB LT MT
FR ER
CD
ABD
ADD
MVE
Legend
Correlation Index (0-1)
0
0.15
0.3

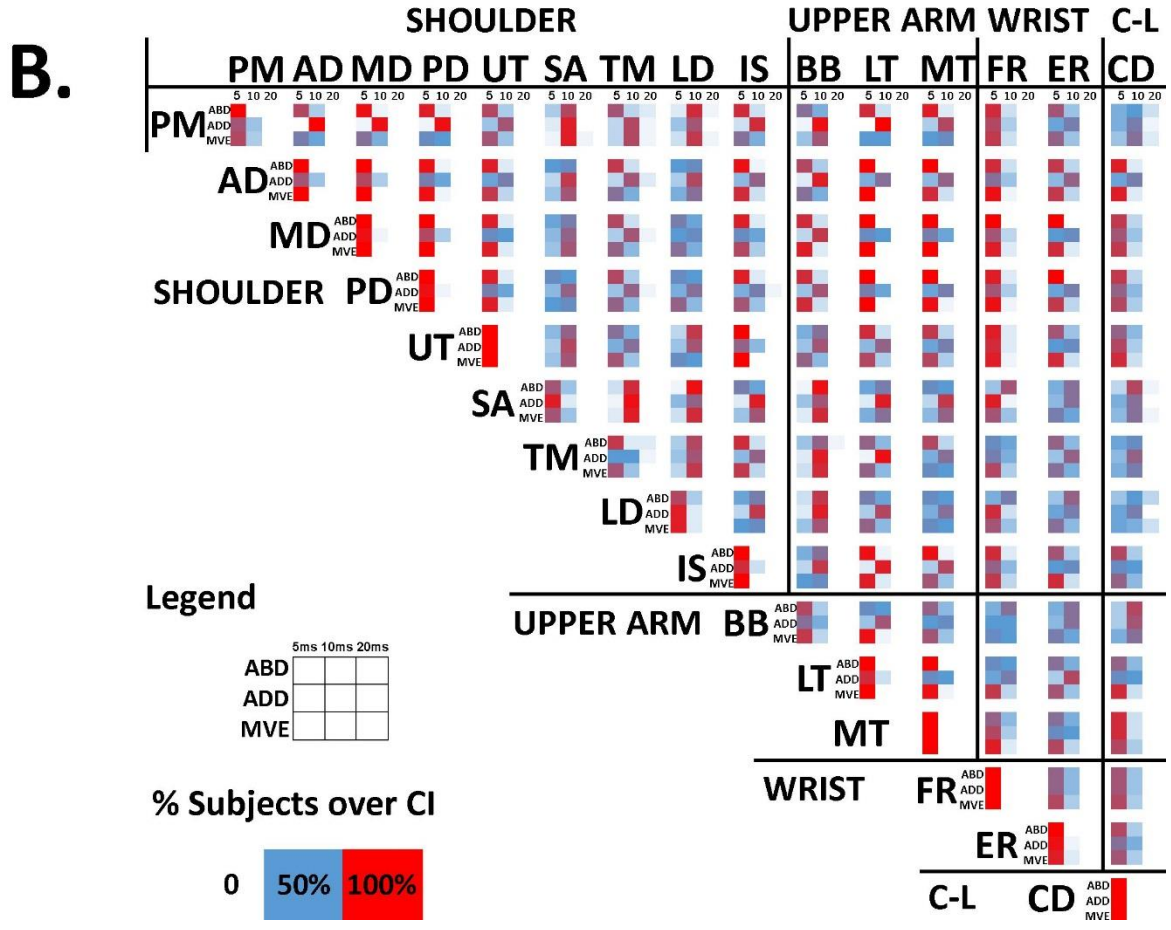
B.
SHOULDER
UPPER ARM
WRIST
C-L
PM AD MD PD UT SA TM LD IS
BB LT MT
FR ER
CD
5 10 20
5ms 10ms 20ms
ABD
ADD
MVE
Legend
% Subjects over CI
0
50%
100%

Figure 4.19. Matrices of cross-correlations between muscle pairs at 120°, compared across tasks. **A.** Group mean absolute peak correlation index. Data are from five 5 s trials per subject (*n* = 21). Legend shows rows corresponding to different tasks and references for colour intensity **B.** Correlation half-widths. For each muscle pair there are 9 squares. Columns correspond to different half-widths (< 5 ms, 5-10 ms and 10-20 ms), and rows correspond to different tasks. Colour intensity relates to the percentage of subjects (*n* = 21) where the half-width falls within that window. C-L – contralateral.

At least 80% subjects showed significant coherence in all bands during ABD and ADD and in the gamma band during MVE (***figure 4.18B***).

Cross-Correlation

Shoulder abductor-elbow flexor correlations (AD-BB) was highest during ADD then ABD then MVE (***figure 4.19A***). During ABD and MVE, half widths were in the 5 ms window in at least 55% of subjects (***figure 4.19B***). During ADD, half-widths were in the 10 ms range for 75% of subjects (***figure 4.19B***).

Shoulder abductor-elbow extensor correlations (PD-MT) were high across all tasks (***figure 4.19A***). Half-widths were in the 5 ms window during ABD and MVE for 90% subjects and divided between 5 and 10 ms during ADD (***figure 4.19B***).

iii. Shoulder-Wrist interactions

Coherence

Shoulder abductor-wrist extensor coherence (AD-ER) was present in the low gamma band during ADD (***figure 4.18A***). Significant coherence was present in around 70% of subjects (***figure 4.18B***).

Cross-Correlation

Shoulder abductor-wrist extensor correlations (AD-ER) were present during ADD. Half widths were in the 5 ms window for 90% subjects during ABD, and 65% subjects during MVE (***figure 4.19B***). During ADD, half-widths divided between the 5 and 10 ms window (***figure 4.19B***).

iv. Shoulder-Contralateral interactions

Coherence

Shoulder-contralateral coherence was minimal (***figure 4.18A***).

Cross-Correlation

Shoulder-contralateral correlations were minimal (***figure 4.19A***).

v. Upper arm-Upper arm interactions

Coherence

Elbow flexor-extensor coherence (BB-LT) was present in all bands during ABD and ADD and in low and high gamma during MVE (***figure 4.18A***). Significant coherence was present in all bands in 90% subjects across tasks with the exceptions of the beta band during MVE and ADD (***figure 4.18B***).

Cross-Correlation

Elbow flexor-extensor correlations (BB-LT) were high during ABD and ADD (***figure 4.19A***). Half-widths were divided between the 5 and 10 ms time window during ABD and ADD, and 75% of subjects in the 5 ms window during MVE (***figure 4.19B***).

vi. Upper arm-Wrist interactions

Coherence

Elbow-wrist extensor coherence (LT-ER) was present in the low gamma band during ABD, and in all bands during ADD (***figure 4.18A***). Significant coherence was present in around 50% of subjects in the low gamma band during ABD, and the beta and high gamma band during ADD. Around 75% subjects showed significant coherence in the low gamma band during ADD (***figure 4.18B***).

Cross-Correlation

Elbow-wrist extensor correlations (LT-ER) were high during ADD (***figure 4.19A***). Half-widths were in the 5 ms time window in 70% of subjects during ABD and MVE, and the 10 ms time window during ADD (***figure 4.19B***).

vii. Upper arm-Contralateral interactions

Coherence

Upper arm-contralateral coherence was minimal (***figure 4.18A***).

Cross-Correlation

Upper arm-contralateral correlations were minimal (***figure 4.19A***).

viii. Wrist-Wrist interactions

Coherence

Wrist flexor-extensor coherence (ER-FR) was high in all bands during ABD and in the beta band and low gamma band during ADD and MVE (***figure 4.18A***). Around 85% subjects showed significant coherence in the beta band during ABD, and at least 60% in the low and high gamma. At least 55% of subjects showed significant beta and low gamma coherence during ADD and all bands during MVE (***figure 4.18B***).

Cross-Correlation

Wrist flexor-extensor correlations (ER-FR) were highest during ABD (***figure 4.17A***). Half-widths were in the 5 ms time window in at least 60% of subjects across all tasks (***figure 4.19B***).

ix. Wrist-Contralateral interactions

Coherence

Wrist-contralateral coherence was minimal (***figure 4.18A***).

Cross-Correlation

Wrist-contralateral correlations were minimal (***figure 4.19A***).

4.4.6 Cluster Analysis

4.4.6.1 Cluster 1

The task matrix for cluster 1 indicates that this cluster primarily consists of muscles which share common drive in the low gamma range across all tasks (***figure 4.20***). Muscles in the network are AD, MD, PD, TM, IS, MT, LT, and BB. The muscles in the network are in a single group. This consists of shoulder abductors (AD, MD, PD, TM, and IS), and upper arm muscles (MT, LT, BB). Adductor muscles and wrist muscles were not integral to this network (***figure 4.20***).

4.4.6.2 Cluster 2

The task matrix for cluster 2 indicates that this network primarily consists of muscles which share common beta-drive across all tasks (***figure 4.20***). Muscles in the network are AD, MD, PD, LT, MT, LD, SA, ER, and FR. There are three groups within this network. The first consists of shoulder abductors (AD, MD, PD) and upper arm extensors (MT and LT), the second consists of shoulder adductors (LD and SA), and the third consists of wrist muscles (ER and FR, ***figure 4.20***).

4.4.6.3 Cluster 3

The task matrix for cluster 3 indicates that this network primarily consists of muscles which share common drive in the high gamma range, across all tasks (***figure 4.20***). Muscles in the network are AD, MD, PD, LT, BB, TM, LD, SA, IS, UT, ER and FR. There are four groups within this network. The first consists of shoulder abductors (AD, MD, PD) an upper arm flexor (BB) and an upper arm extensor (LT), the second consists of shoulder adductors (LD, SA and TM), the third consists posterior shoulder muscles (IS and UT), and the fourth consists of wrist muscles (ER and FR, ***figure 4.20***).

4.4.6.4 Cluster 4

The task matrix for cluster 4 indicates that this network primarily consists of muscles which share common drive in the beta rang during ADD and MVE (***figure 4.20***). Muscles in the network are AD, MD, PD, LT, MT, BB, UT, TM,

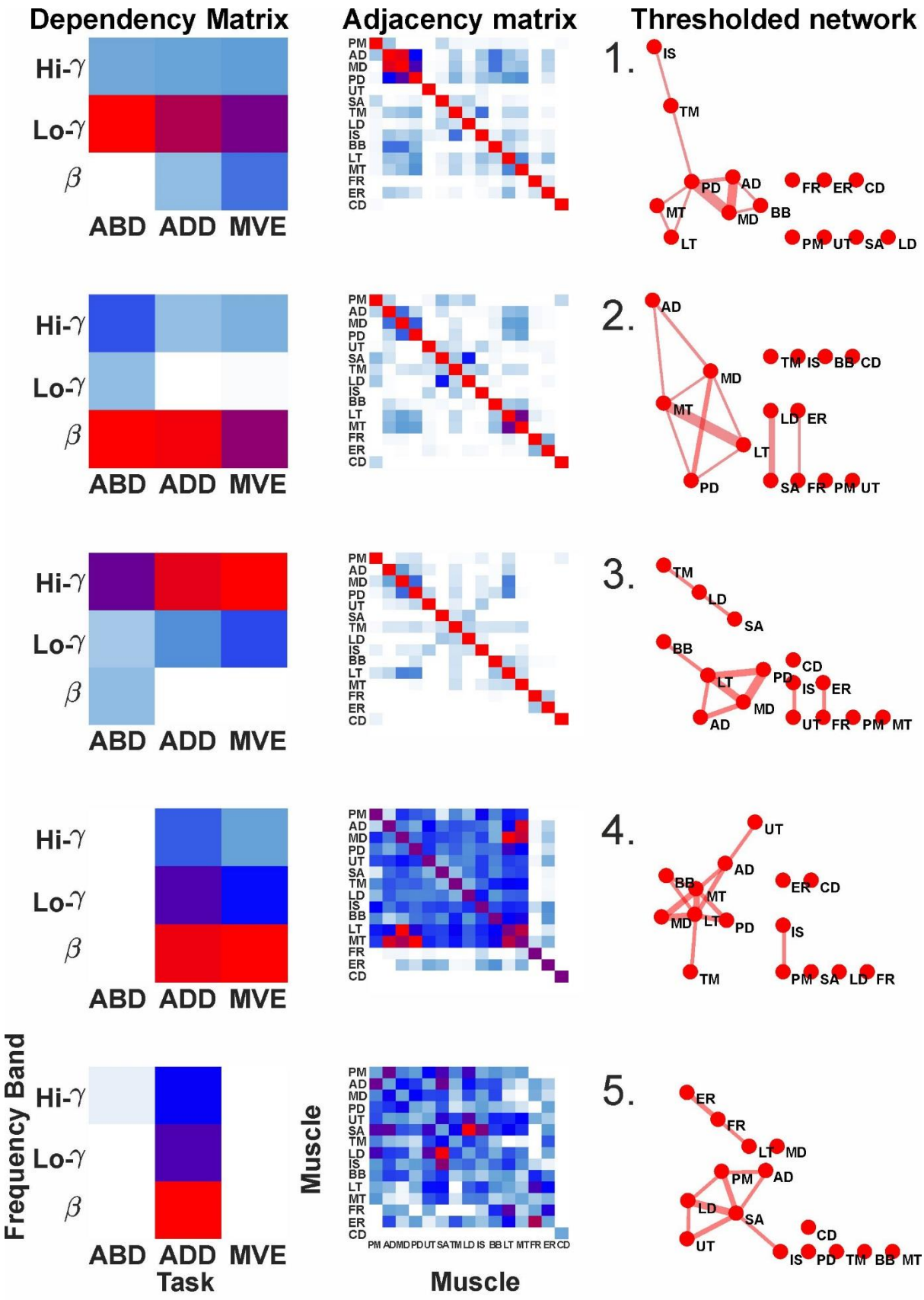
Dependency Matrix
Adjacency matrix
Thresholded network
Hi-γ
Lo-γ
β
ABD ADD MVE
PM AD MD PD UT SA TM LD IS BB LT MT FR ER CD
1.
2.
3.
4.
5.
Frequency Band
Task
Muscle
Muscle

Figure 4.20. Results of cluster analysis. Clusters derived from the coherence analysis of all tasks at 75°. Five was determined as the optimum number of clusters (different rows) for the output by running the analysis with different numbers of clusters and checking the residual error. Group mean coherence was subjected to an NMF analysis whereby muscle networks are identified based on a clustering coefficient. The dependency matrix identifies which dependent variables (task, frequency band) produce the network. The adjacency matrix identifies the muscles involved in the network. This adjacency matrix is then translated into a diagrammatic representation to produce the thresholded network where clusters are illustrated based on the connectivity between muscle pairs. The line thickness reflects the coupling strength of each muscle pair. For the dependency matrix and the adjacency matrix, red represents the highest values, blue represents mid-range values, and white represents the lowest values.

IS and PM. There are two groups within this network. The first consists of shoulder muscles (AD, MD, PD, UT, and TM) and an upper arm muscles (LT, MT and BB) and the second consists of a shoulder abductor and adductor (IS and PM, ***figure 4.20***).

4.4.6.5 Cluster 5

The task matrix for cluster 5 indicates that this network primarily consists of muscles which share common drive during the ADD task (***figure 4.20***). This is primarily in the beta range, but to a lesser extent also the low and high gamma range. Muscles in the network are AD, PM, LD, UT, SA, IS, LT, ER, and FR. There are two groups within this network. The first consists primarily of shoulder adductors (PM, SA, LD) and shoulder abductors (IS, UT, AD) and the second consists of an upper arm extensor (LT) and wrist muscles (ER and FR, ***figure 4.20***).

4.5 Discussion

The primary objectives of this experiment were three-fold: (1) to explore how muscle interactions are altered depending on the task at hand (2) to explore how muscle interactions are altered with a change of shoulder position and (3) to apply a novel MVE task which can be used in conjunction with or to replace MVCs. The goal was to provide a reference catalogue of muscle interactions and inter-subject variability across two MVC tasks (ABD, ADD) and one MVE task. The MVE task is intended to be easily adapted to the clinic and therefore requires minimum motor capability. Patients would perform an MVE in a set arm position. For comparisons between tasks, we use results from the data collected at 75° since this represents mid-range of motion, and

therefore has less innate postural bias than 30° or 120°. Secondary objectives in this experiment were to explore interactions of muscles across joints and functional antagonists during isometric tasks. We will discuss interactions using MD as reference for a prime mover during ABD and MVE, and PM as a reference for a prime mover during the ADD task.

4.5.1 Cluster Analysis

The group mean peak coherence data collected at 75° were subjected to a cluster analysis in order to determine the dependency of muscle networks on both task and frequency band (***figure 4.20***). Based on the relationship between the number of clusters and the residual error, it was determined that 5 clusters was the optimum number to describe the dataset. Overall, the resultant clusters were each dependent on specific factors or included functionally related muscles. Of the 5 clusters, there was one cluster dependent on each frequency band (beta – cluster 2, low gamma – cluster 1, high gamma – cluster 3, ***figure 4.20***), one which included primarily abductor muscles (cluster 4, ***figure 4.20***), and one which included primarily adductor muscles (cluster 5, ***figure 4.20***).

In Chapter 2, we argued that the corticospinal pathway produces EMG activity at 15-60 Hz, the reticulospinal pathway at 35-60 Hz, and spinal pathways at 60-100 Hz. With this in mind, it is interesting to look at the networks from the cluster analysis in terms of the pathways and task context. For example, the muscles in the networks formed by the clusters for the low and high gamma band (cluster 1 and 3 respectively, ***figure 4.20***) are mostly proximal muscles, both of the shoulder and upper arm. This implies that these muscles receive inputs from subcortical pathways. In cluster 3, which is mostly high gamma muscles, wrist muscles are also included, suggesting that they also receive subcortical drive.

The clusters show us interesting insights into the interconnectivity of wrist muscles. Firstly, they are only included in 3 of the 5 clusters. When they do appear, they only once are grouped with any muscle except each other (cluster 5, LT, ***figure 4.20***). This shows us that they few shared inputs across joints. The second point of interest is that 2/3 of the clusters they are included

in are highly dependent on beta band coherence, which is hypothetically cortical drive. This contrasts with many shoulder muscles, which appear more indiscriminately across frequency bands (AD, MD, PD, and TM). This is interesting because it suggests that whilst there may be subcortical inputs to wrist muscles, in this context, control of wrist muscles is mostly dependent on corticospinal inputs.

Cluster 4 and cluster 5 mostly include shoulder abductors and shoulder adductors respectively (***figure 4.20***). This is interesting because it suggests that more specific muscle groups may share corticospinal input. In contrast, cluster 3 includes both abductors and adductors and relies mostly on high gamma activity. However, abductors and adductors are in separate groups within the network. This could be an indication that specific muscle groups are activated by cortical input whereas spinal circuits activate muscles in smaller subgroups depending on the task. The next sections focus on explaining and theorising these results based on individual muscle interactions.

4.5.2 Cross-joint Interactions

4.5.2.1 Corticospinal Bias for Proximal Muscle Pairs and Reticulospinal Bias between Distal Muscle pairs

Coherence between shoulder muscles was most common in gamma range. Beta band coherence was only present when muscles pairs were in close anatomical proximity (deltoid-deltoid) or played a task dependent, functionally related role (at 75°, SA-LD during ABD and MVE, TM-IS during ADD, ***figure 4.16B***). In contrast, between upper arm (BB-LT) and wrist (ER-FR) flexor and extensors, beta band coherence was more common than amongst proximal muscles (clusters 2, 4 and 5). Coherence is usually measured in the beta band since it is thought to represent coupling of the cortical and spinal motoneurones (Farmer et al., 1993). The relatively rare occurrence of beta band coherence between shoulder muscles compared to wrist muscles might be explained by difference in termination patterns of these descending pathways onto these motoneurones. In primates, there are differences between the neural pathways supplying motoneurones of proximal compared to distal muscles (Phillips and Porter, 1964; Lemon, 1993; Lemon, 2008).

Distal muscles receive more corticospinal innervation (as well direct reticulospinal inputs, Baker, 2011) whereas proximal muscles receive more reticulospinal innervation. Different pathways may produce muscle activity in different frequency bands; the corticospinal primarily in the beta band (15-35 Hz) (Farmer et al., 1993; Halliday et al., 2000), the reticulospinal primarily in the low gamma band (35-50 Hz) (Brown, 2000; Nishimura et al., 2009) and spinal pathways (50-100 Hz band – Chapter 3). Taking this into consideration, higher beta band coherence between distal muscle pairs is not surprising, since the different levels of coherence may reflect the number of inputs from the corticospinal or reticulospinal pathway (***figure 4.21***). However, factors such as divergence and flexor/extensor bias of descending pathways mean the full picture is likely to be more complex. The contribution of the common cortical/reticular drive will vary based on their relative proportions of inputs to the motor pool, and their involvement in a given task.

Whilst coherence analysis can be useful for identifying common inputs (Farmer et al., 1993) and determining directionality (Witham et al., 2011), it does not give any details of the presynaptic pathway. Taking correlation half-widths into account as well as coherence can provide more insight. A narrow central peak in the cross-correlogram suggests a common presynaptic input, and a broad peak suggests common input from divergent sources (Kirkwood et al., 1982; Vaughan and Kirkwood, 1997). Both can be present in the cross-correlogram since it is possible for a narrow correlation peak to have a broad base. Correlation half-widths are a convenient measure of the overall shape of a correlation peak. At the shoulder, TM-IS shows both beta and gamma coherence is present during ADD, and half-widths were mainly in the 10 ms window (***figure 4.17B***). During ABD, only gamma coherence is high, and 90% of half-widths are in the 5 ms window. This suggests a predominantly reticulospinal input during ABD whilst both cortico- and reticulospinal inputs are active during ADD. At the wrist, presence of beta band coherence in conjunction with a 5 ms correlation peak reflects a dominant corticospinal input. Previous studies have not found coherence between motor unit pairs in paraspinal muscles. However, there is less need for voluntary control from descending pathways in these muscles (Marsden et al., 1999).

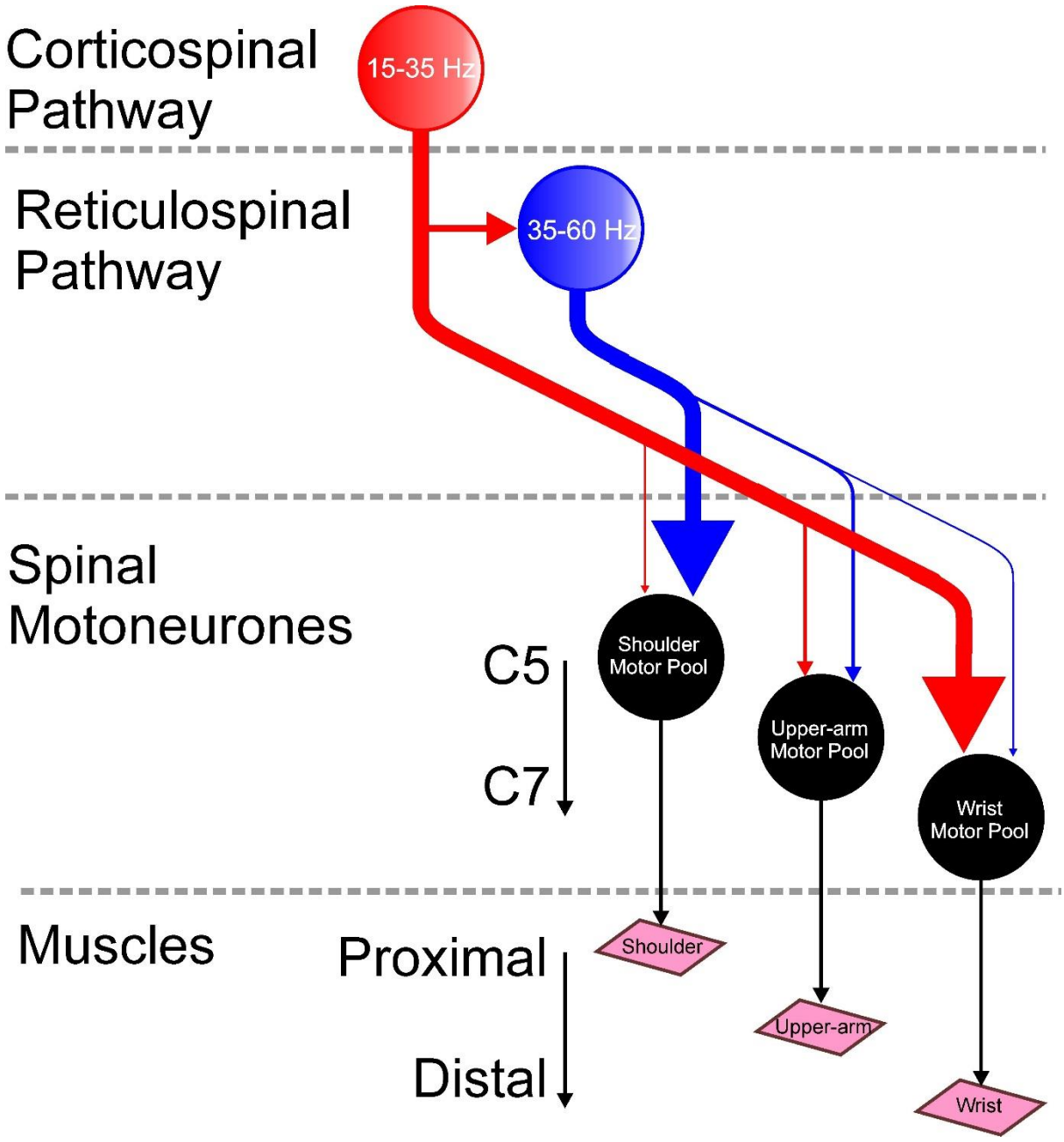

Figure 4.21. Differences in proximal and distal innervation from corticospinal and reticulospinal pathway. Schematic showing how differences of coherence between muscles acting at different joints may be explained by different proportions of inputs to the respective motor pools. In this instance, thickness of the arrow represents number of synaptic contacts.

4.5.2.2 Cross-joint Beta Band Coherence is Task Dependent

There are few studies where intermuscular coherence between the proximal and distal muscles of the arm is used to explore how the corticospinal and reticulospinal inputs are shared across joints. Lee et al. (2014) studied distal muscle coherence during a proximal task, but did not discuss distal-proximal

or proximal-proximal coherence. We found that cross-joint interactions with wrist flexor muscles were rare, and interactions at the upper arm were heavily dependent on task. MD-ER and MD-FR interactions were only present during ABD and ADD (***figure 4.16B***). MD-BB, MD-LT, and LT-ER showed similar shifts across different tasks. In the cluster analysis, ER and FR were rarely integral to clusters consisting of muscles at the shoulder, and only once with a muscle in the upper arm. Farmer et al. (1993) showed that coherence between biceps motor units was much lower than that of hand muscles. In the present study, MD-BB coherence was observed, though it was dependent on the task, which may explain why it was not observed by Farmer et al. During ABD and MVE, gamma range coherence and half-widths were in the 5 ms window, suggesting a common monosynaptic input, possibly reticulospinal. However, during ADD, both beta and gamma range coherence was present and half-widths were mainly in the 10 ms window. Coherence in cross-joint muscles (MD-BB, MD-ER, LT-ER) was also relatively strong during the ADD task. Disruption of this pathway may cause the pathological coupling of activity in shoulder abductors with wrist, elbow, and hand muscles common post-stroke (Brunnstrom, 1966). Presence of both beta and gamma coherence in conjunction with a 10 ms half-width suggests this could be a mixed corticospinal and corticoreticulospinal input. In primates, the corticospinal and reticulospinal pathways have different flexor/extensor bias as well distal/proximal distribution (Shepherd, 1994). Post-stroke disruption of muscle coordination across joints could result from damage to the corticospinal component of this pathway which is prominent during the ADD task (***figure 4.22***). Lee et al. show how activation of proximal muscles caused a reduction in coherence between distal muscles, particularly during an elbow flexion task (Lee et al., 2014). Similarly, we observed that during ADD where shoulder abductor-elbow flexor (MD-BB) coherence was high, wrist flexor-extensor coherence was drastically lower than during other tasks.

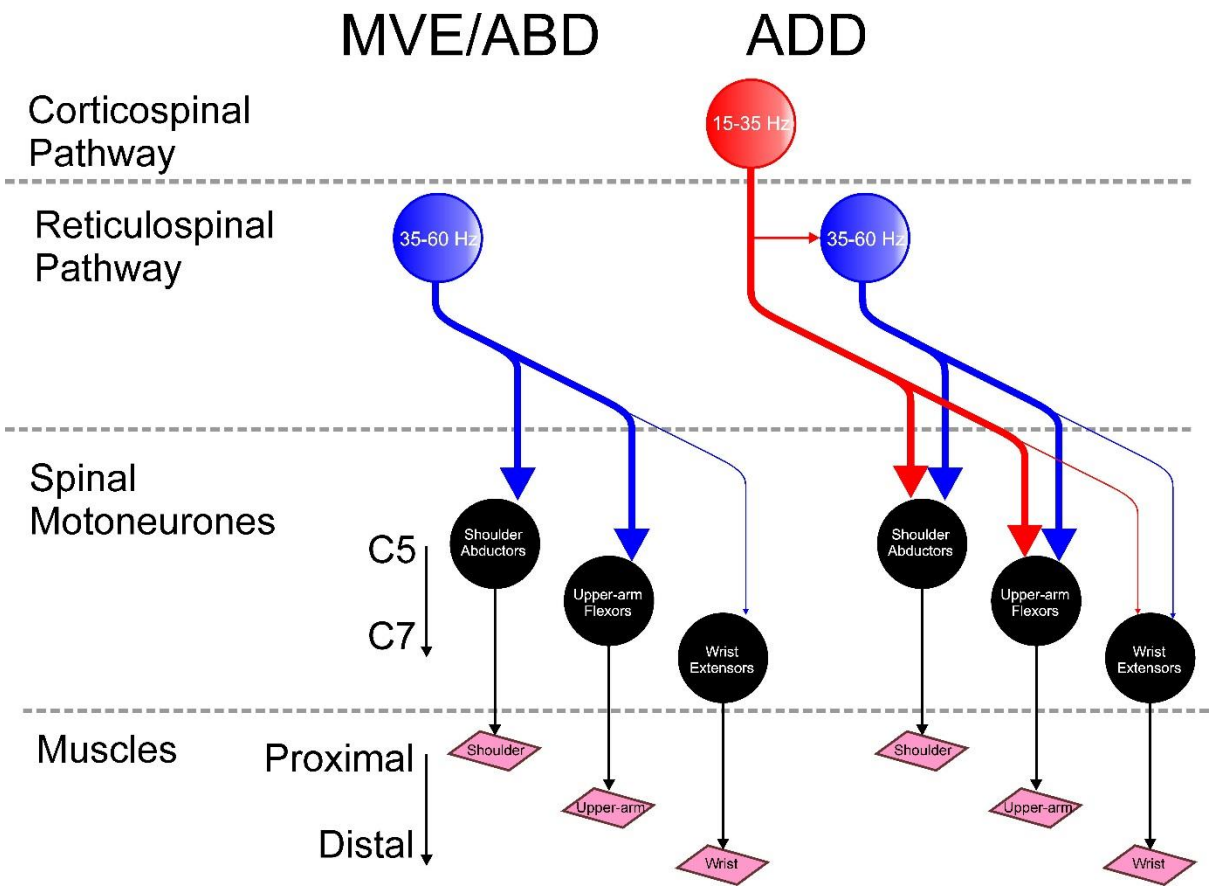

Figure 4.22. Task-dependent involvement of descending pathways. During MVE and ABD, common drive is sourced from one pathway. However, during ADD, multiple inputs are active. This may be due to the flexor/extensor bias of the pathways and the task demand. Imbalance of excitation following injury may cause these interactions to be expressed pathologically.

4.5.3 Involvement of Peripheral Pathways in Defining Muscle Interactions

4.5.3.1 Task Dependent changes in Neural Drive to Muscle Pairs Reveals Inherent flexibility of Motor Primitives

We identified that the levels of coherence between muscle pairs were altered depending on the task. Even interactions between close synergists are task-dependent. For example, coherence between muscles involved in adduction (PM-SA and PM-LD) was very high at 75° and 120° during the ABD task (***figure 4.8A***), yet during the ADD and MVE task, the magnitude of coherence is almost half (max 0.28 PM-SA and 0.24 PM-LD during ABD, and max 0.17 PM-SA and 0.15 PM-LD during ADD or MVE, ***figure 4.10A*** and ***4.12A***). Illert

(1996) proposes that arrangements of neurones (or motor primitives) in the spinal cord produce stereotypical movements. Baldissera (1981) describes how motor primitives could be combined as ‘spinal functional units’ partly through the synaptic distribution of reflex pathways to motor pools of different muscles. Our results illustrate how we can identify that the muscle interactions are altered to meet the demands of the task. This is a reflection of how sensory pathways could induce flexibility amongst motor primitives through their effect on motoneurones of individual muscles. Sensory inputs contact many interneuronal populations in the spinal cord, such as Ia interneurones, propriospinal neurones, and Renshaw cells as well (Martin et al., 2007; Tan et al., 2012; Smith et al., 2017). The net effect of inhibition or excitation onto motoneurones could alter how a muscle is recruited into a motor primitive (Martin et al., 2007).

4.5.3.2 Presynaptic Inhibition and Primary Afferent Depolarisation (PAD)

One aim of this study was to use the ABD and ADD tasks to study how muscle interactions differ between two tasks performed at the same position but when force is applied in opposing directions. The application of force requires activation of different agonists and antagonist muscle groups depending on the direction (shoulder abductors and adductors), in turn producing different patterns of incoming information via afferent pathways. Whilst it is not clear what effect sensory information has on coherence, it has been proposed that alpha band coherence during dynamic movements has a peripheral origin (Mehrkanoon et al., 2014). Currently, it is not fully understood how activity in different afferent fibre types will be modulated throughout an isometric contraction, or how the incoming signal is integrated at a spinal level. Transient changes in EMG coherence are unlikely to be detected using FFT methods since it has no time resolution (we propose using a wavelet transform to approach this problem - see Chapters 2 and 3). Interactions influenced by afferent inflow could affect muscle interactions without manifesting in specific frequency bands through presynaptic inhibition of inputs to motoneurones (Iles, 1996; Rudomin et al., 1998). Rudomin (1981) showed that intraspinal application of $GABA_A$ agonists can depolarise the terminals of afferent fibres

in the cat, and later in rats and mice (Rudomín et al., 1981). Later shown in humans (Iles, 1996), this mechanism is known as primary afferent depolarisation (PAD), as the depolarisation of afferent terminals prevents transmission of signals to the postsynaptic cell. There are complex patterns of presynaptic inhibition which can alter transmission from afferent-afferent, flexor-extensor, afferent-descending pathways. Task related changes in presynaptic inhibition could affect recruitment patterns of muscles into motor primitives (***figure 4.23***). The changes in presynaptic inhibition may affect the magnitude of coherence between muscles without discriminately altering specific frequency bands.

4.5.4 Coherence between Agonist and Antagonists at the Shoulder

4.5.4.1 Shoulder Adductor (Task Antagonists) Interactions are highest during ABD Task whilst Opposing Force Direction

Counter-intuitively, shoulder adductor muscles showed higher coherence during ABD than during ADD (max 0.26 PM-SA and 0.22 PM-LD during ABD, and max 0.16 PM-SA and 0.11 PM-LD during ADD). These muscles could have been recruited due to the biomechanical demands of an isometric task through common afferent as well as descending inputs. As the subject performs the ABD task, sensory receptors across the upper limb respond to the force. Change in activity from sensory receptors could mediate this effect through higher threshold spinal afferent pathways projecting from Golgi Tendon Organs GTO's (group Ib) or the spindle secondaries (group II) through excitatory interneurones to the motor pool of PM, SA and LD. Half-widths were in 10 ms time window during all tasks, so a common di-synaptic input could be an important neural mechanism for control of these muscles in the context of isometric shoulder contractions.

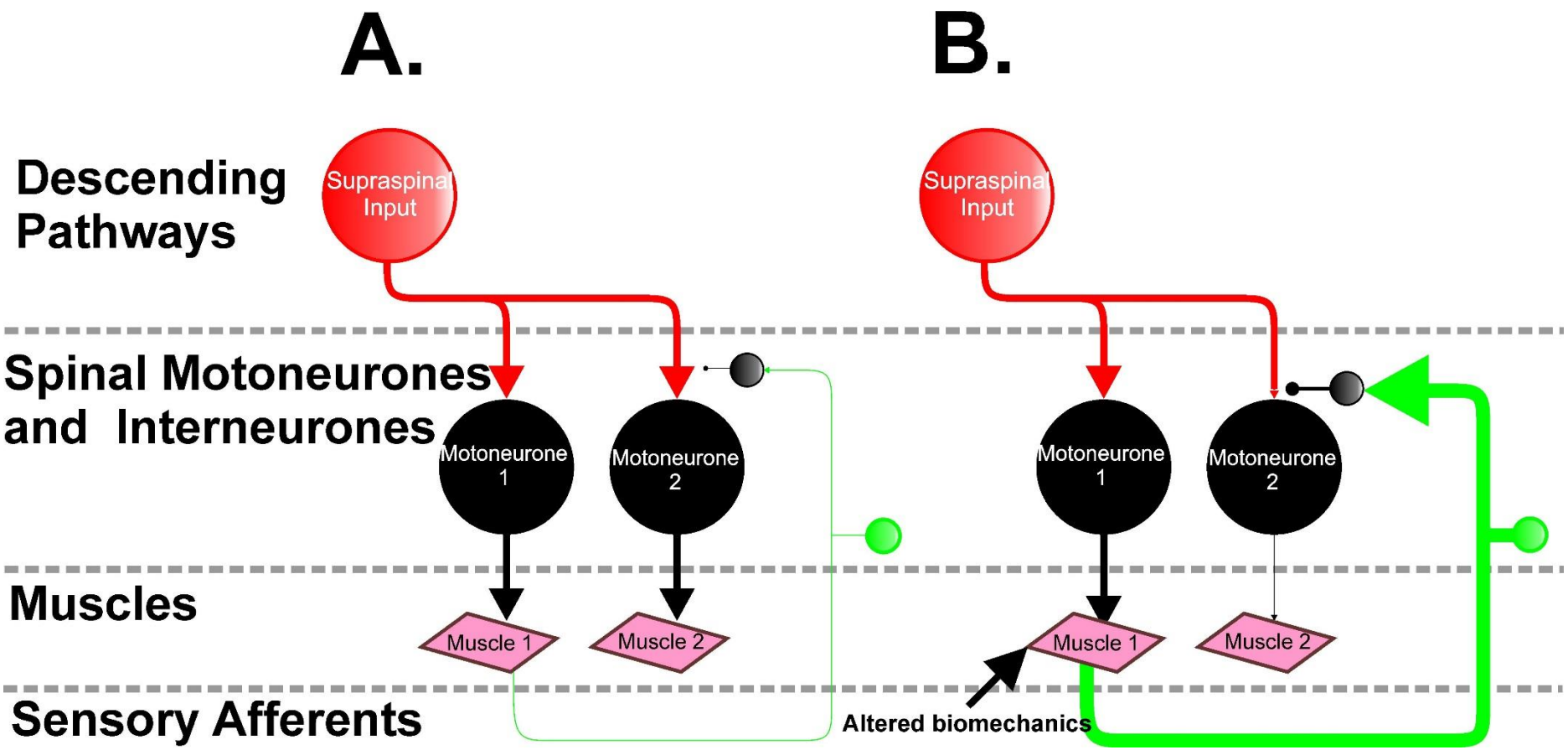

Figure 4.23. Possible effect of presynaptic inhibition on muscle interactions. Shows two situations where altered biomechanics in situation **A.** and **B.** changes peripheral drive, and affects motoneurone interactions through a shift in the level of presynaptic inhibition through a GABAergic interneurone. This example shows presynaptic inhibition of a peripheral pathway onto a descending input which would have a deleterious effect on coherence. However, complex patterns of presynaptic act on terminals from various sources, so presynaptic inhibition could be acting between many pathways.

4.5.4.2 Shoulder Abductor (Task Agonists) Interactions are highest during ABD Task whilst Contributing to Force Direction

Unlike coherence between adductor muscles, coherence between abductor muscles and agonists was higher during the ABD task than the ADD or MVE task. MD-UT and MD-IS, both show high coherence during ABD and ADD but not during MVE (max 0.21 MD-UT and 0.24 MD-IS during ABD, and max 0.16 MD-UT and 0.16 MD-IS during ADD or MVE). At 75° and 120°, MD-UT and MT-IS half-widths are most commonly within a 5 ms time window, suggesting that they receive a direct common presynaptic input. Since involvement of these muscles is high during shoulder abduction, a common descending input through pathways such as the corticospinal or reticulospinal pathway is likely. During ADD and MVE, and at 30° during ABD, half-widths are split 50/50 between subjects in the 5 and 10 ms time window. This suggests that in these conditions, there is greater involvement of polysynaptic pathways. It may be that shoulder abductors are primarily controlled by direct descending pathways but can be subject to polysynaptic influence depending on the task and shoulder position (***figure 4.24***). More subjects have half-widths in the polysynaptic window for shoulder adductors which could suggest more involvement of afferent pathways.

4.5.5 Maximum Voluntary Effort Task to Differentiate Peripheral and Descending Interactions

4.5.5.1 MVE Reveals Core Modules Receiving Shared Descending Drive

Subjects performed MVEs of a major shoulder abductor (MD). No force was applied to the handle, which produced different activation patterns to the either of the MVC tasks. Whereas in the MVC tasks, where muscles which were activated were primarily abductors (ABD) or adductors (ADD), during MVE, both muscle groups were activated together. This meant that the MVE effectively served as a co-contraction task in which muscles were co-activated with MD based on descending input, including PM, a functional antagonist. In contrast, the MVC tasks were influenced by peripheral pathways activated by the loading of the limb. This allows interactions during MVE to be used as an indicator of in-tact descending pathway (***figure 4.25***). Additional interactions

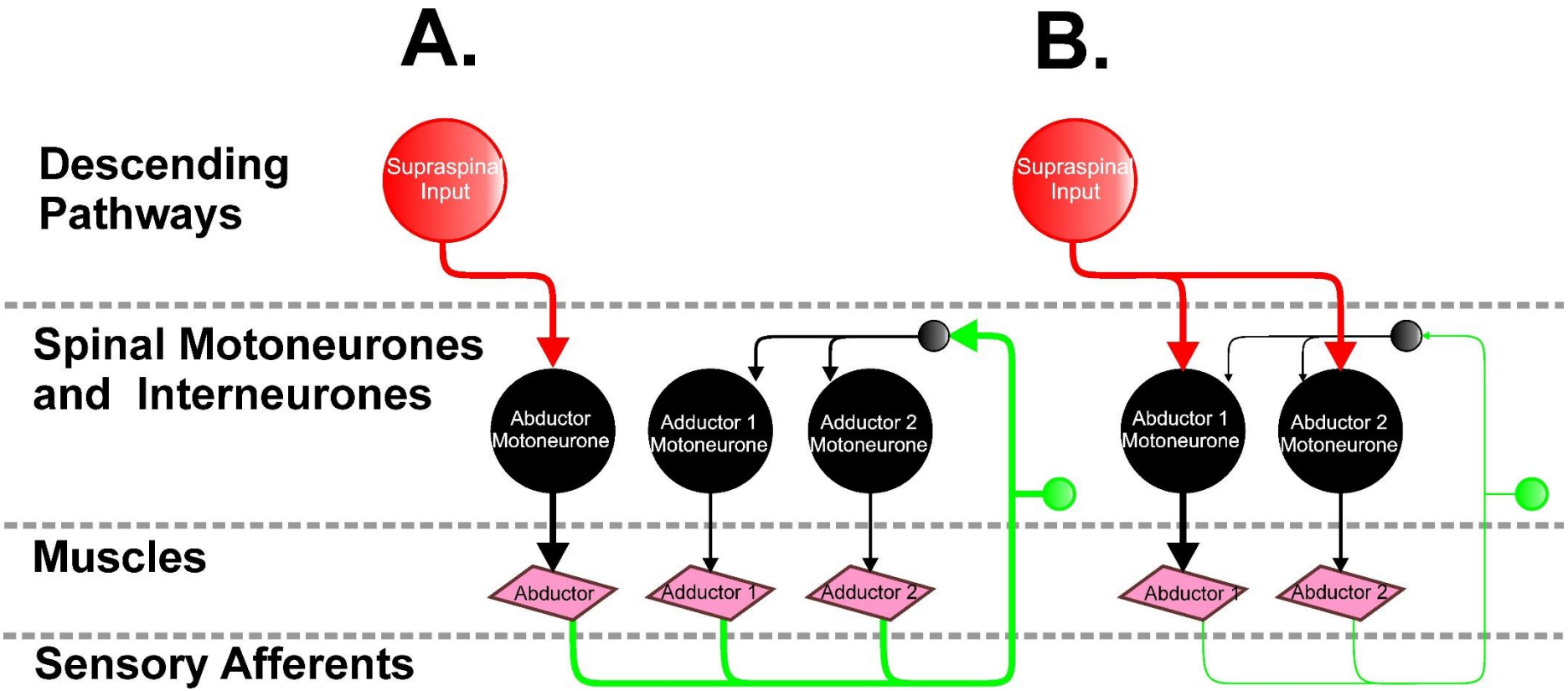

***Figure 4.24. Effect of afferent drive on muscle interactions*. A.** Shows a situation where high descending drive during ABD causes common afferent drive to antagonist through afferent pathway activated during task, consequently reducing the drive between muscles primarily activated reflexively. **B.** ABD motoneurones are primarily activated by descending drive but may also have an afferent component. These schematics also show how afferent drive could induce flexibility in motor primitives.

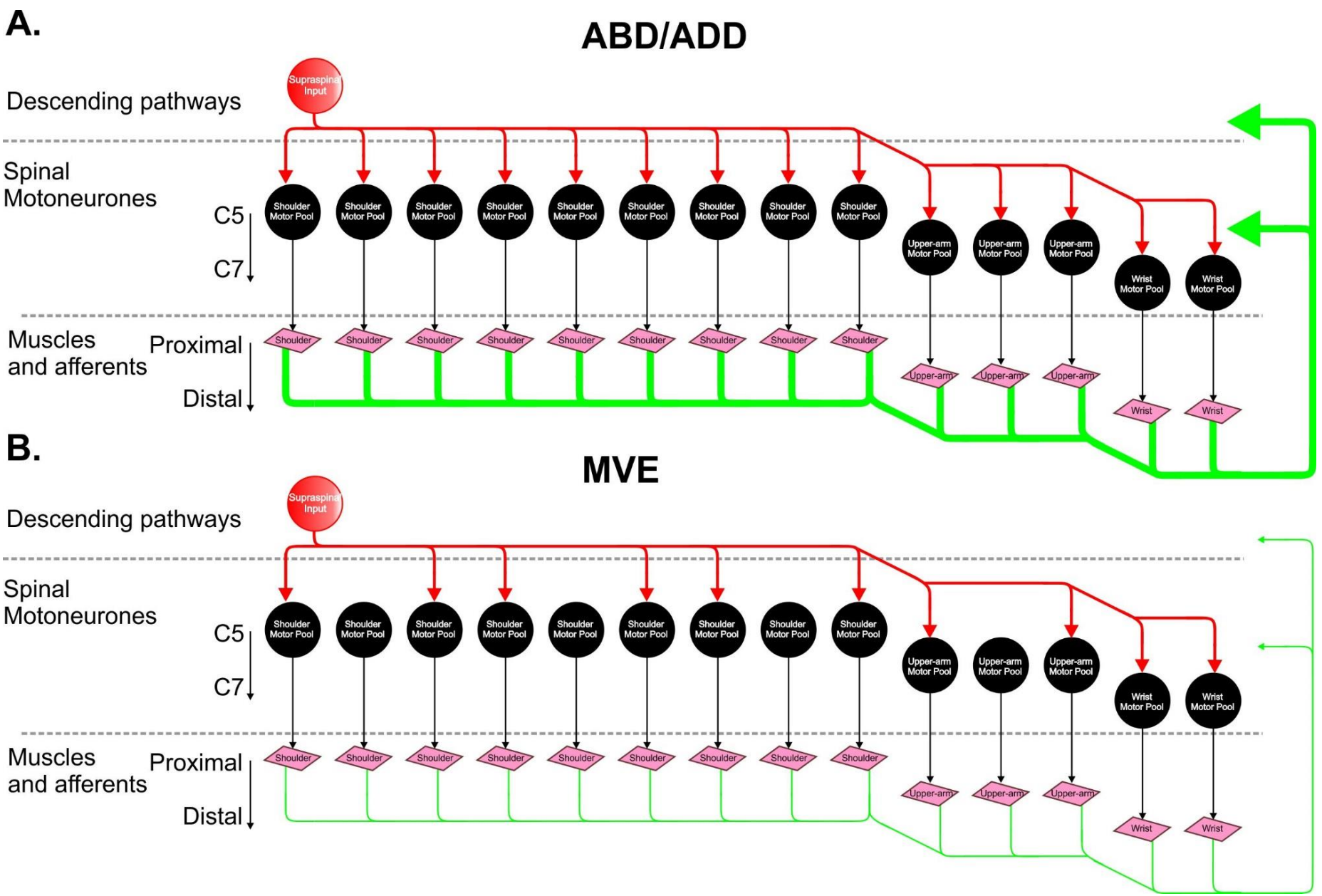
A.
ABD/ADD
Descending pathways
Supraspinal Input
Spinal Motoneurones
C5
C7
Shoulder Motor Pool
Upper-arm Motor Pool
Wrist Motor Pool
Muscles and afferents
Proximal
Distal
Shoulder
Upper-arm
Wrist
B.
MVE
Descending pathways
Supraspinal Input
Spinal Motoneurones
C5
C7
Shoulder Motor Pool
Upper-arm Motor Pool
Wrist Motor Pool
Muscles and afferents
Proximal
Distal
Shoulder
Upper-arm
Wrist

Figure 4.25. Utility of MVE task to identify descending modules. Shows schematics whereby increased peripheral drive during ABD or ADD in A. induces interactions in large number of muscle pairs. However, during MVE in B. peripheral drive is reduced so fewer muscles interact but these muscles are receiving common input from descending pathways.

present during ABD and ADD are likely due to peripheral drive are. For example, MD-IS interactions are consistently low during MVE, but higher during both ABD and ADD. During ABD, MD-IS coherence increases, particularly at low angles. During ADD, MD-IS coherence is consistently higher than during MVE and is maintained at a similar level across angles.

4.5.5.2 Minimal Peripheral Feedback during MVE allows examination of Posture-dependent Changes in Neural Drive

Upper limb position is known to affect the corticospinal excitability of arm muscles via the spinal circuits (Nuzzo et al., 2016). The same mechanisms could affect muscle interactions at different shoulder angles. Posture dependent alterations in muscle interactions were variable. Some interactions changed with angle during MVE. This could be due to a change in the biomechanics altering afferent feed from one muscle to motoneurones of another muscle. For example, during ABD and MVE, MD-TM coherence was high at 30° and progressively decreased as shoulder elevation increased to 120° (***figure 4.8A***). Loading of Golgi tendons at higher angles could inhibit MD-TM through the Ib pathway. During ADD, MD-TM coherence is consistently high at all angles.

4.5.6 Inter-subject Variability as a Useful Clinical Tool

4.5.6.1 Exploring Task-dependent Interactions across the Population

In studies looking at patterns of muscle activity, a high degree of variability amongst subjects is common. We can use the MVE task to identify interactions which are most consistently, or rarely present with MD activity. The goal is to determine common functional units activated by descending pathways in every healthy subject. In mid-range of motion (75°) during MVE, significant coherence with MD was present in at least 75% of the sample with PM and TM in low gamma only, MT in low and high gamma, and AD, PD and LT in all bands. In a clinical population, we could also use this data to identify aberrant interactions by contrasting MVE with the ABD and ADD. For example, MD-BB beta band coherence is significant in 95% of subjects during ADD. However, during ABD and MVE, only 20% and 33% of the sample

respectively show significant beta band coherence (***figure 4.26***). Since beta band coherence is associated with corticospinal activity, presence of MD-BB beta band coherence during ABD or MVE, or absence of it during ADD could be a marker of damage to the corticospinal tract. Likewise, significant MD-LD coherence is only present in 33% subjects during MVE, but in 80% during ABD.

4.5.6.2 Intermuscular Coherence to Improve Clinical Diagnostics

Following stroke, damage to the motor cortex has been shown to disrupt connectivity with the spinal cord causing muscle synergies to be merged, fractionated, or preserved (Cheung et al., 2012). The authors suggest that these patterns could be used as markers to quantify damage to the motor

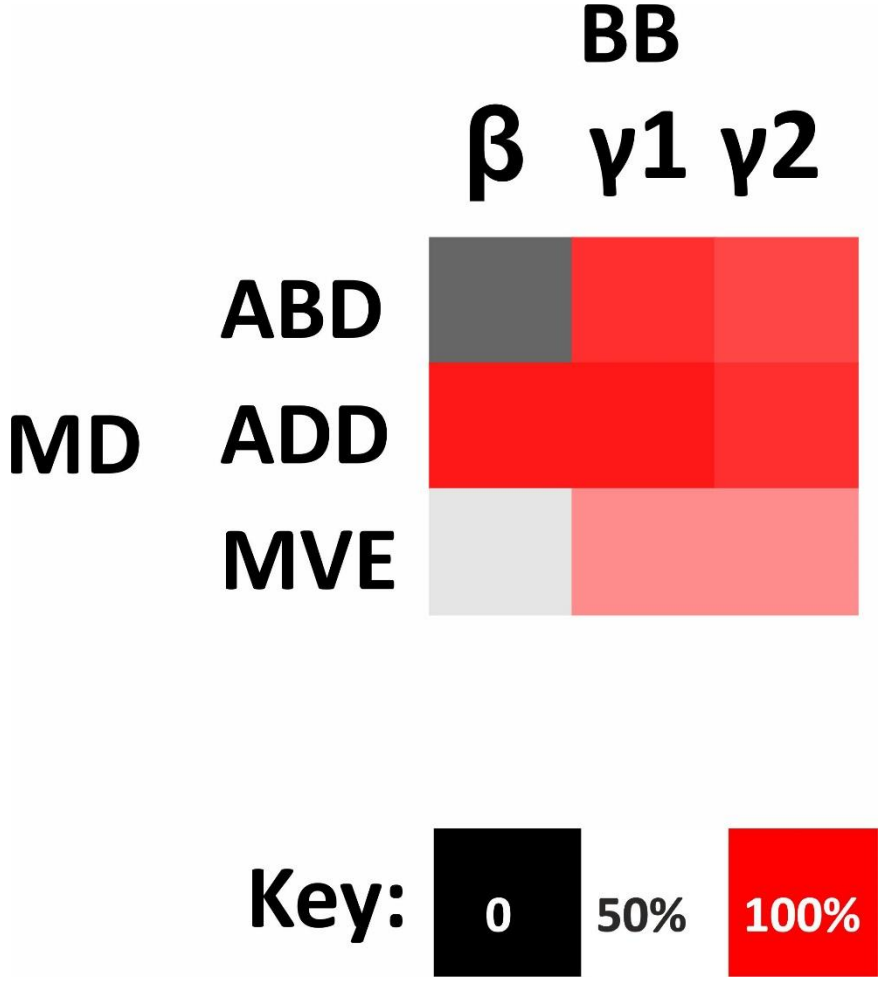

Figure 4.26. Variability across the sample. Shows interactions between MD-BB at 75°. A pair of muscles which would be clinically useful is one where 0% of the sample (black) showed coherence during one task and 100% (red) showed coherence during another (i.e. beta band activity).

cortex. Here we propose that a simpler clinical examination could be performed by looking at coherence patterns between fewer muscles. For example, recording from just 3 muscles: a shoulder abductor (MD), and an elbow flexor and extensor pair (BB and MT) may provide sufficient information. MD-BB and MD-MT interactions are absent during MVE in a healthy scenario. However, MD-BB or MD-MT interactions during MVE could indicate damage to descending pathways and aberrant co-activation of shoulder abductors and elbow flexors which occurs in the flexion synergy (Brunnstrom, 1966).

4.5.7 Experimental Limitations

Throughout the experiment, the best efforts were made to keep limb secured by using a rest in the mid portion of the arm to support the limb. However, wrist braces were not worn through the experiment which would have been preferably considering wrist muscle reflexes can affect more proximal muscles (Alexander and Harrison, 2003; Manning and Bawa, 2011).

Since EMGs were taken from shoulder, many muscles were close to the abdomen and subsequently contaminated with ECG activity from the heart and circulatory system. Depending on the subject, PM, AD, SA, TM, IS, LD suffered the worst contamination. All steps were taken to try and reduce contamination by ECG during electrode placement. We tried many methods for removing ECG artefacts post-hoc, but most either require a dedicated ECG channel or have consequences for the frequency domain (Lu et al., 2009; Abbaspour et al., 2015) so were not included in the final analysis.

The MVE task is intended to be easily adapted to the clinic. In practical purposes, this may not be possible in the clinic since many patients with injury to descending pathways suffer from increased muscle tone in the biceps brachii which prevents them from extending the elbow (a symptom of the flexor synergy) (Brunnstrom, 1966). However, the same principle can be applied with different limb configurations based on the symptoms of the condition being studied.

EMGs were recorded from the shoulder joint, where many muscles overlap or are in close proximity, increasing the possibility for crosstalk from overspill of

muscle activity between sensors (for example: PD-TM, TM-IS). Crosstalk can be measured by taking the square of the peak correlation index (Winter et al., 1994). Different shoulder positions also lead to a change in the configuration of muscles beneath the electrode possibly affecting coherence. This can be checked by observing coherence levels during different tasks at the same angle. If the change in coherence with angle is the same across tasks, this is possibly the effects of crosstalk. However if from task to task coherence levels vary then this is probably due to physiological not postural change.

The EMG system used here (Delsys Trigno™) applies filters between 20-450 Hz at the time of collection which cannot be removed. Subsequently, all analysis was carried out on frequency bands within this range which made observation of lower frequency bands impossible (alpha 8-12 Hz).

Most studies use a statistical framework to define a confidence limit which indicates a significant interaction between two muscles (Rosenberg et al., 1989; Amjad et al., 1997). In this method, the confidence interval is based on the number if disjointed sections used for analysis. For the typical amount of data for one subject (5 x 5s = 25 s), this meant that the confidence interval for coherence was in the region of 0.06, and for cross correlations was 0.02. Pooled coherence measures can overestimate significance (Baker, 2000). In our study, this problem was averted since all data for a given task was collected in the same session. However, since our measure of subject variability was a simple count of subjects over the confidence interval, this does not necessarily correlate well with the mean peak coherence measure.

4.5.8 Conclusions

Beta band corticomuscular coherence increases as a function of force during a sustained contraction (Kilner et al., 2000), and disappears to be replaced by gamma band coherence during dynamic tasks (Mehrkanoon et al., 2014). Both gamma and beta band corticomuscular coherence have shown to be sensitive to changes in peripheral activity (McClelland et al., 2012a; Schmied et al., 2014). This is usually attributed to long sensory loops involving the brain (Kasuga et al., 2017). Studies which measure corticomuscular coherence have a bias towards circuits at a cortical level. Local spinal circuits are rarely

considered to be a factor. Here we measured intermuscular coherence between multiple muscles. Whilst spinal involvement may not be directly identifiable from EMG-EMG coherence, we propose that by using coherence measures as an outcome by which to map common inputs across multiple muscles, intermuscular coherence could be a better tool for evaluating spinal pathways than corticomuscular coherence. Coherence patterns across multiple muscles can reveal shifts in coherence across motor pools rather than through a putative single pathway as with corticomuscular coherence. Motoneurones of muscles sharing input from an afferent pathway can be identified by observing the correlation half-width and coherence of agonists and antagonists. We can also use this information to identify monosynaptic information from descending or peripheral sources. We propose that with the relevant catalogues of the most ubiquitous interactions and pathways across healthy participants, we may should be able to easily diagnose injury to descending pathways by key muscle interactions, for example aberrant MD-BB interactions during MVE as a marker for damage to the corticospinal tract.

Chapter 5: Regulation of Group I and II reflexes from the forearm and hand to the human upper limb during arm cycling and tonic contractions

5.1 Abstract

In humans, details of heteronymous reflexes across joints of the upper limb are incomplete. Moreover, we do not know how group I and group II reflexes are differentially regulated during dynamic and static motor tasks. Dynamic tasks, such as locomotion can engage central pattern generator (CPG) networks in the spinal cord, which gate incoming signals from the periphery when active. However, nobody has yet shown how group I and II afferent pathways are regulated during CPG activity in the upper limb. To explore this, we recorded EMGs from 8 shoulder and arm muscles which serve different functions across the arm (pectoralis major, middle deltoid, biceps brachii, upper trapezius, lateral and medial triceps, flexor and extensor carpi radailis). Subjects (n = 4) performed isometric contractions, an arm cycling task, or were at rest. We assessed responses to ulnar nerve stimuli over a range of stimulation intensities (1 and 3T) and time windows (0-40 and 40-100, and 100-200ms respectively) to explore group I and group II activation. Short and long latency responses in elbow and wrist muscles were both easier to evoke during an isometric contraction than at rest even at low stimulation intensities, showing how reflexes are modulated at rest compared to a task with constant levels of contraction. Putative group II responses in shoulder muscles were present during arm cycling, but rarely at rest or during isometric contractions. We hypothesise that the difference in regulation between cycling and isometric tasks is likely related to activation of the spinal CPG.

5.2 Introduction

Effective positioning of the hand requires a stable base of support at the shoulder joint (Levin, 1996). This relies on cross-joint reflexes from afferent pathways from hand muscles to the shoulder joint. There is detailed literature on homonymous and heteronymous group I and group II in the cat (Baldissera et al., 1981; Edgley et al., 1988; Illert, 1996; Jankowska et al., 2002), and cross-joint interactions through Ia pathways in the baboon (Hongo et al., 1984). However, in humans, details of heteronymous reflexes across joints are incomplete. In humans, reflex responses can be elicited in the shoulder muscles by electrical stimulation of the median, and ulnar nerve at the level of the wrist and elbow, and the radial nerve at the level of the elbow and shoulder during weak contractions (Alexander and Harrison, 2003; Elliott et al., 2011). High stimulation intensities used during these studies means that these responses could involve activation of higher threshold afferents such as group II and maybe group III /IV fibres. Lourenço et al. have used nerve cooling and pharmacological approaches to isolate responses of group II pathways in wrist and hand muscles (Lourenço et al., 2006). However, we do not yet have data with which we can differentiate group I and group II responses in shoulder muscles.

Edgely and Jankowska (1987) showed that in the cat, group II afferent responses are elicited between 1.4 and 2.5 times motor threshold (Jankowska, 1987). The same group later showed how these pathways are involved in locomotion (Edgley et al., 1988). During locomotion, activity from peripheral pathways including group I and II afferents is regulated by neuronal networks known as central pattern generators (CPGs), which are conserved across vertebrates (Grillner, 1981; McCrea and Rybak, 2008). In the cat, CPGs depress group I, II and cutaneous afferent activity during locomotion (Perreault et al., 1999). In the human, lower limb CPG has been well documented. Humans with complete spinal injuries are capable of generating gait patterns with locomotor training (Dietz and Harkema, 2004), and cutaneous and proprioceptive reflexes are depressed or facilitated depending on the phase of the gait cycle (Zehr and Duysens, 2004). However, work on the human upper limb CPG is less comprehensive. Zehr has shown

presynaptic modulation of reflex pathways and regulation of cutaneous inputs during arm cycling, which provides strong evidence for the existence of a human upper limb CPG (Zehr et al., 2004; Hundza and Zehr, 2006). However, nobody has yet shown how group I and II afferent pathways are regulated during CPG activity in the upper limb.

In the study in this chapter, we used different stimulation intensities based on those outlined in the cat literature to elicit responses from group I and group II afferent fibres (Jankowska, 1987). Since we do not currently know how these pathways are regulated during different human behaviours, we studied responses at rest, during an isometric contraction, and during the flexion phase of an arm cycling task. The ulnar nerve innervates the anterior compartment of the forearm and intrinsic muscles of the hand. We stimulated the ulnar nerve at the level of the wrist whilst recording from multiple shoulder muscles and flexors and extensors of the elbow and wrist. This is towards developing a model of regulation of group I and II afferent activity at rest, during isometric contractions, and during dynamic movements.

5.3 Methods

Methods are described in the General Methods Chapter.

5.4 Results

Reflexes were evoked differentially in different muscles depending on the task and the stimulus intensity. At a low intensity, many muscles showed a short latency response. As the stimulus increased, medium and long latency responses were more common (***figure 5.1***).

5.4.1 Responses between different behavioural tasks

Responses were highly dependent on the task (***figure 5.2*** **and** ***5.3***). At rest, it was very rare for a response to be elicited in any muscle except wrist muscles. At 3T, short, medium and latency responses (0-40, 40-100 and 100-200 ms respectively) were present in ER and FR in at least 50% of subjects. In one subject, responses were present at all latencies at both 1T and 3T in LT and

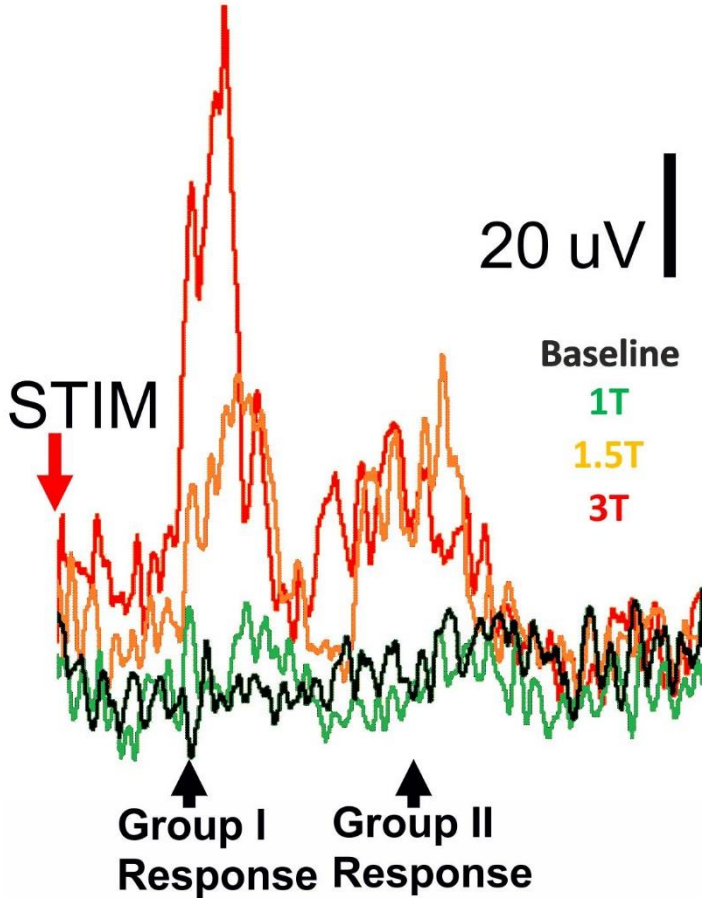

Figure 5.1. Example of group I and group II responses. Putative group I and group II responses evoked by stimulation of the ulnar nerve, recorded from FR. Each trace is the rectified average of 100 stimuli.

MT, and in PM at 3T. However, heteronymous reflexes were more prevalent in elbow and wrist muscles when subjects performed an isometric contraction. For example, short, medium and long latency responses were visible in UT, BB, LT, MT FR and ER in most subjects during tonic isometric contractions, and more so at 3T than at 1T. During tonic contractions, responses in PM were present at all latencies in one subject at 1T, and two subjects at 3T. Responses at medium and long latencies were present in all subjects in UT at 3T. During the flexion phase of arm cycling, responses were present more often than at rest or during tonic contractions, and more consistently across muscles.

5.4.2 Responses at different stimulation intensities

Different stimulation intensities elicited different heteronymous responses depending on the muscle (***figure 5.2* and *5.3***). In shoulder muscles (MD and UT), higher intensity stimulations elicited medium and long latency responses which were not present at lower stimulation intensities. At high intensities, long latency responses in elbow muscles (BB, LT and MT) were large.

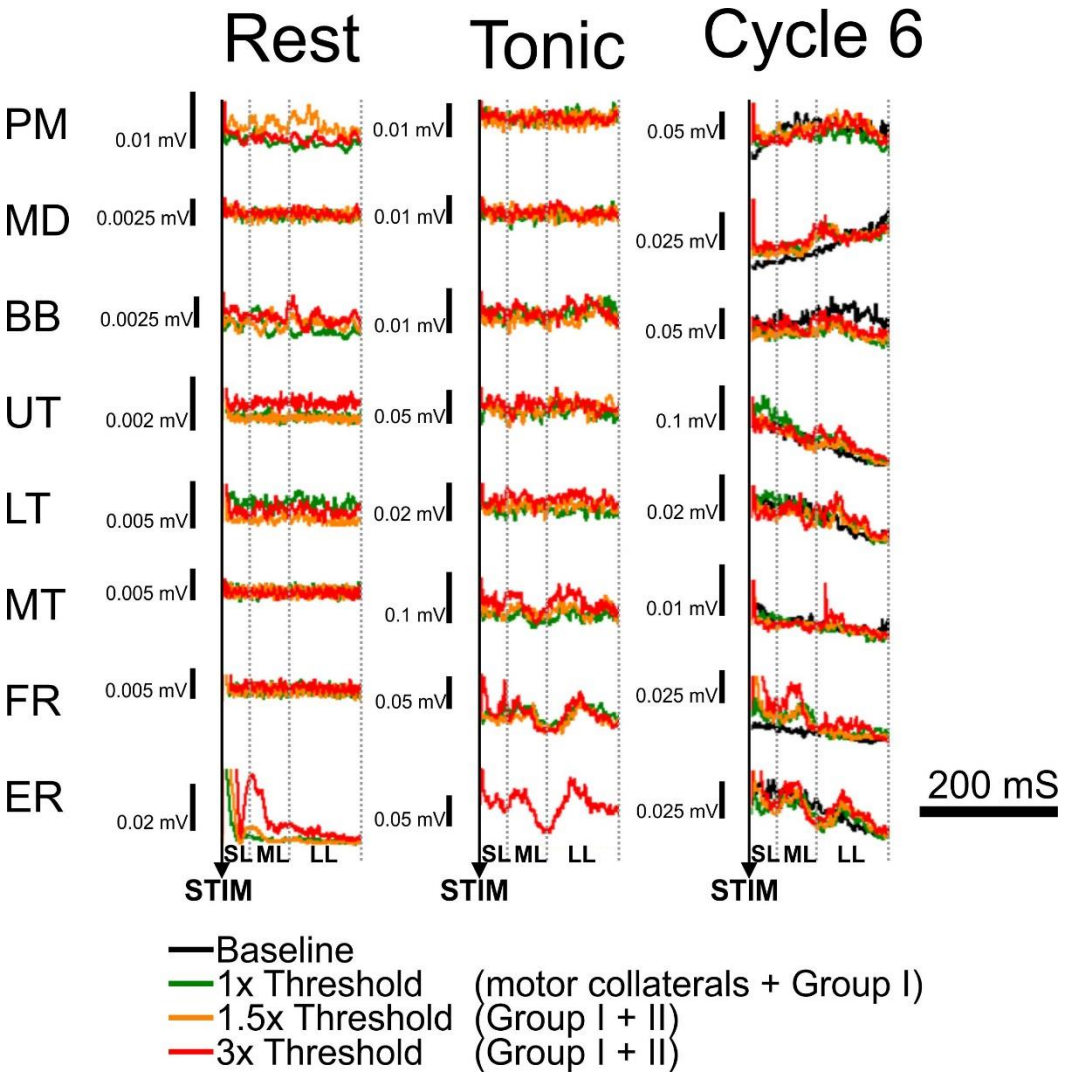

Figure 5.2. Representative traces from one subject. In one subject, responses were recorded at 1T, 1.5 and 3T. Traces show rectified averages of 100 stimuli. Dashed vertical lines demarcate the three time windows used for analysis – short latency (0-40 ms), medium latency (40-100 ms), and long latency (100-200 ms). Continuous vertical line shows stimulus time.

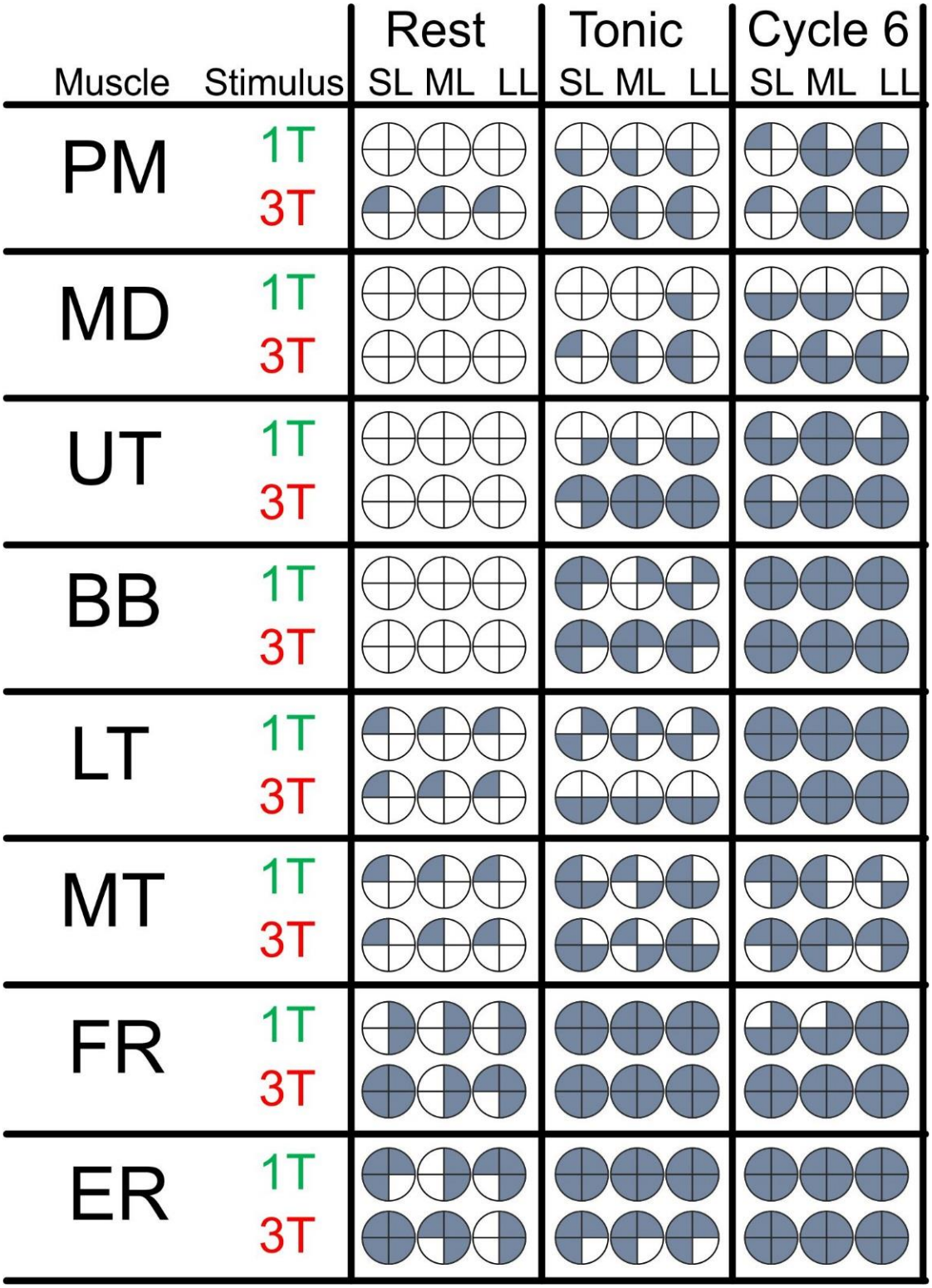

Figure 5.3. Summary table of evoked responses. Summary of evoked responses visually identified from 100 rectified and averaged traces across the sample. Each quarter of a circle represents on subject: top left – subject 1, top right – subject 2, bottom left – subject 3, bottom right – subject 4. Filled quarters indicate presence of a reflex.

5.5 Discussion

These data describe how group I and group II afferent fibres are modulated during different tasks. We presented responses to stimulation at 1T and 3T at rest, during an isometric contraction of the biceps brachii, and during the flexion phase of an arm cycling task. At rest, heteronymous responses are rare across the upper limb except in wrist muscles. During a tonic contraction of the biceps brachii, short, medium and long latency responses in elbow and wrist muscles became more prevalent, and during the flexion phase of arm cycling, medium and long latency responses in shoulder muscles were a common feature. The isometric contraction here was based around maintaining a constant level of activity on biceps brachii. This means that involvement of shoulder muscles in the task was probably minimal. However, during the cycling task, shoulder muscles are highly involved, and in this situation we can clearly see heteronymous responses in most muscles. This shows how reflex pathways are differently modulated during a repetitive task compared to one which requires maintenance of a constant level of contraction in a target muscle. The difference between the regulation between the two tasks is likely related to activation of the spinal CPG.

So far, nobody has shown differential regulation of group I and group II muscle afferents from hand muscles to the shoulder. This study illustrates that heteronymous responses depend highly both on the muscle, and the task at hand. It is perhaps not surprising that responses in shoulder muscles from wrist muscles afferents were minimal at rest, considering the results outlined in Chapter 4. In Chapter 4, we showed that cross-joint communication between the wrist and shoulder was minimal during an isometric task, and only present at low levels during specific tasks. However, we did not present any data recorded during a dynamic movement in Chapter 4. The results presented here show that afferent pathways from the wrist can affect more proximal muscles but this only occurs during dynamic movements.

Future studies will extend these results to outline how responses vary depending on different phases of the cycling task. More research is also needed to explain whether peripheral involvement during dynamic

movements affects intermuscular coherence measured using a similar technique applied in Chapter 4. Since FFT frequency coherence is not well suited to dynamic movements, a wavelet coherence may be more appropriate for these studies. We can also compare data from a frequency analysis to data showing how afferent pathways are regulated to determine whether a particular frequency band correlates with activity in an afferent pathway.

Heteronymous responses are small so it is a common requirement to average at least 30 traces of rectified data in order to identify reflexes in EMG data (Alexander and Harrison, 2003; Elliott et al., 2011). We recorded 100 traces to ensure reflexes would be visible in the data. Technically, it is difficult to differentiate between group I and group II responses. In the human forearm, arrival of group II responses coincides with that of group I responses from a putative transcortical pathways (Lourenço et al., 2006). In this study we differentiate group I responses from group II responses based on their latency and the stimulation intensity required to elicit the response. This is based on the fact that incrementally increasing the stimulus intensity will gradually recruit higher threshold afferent fibres. Longer latency responses correspond with activation of group II pathways (Jankowska, 1987).

Chapter 6: General Discussion

6.1 Summary of Findings

The role of the spinal cord and subcortical neural pathways in neuromuscular control is often overlooked. In turn, so is their possible utility as a target for rehabilitation. A large part of the studies presented here have focussed on methods to identify involvement of these pathways by applying frequency analysis to EMGs recorded non-invasively, and with the application of pathway-specific tasks and stimulation. This is an area of critical importance to the field of neurophysiology since at present, we cannot measure these pathways non-invasively. In cats, rats, and primates, we have detailed schematics of connections between these pathways, but the difficulty of identifying them in humans has until now prevented this data from being generated. This thesis exhibits novel experimental and analytical approaches with which we can probe subcortical and spinal pathways through patterns of EMG activity and patterns of inter-connectivity between muscles.

In the first chapter I have highlighted that key frequency bands relate to specific pathways; namely the corticospinal pathway (15-60 Hz), the reticulospinal pathway (35-100 Hz), and spinal pathways (60-100 Hz). I have shown for the first time that a time-frequency analysis of response to stimulation of specific pathways can enable us to determine neural drive to muscles in a muscle pair. Next, I used these frequency bands to identify task-dependent common drive to motoneurones of muscle pairs across the upper limb. In this study, I have shown a novel application of intermuscular frequency coherence analysis as a means to enable us to identify muscle synergies based on their neural drive. I also showed that with a novel MVE task, we can identify muscle interactions which make up key components of descending neural drive, and have shown how these are altered with activation of additional pathways. Finally, I showed data which details how specific afferent

pathways are regulated during different phases of dynamic movements, which has never been shown before in humans.

6.2 Discussion of Key Results

6.2.1 Contribution of Different Pathways to Specific Frequency Bands

Initially, we established a technique for applying a time-frequency analysis with high time and frequency resolution to evoked potentials. We were able to corroborate our findings with those using conventional neurophysiological methods using data from a previously published study (Forman et al., 2014). By applying this method to data recorded during specific tasks, we were able to reveal neural drive to muscles. Data collected during an arm cycling task engages CPG pathways. By contrasting EMGs recorded during this task to an amplitude-matched isometric task, we showed that with no stimulation, during the cycling task, frequencies above 60 Hz were increased in comparison to the tonic task. Since the arm cycling task engages CPG pathways, we hypothesised that frequencies above 60 Hz were related to CPG activity. By stimulating different levels of the CNS, namely the motor cortex and the pyramidal tract, we were able to show that in fact it is likely that frequencies above 60 Hz are predominantly spinal in origin. This is exhibited by the fact that when TMES was delivered during cycling, the 60-100 Hz band was still increased. This is in agreement with studies which have recorded from muscle or motoneurones from muscles with CPG input (Bruce and Ackerson, 1986; Smith and Denny, 1990). We were also able to identify that subcortical, probably reticulospinal pathways contribute to the 35-60 Hz band since this band is increased with TMS during cycling, which is supported by findings in the primate (Nishimura et al., 2009) and human stroke patients (Rossiter et al., 2013). We were also able to show that the frequencies associated with corticospinal activity are predominantly within the range of 15-60 Hz, which is in general agreement with the bands cited in the literature (Conway et al., 1995; Ritterband-Rosenbaum et al., 2016). This is the first time that it has been shown that at physiologically relevant latencies, the frequency content of EMG in response to stimulation correlates with activity from specific

pathways. Another important finding in these results is that high frequencies within the EMG which are often overlooked may contain valuable data relating to activation of spinal pathways.

6.2.2 High Resolution Wavelet Transform Reveals Frequency Content of Evoked Potentials at Physiologically Relevant Latencies

Commonly, frequency analysis is undertaken using the FFT. This has the disadvantage of having no time resolution meaning that we cannot assess frequency changes over a short frame. We used a Wavelet Synchro-Squeezed Transform to transform EMG data with both optimal time and optimal frequency resolution. This meant that we were able to apply this to measure the frequency content of MEPs in response to stimulation – something which has not been possible before. To measure frequency bands of interest, we applied a filter to the signal of each band before applying the transform. This allowed us to mitigate side lobes and bleeding between bands and provide a clear signal for each frequency band in the spectrogram. This is a common step for engineers utilising digital signal processing. However, it is not commonly applied to EMG data. We propose that this will allow a more sensitive method to detect transient changes within a given frequency band.

6.2.3 Intermuscular Coherence Reveals Neural Muscle Synergies and Task-Dependent Shift in Neural Drive

The next part of my studies involved applying the frequency bands outlined in the first chapter to an intermuscular coherence analysis by which we could identify task-dependent neural drive to muscles. Due to the high quantity of data produced by the many dimensions of the dataset (e.g. muscles x frequency bands x tasks), this was a considerable task. This was eventually possible through automating different levels of the analysis. By measuring coherence between muscle pairs, we were able to show that interactions between muscle pairs were altered, and often showed a shift in the neural pathways generating muscle activity depending on the task at hand. This is an interesting finding since it is often thought that neural correlates of motor primitives are hard wired into the nervous system. We believe that this could

be a demonstration of the flexibility of the spinal functional units depending on the incoming neural information (Baldissera et al., 1981; Illert, 1996).

Muscle synergy analysis shows interesting clinical applications if we are able to relate activity patterns to specific pathways (Cheung et al., 2012). However, at current, most studies which apply muscle synergy analysis use methods which do not reveal the neural drive to muscles (Tresch et al., 2006; Roh et al., 2013). By applying intermuscular coherence to a muscle synergy analysis, we have shown that it is possible to identify neural correlates of muscle synergies. Very few have attempted this previously, although recently there has been a move towards similar methods of analysis in the field (Kerkman et al., 2018). We were able to show that many muscle pairs (BB-MD, TM-IS, MD-ER) were receiving greatly different neural input between different tasks. We were also able to show common input to muscles acting across joints, and how these interactions depend on specific pathways.

6.2.4 MVE Task as a Means to Reveal Muscle Pairs Receiving Shared Descending Drive

In this study, we employed a novel MVE task. Since no force was applied during MVE, interactions can be used as an indicator of intact descending pathway. This allows us to assess muscle interactions which are not influenced by common neural drive from peripheral pathways as the case when recording conventional MVCs. There are many systematic problems with recording MVCs, and important information is lost commonly only the muscle of interest is recorded during MVCs. We believe that implementing MVEs might be a better way to assess descending pathways in a clinical situation. EMGs can be recorded from key muscles which we have previously identified as receiving a common descending input to use as a marker for damage to descending systems.

6.2.5 Inter-Subject Variability

Current predictions of recovery following stroke do not correlate well with the actual recovery (Prabhakaran et al., 2007). A high degree of variability in muscle activation patterns between subjects is also common. In order to

address inter-subject variability in a healthy population, we provided a count of how many subjects across the sample showed significant coherence between muscle pairs. During the MVE task, we wanted to identify interactions which are most consistently, or rarely present with MD activity. We determined that in at least 75% of the sample, MD showed significant coherence with PM and TM in low gamma only, MT in low and high gamma, and AD, PD and LT in all bands. We propose that identifying key muscle interactions which are homogenous across the sample will be useful for patient stratification in a clinical scenario.

6.3 Transferability of Methods to other Contexts

6.3.1 Custom-Written System for Time-Frequency Analysis of Evoked Potentials

Here, we generated a system of scripts which can be used to record time points from standard electrophysiological measurements (such as peak, onset etc.) which can then be exported to a time-frequency analysis. The script library encompasses scripts written in languages for different programs suited to different analysis techniques. We applied this system to gather data about frequency content of a signal at the peak response time of an evoked potential by TMS or TMES. This system is readily transferable to many different electrophysiological contexts. For example, it could be used for peripheral nerve stimulation, or for long latency loops. As well as power spectral density using WSST, we also have scripts to measure frequency coherence between two wavelet transforms. This transferability means that these scripts and this system can be easily adapted to address many other experimental questions.

6.3.2 Custom-Written System for Onset/Offset, Amplitude, Power, Coherence, Phase, and Cross-Correlation Analysis

The scripts written for Chapter 3 are also widely transferable and can easily be adapted to answer other experimental questions. Once users have marked the onset and offset of different muscles, it is easy to obtain many different analytical measurements, including amplitude analysis and relative measurements of time points in different muscles (peak, onset, offset). In this

study we addressed a specific question related joint angle and task context during constant isometric tasks and focussed on FFT based frequency coherence and cross-correlation analysis. Whilst this system was optimised to meet this criteria, it is not limited to the study of isometric tasks. The core of this system is based on studies in the cat which assess muscle onset and offset in relation to gait cycles in the cat (Duysens, 1977; Drew and Rossignol, 1987). It can therefore be easily applied to muscle synergy analysis during dynamic tasks, cycling tasks, walking etc.

6.4 A Catalogue of Common Synaptic Inputs to Motoneurones across the Human Upper Limb

Studies of neural pathways innervating forelimb muscles in animals are comprehensive. In primates we have details of descending pathways from the brain and subcortical structures (Kuypers, 1981; Lemon, 2008), we have details of cross joint interactions through Ia pathways in the baboon (Hongo et al., 1984), and details of group I and II pathways in the forelimb of the cat (Baldissera et al., 1981; Jankowska et al., 2002). However, due to the difficulty of accessing these pathways experimentally, details of muscle interactions between the human shoulder and upper limb are incomplete (Pierrot-Deseilligny and Burke, 2012). One of the primary objectives of this work was to bring details of muscle interactions in humans closer to data from animal models by creating a catalogue of shared inputs to muscle pairs at the shoulder and across the upper limb. We have provided details of muscle interactions of major muscle groups across the human upper limb including details of cross joint interactions. This is towards an objective, synergy-based assessment of patients which could be used to improve current clinical measures and predictions of recovery.

6.5 Clinical significance

6.5.1 Assessment of Descending Pathways by Time-Frequency Analysis of Evoked Responses

Current methods of assessing damage to descending pathways are variable. Imaging approaches such as fMRI are costly and require a high level of technical expertise. Importantly, no methods are currently available to assess the integrity of descending pathways using a physiological measure. We have presented a method potential by which we can non-invasively examine fidelity of cortical and subcortical circuits by observing the frequency content of EMG signals in response to TMS. This will be useful to assess connectivity in residual pathways following an injury such as stroke or spinal cord injury in hemiplegic patients with some residual capacity for movement on the unaffected side. Subjects could be asked to attempt a cycling task or an MVC, during which a TMS pulse could be delivered. By comparing the frequency spectra between the two tasks, we could assess the extent of injury by examining which frequencies are altered in the response.

6.5.2 Arm Cycling as an Activity Based Therapy

Several studies have attempted to use arm cycling as a therapeutic intervention following stroke (Broeks et al., 1999; Diserens et al., 2007) though long term, loss of arm function is still a common problem. The CPG in the human upper limb appears to be involved in regulating input to the motor pool during repetitive movements (Zehr et al., 2004). We propose that with more data relating to the regulation of descending, spinal, and afferent pathways, stimulation could be timed according to the cycle in order to encourage plasticity in the deficient pathways.

6.5.3 Intermuscular Coherence to Improve Clinical Diagnostics

Following stroke, muscle activation patterns show distinctive patterns of activity such as the flexion synergy (Brunnstrom, 1966) or merging and fractionation (Cheung et al., 2012). Assessment of muscle synergies could be a useful tool to quantify damage to the motor cortex. Here we have proposed

that we could use coherence analysis to reduce the complexity of a clinical muscle synergy analysis by identifying key muscle pairs which can tell us about the integrity of descending pathways. From the data presented here, we suggest that recording from just 3 muscles may be enough to give us this information by recording MD (a shoulder abductor), BB (an elbow flexor) and MT (an elbow extensor). MD-BB and MD-MT interactions are absent during MVE in a healthy scenario, but during ABD and ADD these interactions are present. MD-BB or MD-MT interactions during MVE could indicate damage to descending pathways. We will develop an App for a tablet or smart phone which is user friendly in order that practitioners with little or technical expertise can apply it in a clinical scenario (***figure 6***). The App will interpret EMG data based on muscle interactions during a predefined MVE task where the limb is in a specific position. A coherence analysis will be performed on the EMG data and a clinical summary of remaining pathways and predicted recovery will be returned to the examiner.

6.6 Future directions

6.6.1 Incorporation of Clinical Data

The data presented here describes measurements taken from healthy adults. We have presented a description of specific frequency bands which relate to neural drive to muscle, and a catalogue of muscles which share common drive. The next steps is to repeat these studies in individuals with a known loss. This data would allow us to confirm which muscle pairs would be useful to use in a frequency analysis for diagnostic examination of specific pathways.

6.6.2 Moving forward with the study of High frequency components of EMG

We have outlined that high frequency components of EMG signals could contain valuable information relating to activation of subcortical and spinal pathways. However, these aspects of EMG data are often overlooked because i. high frequencies are commonly assumed to be noise

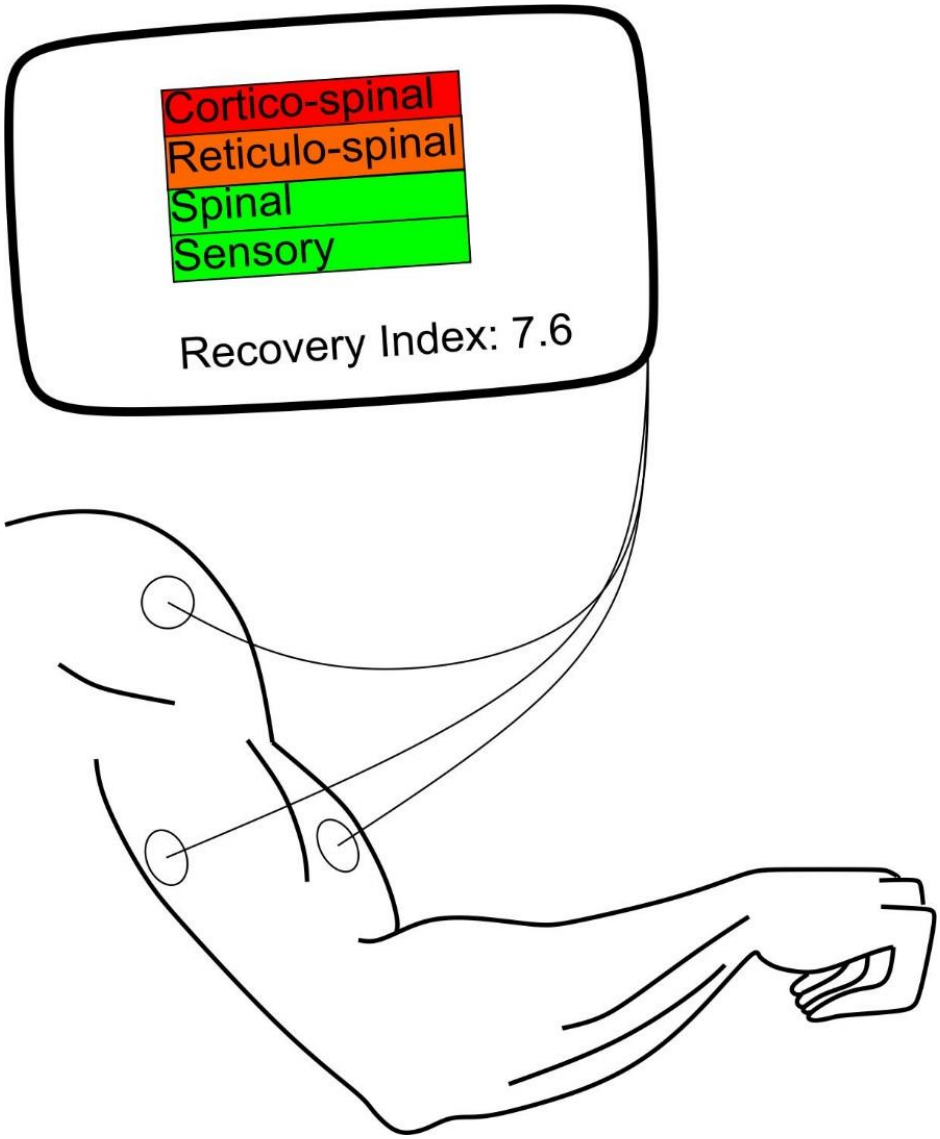

Figure 6. Proposed diagnostic App for use in the clinic. Coherence could be measured between key muscle pairs, and a battery of tasks could be performed to identify which pathways are still intact. The frequency bands for specific pathways were outlined in Chapter 3 and the tasks when specific pathways are expected to be active were outlined in Chapter 4.

(De Luca and Erim, 1994) and ii. before coherence analysis is performed, data is almost always rectified, which shifts power from higher frequencies to lower frequencies (Boonstra and Breakspear, 2012). At current, we still do not know whether high frequencies in the EMG relate to motor unit activity. Motor unit firing above 25 Hz has rarely been described in the literature, possibly because of experimental conditions required for recording single motor unit activity (restricted movement, low force contractions, use of anaesthetised animal preparations) , as well as analytic measures (e.g. mean rather than range) (Linnamo, 2002; Kallio et al., 2013; Johnson et al., 2017). Using high-

density surface EMGs, it is possible to extract recordings of individual motor units from the skin surface (Farina & Holobar, 2016). Future studies should focus on identifying a central or peripheral source for motor unit action potentials using these techniques and follow up with how this may manifest in whole-muscle EMG.

6.6.3 Investigating Differences in Proximal and Distal Innervation in Relation to Coherence

The data presented here was recorded mainly from proximal muscles. This may explain why occurrence of beta band activity was relatively uncommon in these data sets. Most coherence studies use muscles of the hand when studying corticomuscular coherence, where beta band activity is common. These discrepancies may be explained by differences in the innervation of proximal and distal muscles (Lemon, 1993; Lemon, 2008). If beta band (15-35 Hz) and gamma band (35-100 Hz) coherence are seen in distal and proximal muscles respectively, this may be a useful physiological marker of corticospinal and reticulospinal innervation. Future studies should seek to further investigate cross-joint coherence. Based on the data presented here, it seems likely that the anatomy of the pathways innervating the proximal and distal limb will correlate with differences in coherent frequencies. It is also pertinent to learn more about how innervation from different pathways is distributed across joints.

6.7 Concluding Remarks

We set out with the objective of developing tools and data which allow non-invasive ways to measure activity in inaccessible but important pathways, such as those in the spinal cord and brainstem. To achieve this, we applied pathway-specific tasks and stimulation in order to associate define frequency bands in the EMG which relate to activity in specific pathways. This required the development of an analysis pipeline which could be used to demarcate time points of interest and then measure the frequency distribution or frequency coherence at the required time point. Using this system, we have shown evidence that the corticospinal pathway produces EMG activity in the

15-60 Hz, subcortical pathways in the 35-100 Hz range, and spinal pathways in the 60-100 Hz range. The justification for this was based on alterations in the frequency domain due to tasks or stimulation which activated specific pathways. Using this information, we applied intermuscular coherence to a muscle synergy analysis which we were able to use to identify key modules of muscles activated by descending pathways, catalogue muscle interactions across the upper limb, and identify shifts in muscle interactions which were dependent on task and limb position. This involved constructing a system based on studies of gait analysis in cats which could be used to take different measurements from the data based off of onset and offset time points of muscle bursting. Finally, we demonstrated the involvement of high and low threshold peripheral pathways in a dynamic and static task of the upper limb. These works have produced techniques with potential applications to clinical practice by providing metrics by which we can assess functional descending pathways, and using frequency coherence analysis as a diagnostic tool. We have also shown patient-friendly behavioural tasks which can be useful for clinical assessment, and a means by which we can assess variability in a healthy and patient population. Repeating these experiments in a clinical population will be valuable to contrast with the results described here.

References

Abbaspour, S., Linden, M. and Gholamhosseini, H. 2015. ECG artifact removal from surface EMG signal using an automated method based on wavelet-ICA. *Stud. Health Technol. Inform.* **211**(May), pp.1–6.

Alexander, C.M. and Harrison, P.J. 2003. Reflex connections from forearm and hand afferents to shoulder girdle muscles in humans. *Experimental Brain Research*. **148**(3), pp.277–282.

Amjad, A.M., Halliday, D.M., Rosenberg, J.R. and Conway, B.A. 1997. An extended difference of coherence test for comparing and combining several independent coherence estimates: Theory and application to the study of motor units and physiological tremor. *Journal of Neuroscience Methods*. **73**, pp.69–79.

Armstrong, D. and Drew, T. 1985. Forelimb electropyographic responses to motor cortex stimulation during locomotion in the cat. *J Physiol*. **367**, pp.327–351.

Baker, M.R. and Baker, S.N. 2003. The effect of diazepam on motor cortical oscillations and corticomuscular coherence studied in man. *The Journal of physiology*. **546**(Pt 3), pp.931–942.

Baker, S.N. 2007. Oscillatory interactions between sensorimotor cortex and the periphery. *Current Opinion in Neurobiology*. **17**(6), pp.649–655.

Baker, S.N. 2000. 'Pooled coherence' can overestimate the significance of coupling in the presence of inter-experiment variability. *Journal of Neuroscience Methods*. **96**(2), pp.171–172.

Baker, S.N. 2011. The primate reticulospinal tract, hand function and functional recovery. *The Journal of physiology*. **589**, pp.5603–12.

Baldissera, F., Hultborn, H. and Illert, M. 1981. Integration in spinal neuronal systems. *Comprehensive Physiology*.

Bernshteĭn, N. 1967. The co-ordination and regulation of movements.

Bizzi, E., Cheung, V.C.K., D'Avella, A., Saltiel, P. and Tresch, M. 2008. Combining modules for movement. *Brain Research Reviews*. **57**, pp.125–133.

Bohannon, R.W. and Smith, M.B. 1987. Interrater reliability of a modified Ashworth scale of muscle spasticity. *Physical therapy*. **67**(2), pp.206–207.

Boonstra, T.W. and Breakspear, M. 2012. Neural mechanisms of intermuscular coherence: implications for the rectification of surface electromyography. *Journal of Neurophysiology*. **107**(3), pp.796–807.

Boonstra, T.W., Danna-Dos-Santos, A., Xie, H.-B., Roerdink, M., Stins, J.F. and Breakspear, M. 2015. Muscle networks: Connectivity analysis of EMG activity during postural control. *Scientific Reports*. **5**, p.17830.

Broeks, J.G., Lankhorst, G.J., Rumping, K. and Prevo, A.J. 1999. The long-term outcome of arm function after stroke: results of a follow-up study. *Disability and rehabilitation*. **21**(8), pp.357–64.

Brown, P. 2000. Cortical drives to human muscle: The Piper and related rhythms. *Progress in Neurobiology*. **60**(1), pp.97–108.

Brown, P., Salenius, S., Rothwell, J.C. and Hari, R. 1998. Cortical correlate of the Piper rhythm in humans. *Journal of neurophysiology*. **80**(6), pp.2911–7.

Bruce, E.N. and Ackerson, L.M. 1986. *High-Frequency Oscillations in Human Electromyograms During Voluntary Contractions*.

Brunnstrom, S. 1966. Motor testing procedures in hemiplegia: based on sequential recovery stages. *Physical therapy*. **46**(4), pp.357–75.

Buchanan, T.S. and Almdale, D.P.J. 1986. Characteristics of synergic relations during isometric contractions of human elbow muscles. *Journal of neurophysiology*. (5).

Budini, F., McManus, L.M., Berchicci, M., Menotti, F., Macaluso, A., Di Russo, F., Lowery, M.M. and De Vito, G. 2014. Alpha Band Cortico-Muscular Coherence Occurs in Healthy Individuals during Mechanically-Induced Tremor. *PloS one*. **9**(12), p.e115012.

Burke, R.E. 1981. Motor units: anatomy, physiology, and functional organization. *Comprehensive Physiology*. (543).

Carod-Artal, F.J. and Egido, J.A. 2009. Quality of life after stroke: The importance of a good recovery. *Cerebrovascular Diseases*. **27**(SUPPL. 1), pp.204–214.

Carroll, T.J., Baldwin, E.R.L., Collins, D.F. and Zehr, E.P. 2006. Corticospinal excitability is lower during rhythmic arm movement than during tonic contraction. *Journal of neurophysiology*. **95**(2), pp.914–21.

Castronovo, A.M., Negro, F., Conforto, S. and Farina, D. 2015. the Proportion of Common Synaptic Input To Motor Neurons Increases With an Increase in Net Excitatory Input. *Journal of Applied Physiology*., jap.00255.2015.

Chakarov, V., Naranjo, J.R., Schulte-Monting, J., Omlor, W., Huethe, F. and Kristeva, R. 2009. Beta-Range EEG-EMG Coherence With Isometric Compensation for Increasing Modulated Low-Level Forces. *Journal of Neurophysiology*. **102**(2), pp.1115–1120.

Chang, Y.-J., Chou, C.-C., Chan, H.-L., Hsu, M.-J., Yeh, M.-Y., Fang, C.-Y., Chuang, Y.-F., Wei, S.-H. and Lien, H.-Y. 2012. Increases of

Quadriceps Inter-Muscular Cross-Correlation and Coherence during Exhausting Stepping Exercise. *Sensors*. **12**(12), pp.16353–16367.

Cheung, V.C.K., D'Avella, A., Tresch, M.C. and Bizzi, E. 2005. Central and sensory contributions to the activation and organization of muscle synergies during natural motor behaviors. *The Journal of neuroscience : the official journal of the Society for Neuroscience*. **25**(27), pp.6419–6434.

Cheung, V.C.K., Turolla, a., Agostini, M., Silvoni, S., Bennis, C., Kasi, P., Paganoni, S., Bonato, P. and Bizzi, E. 2012. Muscle synergy patterns as physiological markers of motor cortical damage. *Proceedings of the National Academy of Sciences*. **109**(36), pp.14652–14656.

Clough, J.F., Kernell, D. and Phillips, C.G. 1968. The distribution of monosynaptic excitation from the pyramidal tract and from primary spindle afferents to motoneurones of the baboon's hand and forearm. *The Journal of physiology*. **198**(1), pp.145–66.

Conway, B.A., Halliday, D.M., Farmer, S.F., Shahani, U., Maas, P., Weir, A.I. and Rosenberg, J.R. 1995. Synchronization between motor cortex and spinal motoneuronal pool during the performance of a maintained motor task in man. *The Journal of physiology*. **489**(3), pp.917–924.

d'Avella, A., Fernandez, L., Portone, A. and Lacquaniti, F. 2008. Modulation of phasic and tonic muscle synergies with reaching direction and speed. *Journal of neurophysiology*. **100**(3), pp.1433–1454.

Darby, S.A. and Frysztak, R.J. 2013. Chapter 9 - Neuroanatomy of the Spinal Cord *In*: *Neuroanatomy of the Spinal Cord*. Mosby, pp.341–412.

Delagi, E., Iazzetti, J., Perotto, A. and Morrison, D. 2011. *Anatomical guide for the electromyographer: the limbs and trunk*. Charles C Thomas.

Dewald, J.P.A., Pope, P.S., Given, J.D., Buchanan, T.S. and Rymer, W.Z. 1995. Abnormal muscle coactivation patterns during isometric torque generation at the elbow and shoulder in hemiparetic subjects. *Brain*. **118**(2), pp.495–510.

Dietz, V. and Harkema, S.J. 2004. Locomotor activity in spinal cord-injured persons. *Journal of applied physiology (Bethesda, Md. : 1985)*. **96**, pp.1954–1960.

Diserens, K., Perret, N., Chatelain, S., Bashir, S., Ruegg, D., Vuadens, P. and Vingerhoets, F. 2007. The effect of repetitive arm cycling on post stroke spasticity and motor control Repetitive arm cycling and spasticity.

Drew, T., Kalaska, J. and Krouchev, N. 2008. Muscle synergies during locomotion in the cat: a model for motor cortex control. *The Journal of physiology*. **586**, pp.1239–1245.

Drew, T. and Rossignol, S. 1987. A kinematic and electromyographic study of cutaneous reflexes evoked from the forelimb of unrestrained walking

cats. *Journal of neurophysiology*. **57**(4), pp.1160–84.

Duysens, J. 1977. *Reflex Control of Locomotion as Revealed by Stimulation of Cutaneous Afferents in Spontaneously Walking Premammillarv Cats*.

Eccles, J.C., Eccles, R.M. and Lundberg, A. 1957. The convergence of monosynaptic excitatory afferents on to many different species of alpha motoneurones. *The Journal of Physiology*. **137**(1), pp.22–50.

Edgley, S.A., Jankowska, E. and Shefchyk, S. 1988. Evidence that mid-lumbar neurones in reflex pathways from group II afferents are involved in locomotion in the cat. *The Journal of Physiology*. **403**(1), pp.57–71.

Elliott, S.C., Hanson, J.R., Wellington, J. and Alexander, C.M. 2011. Reflex control of posterior shoulder muscles from arm afferents in healthy people. *Journal of Electromyography and Kinesiology*. **21**(6), pp.1087–1091.

Engberg, I., Lundberg, A. and Ryall, R.W. 1968. *Reticulospinal Inhibition of Transmission in Reflex Pathways*.

Farina, D., Negro, F. and Jiang, N. 2013. Identification of common synaptic inputs to motor neurons from the rectified electromyogram. *The Journal of physiology*. **591**(Pt 10), pp.2403–18.

Farmer, S.F. 1998. Rhythmicity, synchronization and binding in human and primate motor systems. *Journal of Physiology*. **509**(1), pp.3–14.

Farmer, S.F., Bremner, F.D., Halliday, D.M., Rosenberg, J.R. and Stephens, J.A. 1993. The frequency content of common synaptic inputs to motoneurones studied during voluntary isometric contraction in man. *Journal of Physiology*. **470**, pp.127–155.

Fetz, E.E. and Finocchio, D. V. 1975. Correlations between activity of motor cortex cells and arm muscles during operantly conditioned response patterns. *Experimental Brain Research*. **23**(3), pp.217–240.

Fisher, K.M., Zaaimi, B. and Baker, S.N. 2012. Reticular formation responses to magnetic brain stimulation of primary motor cortex. *The Journal of physiology*. **590**, pp.4045–60.

Flash, T. and Hochner, B. 2005. Motor primitives in vertebrates and invertebrates. *Current Opinion in Neurobiology*. **15**(6), pp.660–666.

Forman, D., Raj, A., Button, D.C. and Power, K.E. 2014. Corticospinal excitability of the biceps brachii is higher during arm cycling than an intensity-matched tonic contraction Corticospinal excitability of the biceps brachii is higher during arm cycling than an intensity-matched tonic contraction. *Journal of Neurophysiology*. (June 2014), pp.1142–1151.

Gandevia, S.C. 2001. Spinal and supraspinal factors in human muscle fatigue. *Physiological reviews*. **81**(4), pp.1725–89.

Georgopoulos, A.P. and Stefanis, C.N. 2007. Local shaping of function in the motor cortex: Motor contrast, directional tuning. *Brain Research Reviews*. **55**(2 SPEC. ISS.), pp.383–389.

Gladstone, D.J., Danells, C.J. and Black, S.E. 2014. The Fugl-Meyer Assessment of Motor Recovery after Stroke: A Critical Review of Its Measurement Properties.

Grillner, S. 1981. Control of Locomotion in Bipeds, Tetrapods, and Fish *In*: *Comprehensive Physiology*.

Gross, J., Tass, P.A., Salenius, S., Hari, R., Freund, H.J. and Schnitzler, A. 2000. Cortico-muscular synchronization during isometric muscle contraction in humans as revealed by magnetoencephalography. *Journal of Physiology*. **527**(3), pp.623–631.

Grosse, P., Cassidy, M.J. and Brown, P. 2002. EEG-EMG, MEG-EMG and EMG-EMG frequency analysis: Physiological principles and clinical applications. *Clinical Neurophysiology*. **113**(10), pp.1523–1531.

Guzmán-López, J., Selvi, A., Solà-Valls, N., Casanova-Molla, J. and Valls-Solé, J. 2015. Effects of postural and voluntary muscle contraction on modulation of the soleus H reflex by transcranial magnetic stimulation. *Experimental Brain Research*. **233**(12), pp.3425–3431.

Halliday, D.M., Conway, B. a, Farmer, S.F., Shahani, U., Russell, a J. and Rosenberg, J.R. 2000. Coherence between low-frequency activation of the motor cortex and tremor in patients with essential tremor. *Lancet*. **355**(9210), pp.1149–1153.

Halliday, D.M., Conway, B.A., Farmer, S.F. and Rosenberg, J.R. 1998. Using electroencephalography to study functional coupling between cortical activity and electromyograms during voluntary contractions in humans. *Neuroscience Letters*. **241**(1), pp.5–8.

Halliday, D.M., Rosenberg, J.R., Amjad, A.M., Breeze, P., Conway, B.A. and Farmer, S.F. 1996. A framework for the analysis of mixed time series/point process data-Theory and application to the study of physiological tremor, single motor unit discharges and electromyograms. *Progress in Biophysics and Molecular Biology*. **64**(2–3), pp.237–278.

Hilt, P.M., Delis, I., Pozzo, T. and Berret, B. 2018. Space-by-Time Modular Decomposition Effectively Describes Whole-Body Muscle Activity During Upright Reaching in Various Directions. *Frontiers in Computational Neuroscience*. **12**(April), pp.1–19.

Hirashima, M. and Oya, T. 2016. How does the brain solve muscle redundancy? Filling the gap between optimization and muscle synergy hypotheses. *Neuroscience Research*. **104**, pp.80–87.

Hongo, T., Lundberg, A., Phillips, C.G. and Thompson, R.F. 1984. The pattern of monosynaptic Ia-connections to hindlimb motor nuclei in the

baboon: a comparison with the cat. *Proc R Soc Lond B Biol Sci*. **221**(1224), pp.261–289.

Hultborn, H., Jankowska, E. and Lindström, S. 1971. Recurrent inhibition of interneurones monosynaptically activated from group Ia afferents. *The Journal of physiology*. **215**, pp.613–636.

Hundza, S.R. and Zehr, E.P. 2006. Cutaneous reflexes during rhythmic arm cycling are insensitive to asymmetrical changes in crank length. *Experimental Brain Research*. **168**(1–2), pp.165–177.

Iles, J.F. 1996. Evidence for cutaneous and corticospinal modulation of presynaptic inhibition of Ia afferents from the human lower limb. *The Journal of physiology*. **491 (Pt 1**, pp.197–207.

Iles, J.F. 1986. Reciprocal inhibition during agonist and antagonist contraction. *Experimental Brain Research*. **62**(1), pp.212–214.

Iles, J.F. and Pisini, J. V 1992. Cortical modulation of transmission in spinal reflex pathways of man. *The Journal of physiology*. **455**, pp.425–446.

Illert, M. 1996. Monosynaptic Ia pathways and motor behaviour of the cat distal forelimb *In*: *Acta Neurobiologiae Experimentalis*., pp.423–433.

Isa, T., Ohki, Y., Alstermark, B., Pettersson, L.-G. and Sasaki, S. 2007. Direct and indirect cortico-motoneuronal pathways and control of hand/arm movements. *Physiology (Bethesda, Md.)*. **22**, pp.145–152.

Jankowska, E. 1987. Field Potentials Generated by Group II Muscle Afferents in the Middle Lumbar Segments of the Cat Spinal Cord. *October*. (1987), pp.393–413.

Jankowska, E., Slawinska, U. and Hammar, I. 2002. On organization of a neuronal network in pathways from group II muscle afferents in feline lumbar spinal segments. *The Journal of physiology*. **542**, pp.301–314.

Johnson, M.D., Thompson, C.K., Tysseling, V.M., Powers, R.K. and Heckman, C.J. 2017. The potential for understanding the synaptic organization of human motor commands via the firing patterns of motoneurons. *Journal of Neurophysiology*. **118**(1), pp.520–531.

Kallio, J., Søgaard, K., Avela, J., Komi, P. V, Selänne, H. and Linnamo, V. 2013. Motor Unit Firing Behaviour of Soleus Muscle in Isometric and Dynamic Contractions. *PLoS ONE*. **8**(2).

Kasuga, S., Momose, N., Ushiyama, J. and Ushiba, J. 2017. Corticomuscular coherence reflects somatosensory feedback gains during motor adaptation. *Neuroscience Research*. **131**, pp.10–18.

Kattla, S. and Lowery, M.M. 2010. Fatigue related changes in electromyographic coherence between synergistic hand muscles. *Experimental Brain Research*. **202**(1), pp.89–99.

Katz, R. and Pierrot-Deseilligny, E. 1999. Recurrent inhibition in humans. *Progress in Neurobiology*. **57**(98), pp.325–355.

Kendall, F.P., McCreary, E.K., Provance, P.G., Rodgers, M. and Romani, W. 2013. *Muscles: Testing and Function, with Posture and Pain*.

Kerkman, J.N., Daffertshofer, A., Gollo, L.L., Breakspear, M. and Boonstra, T.W. 2018. Network structure of the human musculoskeletal system shapes neural interactions on multiple time scales. *bioRxiv*., pp.1–22.

Kilner, J.M., Baker, S.N., Salenius, S., Hari, R. and Lemon, R.N. 2000. Human cortical muscle coherence is directly related to specific motor parameters. *The Journal of neuroscience : the official journal of the Society for Neuroscience*. **20**(23), pp.8838–8845.

Kilner, J.M., Baker, S.N., Salenius, S., Jousmäki, V., Hari, R. and Lemon, R.N. 1999. Task-dependent modulation of 15-30 Hz coherence between rectified EMGs from human hand and forearm muscles. *Journal of Physiology*. **516**(2), pp.559–570.

Kilner, J.M., Salenius, S., Baker, S.N., Jackson, A., Hari, R. and Lemon, R.N. 2003. Task-Dependent Modulations of Cortical Oscillatory Activity in Human Subjects during a Bimanual Precision Grip Task. *NeuroImage*. **18**(1), pp.67–73.

Kirkwood, P.A. and Sears, T.A. 1978. The Synaptic Connexions to Intercostal Motoneurones as Revealed by the Average Common Excitation Potential. *J. Physiol*. **275**, pp.103–134.

Kirkwood, P.A., Sears, T.A., Tuck, D.L. and Westgaard, R.H. 1982. Variations in the time course of the synchronization of intercostal motoneurons in the cat. *Journal of Physiology (London)*. **327**, pp.105–135.

Knikou, M., Rymer, Z. and Rymer, W. 2002. Effects of changes in hip joint angle on H-reflex excitability in humans. *Experimental brain research*. **143**(2), pp.149–159.

Kristeva, R., Patino, L. and Omlor, W. 2007. Beta-range cortical motor spectral power and corticomuscular coherence as a mechanism for effective corticospinal interaction during steady-state motor output. *NeuroImage*. **36**(3), pp.785–792.

Kutch, J.J. and Valero-Cuevas, F.J. 2012. Challenges and new approaches to proving the existence of muscle synergies of neural origin. *PLoS Computational Biology*. **8**(5).

Kuypers, H.G. 1981. Anatomy of the descending pathways *In*: *Handbook of Physiology*. Hoboken, NJ, USA: John Wiley & Sons, Inc., pp.597–666.

Laine, C.M., Martinez-valdes, E., Falla, D., Mayer, F. and Farina, D. 2015. Motor Neuron Pools of Synergistic Thigh Muscles Share Most of Their Synaptic Input. *Journal of Neuroscience*. **35**(35), pp.12207–12216.

Lee, D. and Seung, H. 2001. Algorithms for non-negative matrix factorization. *Advances in neural information processing systems*. (1), pp.556–562.

Lee, S.W., Landers, K. and Harris-Love, M.L. 2014. Activation and intermuscular coherence of distal arm muscles during proximal muscle contraction. *Experimental Brain Research*. **232**(3), pp.739–752.

Lemon, R.N. 1993. Cortical control of the primate hand. *Experimental Physiology*. **78**, pp.263–301.

Lemon, R.N. 2008. Descending pathways in motor control. *Annual review of neuroscience*. **31**(Cm), pp.195–218.

Levin, M.F. 1996. Interjoint coordination during pointing movements is disrupted in spastic hemiparesis. *Brain*. **119**(1), pp.281–293.

Linnamo, V. 2002. *Motor Unit Activation and Force Production during Eccentric , Concentric and Isometric*.

Lloyd, D.P.C. 1943. Neuron patterns controlling transmission of ipsilateral hind limb reflexes in cat. *Journal of Neurophysiology*. **6**(4), pp.293–315.

Lourenço, G., Iglesias, C., Cavallari, P., Pierrot-Deseilligny, E. and Marchand-Pauvert, V. 2006. Mediation of late excitation from human hand muscles via parallel group II spinal and group I transcortical pathways. *The Journal of physiology*. **572**(Pt 2), pp.585–603.

Lu, G., Brittain, J.-S., Holland, P., Yianni, J., Green, A.L., Stein, J.F., Aziz, T.Z. and Wang, S. 2009. Removing ECG noise from surface EMG signals using adaptive filtering. *Neuroscience Letters*. **462**(1), pp.14–19.

De Luca, C.J. and Erim, Z. 1994. Common drive of motor units in regulation of muscle force. *Trends Neurosci*. **17**(7), pp.299–305.

Macefield, G., Gandevia, S.C. and Burke, D. 1989. Conduction velocities of muscle and cutaneous afferents in the upper and lower limbs of human subjects. *Brain : a journal of neurology*. **112 (Pt 6**, pp.1519–1532.

Manning, C.D. and Bawa, P. 2011. Heteronymous reflex connections in human upper limb muscles in response to stretch of forearm muscles. *Journal of neurophysiology*. **106**(3), pp.1489–1499.

Marsden, J.F., Farmer, S.F., Halliday, D.M., Rosenberg, J.R. and Brown, P. 1999. The unilateral and bilateral control of motor unit pairs in the first dorsal interosseous and paraspinal muscles in man. *Journal of Physiology*. **521**(2), pp.553–564.

Martin, J.H., Friel, K.M., Salimi, I. and Chakrabarty, S. 2007. Activity- and use-dependent plasticity of the developing corticospinal system. *Neuroscience and biobehavioral reviews*. **31**(8), pp.1125–35.

Matlab® 2018. Confidence Intervals for Sample Autocorrelation - MATLAB &

Simulink - MathWorks United Kingdom. [Accessed 27 February 2019]. Available from: https://uk.mathworks.com/help/signal/ug/confidence-intervals-for-sample-autocorrelation.html.

Matlab® 2016. Wavelet coherence and cross-spectrum - MATLAB wcoherence - MathWorks United Kingdom. [Accessed 27 February 2019]. Available from: https://uk.mathworks.com/help/wavelet/ref/wcoherence.html.

McAuley, J.H., Rothwell, J.C. and Marsden, C.D. 1997. Frequency peaks of tremor, muscle vibration and electromyographic activity at 10 Hz, 20 Hz and 40 Hz during human finger muscle contraction may reflect rhythmicities of central neural firing. *Experimental Brain Research*. **114**(3), pp.525–541.

McClelland, V.M., Cvetkovic, Z. and Mills, K.R. 2014. Inconsistent effects of EMG rectification on coherence analysis. *The Journal of physiology*. **592**(Pt 1), pp.249–250.

McClelland, V.M., Cvetkovic, Z. and Mills, K.R. 2012a. Modulation of corticomuscular coherence by peripheral stimuli. *Exp Brain Res*. **219**(2), pp.275–292.

McClelland, V.M., Cvetkovic, Z. and Mills, K.R. 2012b. Rectification of the EMG is an unnecessary and inappropriate step in the calculation of Corticomuscular coherence. *Journal of Neuroscience Methods*. **205**(1), pp.190–201.

McCrea, D.A. and Rybak, I.A. 2008. Organization of mammalian locomotor rhythm and pattern generation. *Brain Research Reviews*. **57**(1), pp.134–146.

Mehrkanoon, S., Breakspear, M. and Boonstra, T.W. 2014. The reorganization of corticomuscular coherence during a transition between sensorimotor states. *NeuroImage*. **100**, pp.692–702.

Mendell, L.M. and Henneman, E. 1970. Terminals of Single Ia Fibers: Location, Density, Within a Pool of Motoneurons and Distribution. *Journal of Neurophysiology*. **34**, pp.171–187.

Miller, L.C. and Dewald, J.P.A.A. 2012. Involuntary paretic wrist/finger flexion forces and EMG increase with shoulder abduction load in individuals with chronic stroke. *Clinical Neurophysiology*. **123**(6), pp.1216–1225.

Miller, T.A., Mogyoros, I. and Burke, D. 1995. Homonymous and heteronymous monosynaptic reflexes in biceps brachii. *Muscle & Nerve*. **18**(6), pp.585–592.

Mima, T. and Hallett, M. 1999. Corticomuscular coherence: a review. *Journal of clinical neurophysiology : official publication of the American Electroencephalographic Society*. **16**(6), pp.501–511.

Murthy, V.N. and Fetz, E.E. 1992. Coherent 25- to 35-Hz oscillations in the sensorimotor cortex of awake behaving monkeys. *Proceedings of the National Academy of Sciences of the United States of America*. **89**(12), pp.5670–4.

Murthy, V.N. and Fetz, E.E. 1996. Oscillatory activity in sensorimotor cortex of awake monkeys: synchronization of local field potentials and relation to behavior. *Journal of Neurophysiology*. **76**(6), pp.3949–3967.

Neto, O.P., Baweja, H.S. and Christou, E. a. 2010. Increased voluntary drive is associated with changes in common oscillations from 13 to 60 Hz of interference but not rectified electromyography. *Muscle and Nerve*. **42**(September), pp.348–354.

Nielsen, J.B., Conway, B. a, Halliday, D.M., Perreault, M.-C. and Hultborn, H. 2005. Organization of common synaptic drive to motoneurones during fictive locomotion in the spinal cat. *The Journal of physiology*. **569**(Pt 1), pp.291–304.

Nishimura, Y., Morichika, Y. and Isa, T. 2009. A subcortical oscillatory network contributes to recovery of hand dexterity after spinal cord injury. *Brain*. **132**(3), pp.709–721.

Nuzzo, J.L., Trajano, G.S., Barry, B.K., Gandevia, S.C. and Taylor, J.L. 2016. Arm-posture-dependent changes in corticospinal excitability are largely spinal in origin. *Journal of Neurophysiology*. **115**(4), jn.00885.2015.

Omlor, W., Patino, L., Hepp-Reymond, M.C. and Kristeva, R. 2007. Gamma-range corticomuscular coherence during dynamic force output. *NeuroImage*. **34**(3), pp.1191–1198.

Overduin, S.A., d'Avella, A., Carmena, J.M. and Bizzi, E. 2012. Microstimulation activates a handful of muscle synergies. *Neuron*. **76**(6), pp.1071–1077.

Overduin, S.A., d'Avella, A., Roh, J., Carmena, J.M. and Bizzi, E. 2015. Representation of Muscle Synergies in the Primate Brain. *The Journal of neuroscience : the official journal of the Society for Neuroscience*. **35**(37), pp.12615–24.

Patino, L., Omlor, W., Chakarov, V., Hepp-Reymond, M.-C. and Kristeva, R. 2008. Absence of gamma-range corticomuscular coherence during dynamic force in a deafferented patient. *Journal of neurophysiology*. **99**(4), pp.1906–1916.

Perreault, M.C., Shefchyk, S.J., Jimenez, I. and McCrea, D.A. 1999. Depression of muscle and cutaneous afferent-evoked monosynaptic field potentials during fictive locomotion in the cat. *The Journal of physiology*. **521 Pt 3**(3), pp.691–703.

Phillips, C.G. and Porter, R. 1964. The Pyramidal Projection to Motoneurones of Some Muscle Groups of the Baboon's Forelimb.

Progress in Brain Research. **12**, pp.222–245.

Pierrot-Deseilligny, E. and Burke, D. 2012. *The Circuitry of the Human Spinal Cord*. Cambridge: Cambridge University Press.

Poosapadi Arjunan, S., Kumar, D.K., Wheeler, K., Shimada, H. and Siddiqi, A. 2016. Effect of number of motor units and muscle fibre type on surface electromyogram. *Medical & Biological Engineering & Computing*. **54**(4), pp.575–582.

Prabhakaran, S., Zarahn, E., Riley, C., Speizer, a., Chong, J.Y., Lazar, R.M., Marshall, R.S. and Krakauer, J.W. 2007. Inter-individual Variability in the Capacity for Motor Recovery After Ischemic Stroke. *Neurorehabilitation and Neural Repair*. **22**(1), pp.64–71.

Raethjen, J., Lindemann, M., Dümpelmann, M., Wenzelburger, R., Stolze, H., Pfister, G., Christian, E.E., Timmer, J. and Deuschl, G. 2002. Corticomuscular coherence in the 6-15 Hz band: is the cortex involved in the generation of physiologic tremor? *Experimental Brain Research*. **142**(1), pp.32–40.

Reyes, A., Laine, C.M., Kutch, J.J. and Valero-Cuevas, F.J. 2017. Beta Band Corticomuscular Drive Reflects Muscle Coordination Strategies. *Frontiers in Computational Neuroscience*. **11**(April), pp.1–10.

Richards, T.C., Desai, A.D. and Chakrabarty, S. 2018. Scripts associated with 'Identifying Shared Pathways Across Multiple Muscle Groups of the Human Upper Limb'. *University of Leeds [Dataset]*. [Online]. [Accessed 20 May 2019]. Available from: https://doi.org/10.5518/592.

Riddle, C.N., Baker, M.R. and Baker, S.N. 2004. The effect of carbamazepine on human corticomuscular coherence. *NeuroImage*. **22**(1), pp.333–340.

Riddle, C.N. and Baker, S.N. 2006. Digit displacement, not object compliance, underlies task dependent modulations in human corticomuscular coherence. *NeuroImage*. **33**(2), pp.618–627.

Ritterband-Rosenbaum, A., Herskind, A., Li, X., Willerslev-Olsen, M., Olsen, M.D., Farmer, S.F. and Nielsen, J.B. 2016. A critical period of Corticomuscular and EMG-EMG coherence detection in 9-25 week old healthy infants. *The Journal of Physiology*. **8**, pp.2699–2713.

Roh, J., Cheung, V.C.-K.K. and Bizzi, E. 2011. Modules in the brain stem and spinal cord underlying motor behaviors. *Journal of neurophysiology*. **106**(3), pp.1363–1378.

Roh, J., Rymer, W.Z., Perreault, E.J., Yoo, S.B. and Beer, R.F. 2013. Alterations in upper limb muscle synergy structure in chronic stroke survivors. *Journal of neurophysiology*. **109**(3), pp.768–81.

Rosenberg, J.R., Amjad, A.M., Breeze, P., Brillinger, D.R. and Halliday, D.M. 1989. The Fourier approach to the identification of functional coupling

between neuronal spike trains. *Progress in Biophysics and Molecular Biology*. **53**(1), pp.1–31.

Rossiter, H.E., Eaves, C., Davis, E., Boudrias, M.H., Park, C.H., Farmer, S., Barnes, G., Litvak, V. and Ward, N.S. 2013. Changes in the location of cortico-muscular coherence following stroke. *NeuroImage: Clinical*. **2**(1), pp.50–55.

Rothwell, J.C. 1987. Control of Human Voluntary Movement. , p.325.

Rudomín, P., Engberg, I. and Jiménez, I. 1981. Mechanisms involved in presynaptic depolarization of group I and rubrospinal fibers in cat spinal cord. *Journal of neurophysiology*. **46**(3), pp.532–48.

Rudomin, P., Romo, R. and Mendell, L.M. 1998. *Presynaptic Inhibition and Neural Control*. Oxford University Press.

Salenius, S., Portin, K., Kajola, M., Salmelin, R. and Hari, R. 1997. Cortical control of human motoneuron firing during isometric contraction. *Journal of neurophysiology*. **77**(6), pp.3401–3405.

Schepens, B. 2004. Independent and Convergent Signals From the Pontomedullary Reticular Formation Contribute to the Control of Posture and Movement During Reaching in the Cat. *Journal of Neurophysiology*. **92**(4), pp.2217–2238.

Schmied, A., Forget, R., Vedel, J.-P., Halliday, D.M., Turker, K.S., Des, P. and Rythmiques, R.M. 2014. Motor unit firing pattern, synchrony and coherence in a deafferented patient. *Frontiers in Human Neuroscience*. **8**(October), pp.1–16.

Scott, S.H. 2004. Optimal feedback control and the neural basis of volitional motor control. *Nature Reviews Neuroscience*. **5**(7), pp.532–546.

Sergio, L.E., Hamel-Pâquet, C. and Kalaska, J.F. 2005. Motor Cortex Neural Correlates of Output Kinematics and Kinetics During Isometric-Force and Arm-Reaching Tasks. *J Neuro-physiol*. **94**, pp.2353–2378.

Shepherd, G.M. 1994. *Neurobiology* 3rd ed. Ney York, Oxford: Oxford University Press.

Sherrington, C.S. 1906. The Integrative Action of the Nervous System. *Yale University Press*. **57**.

Sinkjaer, T., Andersen, J.B., Ladouceur, M., Christensen, L.O. and Nielsen, J.B. 2000. Major role for sensory feedback in soleus EMG activity in the stance phase of walking in man. *The Journal of physiology*. **523 Pt 3**, pp.817–827.

Smith, A. and Denny, M. 1990. High-frequency oscillations as indicators of neural control mechanisms in human respiration, mastication, and speech. *Journal of neurophysiology*. **63**(4), pp.745–758.

Smith, C.C., Paton, J.F.R., Chakrabarty, S. and Ichiyama, R.M. 2017. Descending Systems Direct Development of Key Spinal Motor Circuits. *The Journal of neuroscience : the official journal of the Society for Neuroscience*. **37**(26), pp.6372–6387.

Srinivasan, R., Nunez, P.L., Tucker, D.M., Silberstein, R.B. and Cadusch, P.J. 1996. Spatial sampling and filtering of EEG with spline laplacians to estimate cortical potentials. *Brain Topography*. **8**(4), pp.355–366.

Stegeman, D. and Hermens, H. 2007. Standards for surface electromyography: The European project Surface EMG for non-invasive assessment of muscles (SENIAM). *Línea). Disponible en: http://www. med. …*., pp.108–112.

Sukal, T.M., Ellis, M.D. and Dewald, J.P.A. 2007. Shoulder abduction-induced reductions in reaching work area following hemiparetic stroke: Neuroscientific implications. *Experimental Brain Research*. **183**(2), pp.215–223.

Tan, A.M., Chakrabarty, S., Kimura, H. and Martin, J.H. 2012. Selective corticospinal tract injury in the rat induces primary afferent fiber sprouting in the spinal cord and hyperreflexia. *The Journal of neuroscience : the official journal of the Society for Neuroscience*. **32**(37), pp.12896–12908.

Taylor, J.L. 2006. Stimulation at the cervicomedullary junction in human subjects. *Journal of Electromyography and Kinesiology*. **16**(3), pp.215–223.

Tazoe, T. and Perez, M.A. 2017. Cortical and reticular contributions to human precision and power grip. *Journal of Physiology*. **595**(8), pp.2715–2730.

Ting, L.H. and Macpherson, J.M. 2005. A limited set of muscle synergies for force control during a postural task. *Journal of neurophysiology*. **93**(1), pp.609–13.

Torres-Oviedo, G. 2007. Muscle synergies characterizing human postural responses. *Journal of neurophysiology*., pp.2144–2156.

Tresch, M.C., Cheung, V.C.K. and d'Avella, A. 2006. Matrix factorization algorithms for the identification of muscle synergies: evaluation on simulated and experimental data sets. *Journal of neurophysiology*. **95**(January 2006), pp.2199–2212.

Tresch, M.C., Saltiel, P. and Bizzi, E. 1999. The construction of movement by the spinal cord. *Nature neuroscience*. **2**, pp.162–167.

Tresch, M.C., Saltiel, P., D'Avella, A. and Bizzi, E. 2002. Coordination and localization in spinal motor systems. *Brain Research Reviews*. **40**, pp.66–79.

Twitchell, T.E. 1951. The Restoration of Motor Function Following

Hemiplegia in Man. *Brain*. **74**, pp.443–480.

Ushiyama, J., Takahashi, Y. and Ushiba, J. 2010. Muscle dependency of corticomuscular coherence in upper and lower limb muscles and training-related alterations in ballet dancers and weightlifters. *Journal of Applied Physiology*. **109**(4), pp.1086–1095.

Ushiyama, J., Yamada, J., Liu, M. and Ushiba, J. 2016. Individual difference in β-band corticomuscular coherence and its relation to force steadiness during isometric voluntary ankle dorsiflexion in healthy humans. *Clinical Neurophysiology*. **128**(2), pp.303–311.

Vaughan, C.W. and Kirkwood, P.A. 1997. Evidence from motoneurone synchronization for disynaptic pathways in the control of inspiratory motoneurones in the cat. *Journal of Physiology*. **503**(3), pp.673–689.

de Vries, I.E.J., Daffertshofer, A., Stegeman, D.F. and Boonstra, T.W. 2016. Functional connectivity in the neuromuscular system underlying bimanual coordination. *Journal of Neurophysiology*. **116**(6), pp.2576–2585.

Wada, N. and Shikaki, N. 1999. Neuronal pathways for spinal reflexes activated by group I and group II muscle afferents in the spinal segment (Co1) innervating the tail in the low spinalized cat. *Experimental Brain Research*. **125**, pp.129–138.

Ward, N.J., Farmer, S.F., Berthouze, L. and Halliday, D.M. 2013. Rectification of EMG in low force contractions improves detection of motor unit coherence in the beta-frequency band. *Journal of neurophysiology*. **110**(8), pp.1744–50.

Wargon, I., Lamy, J.C., Baret, M., Ghanim, Z., Aymard, C., Pénicaud, A. and Katz, R. 2006. The disynaptic group I inhibition between wrist flexor and extensor muscles revisited in humans. *Experimental Brain Research*. **168**(1–2), pp.203–217.

Welch, P.D. 1967. The Use of Fast Fourier Transform for the Estimation of Power Spectra: A Method Based on Time Averaging Over Short, Modified Periodograms. *IEEE Transactions on Audio and Electroacoustics*. **15**(2), pp.70–73.

Winter, D.A., Fuglevand, A.J. and Archer, S.E. 1994. Crosstalk in surface electromyography: Theoretical and practical estimates. *Journal of Electromyography and Kinesiology*. **4**(1), pp.15–26.

Witham, C.L., Riddle, C.N., Baker, M.R. and Baker, S.N. 2011. Contributions of descending and ascending pathways to corticomuscular coherence in humans. *The Journal of physiology*. **589**(Pt 15), pp.3789–3800.

Wolf, S.L., Winstein, C.J., Miller, J.P. and Morris, D. 2006. Effect of Constraint-Induced Movement Therapy on Upper Extremity Function 3 to 9 Months After Stroke. *Journal of the American Medical Association*. **296**(17), pp.2095–2104.

Yakovenko, S., Krouchev, N. and Drew, T. 2011. Sequential activation of motor cortical neurons contributes to intralimb coordination during reaching in the cat by modulating muscle synergies. *Journal of neurophysiology*. **105**(1), pp.388–409.

Yamaguchi, T. 2004. The central pattern generator for forelimb locomotion in the cat. *Progress in Brain Research*. **143**, pp.115–122.

Zaaimi, B., Edgley, S. a., Soteropoulos, D.S. and Baker, S.N. 2012. Changes in descending motor pathway connectivity after corticospinal tract lesion in macaque monkey. *Brain*. **135**(7), pp.2277–2289.

Zehr, E.P., Carroll, T.J., Chua, R., Collins, D.F., Frigon, A., Haridas, C., Hundza, S.R. and Thompson, A.K. 2004. Possible contributions of CPG activity to the control of rhythmic human arm movement. *Canadian Journal of Physiology and Pharmacology*. **82**(8–9), pp.556–568.

Zehr, E.P. and Duysens, J. 2004. *Regulation of Arm and Leg Movement during Human Locomotion*. Sage PublicationsSage CA: Thousand Oaks, CA.

Zehr, E.P. and Kido, A. 2001. Neural control of rhythmic, cyclical human arm movement: task dependency, nerve specificity and phase modulation of cutaneous reflexes. *Journal of Physiology*. **537**(3), pp.1033–1045.

Appendix

Appendix 1. Scripts associated with Chapter 3

These scripts are available, with permission, from the University of Leeds Data Repository at: https://doi.org/10.5518/592 (Richards et al., 2018).

i. Latency Analysis

Spike 2

Curlat.s2s: Sets cursors for measurements: Stim, Onset, P1, P2.

Overdraw.s2s: Enables overdrawing of traces aligned to stimulus.

Rect.s2s: Rectifies waveforms.

TMSthresh.s2s: Removes DC offset (using 2s time window), Rectifies waveforms. Adds virtual channels to mark stimulus artefact. Searches selected channel for stimulus artefact – marker added by confirmation from user. Searches for Onset, P1, and P2 using active cursors to mark events. Confirmation by user exports results to .txt file to be copied to excel document.

WavfmAvg.s2s: Generates a waveform average aligned to stimulus markers set by user for included trials.

VBA

MACROS_Canda_Latency_FINAL.xlsm: Formats excel of results exported from TMSthresh.s2s. Copies results from individual subjects into column format for input to Matlab® for time-frequency analysis.

R

Latency.R: Calculates group mean, generates bar graphs (mean ± SEM).

ii. Time-Frequency Analysis

BASH

Run#.SH: HPC submission script. Load Matlab® license, submit to HPC queue, run scripts from console.

Matlab®

Run.m: points to correct directory and calls Processall.m.

Processall.m: sorts data, runs loops and acts as master for parallel processing. Calls Findlat.m.

Findlat.m: Call bandpower.m to obtain wavelet transform then extract Power Spectral Density (PSD) at latency x.

Bandpower.m: generate Wavelet Synchro-Squeezed Transform of data.

iii. Wavelet Coherence Analysis

BASH

Run#.SH: HPC submission script. Load Matlab® license, submit to HPC queue, run scripts from console.

Matlab®

Runcoh.m: points to correct directory and calls Processallcoh.m.

Processallcoh.m: sorts data, runs loops and acts as a master for parallel processing. Calls Findlatcoh.m.

Findlatcoh.m: Call bandcoh.m to obtain wavelet coherence.

Bandcoh.m: perform wavelet coherence on two signals.

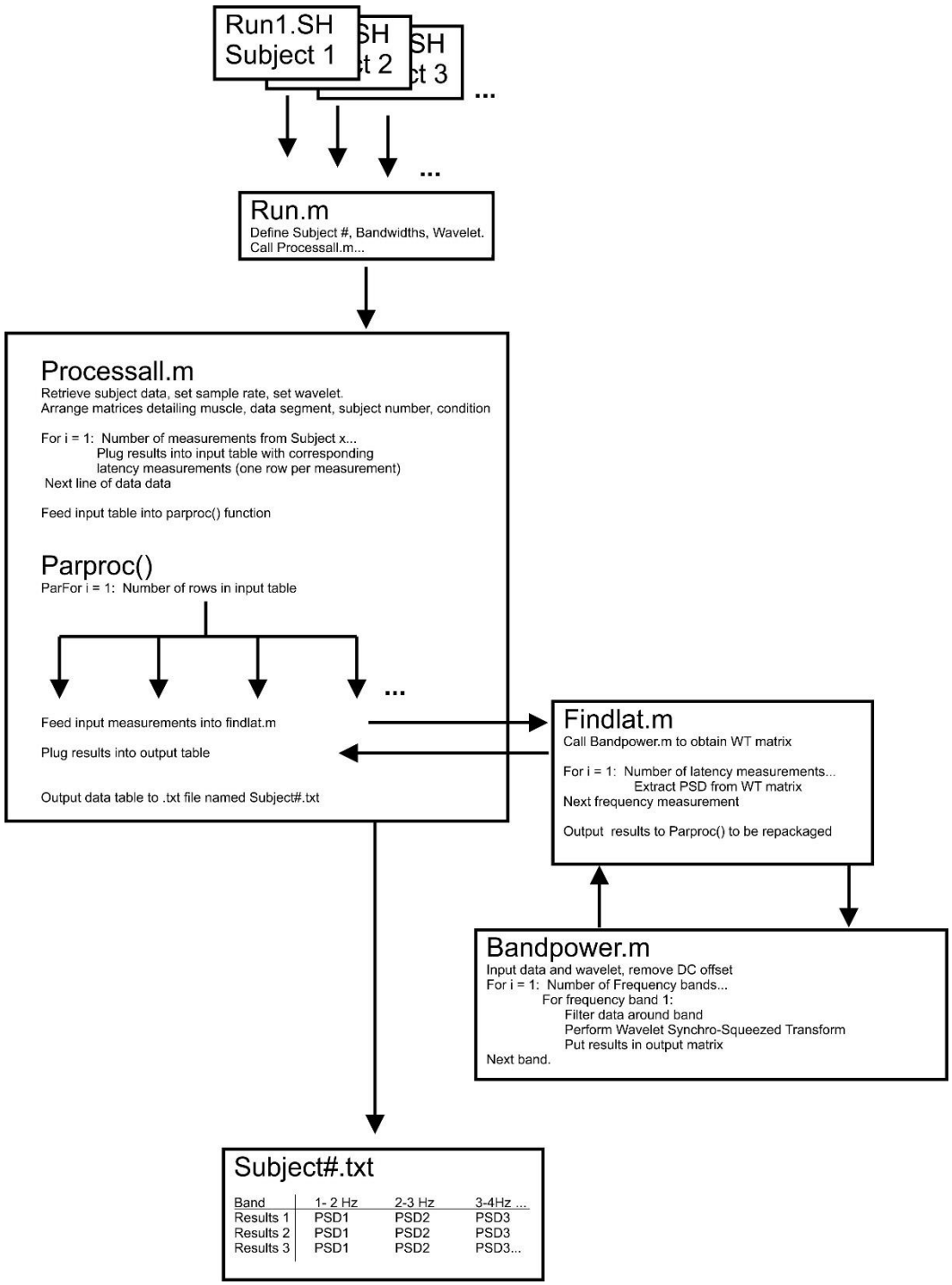

Appendix figure 1. Flowchart detailing the parallel processing sequence used for wavelet analysis.

Appendix 2. Scripts associated with Chapter 4

These scripts, or information on where to obtain them, are available with permission from the University of Leeds Data Repository at: https://doi.org/10.5518/592 (Richards et al., 2018).

i. Onset/Offset Marking

Spike 2

RelTxtAllChans.s2s: Removes Dc offset, Rectifies data, identifies onset/offset, user confirmation, saves onset and offset to marker channel, takes measurements relative to a reference muscle (REF, selected by user), and exports all results to .txt file. Automatically iterates through burst by burst, channel by channel. All parameters are adjustable by user. Measurements: Absolute Max (Raw), RMS Amplitude (between onset and offset), Onset time, Offset time, Burst duration, Amplitude at T=REFmax, Onset relative to REF, Offset relative to REF, T Max relative to T REF onset, T Max relative to T REF max.

RelTxtSingleChan.s2s: Same as RelTxtAllChans.s2s but on single channel if user needs to make corrections on only one channel.

RelMark.s2s: Takes relative measurements from files with existing marker channels and exports to .txt file. Can be modified to take any new measurements.

VBA

Template.xlsx: Spreadsheet to copy data into. Automatically generates averages, bar charts, and onset offset comparison for each subject.

ii. Coherence Analysis

Spike 2

Int_Batch.s2s: This script removes data at the start of the file where EMG drift was present. This is so DC offset could be removed in Matlab®.

BatchCoher+Phase.s2s: Automatically calculates power spectrum, coherence and phase based on pre-determined onset and offset measurements for all bursts for all channels for a given file. Automatically saves results in specified folders.

PrintSigResultsPeak_Batch.s2s: Batch-processing of results files to calculate mean peak from results files generated from BatchCoher+Phase.s2s.

PrintSigResultsCI_Batch.s2s: Batch-processing of results files to number of subjects above CI from results files generated from BatchCoher+Phase.s2s.

Matlab®

Butter.m: Removes DC offset and applies 4^{th} order Butterworth filter.

VBA

Coh_MeanPeak_Macro.xlsm: Automatically sorts data pasted from peak analysis into format for figures.

Coh_CI_Macro.xlsm: Automatically sorts data pasted from CI analysis into format for generating figures.

iii. Cross-correlation Analysis

Spike 2

PrintSigResultsPeak_BatchCor_MeanAbsPeak.s2s: Batch-processing of results files to calculate mean absolute peak from result files.

PrintSigResults_BatchCor_SubsAboveCI_HW.s2s: Batch-processing of results files to count number of subjects above CI from results files.

VBA

Cor_MeanPeak_Macro.xlsm: Automatically sorts data pasted from peak analysis into format for figures.

Cor_CI_HW_Macro.xlsm: Automatically sorts data pasted from CI analysis into format for generating figures.

iv. Cluster Analysis

Matlab®

PerformNMF.m: Performs NMF cluster analysis and displays resultant clusters as networks.